THE MICROSCOPIC ~~INVESTIGATION~~ STUDY OF PHASE ~~CHANGES~~ TRANSITIONS IN FERROELECTRIC PEROVSKITES

A Thesis

Submitted for the

DEGREE OF DOCTOR OF PHILOSOPHY

IN THE UNIVERSITY OF LONDON

by

HAMISH GEORGE MAGUIRE

Department of Electrical Engineering,

City and Guilds College,

Imperial College,

LONDON.

1969.

ABSTRACT

The fundamental properties which define ferroelectric behaviour in crystals is initially considered and the importance of the occurrence of electric polarisation spontaneously, as a result of temperature change only and not of applied field, is stressed. This is followed by considering the consequences of this on the various physical properties. Attention is drawn to the crystallographic changes which barium titanate undergoes and various theories which have attempted to explain this are considered critically. The problem of growing suitably large good quality crystals for the particular purpose of the microscopic techniques used is described.

Electron spin resonance studies of the effect of a temperature dependent crystal field on substitutional transition metal ions is determined. The further direct effect of this crystal field on the nuclear energy levels is also determined by the measured quadrupole splitting using the Mössbauer effect.

ACKNOWLEDGEMENTS

I wish to gratefully acknowledge the opportunity provided by Professor J.C. Anderson which enabled me to complete this work in the face of unforeseen difficulties and his patience and understanding throughout.

I would also like to thank Dr. E.A.D. White for encouragement and help in connection with the crystal growing.

Sincere thanks are also due to Dr. J.F. Gibson, who so generously provided free and unhindered access to the Varian electron spin resonance spectrometer and with whom I had many illuminating discussions. Thanks are also due to Dr. L.V.C. Rees on whose spectrometer the Mössbauer measurements were performed. Special thanks are due to Dr. R.W. Kibble and K.E. Barnes of the Department of Theoretical Physics, who so generously helped to lay the foundations for the necessary quantumn mechanics involved.

Finally I would like to thank Mr. E.A. Hall, Senior Technician in the Materials Laboratories, and the staff of the general workshops whose able assistance and sound advice cut many corners.

CONTENTS

		Page No.
1.	SURVEY OF FERROELECTRIC PHENOMENA	14
1.1	INTRODUCTION	14
1.2	OBJECTIVES	14
1.3	DEFINITION OF A FERROELECTRIC - OUTSTANDING PROPERTIES	15
1.4	PHENOMENOLOGICAL CLASSIFICATIONS OF FERROELECTRICS	20
1.5	ANTIFERROELECTRICS, FERRIELECTRICS, PARAELECTRICS	25
1.5.1	Antiferroelectrics	25
1.5.2	Ferrielectrics	27
1.5.3	Paraelectrics	28
1.6	CHRONOLOGICAL DEVELOPMENT	29
1.7	THEORETICAL APPROACHES	31
2.	PHENOMENOLOGICAL BEHAVIOUR (MACROSCOPIC)	34
2.1	THE DIELECTRIC CONSTANT	34
2.1.1	Introduction	34
2.1.2	General Behaviour	34
2.1.3	Frequency Effects	39

		Page No.
2.2	ELECTROMECHANICAL BEHAVIOUR	44
2.2.1	Introduction	44
2.2.2	Piezoelectric Behaviour	47
2.2.3	Electrostrictive Behaviour	52
2.2.4	Elastic Behaviour	55
2.3	SPONTANEOUS POLARISATION AND SPONTANEOUS STRAIN	55
2.3.1	Introduction	55
2.3.2	Spontaneous Polarisation	57
2.3.3	Spontaneous Strain	61
2.4	THERMAL BEHAVIOUR	63
2.4.1	Introduction	63
2.4.2	Specific Heat Anomaly	65
2.4.3	Latent part of the Transition Heat	66
2.4.4	Thermal Expansion Coefficient	66
2.5	THE OPTICAL PROPERTIES IN THE VISIBLE RANGE	67
2.5.1	Introduction	67
2.5.2	Electro-optic Effect	67
2.6	THE INFLUENCE OF EXTERNAL STRESSES	71
2.6.1	Introduction	71
2.6.2	The Influence of Electric Fields	71
2.6.3	The Influence of Mechanical Stresses	72
2.7	ELECTRICAL PROPERTIES	73
2.7.1	Introduction	73
2.7.2	Electrical Conductivity	74

		Page No.
3.	GROWTH OF BARIUM TITANATE SINGLE CRYSTAL	75
3.1	INTRODUCTION	75
3.2	METHOD AND TECHNIQUES	76
3.3	CHOICE OF SOLVENT	77
3.4	GENESIS OF BUTTERFLY TWINS	78
3.5	APPARATUS	82
3.6	EXPERIMENTAL METHOD	85
4.	THE CRYSTAL STRUCTURE AND ASSOCIATED ATOMIC PROPERTIES	92
4.1	INTRODUCTION	92
4.1.1	The Structure in the Cubic Phase	92
4.1.2	The Structure in the Tetragonal Phase	93
4.1.3	Bond Lengths and Bond Angles	98
4.2	INFRA-RED PROPERTIES	99
4.2.1	Introduction	99
4.2.2	Results	101
4.3	THE DOMAIN STRUCTURE	104
4.3.1	Introduction	104
4.3.2	Experimental Evidence for Domains	105
4.3.3	The Domain Geometry of Tetragonal Barium Titanate	107
4.3.4	180° Domains	108
4.3.5	90° Domains	109
4.3.6	The Domain Walls	111
4.3.7	180° Walls	111
4.3.8	90° Walls	113

		Page No.
5.	THEORIES FOR BARIUM TITANATE	115
5.1	GENERAL REMARKS	115
5.1.1	Phenomenological Theory and Thermodynamics of the Transition	116
5.2	MODEL THEORIES	128
5.2.1	Introduction	128
5.2.2	Polarisation and Susceptibility	129
5.2.3	The Internal Field	131
5.2.4	Polarisability	132
5.2.5	Mason-Mathias Theory	133
5.2.6	Devonshire's Model Theory	136
5.2.7	Slater's Theory	137
5.2.8	Oxygen Displacement Theory (Jaynes)	140
5.2.9	Electronic Theory	141
5.2.10	Megaw's Theory	143
5.3	LATTICE DYNAMICS THEORY	144
5.3.1	Introduction	144
5.3.2	Theory of Ferroelectricity (Cochran)	144
6.	ELECTRON PARAMAGNETIC RESONANCE (EPR)	151
6.1	INTRODUCTION	151
6.2	THE RESONANCE PHENOMENON	153
6.3	THE CRYSTAL FIELD	154
6.3.1	Introduction	154

		Page No.
6.4	THE FREE ION	155
6.4.1	Effect of a Static Crystalline Field	157
	(a) Strong Crystalline Field	157
	(b) Intermediate Crystal Field	157
	(c) Weak Crystal Field	158
6.5	ENERGY LEVELS OF THE d-ELECTRONS	158
6.5.1	Qualitative outline	158
6.5.2	d-orbital splitting	161
6.5.3	Kramers' Theorem	164
6.6	THE SPIN HAMILTONIAN	165
6.6.1	Introduction	165
6.6.2	The Spectroscopic Splitting Factor - g	168
6.6.3	Fine Structure	169
6.6.4	Magnetic Hyperfine Structure	171
6.6.5	Quadrupole interaction	173
6.6.6	Nuclear interaction with the external field	174
6.6.7	S-state ions	174
6.7	DERIVATION OF ENERGY LEVELS FROM THE SPIN HAMILTONIAN	176
6.7.1	Introduction	176
6.7.2	The matrix representation	176
6.7.3	Angular momentum operators - Dirac notation	178
6.8	THE SPECTROMETER SYSTEM	180
6.9	THE CRYSTAL GONIOMETER	185

		Page No.
6.10	Fe^{3+} - EXPERIMENTAL	188
6.10.1	The room temperature resonance spectrum	188
6.10.2	Rotation of the crystal (spectrum)	188
6.10.3	Temperature dependence	190
6.11	THEORY OF Fe^{3+} IN BARIUM TITANATE	190
6.11.1	Introduction	190
6.11.2	The Matrix elements	193
6.12	EVALUATION OF THE PARAMETERS OF THE SPIN HAMILTONIAN FROM DATA AT $\Theta = 0$	197
6.12.1	(i) g - tensor	198
6.12.2	(ii) D, a, b.	198
6.13	THE ENERGY LEVEL DIAGRAM	199
6.14	Mn^{2+} - EXPERIMENTAL	209
6.14.1	Introduction	209
6.14.2	Experimental	210
6.14.3	ENDOR - Electron nuclear double resonance	211
7.	THE MÖSSBAUER EFFECT	214
7.1	FUNDAMENTAL FEATURES	214
7.1.1	Introduction	214
7.1.2	Emission of gamma rays by nuclei	215
7.1.3	Doppler broadening	219
7.1.4	Cross section for resonance fluorescence	220
7.1.5	Applications of the Mössbauer effect to Barium Titanate	223

		Page No.
7.2	LATTICE VIBRATIONS	224
7.2.1	Introduction	224
7.2.2	Probability of a recoil-free emission (absorption)	226
7.2.3	The Debye Solid	229
7.3	THE ISOMER SHIFT (IS)	231
7.3.1	Introduction	231
7.3.2	Isomer Shift	231
7.4	QUADRUPOLE COUPLING	237
7.4.1	Introduction	237
7.4.2	The quadrupole Hamiltonian	239
7.5	THE ELECTRIC FIELD GRADIENT (EFG)	243
7.6	MAGNETIC HYPERFINE STRUCTURE (hfs)	247
7.6.1	Introduction	247
7.6.2	The Transition Probabilities	249
7.6.3	The Internal (Magnetic) Field	250
7.7	EXPERIMENTAL	252
7.7.1	Introduction	252
7.7.2	The Mössbauer Spectrometer	253
7.7.3	Temperature Variation	256
7.7.4	Sample preparation	257
7.7.5	Location and charge state of the Mössbauer probe	260
7.7.6	Measurements and results.	261

		Page No.
8.	DISCUSSION	269
8.1	INTRODUCTION	269
8.2	ELECTRON SPIN RESONANCE STUDIES	269
8.3	MOSSBAUER STUDIES	274
8.4	CONCLUSION	276
	REFERENCES	277
	APPENDIX A	288
	APPENDIX B - Programme 1	301
	Programme 2	304

TABLE OF FIGURES

CHAPTER 2:

Fig. 2.1 Fig. 2.2	37
Fig. 2.3 Fig. 2.4	42
Fig. 2.5 Fig. 2.6	51
Fig. 2.7 Fig. 2.8 Fig. 2.9	54
Fig. 2.10 Fig. 2.11 Fig. 2.12	59
Fig. 2.13 Fig. 2.14	64

Page No.

CHAPTER 3:

Fig. 3.1
Fig. 3.2 79

Fig. 3.3 83

Fig. 3.4 89

CHAPTER 4:

Fig. 4.1
Fig. 4.2
Fig. 4.3
Fig. 4.4
Fig. 4.5 96

Fig. 4.6
Fig. 4.7 102

Fig. 4.8 112

CHAPTER 5:

Fig. 5.1 120

Fig. 5.2
Fig. 5.3 124

Fig. 5.4
Fig. 5.5
Fig. 5.6 148

CHAPTER 6:

Fig. 6.1
Fig. 6.2 163

Fig. 6.3 181

Fig. 6.4(a) 186

Fig. 6.4(b)
Fig. 6.4(c) 187

Fig. 6.5 189

Fig. 6.6 191

Page No.

CHAPTER 6 (continued):

Fig. 6.7 192

Fig. 6.8
Fig. 6.9 194

Fig. 6.10 201

Fig. 6.11 202

Fig. 6.12 204

Fig. 6.13 205

Fig. 6.14 207

Fig. 6.15 208

Fig. 6.16 212

CHAPTER 7:

Fig. 7.1
Fig. 7.2
Fig. 7.3 218

Fig. 7.4
Fig. 7.5 228

Fig. 7.6 234

Fig. 7.7
Fig. 7.8 246

Fig. 7.9 254

Fig. 7.10 258

Fig. 7.11 262

Fig. 7.12 264

Fig. 7.13 265

Fig. 7.14 266

CHAPTER 8:

Fig. 8.1 273

1. SURVEY OF FERROELECTRIC PHENOMENA

1.1 INTRODUCTION

Ferroelectricity is a somewhat misleading name. Whilst the phenomenology of the dielectric behaviour is more or less analogous to the magnetic counterpart, the underlying mechanisms have really very little in common.

A theory of ferromagnetism must use quantum mechanics, but ferroelectricity is one of the few cooperative phenomena for which an adequate description can, at least to a large extent, be based on the methods of classical physics. This is of course due to the profound difference between the forces acting on the spin of the electrons as compared to those between electric dipoles.

The majority of ferromagnets owe their properties to one of the rather small groups of magnetic elements that stretch from Cr to Ni and over the 4f and 5f series. On the other hand, ferroelectricity can never be tied to one single element.

1.2 OBJECTIVES

It is the purpose of this work to try and determine the mechanisms which are responsible for the occurrence of ferroelectric behaviour in perovskite barium titanate. To this end the experimental techniques involved may differ greatly and considerable work has already been done in order to gain

an understanding of the macroscopic behaviour for the temperature range in which the crystal structure varies from cubic to tetragonal and from non-ferro to ferroelectric. While certain of these measurements do infer the nature and type of the above transition they do not really contribute very much to an understanding of the processes responsible for them.

It is primarily for this reason that an attempt was made towards a better understanding of the microscopic mechanisms which are active in producing ferroelectric behaviour. The techniques which have been drawn upon in this work are those of magnetic resonance and nuclear resonance fluorescence (Mössbauer effect) spectroscopy. This is achieved by the incorporation of suitable probes in the crystal at the lattice points of interest.

1.3 DEFINITION OF A FERROELECTRIC - OUTSTANDING PROPERTIES

The relation between the electric displacement, D, and applied field, E, for a ferroelectric crystal exhibits hysteresis which appears only in certain temperature ranges depending upon the material. In its ferroelectric phase a crystal is spontaneously polarised, i.e. electric polarisation exists in the crystal in the absence of an externally applied field. The most important property of a ferroelectric is that the direction of the spontaneous polarisation

can be altered by an externally applied electric field. In typical ferroelectrics the spontaneous polarisation decreases as the crystal is heated and disappears at a temperature called the "ferroelectric Curie point". For good, pure, single crystals of $BaTiO_3$ this "transition" occurs in the region of 120°C, and recent attempts at growing purer crystal suggests an increase in this transition related to the purity; this temperature is referred to as the Curie temperature or transition temperature.

The dielectric constant is generally high in the direction of the spontaneous polarisation, and shows a very high peak at the Curie point. In the case of $BaTiO_3$ the dielectric constant is greater in a direction perpendicular to that of spontaneous polarisation. Heating beyond the Curie temperature results in a rapid decrease of the dielectric constant which is then inversely proportional to the temperature, according to the Curie-Weiss law.

The spontaneous polarisation is accompanied by a spontaneous strain, and piezoelectric and elastic anomalies accompany the dielectric anomaly. Also, there is generally an anomaly of the specific heat at the transition temperature and the shape of the curve of specific heat against temperature in the region of this anomaly depends upon whether the transition is of the first order, which involves a latent heat,

or of the second order which does not involve a latent heat.* The accumulation of experimental evidence shows that the phase transition of $BaTiO_3$ is of the first order.

Due to the polarisation and strain the symmetry of a crystal in its ferroelectric phase is lower than that of the non-polar phase, (here the word polar is not used in the same sense as that used to describe for example, an ionic crystal). The departure from the higher symmetry is slight, and a macroscopic ferroelectric crystal often consists of multiple twins. An individual twin forms a domain, within which the polarisation is uniformly directed; adjacent domains are oriented and hence polarised in different directions. These orientations can be altered by application of a field. It should be noted that domains are not necessarily the result of twin formation.

The phenomenological properties described above are common to all ferroelectric crystals. Their behaviour is directly attributable to the crystallographic properties and the changes associated with them whenever they undergo a transition from the non-ferroelectric to the ferroelectric phase.

It is well known that crystals can be divided into thirty-two classes according to their rotational symmetries.

* A. Pippard. The elements of classical thermodynamics, p.136.

(W.G. Cady - Piezoelectricity, p.17). Of these thirty-two classes eleven have a centre of symmetry and are called centrosymmetric; the remaining twenty-one are non-centrosymmetric. Crystals in twenty out of the twenty-one non-centrosymmetric classes show the phenomenon of piezoelectricity, i.e. upon the application of an external mechanical stress an electrical polarisation is created within the crystal. Ten out of the twenty piezoelectric classes have the property that for a nuclear and electronic charge density $\rho(r)dV$ the electric dipole moment of the unit cell

$$\int \rho(r).r.dV \neq 0$$

is different from zero, and are called pyroelectric. Crystals in this class are already polarised since they possess at least one axis, though not necessarily the only one, which shows properties in one direction which are different from those in the other direction. The electrical polarisation is usually masked by a surface charge and occasionally by twinning, but it can usually be observed in a non-conducting crystal as a surface charge if the temperature of the crystal is altered and a change in the polarisation occurs - hence the name pyroelectricity. In some pyroelectric crystals the direction of polarity may be reversed by application of a sufficiently high electric field.

Such reversible pyroelectrics are ferroelectrics. This reversal must of course be possible at field strengths below the breakdown strength of the crystal. The reversibility of the direction of spontaneous polarisation is a consequence of the fact that the polar structure of ferroelectrics in the ferroelectric phase is only a slightly distorted non-polar structure in the non-ferroelectric or paraelectric phase. It is this property which leads to non-linear dielectric behaviour and to hysteresis effects in the relation between dielectric displacement and electric field. The field necessary to bring about this reversal of the polarisation is called the "coercive field", the value for single-crystal $BaTiO_3$ being about 500 Vcm^{-1} at room temperature.

The crystallographic properties just mentioned do not label a crystal as ferroelectric, since, whereas one can deduce the presence of piezo- or pyro-electricity as soon as the crystal class has been established, by optical or X-ray means for example, dielectric measurements alone can establish the presence of ferroelectricity - the latter word is thus a dielectric and not a crystallographic term. The crystallographic properties, though not serving to define ferroelectricity, are the necessary conditions for the phenomenon to occur; the phenomenological properties describe the effect of changing temperature. The definition of the phenomena may

be stated thus:

"A ferroelectric is a crystal possessing reversible polarisation, as shown by a dielectric hysteresis loop."

1.4 PHENOMENOLOGICAL CLASSIFICATIONS OF FERROELECTRICS

From a purely phenomenological standpoint ferroelectrics have been divided into various classes, which depend largely on what significant properties are to be discussed. Generally discussions based on macroscopic considerations are as follows:-

a) Ferroelectrics that can polarise along only one axis ("up" or "down")

Rochelle salt and related tartrates.

KH_2PO_4 - type ferroelectrics.

$(NH_4)_2SO_4$ and $(NH_4)_2BeF_4$.

Colemanite, $CaB_3O_4(OH)_3.H_2O$.

Thiourea, triglycine sulphate and selenate.

b) Ferroelectrics that can polarise along several axes that are equivalent in the unpolarised state:

Barium Titanate ($BaTiO_3$) - type ferroelectrics (Perovskite family)

$Cd_2Nb_2O_7$

$PbNb_2O_6$

Certain alums and the Tungsten bronze family.

Both of the above classes show piezoelectric activity in

the polarised phase. Those of class b) often have transition points below the Curie temperatures at which there is a sudden change in magnitude and direction of the spontaneous polarisation.

Another important phenomenological classification is as follows:

a) Ferroelectrics that are piezoelectric in the unpolarised phase:

Rochelle salt and related tartrates

KH_2PO_4 - type ferroelectrics

b) Ferroelectrics that are not piezoelectric in the unpolarised phase:

$BaTiO_3$ type ferroelectrics

$Cd_2Nb_2O_7$

$PbNb_2O_6$

Colemanite

One outstanding property of ferroelectrics of class b) is found to be the "reversibility of the spontaneous polarisation by a mechanical stress", and the very strong dependence of the electromechanical behaviour upon the electrical boundary conditions and the temperature.

A further classification, which is merely an extension of the above, divides ferroelectrics into two types which are not dependent upon the presence or absence in general of piezo-

electric properties in the paraelectric phase, but upon the presence or absence of these properties in the direction of formation of spontaneous polarisation (Shuvalov, 1964). This so-called crystal-physical classification is strictly a classification not of ferroelectric crystals in general but of ferroelectric phases.

However, in any microscopic investigation of phase changes occurring in ferroelectric crystals one must consider the internal effects of any microscopic displacements. It is convenient from this point of view to divide ferroelectric crystals into two groups. The first group comprises hydrogen-bonded crystals such as KH_2PO_4, which undergo an order-disorder transition. Though all atoms in the unit cell are involved in the ferroelectric process, the transition nevertheless seems to be triggered by an ordering of hydrogens in one out of the two possible equilibrium sites in the H-bonds.

In the case of the O-H-O bond the O-O distance is crucial. Below 2.5 Å there will be only a one potential well not permitting two more or less symmetric position for the hydrogen. Above 2.8 Å the hump between the two wells will be already too high to permit any further tunnelling to the hydrogen through it. Therefore, the optimum distance for tunnelling, ordering and hence ferroelectricity is between 2.5 and 2.8 Å. The role of the hydrogen atoms in

these transitions is demonstrated by the isotope effects (Känzig, 1957; Jona and Shirane, 1962), in the Curie temperatures on deuteration and particularly by the huge isotope effects (up to six orders of magnitude) in the ferroelectric domain wall mobilities (Bjorkstom and Oettel, 1966; Blinc and Svetina, 1966) on replacing hydrogen by heavy hydrogen. The enhanced understanding of this group of crystals has been brought about by exploring the formal analogy with the Ising and Heizenberg problems in ferromagnetism (Blinc and Svetina, 1966; De Gennes, 1963; Bersuker, 1966; Brout et al., 1966).

The atomic displacements involved in the transitions are usually small and difficult to study with diffraction techniques. Since symmetry changes on going from the non-polar to the polar phase require an accompanying change in the electric field gradients within the crystal and small atomic displacements may cause large field gradient changes, the quadrupole splittings of nuclear magnetic lines provide a very powerful method for the study of microscopic details of these transitions. Spin-lattice relaxation data and life-time effects in the magnetic resonance line shapes in addition provide information on the dynamics of the ferroelectric state and the elementary excitations involved.

The second group (Jona and Shirane, 1962) of ferroelectric

crystals includes the double oxides, such as $BaTiO_3$, which undergo a transition of the displacive type, and the high electronic polarisability of oxygen octahedra will almost always lead to a spontaneous dielectric polarisation, provided, as pointed out below, the centre ion has a noble gas configuration. Actually, it is possible even to average over the periodic system. Instead of Ti one could substitute, for instance, $\frac{1}{2}$ Sc and $\frac{1}{2}$ Nb. Ferroelectricity is limited to a rather broad range of centre ion-oxygen distances. Above and below these distances antiferroelectricity will usually occur instead (Johnson et al., 1963). The properties of these crystals can be understood in terms of an instability of the crystal lattice against a transverse optical mode as the temperature approaches the Curie temperature. In $BaTiO_3$, this instability seems to be due to electron-phonon coupling, i.e. due to vibronic interactions. It is interesting to note that the above multiple potential well concept of ferroelectricity may also be applicable to $BaTiO_3$ type crystals, since it has been recently pointed out (Brout et al., 1966; Bersuker, 1966) that the Ti ion in $BaTiO_3$ has its potential minimum displaced off the centre of symmetry due to a "pseudo Jahn-Teller effect". Model theories often involve the idea that the driving force for ferroelectric transitions of this type is a temperature

dependent covalent bond. Since the chemical shift of the nuclear resonance provides a sensitive measure for the degree of covalent bonding, a measurement of the temperature dependence of the chemical shifts of all nuclei involved could significantly enhance our understanding of this type of crystal. This field is still relatively unexplored and the results obtained so far are inconclusive.

1.5 ANTIFERROELECTRICS, FERRIELECTRICS, PARAELECTRICS

1.5.1 Antiferroelectrics

Crystals which are isomorphous with ferroelectrics or of closely related structure, often undergo, with decreasing temperature, phase transitions from a state of higher symmetry to a state of lower symmetry, which are connected with slight distortions of the crystal lattice. This is usually accompanied by twinning. Unlike ferroelectric domains, these twins have no net electric dipole moment. Kittel thus defines the antiferroelectric state as one in which "lines of ions in the crystal are spontaneously polarised, but with neighbouring lines polarised in anti-parallel directions, so that the net macroscopic polarisation of the crystal as a whole is zero". The anomaly in the heat capacity at the Curie point closely follows that of a ferro-electric. Thus thermodynamic evidence alone is insufficient to distinguish between a ferro and antiferroelectric. There

seems little doubt that the critical conditions for antiferroelectricity and ferroelectricity are closely related; in fact some antiferroelectrics can be forced into a ferroelectric state by a strong field.

In view of the above, it is pointed out by Megaw that in attempting a definition it is desirable to look for something more exact and more easily stated in terms of observable properties. It seems best to use the dielectric constant as a criterion, since the anomalies in this appear at the transition point, and therefore an antiferroelectric can only be recognised as such at or near the transition: "An antiferroelectric is a substance of non-polar symmetry, showing no dielectric hysteresis, which has a pseudo-symmetric transition to a high symmetry form accompanied by a sharp anomally in the dielectric constant". This definition is handicapped in that the pseudo-symmetry of the transition is not always easy to establish experimentally. Consequently a further criterion is needed and this is provided in the response shown to a d.c. biasing field. To this end it has been shown by Takagi (1952), on theoretical grounds, that the dielectric constant should increase with increasing bias, though slowly at first since it is proportional to E^2, for an antiferroelectric, and increase with decreasing bias, being proportional to E, for a ferro-

electric; this is in fact borne out by experiment. Kittel further points out the very important distinction between the antiferroelectric state not being piezoelectric as a centre of symmetry exists, and the ferroelectric state possessing a large piezoelectric effect. Though this is a distinguishing feature between the two states it does not serve to define either one. Thus we see that, like ferroelectric, it is not possible to define antiferroelectric crystallographically - the definition again involves dielectric behaviour as well as structural properties.

1.5.2 Ferrielectrics

From what has been said above about ferroelectrics and antiferroelectrics it is reasonable to enquire if both these phenomena exist simultaneously in the same crystal. With the above definitions as they stand, this is not so. The spontaneous polarisation of a ferroelectric is unidirectional, and if we restrict our attention at right angles to this, it has no spontaneous polarisation and gives no hysteresis loop, though it may show the pseudosymmetry and anomalous dielectric constant of an antiferroelectric. Hence some ferroelectrics may possess antiferroelectric properties in a direction at right angles to its polar axis. They are called "ferrielectric". The above effects are only detectable in single crystals, since they depend on direction.

In examining the origin of these effects, Megaw considers the individual dipoles, assumed similar, existing in separate parts of the unit cell, to be oriented with respect to the polar axis along a cone whose axis coincides with the polar axis. Thus the components of the dipoles along this axis account for the ferroelectric behaviour, and at right angles to it for the antiferroelectric behaviour. For this reason Megaw refers to these crystals as "Cone ferroelectrics". In the important special case when all the dipoles are parallel, because they lie on rotation axes of symmetry, as in tetragonal $BaTiO_3$, the semi-angle of the cone is zero, and this is then referred to as a "line ferroelectric". Apart from Megaw, these names are not widely used by other authors.

1.5.3 Paraelectrics

The word paraelectric is used to denote the high-symmetry form of a substance which is ferroelectric or antiferroelectric below the transition temperature. It has also been extended to cover substances possessing high symmetry structures in a family which contains ferroelectrics, even if they themselves never undergo a transition.

Throughout the remainder of this account, the word paraelectric refers to the high symmetry non-polar structure existing above the Curie temperature. Thus for the case of $BaTiO_3$, it is paraelectric above about 120°C and obeys a

Curie-Weiss law with increasing temperature. The words paraelectric (-phase) and non-ferroelectric (-phase) are used interchangeably throughout.

1.6 CHRONOLOGICAL DEVELOPMENT

It was as early as 1894 that unusual dielectric, piezoelectric, and electrooptic properties of Rochelle salt were noticed by Pockels in Göttingen and this substance was further investigated after World War I in the United States by Cady, Anderson and Nicholson in connection with ultrasonic underwater communication. However the discovery of the phenomenon is generally attributed to Valasek, who in 1921 pointed out the analogy between the dielectric properties of Rochelle salt and the magnetic properties of ferromagnetic materials, from which the word itself is derived. The word itself first appears to have been used by Mueller in 1935, and is misleading inasmuch as it has nothing to do with iron and in any case is not exactly analagous with ferromagnetism.

It wasn't until around 1943 that Wainer and Soloman in the United States, Wul and Goldman in Russia, and Ogawa in Japan independently discovered the anomalous dielectric properties of $BaTiO_3$. In contrast to earlier ferroelectrics, $BaTiO_3$ has three equivalent mutually perpendicular axes and thus exhibits unusual dielectric and electromechanical properties with variation in temperature in polycrystalline form.

Small single crystals were first grown by the Swiss group (Blattner, Mathias, Merz and Scherrer) at Zurich in 1947, and Remeika, in 1954 developed a method of growing large single crystals; this greatly stimulated basic studies of the material, and among other things, the first single crystal structure study was carried out by Frazer, Danner and Pepinsky using neutron diffraction methods in 1955. The first optical investigations of it's domain structure were performed in 1948 at Bristol, Zurich and M.I.T. In 1949 Devonshire first successfully worked out a phenomenological theory which described its behaviour whilst at about the same period considerable efforts were made, theoretically, to relate the ferroelectric properties to the crystal structure. $BaTiO_3$ was the first dielectric in which relative displacements of sublattices due to polarisation were observed by X-ray diffraction (Känzig, 1951). The middle 1950's saw extensive efforts directed towards the study of the static and dynamic properties of its domain structure in view of possible applications as information storage devices.

In recent years one sees the departure from the conventional macroscopic explanations of the physical properties of $BaTiO_3$, since these have proved inadequate, and more effort being directed towards both microscopic experimental investigation and the attendant theory.

1.7 THEORETICAL APPROACHES

The theoretical treatments put forward, in attempting to explain the phase transition occurring at the Curie temperature, generally fall into two distinct groups; (a) those requiring a molecular model, and (b) those adopting the phenomenological approach.

The most successful phenomenological theory is that due to Devonshire. The free energy function is expanded in terms of the independent variables, polarisation and stress, and use is made of certain measured properties of the crystal to determine co-efficients, and predict others. The difficult point here is to explain the experimental facts with the smallest number of expansion coefficients possible, on the basis of the most reasonable assumptions.

Molecular theories may be further classified into two types. The first is based on dipoles with two positions of equilibrium, introduced by Mason and Mathias, and is related to the earlier Eucken-Buchner theory of dielectric behaviour in certain dielectrics.

The second may be termed the oscillating-ion type in which the ions are assumed to move in a parabolic potential well. This concept prompted Jaynes' "Oxygen displacement theory" which was supported by the structure determinations of Känzig and Evans. Slater extends this further and

considers the titanium ion to be slightly displaced as a result of the oxygen displacements.

Basically both the above treatments are based on the long range forces of dipole interaction.

Other investigators, however, notably Megaw, have approached the problem in another way by considering the transition as associated with a change of the type of chemical bonding rather than a change in the dipole structure. In the above model theories the "Molecular mechanism" accompanying a phase change is little understood at the present time even though the crystal structure and the minute changes at the transition point are.

In addition to the above two theoretical approaches to the problem of ferroelectricity there has emerged in the last decade what is probably the most successful attempt at explaining microscopically the theory for certain crystals. This was initially due to Cochran and is based on the assumption that the ferroelectric transitions result from an instability for a certain normal vibrational mode and may hence be treated as a problem in lattice dynamics. Essentially the theory is based on the argument that, for a crystal which is wholly or partly ionic, the lattice vibrations are accompanied by polarisation oscillation of the same frequency creating a localised field interacting with the ions through

long-range Coulomb forces which, if for one particular mode of vibration have the same magnitude but opposite sign to the short-range forces renders the crystal unstable for this mode. The dielectric constant being connected to the frequency of the critical mode then becomes extremely large as happens at the Curie point.

Actually the connection between the ferroelectric properties of crystals and the dynamical properties may be seen simply and perhaps most naturally through the Lyddane-Sachs-Teller relation which connects the frequencies of the longitudinal optical and transverse optical modes of infinite wavelength in terms of the ratio of the static to high frequency dielectric constant. This was already appreciated by Fröhlich as early as 1949.

2. PHENOMENOLOGICAL BEHAVIOUR (MACROSCOPIC)

2.1 THE DIELECTRIC CONSTANT

2.1.1 Introduction

In solids, for static and low frequency fields, the displacement D is linearly related to the electric field E thus:

$$D = KE$$

The factor K is called the permittivity. It is more convenient to express the permittivity in terms of the permittivity of a vacuum K_o, and for this purpose a dimensionless constant is defined,

$$\epsilon = K/K_o$$

known as the dielectric constant or relative permittivity.

Due to hysteresis effects in the ferroelectric phase the dielectric behaviour is non-linear.

2.1.2 General Behaviour

The dielectric constant of $BaTiO_3$ increases with decreasing temperature in the non-polar phase, passes through a sharp maximum at the Curie point, and then decreases discontinuously with the onset of spontaneous polarisation. Above the Curie point (120°C for $BaTiO_3$) the dielectric constant is found to obey a Curie-Weiss law,

$$\epsilon = \epsilon_o + \frac{C}{T - T_o} \qquad (1)$$

Here ϵ represents the dielectric constant, ϵ_o the electronic contribution to the dielectric constant, C the Curie constant, T the absolute temperature, and T_o the characteristic temperature (also called the extrapolated Curie temperature). T_o lies in the neighbourhood of the transition temperature but about 10 to 20 degrees below it. Also ϵ_o is of the order of unity and may be left out of the above equation since ϵ is several thousands. The dielectric constant is linearly related to the slope of the P vs E curve. Above the Curie temperature in the non-polar phase the relation between polarisation P and field E is linear and therefore the dielectric constant is field independent. As there is cubic symmetry in this phase the value of the dielectric constant is independent of the direction along which a measuring field is applied.

As the crystal is cooled below the Curie point however its structure is altered from cubic to tetragonal - $a = b < c$, $\alpha = \beta = \gamma = 90^{\circ}$, and the existence of a hysteresis loop clearly implies that the value of the dielectric constant depends on the field strength at which it is measured. For tetragonal symmetry of the crystal below the Curie temperature, the tetragonal 'c' axis contains the direction of spontaneous polarisation with 'c' only slightly longer than 'a'. Consequently two dielectric constants are

now necessary in order to describe the dielectric behaviour of the crystal. One, ϵ_c is measured upon applying the a.c. field along the 'c' axis. The other ϵ_a is measured upon applying the a.c. field perpendicular to the 'c' axis. However, a crystal plate which is cooled below the Curie point normally shows a rather complicated domain structure, and hence measurement of dielectric constant in a direction perpendicular to the major surfaces would furnish an average dielectric constant whose value would depend on the relative number of 'c' domains and 'a' domains. ϵ_c is the dielectric constant one measures with the 'c' axis perpendicular to the major surfaces and ϵ_a has the 'c' axis parallel to the major surfaces of a single domain plate. An important result of these measurements in the region of the Curie point is that $\epsilon_a >> \epsilon_c$ (Merz, 1949). The physical meaning of this smaller ϵ_c is that the dipoles are easier to move in the direction perpendicular to polarisation under an electric field. The dielectric constant of ceramic $BaTiO_3$ is approximately $\epsilon = \frac{1}{3}(\epsilon_c + 2\epsilon_a)$. A hysteresis loop is shown in Fig. 2.1. The dielectric susceptibility χ is normally defined as P/E and the dielectric constant as $1 + 4\pi\chi$ in c.g.s. units. In the cubic phase P is linearly related to E and this definition suffices. However in the tetragonal phase, the dielectric constant is not really a constant but depends on

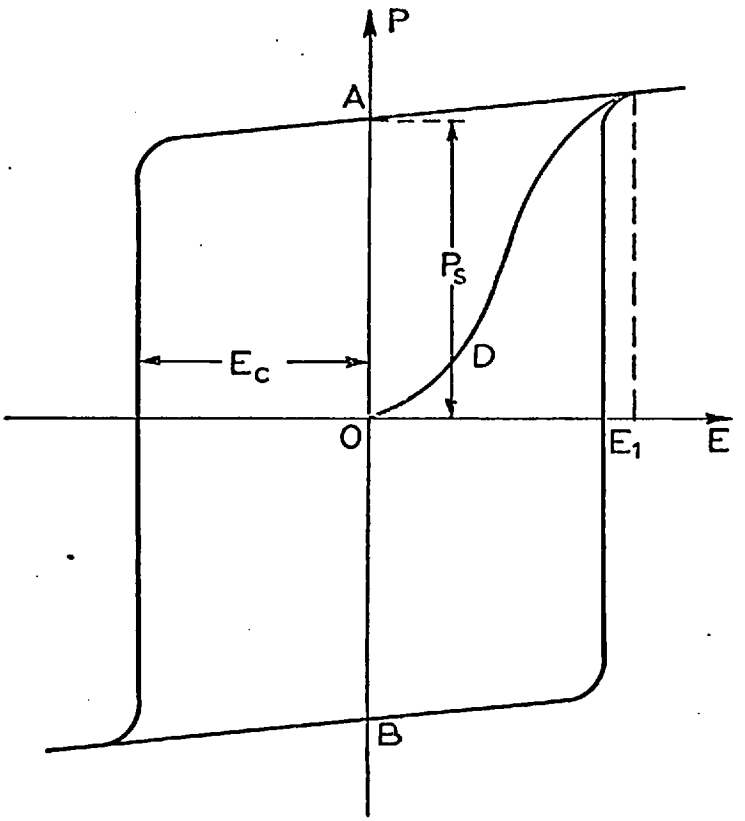

P
A
P_S
D
E_c
O
E_1
E
B

Fig. 2.1

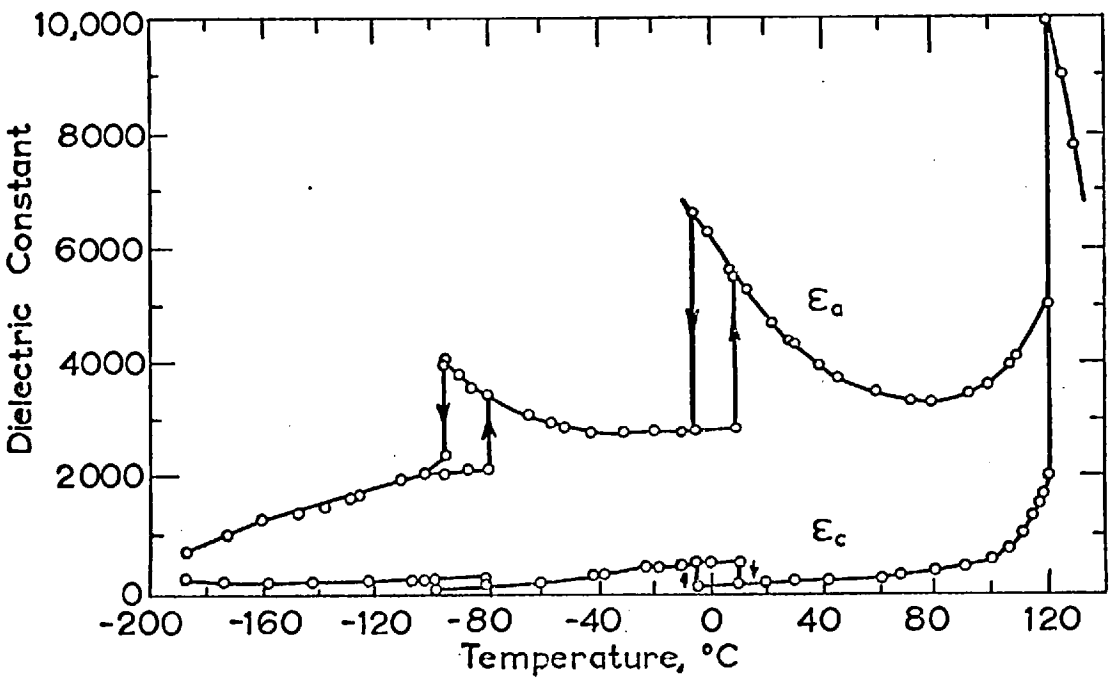

10,000
8000
6000
4000
2000
0
Dielectric Constant
ε_a
ε_c
-200
-160
-120
-80
-40
0
40
80
120
Temperature, °C

Fig. 2.2

the field strength at which it is measured; this is a consequence of the non linear relationship between P and E. We may distinguish between, (Megaw, 1957):

1) the overall susceptibility P_B/E_B, the ratio of the values of P and E at the tip of the loop,
2) the small signal susceptibility at any point of the slope dP/dE,
3) the initial or "small signal" susceptibility, the slope dP/dE at zero external field,
4) the saturation susceptibility, the slope at B.

Now if the applied field is small, no new domains are created and no movement of the domain boundaries takes place. In this case one measures the dielectric constant of the crystal with no interference from the domain structure. This quantity, which is called the initial dielectric constant, is directly proportional to the slope of the virgin curve OD at the zero point. The value of this measuring field is usually of the order of about 1 V cm^{-1}. It follows from the above definitions that the value of the dielectric constant is strongly dependent on the shape of the hysteresis loop, which in turn is dependent on the texture of the crystal.

Consequently it is not surprising that there should be disagreement among different authors about the absolute values they report for the dielectric constant since many of

them have not stated their definition of the constant, nor specified the conditions under which it was measured - for example, whether the crystal was "clamped" or "free". More recent authors generally measure the initial dielectric constant of the free crystal.

2.1.3 Frequency Effects

The existence of permanent dipoles in $BaTiO_3$ in the ferroelectric phase below the Curie point influences the dielectric behaviour, due to the reaction of these dipoles to the frequency of the measuring field.

At static and low frequency fields the dipoles are able to react in step with the applied field. At high frequencies however there is a phase difference between applied field and reaction, and hence between E and P. Using complex notation this situation may be described thus:

$$E = E_o \; e^{j\omega t} \qquad (2)$$

$$D = D_o \; e^{j(\omega t - \delta)} \qquad (3)$$

where δ represents the phase angle by which the dielectric flux density lags the applied field. It may readily be shown that

$$\tan\delta = \epsilon^{11}/\epsilon^{1}, \qquad (4)$$

where the quantity $\tan\delta$ is known as the "dissipation factor" - i.e. energy is dissipated in the material. This is referred to as "dielectric loss".

The introduction of a complex dielectric constant $\epsilon^x = \epsilon^1 - j\epsilon^{11}$ describes this situation where ϵ^1 is the real part or in phase component of the dielectric constant and ϵ^{11} the imaginary part or out of phase component. It may be shown further (Böttcher, 1952) that the dissipated energy per unit volume of the dielectric per second is given by:

$$W = \frac{\omega E_o^2}{8\pi} \epsilon^{11} = \frac{\omega E_o^2}{8\pi} |\epsilon| \sin\delta \qquad (5)$$

This energy is directly proportional to ϵ^{11} and thus to $\sin\delta$. The energy losses are thus proportional to $\sin\delta$, which for this reason is called the "loss factor". However, $\tan\delta$ is frequently referred to as the loss factor, but this is only correct for small values of δ, since then $\sin\delta = \tan\delta$.

The dielectric loss at high frequencies is due to the relaxation effect of the permanent dipoles. This effect may be described by an equation of the form,

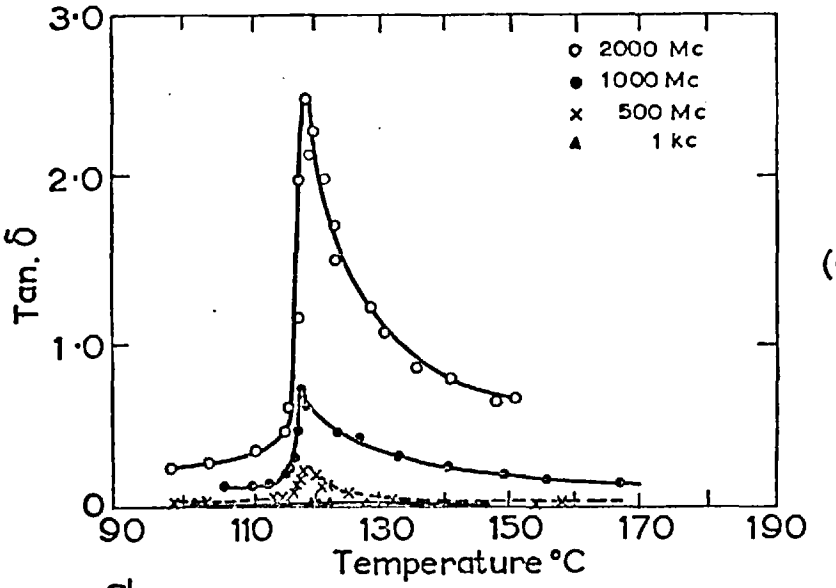
$$P_{dip} = P_{o_{dip}} (1 - e^{t/\tau}) \qquad (6)$$

where P_{dip} is the polarisation due to permanent dipoles at time, t, $P_{o_{dip}}$ the amplitude of the permanent dipoles, and τ a constant, which is a measure of the time lag, called the relaxation time.

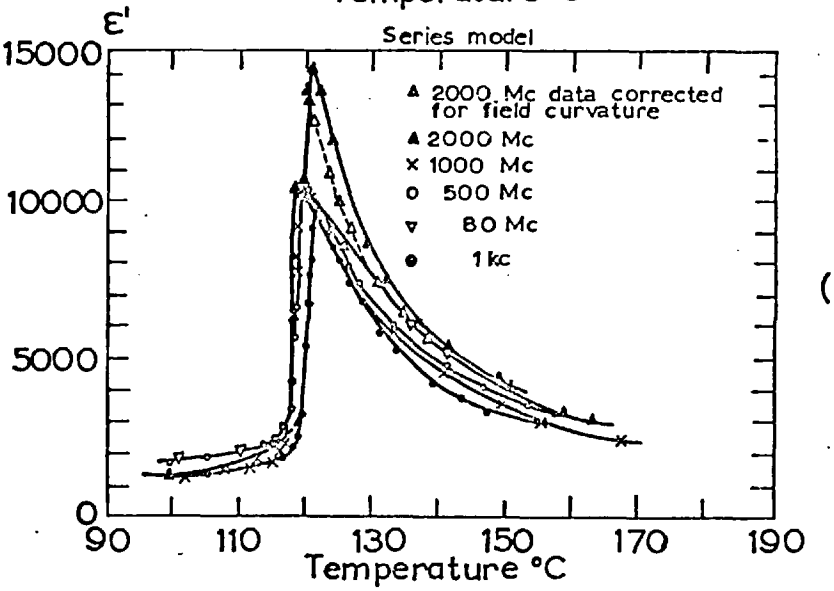
Fig. 2.2 shows the temperature dependence of the small

signal dielectric constant (Merz, 1949) and is typical of several determinations by various workers. Only that part of the curve above about 0°C has a clear physical meaning for reasons already mentioned. Below this temperature the domain configuration is not clearly defined and should have a strong influence on the measured value of ϵ. Hysteresis effects at the Curie point for increasing and decreasing temperatures have also been reported amounting to about 2°C (Drougard and Young, 1954; Känzig and Maikoff, 1949). These hysteresis effects are also observed on poly-crystalline samples (Pickara and Pajak, 1952).

Several measurements have been made on the high-frequency dielectric properties but the only reliable measurements which are easy to interpret are those made on single crystals above the Curie point or on poled single crystals below the Curie point. Measurements in the paraelectric region of 10° above the Curie point of the real part of the dielectric constant and of the loss tangent $\tan\delta$ over a frequency range from 1 kc/s to 2000 Mc/s are shown in Figs. 2.3 (a) and (b) respectively (Stern and Lurio, 1961). Measurements have also been performed at 24,000 Mc/s in the paraelectric region and in the 'a' direction of carefully poled single crystals in the ferroelectric region (Benedict and Durrand, 1958). These results are shown in Fig. 2.4 where the broken line



(a)



(b)

Fig. 2.3

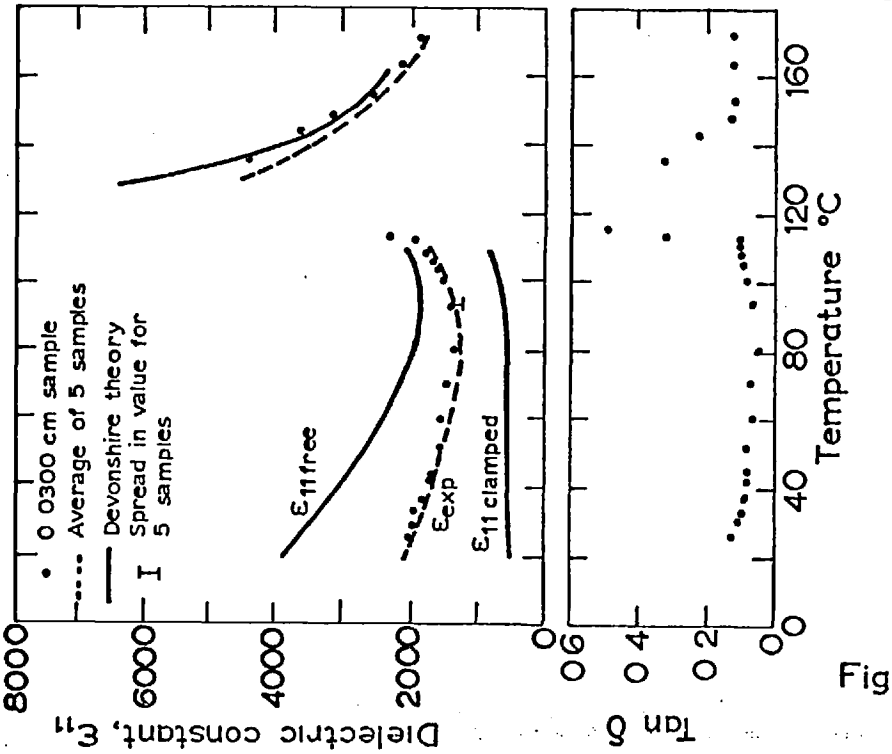


Fig. 2.4.

gives the best fit for the experimental points and the solid line above the Curie point and the upper solid line below the Curie point represent values found experimentally at very low frequencies and also those given by the thermodynamic theory (see Chapter 5). The lower solid line shows the value of the dielectric constant for the clamped crystal as calculated from the thermodynamic theory. Above the Curie point the values for the clamped and the free crystal practically coincide (since the crystal is not piezoelectric, as expected for cubic symmetry). Below the Curie point however one would expect to find points lying on the lower solid line since at the high-frequencies used in the experiment the mechanical oscillations of the crystal certainly cannot follow the alternating field. However, from Fig. 2.4 it appears that the experimental values lie somewhere in between those for the free and clamped crystal, a fact which has not yet been satisfactorily explained. We may, however, conclude from measurements in the paraelectric region that the dielectric dispersion in $BaTiO_3$ occurs above 24 Gc/s.

Several workers have performed dielectric constant and loss tangent measurements through the Curie point on ceramic specimens in the X band (Lipaova and Sharani, 1960; Powles and Jackson, 1949; Schmitt, 1957). A common factor which has emerged from these measurements is the sudden decrease in

$\tan\delta$ above the Curie point and we may assume that the reason for the lower loss occurring above the Curie point is that in polarising the specimen in the paraelectric region one does not have to overcome a pre-existing pattern.

Several workers have also measured the above two quantities through the Curie point as a function of frequency. The most complete spectrum being that of Westphal (1954). His results show a relaxation spectrum commencing at about 10^8 c/s. However, these results may be discarded as calculations have shown that the dispersion at high frequencies is due to domain wall oscillations which is due to the inertia of the ions changing position slightly as their dipole moments change direction on motion of the wall.

2.2 ELECTROMECHANICAL BEHAVIOUR

2.2.1 Introduction

If a stress is applied to certain crystals they develop an electric moment whose magnitude is proportional to the applied stress. This is known as the direct piezoelectric effect. In general a state of stress is described by a second-rank tensor with nine components, while the polarisation of the crystal, being a vector is specified by three components. It is found that when a general stress σ_{ij} acts on a piezoelectric crystal each component of the polarisation P_i is linearly related to all the components of σ_{ij}. Thus in

general the relationship between P_i and σ_{ij} is:

$$P_i = d_{ijk}\,\sigma_{ij} \qquad (1)$$

The d_{ijk} are the "piezoelectric moduli" consisting of 27 coefficients. For the particular case of $BaTiO_3$ which is spontaneously polarised below the Curie point, P_i must be interpreted as the change in the polarisation caused by the stress. As is implied by equation (1) a change from a tensile stress to an equal compressive stress reverses the direction of the polarisation.

When an electric field is applied to a piezoelectric crystal, its shape changes slightly. This is known as the "converse piezoelectric effect", its existence being a thermodynamic consequence of the direct effect. It is found that there is a linear relation between the components of the vector E_i, giving the electric field intensity within the crystal, and the components of the strain tensor Ω_{ij} which describe the change of shape. It may be shown by thermodynamic reasoning that the coefficients connecting the field and the strain in the converse effect are the same as those connecting the stress and the polarisation in the direct effect. The converse effect is written

$$\Omega_{jk} = d_{ijk}\,E_i \qquad (2)$$

when the direct effect is described by equation (1) above.

By considering the nature of the stresses introduced

into the crystal, it may be shown that the number of independent moduli above is reduced to six. Further, by adopting the matrix notation, (1) and (2) above may be rewritten

$$P_i = d_{ij}\ \sigma_j \quad (i=1,2,3,\ j=1,\ldots 6) \qquad (3)$$

$$\text{and}\quad \Omega_j = d_{ij}\ E_i \quad (i=1,2,3,\ j=1,\ldots 6) \qquad (4)$$

the d_{ij} forming the matrix of coefficients. By appealing to pure symmetry arguments, and also, using the fact that a crystal with a centre of symmetry cannot be piezoelectric, further reduction in the number of independent moduli is obtained.

The elastic behaviour we shall consider falls within the framework of Hookes law which relates the amount of strain to the magnitude of the applied stress thus, for the simple case:

$$\Omega = s\sigma \qquad (5)$$

where s is a constant called the "compliance". Alternatively we may write $\sigma = C\Omega$, where $C = 1/S$ and is called the "stiffness"; it is also Youngs Modulus. By similar reasoning to that adopted above for the piezoelectric moduli, we may rewrite these two equations for general stresses and strains in the form

$$\Omega_i = S_{ij}\ \sigma_j \quad (i,j = 1.....6) \qquad (6)$$

$$\sigma_i = C_{ij}\ \Omega_j \quad (i,j = 1.....6) \qquad (7)$$

Below the Curie point, ferroelectric $BaTiO_3$ is non-symmetrical and exhibits piezoelectricity, the strain being linearly related to the applied field. Above the Curie point however it is centro-symmetrical and application of a field will move the atoms into non-symmetrical positions resulting in distortion. Reversal of the field, because of the symmetry, produces the same sign of striction, and the strain is thus proportional to quadratic powers of the applied field. This is known as the "electrostrictive effect" and is responsible for piezoelectric activity above the Curie point. We may define the electrostrictive constant ϕ, thus

$$\varepsilon = \phi P^2, \text{ where P is the polarisation.}$$

2.2.2 Piezoelectric Behaviour

Ferroelectric $BaTiO_3$ is piezoelectric and when subjected to an rf electric field resonates at particular frequencies dependent on its geometry and the method of excitation. The resonant condition is indicated by a large decrease of crystal impedance to a minimum value. At a slightly higher frequency an impedance maximum occurs; this is the antiresonant frequency ν_a. For a longitudinally vibrating piezoelectric crystal its resonance frequency is

$$\nu_r = \frac{1}{2l}\sqrt{\rho S^E} \qquad (8)$$

where l = length of crystal, ρ its density, and S^E the

elastic compliance at constant field (Mason, 1951). The difference between the "free" and "clamped" behaviour is determined by the "electromechanical coupling factor" which is defined as the square root of the ratio of mechanical energy stored, for a given type of displacement, to the total input electrical energy stored. This factor is given by Mason (1951),

$$k = d/\sqrt{\frac{\epsilon^T S^E}{4\pi}} \qquad (9)$$

where d is the piezoelectric constant, ϵ^T is the stress free dielectric constant, and S^E is the field free elastic compliance. He has also shown that the resonant and anti-resonant frequencies are related thus

$$k^2 = \frac{\pi^2}{4} \frac{\Delta\nu}{\nu_r} \qquad (10)$$

where $\Delta\nu = \nu_A - \nu_R$

The matrix d_{ij} for $BaTiO_3$ in the ferroelectric phase belongs to class 4mm and is given by

$$\begin{pmatrix} 0 & 0 & 0 & 0 & d_{15} & 0 \\ 0 & 0 & 0 & d_{15} & 0 & 0 \\ d_{31} & d_{31} & d_{33} & 0 & 0 & 0 \end{pmatrix}$$

- the coefficients d_{31} and d_{33} being of particular interest here because they relate to the polarisation along the ferroelectric axis. For a 'c' plate crystal the coefficient d_{31} is equal to the ratio of the strain induced in the (100)

direction to the field applied in the (001) direction (c axis) which produced this strain. d_{33} relates the strain and field in the direction of polarisation, hence:

$$\left.\begin{aligned} \Omega_x = \Omega_y &= d_{31} E_Z \\ \Omega_z &= d_{33} E_Z \end{aligned}\right\} \qquad (11)$$

where E_Z is the externally applied field in the (001) direction, its sign being considered with respect to the direction of the polarisation. Since E_Z is applied parallel to the direction of spontaneous polarisation the crystal expands in this direction and contracts at right angles to it. Hence d_{33} is positive and d^{31} negative, and Ω_x, Ω_y above correspond to contractions, and Ω_z to an expansion. For the piezoelectric modulus d_{31} equation (9) becomes

$$d_{31} = k\left[\frac{\overset{T}{33}}{4} S^E_{11}\right]^{\frac{1}{2}}.$$

It has been shown (Merz, 1949) that since the crystal is piezoelectric in the polarised state, the total strains Ω_x ($=\Omega_y$) and Ω_z are proportional to the square of the total polarisation (spontaneous plus induced):

$$\left.\begin{aligned} \Omega_x &= \mu P_z^2 \\ \Omega_z &= \rho P_z^2 \end{aligned}\right\} \qquad (12)$$

at zero applied stress, where μ and ρ are constants where it has been shown that

$$\mu = 2\, d_{31}/P_z \overset{T}{\Omega}_{33} \qquad (13)$$

and that the following relations are readily derivable from equation (12)

$$d_{31} = 2\chi_c \mu P_s$$

$$d_{33} = 2\chi_c \rho P_s \qquad (14)$$

where χ_c is the susceptibility measured along the c axis, and P_s is the spontaneous polarisation.

As the magnitude of spontaneous polarisation is dependent upon both temperature and applied field the piezoelectric coefficients also depend upon these parameters. The existence of domains complicates the measurement of the piezoelectric coefficient since the domain structure changes with the applied field and thus causes additional changes in the strain components. Hence the only reliable measurements are on single domain crystals.

Measurements of the temperature variation on single crystal plates of the d_{31} coefficient by a static method using the converse piezoelectric effect is shown in Fig. 2.5 (Merz and Caspari, 1950; Rzhanov, 1960). These experimental results have been verified theoretically using equation (14) and a value of μ substituted from equation (12).

The variation of ν_r the piezoelectric resonance frequency, and $\Delta\nu$ $(= \nu_A - \nu_R)$ is shown to undergo an anomaly (Blattner, Känzig, and Merz, 1949) for crystals with a minimum of internal strains, and free of domains perpendicular to the major surfaces.

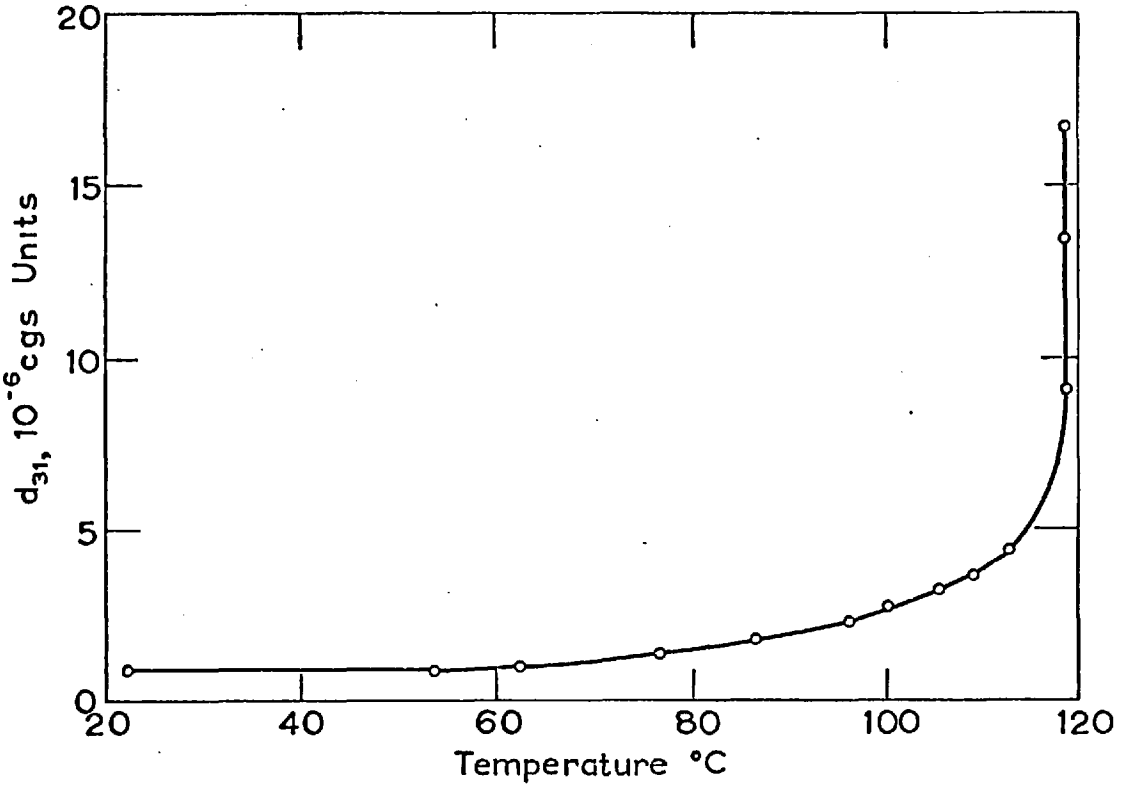

20
15
10
5
0
d_{31}, 10^{-6} cgs Units
20
40
60
80
100
120
Temperature °C

Fig. 2.5.

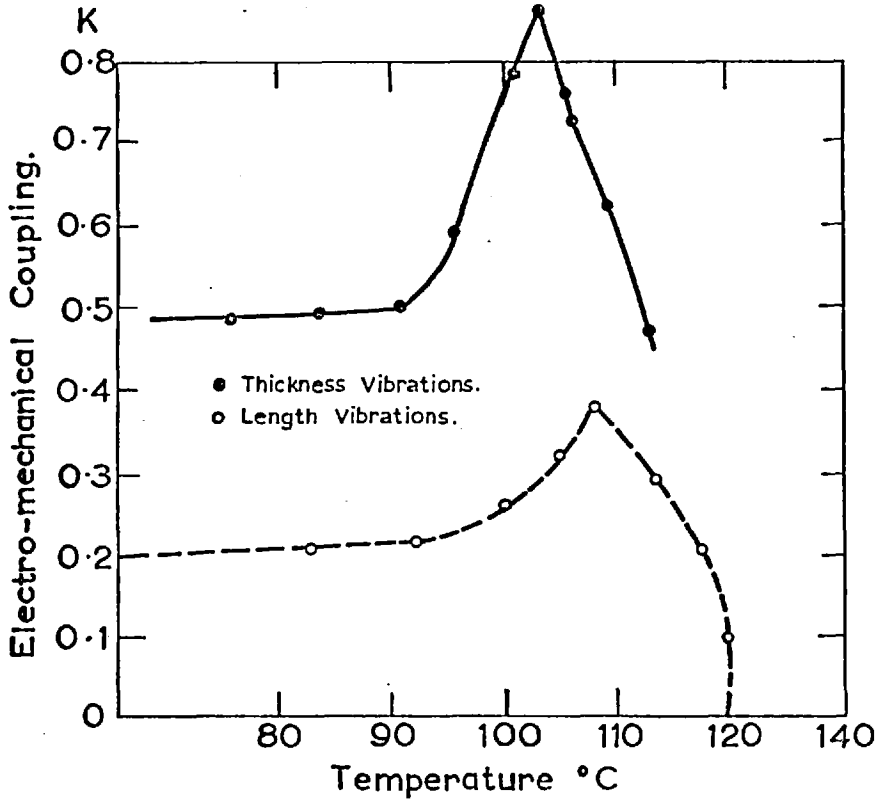

K
0·8
0·7
0·6
0·5
0·4
0·3
0·2
0·1
0
Electro-mechanical Coupling.
● Thickness Vibrations.
○ Length Vibrations.
80
90
100
110
120
140
Temperature °C

Fig. 2.6.

On calculating the d_{31} coefficient from these results the peak value occurring at the Curie point is found to be much higher than that measured experimentally (Huibregtse, Bessey and Drougard, 1959), and it is not clear why this should be so. The increase of d_{31} on approaching the Curie point clearly indicates the increase of the dielectric susceptibility χ_c since the polarisation P_s does not vary significantly before dropping to zero.

The electromechanical coupling coefficient K, which has been measured for thickness vibrations, is shown in Fig. 2.6 (Drougard and Young, 1955). The calculated curve (dotted) was taken from the results of Caspari and Merz using Fig. 2.5 and equation (10), and though the aspect is the same, a greater coupling efficiency is obtained with thickness clamped crystal. However, on looking at the profile of these curves one may reasonably attribute the increase in the coupling coefficient K on either side of the Curie point as being due to a "softening" of the crystal at these temperatures (see next section).

2.2.3 Electrostrictive Behaviour.

Owing to the fact that $BaTiO_3$ is not piezoelectric in the non-polar phase the discussion of the electrostrictive effect is particularly simple. As mentioned previously electrostriction is a quadratic effect and occurs in all crystals, i.e., when an electric field is applied to a

crystal strains are produced proportionally to the field. Using the Voigt notation with two suffixes instead of four (see e.g., Forsbergh, 1956), the matrix of the electrostrictive constants for cubic crystals is:

$$\begin{pmatrix} Q_{11} & Q_{12} & Q_{12} & 0 & 0 & 0 \\ Q_{12} & Q_{11} & Q_{12} & 0 & 0 & 0 \\ Q_{12} & Q_{12} & Q_{11} & 0 & 0 & 0 \\ 0 & 0 & 0 & Q_{44} & 0 & 0 \\ 0 & 0 & 0 & 0 & Q_{44} & 0 \\ 0 & 0 & 0 & 0 & 0 & Q_{44} \end{pmatrix}$$

The electrostrictive constants are related to the piezoelectric moduli d_{ik} thus:

$$d_{ik} = Q_{ik} P_s \frac{\Omega c}{2\pi} \qquad (15)$$

Q_{33} is found to be invariant with temperature in the paraelectric region (Allsop and Gibbs, 1959). They have also found this to hold for ceramics in the paraelectric phase, but with a dip occurring in the coefficient on traversing the Curie point thereafter decreasing smoothly (also Schmitt, 1956). The thermal behaviour of Q_{12} is shown in Fig. 2.7 (Huibregtse, Bessey, and Drougard, 1959). As Q_{ik} is practically temperature independent equation (15) shows that the moduli d_{31} and d_{33} behave anomalously as a function of temperature as does also Ω_c and drop to zero above the Curie temperature.

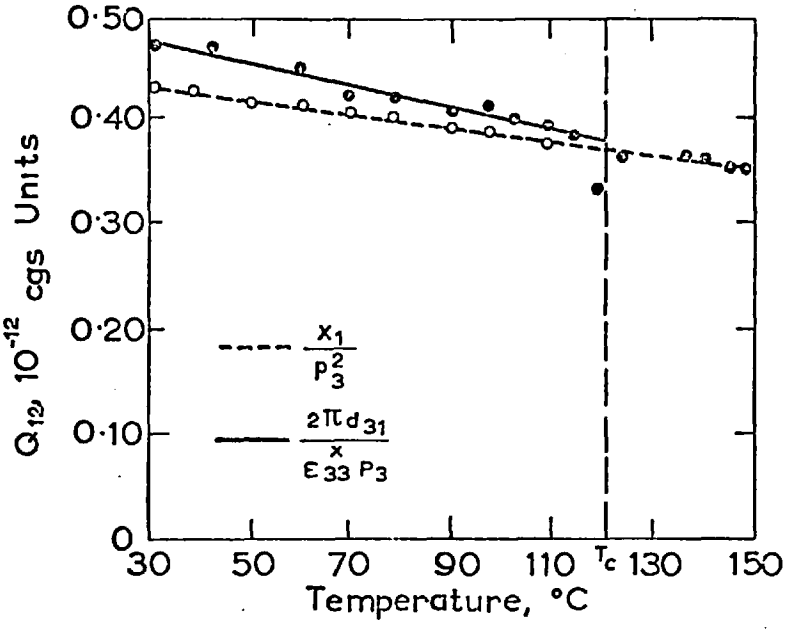


Fig. 2.7.

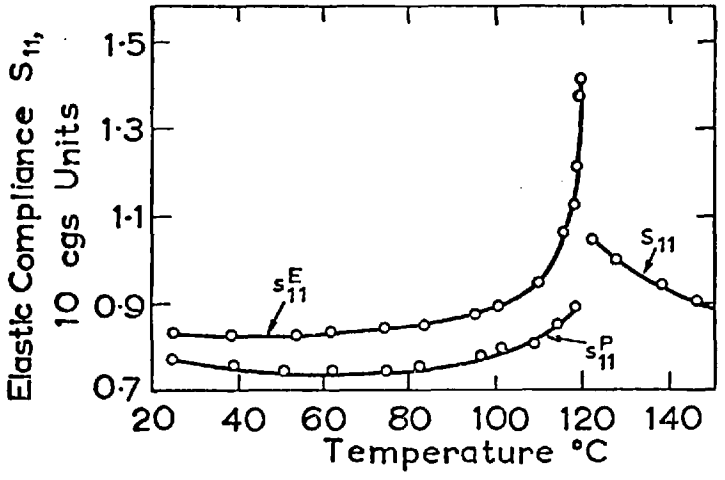


Fig. 2.8.

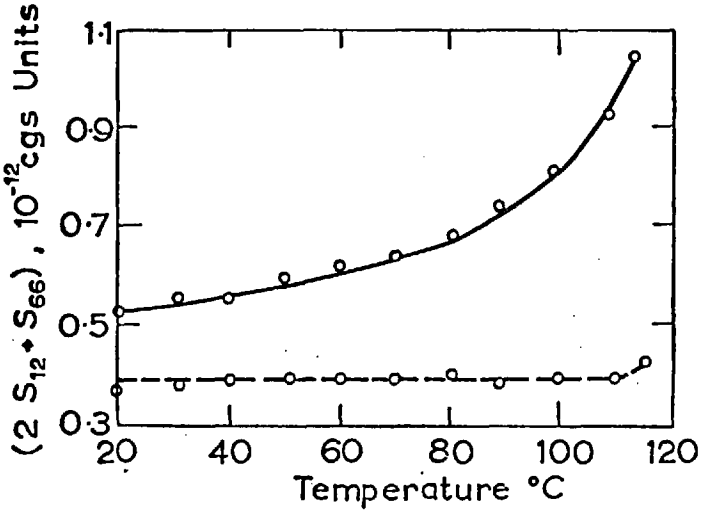


Fig. 2.9.

2.2.4 Elastic Behaviour.

The temperature variation of the compliance coefficients S_{11}^{E} and S_{11}^{P} are shown in Fig. 2.8 (Huibregtse, Drougard and Young, 1955). Using the piezoelectric resonance technique S_{11}^{E} and S_{11}^{P} are indistinguishable above the Curie point, and since in the tetragonal phase S_{11}^{E} reflects the behaviour of the dielectric constant as expected, S_{11}^{P} contrary to expectations shows a small anomaly in the vicinity of the Curie temperature. This is probably due to domain effects in this region. This shows quite clearly the elastic softening occurring near the transition point and it would appear that in the cubic phase the crystal is harder. The quantity $(2S_{12}^{P} + S_{66}^{P})$ on the other hand responds to expectations in that it is practically temperature independent, while the same quantity at constant electric field $(2S_{12}^{E} + S_{66}^{E})$ exhibits a marked anomally at the Curie point, Fig. 2.9 (Huibregtse, Bessey and Drougard, 1959).

2.3 SPONTANEOUS POLARISATION AND SPONTANEOUS STRAIN

2.3.1 Introduction

Since the spontaneous polarisation of a ferroelectric can be reversed it may be measured directly, in contrast to the polarisation of ordinary pyroelectrics. Direct observation of a hysteresis loop on an oscilloscope screen is due to the conventional circuit originally devised by

Sawyer and Tower (1930). In this circuit the X-plate voltage is proportional to the generator voltage which is proportional to the potential difference across C_1, since $C_2 >> C_1$. The Y-plate voltage is proportional to the charge on C_2 which equals the charge on C_1 and is proportional to the polarisation of the specimen, Fig. 2.10.

The information derivable from such hysteresis loops may be seen from Fig. 2.1. Beyond E_1 the relation between P and E is linear and is due to the induced polarisation only. It is generally assumed that the spontaneous polarisation P_s may be deduced by extrapolating the above linear portion to E = 0. However considerable errors may arise from the fact that there are domains which cannot be reversed easily. The total polarisation P_t existing for a field $> E_1$ consists of two parts, P_s the spontaneous polarisation, and P_i the induced polarisation. Hence P_i may be determined directly. E_c is the value of the "coercive field", i.e. the field necessary to reverse the direction of the polarisation, and P_r the remanent polarisation for zero applied field.

It is found that the exact shape of the loop obtained experimentally depends on a number of factors: the dimensions of the sample, the temperature, the texture of the crystal and its previous thermal and electrical history. For good single

crystals the loop is approximately a parallelogram, and the changes in polarisation at the coercive field happen in a single discontinuous jump. However, real crystals are never perfect, but subject to local stresses, and because of the piezoelectric effect, imply local electric fields. According to the direction of these, the external field required for reversal is greater or less than the coercive field. Hence even for the best single crystals the loop is always somewhat rounded at the corners.

As the temperature approaches the Curie point the sides of the loop close in, and the coercive force gets smaller, finally approaching zero, as the loop becomes a straight line.

2.3.2 Spontaneous polarisation

The effects of imperfections on crystals, as mentioned above, were reflected in the early measurements of the spontaneous polarisation by a hysteresis loop. Early measurements gave for P_s at room temperature a value of about 16 $\mu C\ cm^{-2}$ together with a continuous increase with falling temperature through the Curie point, which is attributed to domain effects (Hulm, 1947; Merz, 1949). However, later measurements on good single crystals clearly show a discontinuous increase in the spontaneous polarisation at the Curie point followed thereafter by a continuous increase to a value of about 26 $\mu C\ cm^{-2}$ at room temperature (Känzig and

Meier, 1949; Merz, 1953; Cross, 1953), Fig. 2.11. Temperature hysteresis at the discontinuity of $4^{o}C$ have also been detected (Kay and Vousden, 1949).

The temperature variation through the Curie point of the coercive field E_c for single crystals does not appear to have been investigated systematically at the Curie point, but only at the two lower transitions where it undergoes discontinuities and exhibits hysteresis (Weider, 1955). The value of the coercive field measured at room temperature varies from a minimum of 500V/cm to a maximum of about 2,000V/cm (Weider, 1955; Merz, 1953; Landauer et al., 1956).

A convenient method of describing the state of polarisation of $BaTiO_3$ has been carried out on single 'c' plate crystals making use of the "pyroelectric" effect, which is the change in the polarisation of a crystal when it undergoes a variation in its temperature (Chynoweth, 1956). The basis of the technique is as follows: if P_s is the spontaneous polarisation of the crystal at a temperature T, then a small change dT produces a change dP_s in P_s, and if this happens in a time dt then the rate of change of polarisation (dP_s/dt) is equivalent to a current i flowing in the external circuit.

Thus the current per unit area of the crystal is:

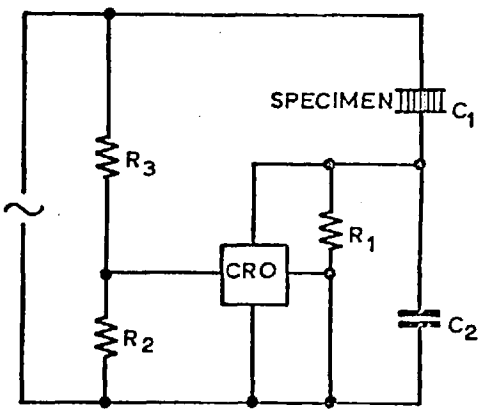


Fig. 2.10.

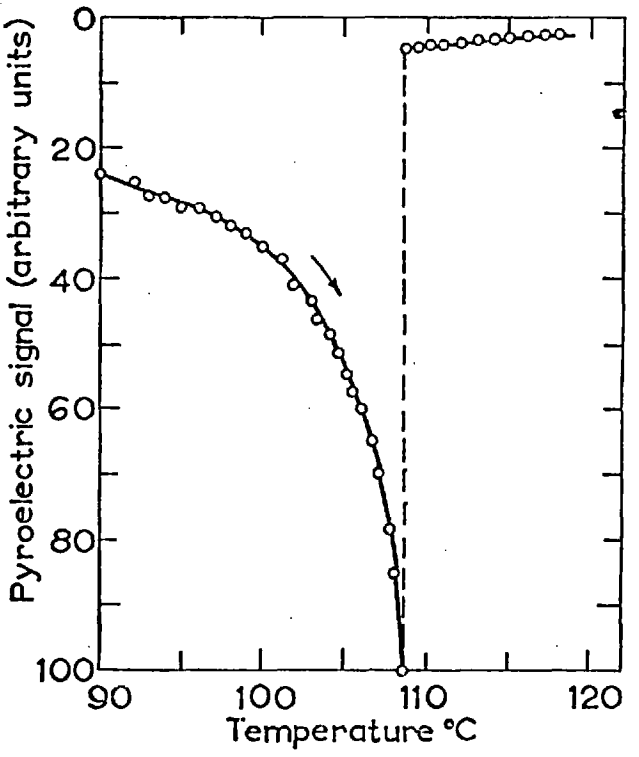
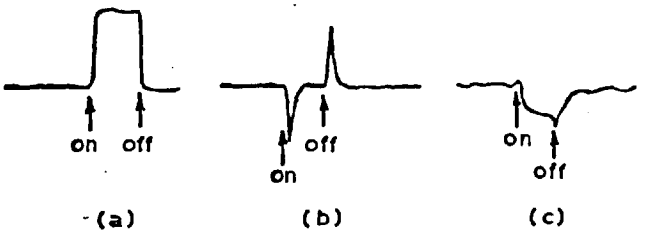


Fig. 2.12.



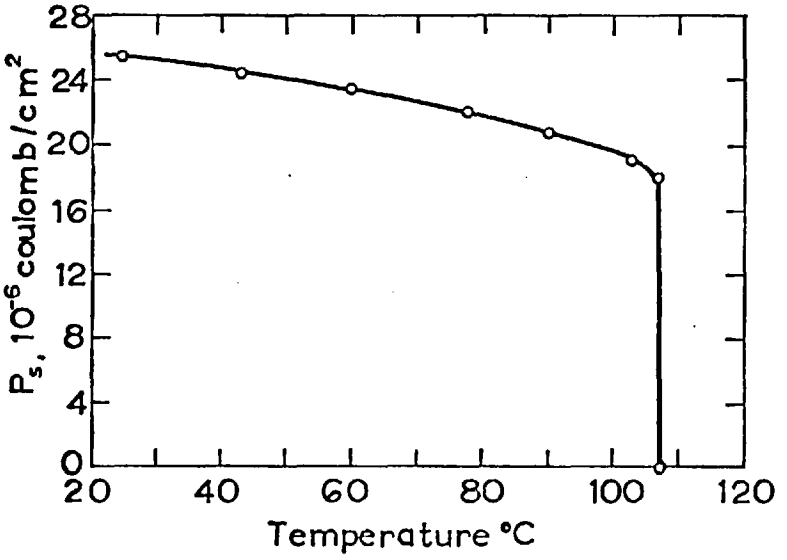


Fig. 2.11.

$$i = \left(\frac{dP_s}{dt}\right) = \left[\left(\frac{dP_s}{dT}\right)\left(\frac{dT}{dt}\right)\right]T = T \qquad (1)$$

For small ΔT, (dP_s/dT) can be regarded as constant for that temperature and the current then depends only on the rate of change of temperature. The heating was performed by intermittent illumination with infra-red flashes, and the nature of the pyroelectric current during a light-dark cycle obtained was such as to exclude the possibility of disturbance by bolometric, thermoelectric and photoconductive processes. To determine the pyroelectric coefficient in absolute units from i it is necessary to know the initial rate of change of temperature $\left(\frac{dT}{dt}\right)$ which is difficult to measure accurately. The value so calculated can be compared with that from measurements on hysteresis loops; results are in good agreement showing that the pyroelectric technique can be used to determine accurately the spontaneous polarisation. In Fig. 2.12 the pyroelectric current is plotted against temperature for a $BaTiO_3$ crystal which was previously saturated with a negative field (Chynoweth, 1956). The sudden discontinuity observed reflects the discontinuity in $\left(\frac{dP_s}{dT}\right)$. Above the Curie point the pyroelectric signal should be zero, because $P_s = 0$, but a signal can be observed even above this temperature. This can be explained by assuming the presence of a surface layer which remains permanently polarised even above the Curie point when the bulk polarisation vanishes. By observing the wave

forms of the pyroelectric current signals, he concluded tentatively that space large layers of up to 10^{-5} cms reside at the surface of the crystal. The reason for the presence of this layer is not understood.

The above decrease in the pyroelectric current occurring at the Curie point confirms that the transition is of the first order.

The advantage of the method lies in its ability to study the polarisation under conditions where hysteresis loops cannot be obtained, or where it is desirable not to interfere with the state of polarisation. Thus the method provides a non-destructive means for "reading out" the state of polarisation.

Strictly, the pyroelectric current measured above is due to the "secondary pyroelectric effect" which is the additional pyroelectricity produced because the crystal is free to deform, the thermal expansion causing a strain, which by the piezo-electric effect produces an electrical displacement (Nye, 1957).

2.3.3 Spontaneous Strain

On cooling through the Curie point, the spontaneous strain corresponds to an expansion along the polar axis and to a contraction at right angles to it. These changes in axial lengths have been established as discontinuous, which the early work of Megaw (1947) had failed to distinguish. The results of measurements on good single crystals by optical

means are shown in Fig. 2.13 (Kay and Vousden, 1949), the change in the dimensions of the 'c' axis (+ve) being about twice that for the 'a' axis (-ve). Also a slight but discontinuous change in the volume has been found (Shirane and Takeda, 1952). It has been shown further that comparing values of the spontaneous polarisation P_s with the calculated values of $\Delta c/c$ and $\Delta a/a$ from Megaw's measurements the spontaneous strain is proportional to the square of the spontaneous polarisation, in the region of the Curie point at any rate, there being an ever increasing departure from this with decreasing temperatures below about $90^{\circ}C$.

An anomaly of the tetragonal strain in a thin surface layer of about 100 A° thick has been detected by means of electron diffraction (Anliker, Brugger and Känzig, 1954). This anomalous strain was found to be slightly larger than the strain in the bulk, and does not vanish when the crystal is heated above the Curie temperature; presumably remaining constant. It has been suggested that since $BaTiO_3$ exhibits semi-conducting properties then this observed surface strain could be due to a thin electronic or ionic space charge layer near the surface which becomes trapped in surface states (Känzig, 1955).

2.4 THERMAL BEHAVIOUR

2.4.1 Introduction

Since energy must be supplied over a range of temperatures to a ferroelectric crystal in order to destroy its spontaneous polarisation, this would thus involve a change in the internal energy of the crystal giving rise to an anomaly in the specific heat at the Curie temperature. The transition heat is the total area contained between the normal and anomalous part of the specific heat-temperature curve, while the transition entropy is defined as the total heat anomaly divided by the temperature at which the above peak in the specific heat occurs.

Most measurements appear to have been made on powders, polycrystalline material, or multi-domain crystals, and are therefore inherently inaccurate because of domain wall contributions, surface effects, and depolarising fields.

A first order change occurs abruptly at the Curie point and is accompanied by a latent heat whilst a second order change is characterised by a smooth variation over a range of several degrees. Consequently it is very difficult to decide purely on the basis of specific heat measurements which of these two types of transitions takes place, as even a first order transition is always spread over a temperature range of several degrees for the reasons mentioned above.

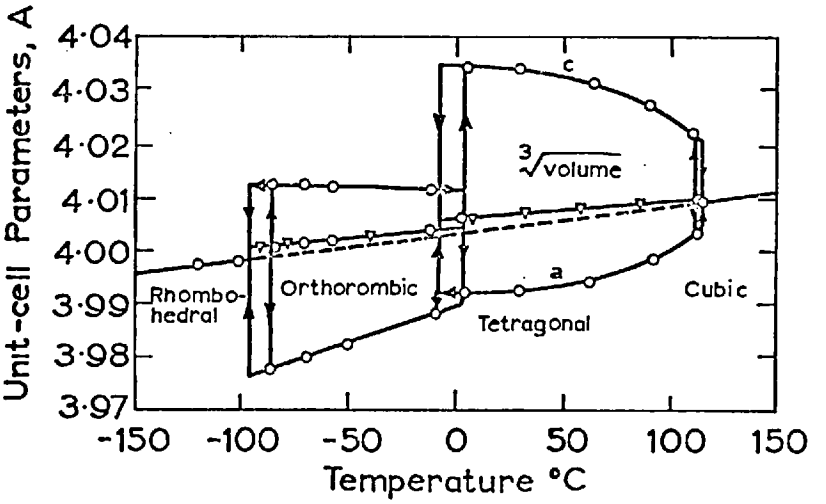


Fig. 2.13.

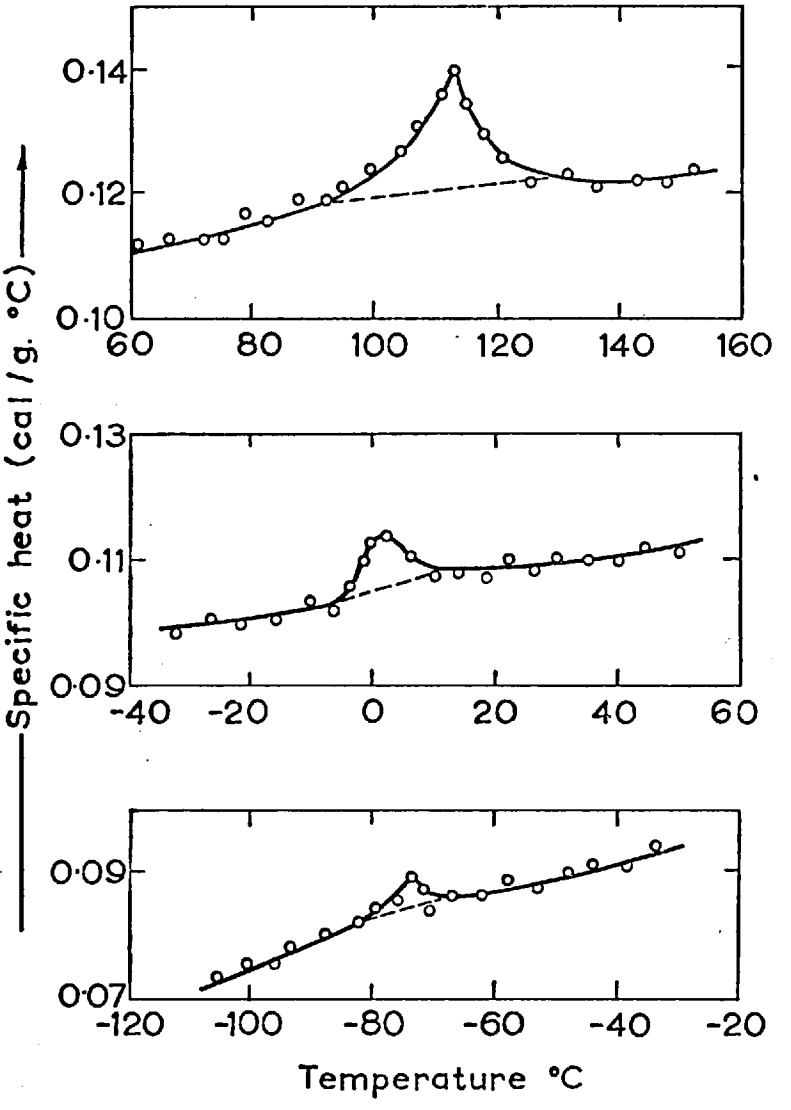


Fig. 2.14.

2.4.2 Specific Heat Anomaly

The phase transitions of ferroelectric $BaTiO_3$ with temperature are discontinuous transitions followed by continuous changes. Therefore a latent heat should be superimposed to a continuous anomaly of the specific heat. However domain effects, internal strains, surface effects, and inhomogeneities broaden the transition so that only a more or less sharp peak of the specific heat is observed at the transition point.

Results of measurements of the specific heat (Volger, 1952; Blattner et al, 1949; Todd and Lorensen, 1952; Busch et al, 1948) as a function of temperature are shown (Shirane and Takeda, 1952) Fig. 2.14. Three peaks are observed, corresponding with the three transitions, which are not as sharp as one would expect in a first order transition. The heats of transition ΔQ and the changes in the entropy ΔS derived from the curves of Fig. 2.14 are listed in the table below

Transitions	ΔQ (cal/mole)	ΔS (cal/mole °C)
120°C (tetragonal-cubic)	50 ± 5	0.125
5°C (orthorhombic-tetragonal)	22 ± 4	0.076
-70°C (trigonal-orthorhombic)	8 ± 2	0.04

2.4.3 Latent part of the transition heat

Since the observed specific heat changes occur over an interval of several degrees then the tetragonal to cubic phase transition cannot be termed a first order change as no latent heat was detectable.

However, an ingenious method has been used for "detecting" the latent part of the transition heat (Roberts, 1952). This latent heat of transition was detected in the form of a temperature rise when an electric field was suddenly impressed on a ceramic disc just above the Curie point, the temperature reverting to its original value on removal of this field. This temperature change may be interpreted as that accompanying an adiabatic transition from the cubic to the tetragonal phase. A similar temperature rise was detected just below the Curie point but this time irreversibly so. Estimates for this latent heat of transition amounting to 15 cals $mole^{-1}$ were obtained by assuming a value for the average specific heat.

2.4.4 Thermal expansion coefficient

The linear thermal expansion coefficient undergoes a contraction in a range of approximately $10^{\circ}C$ through the transition point. Measurements on ceramic samples indicate that the linear expansion coefficient is different for the two phases being greater in the cubic phase (Shirane and Takeda, 1952), the rather sharp contraction resulting in a volume change of -0.62Å.

2.5 THE OPTICAL PROPERTIES IN THE VISIBLE RANGE

2.5.1 Introduction

The large dielectric polarisation that occurs in $BaTiO_3$ (induced above the Curie point, spontaneous below) corresponds to a substantial change in the crystal symmetry and hence in the refractive properties. With zero applied field birefringence is still exhibited on entering the temperature region at which there is spontaneous polarisation. This permits the direct observation of the ferroelectric domains. It follows that the "overall" birefringence of the polarised phase depends upon the domain structure.

2.5.2 Electro-optic effect

The index ellipsoid or indicatrix characterises the optical properties of a crystal thus:

$$\frac{x^2}{n_1^2} + \frac{y^2}{n_2^2} + \frac{z^2}{n_3^2} = 1$$

where n_1, n_2 and n_3 are the principal refractive indices. An electric field applied to the crystal deforms the indicatrix and its equation becomes generally

$$a_{11}x^2 + a_{22}y^2 + a_{33}z^2 + 2a_{23}yz + 2a_{31}zx + 2a_{12}xy = 1$$

This deformation changes the optical properties, the effect is called the electro-optic effect; the indices a_{ik} are known as polarising constants.

Changes in a_{ik} can be caused by mechanical stress in addition to an electric field, that is, besides an electro-optical effect there can also be an elastic-optical (piezo-optical) effect. The modified a_{ik} are generally given by an expression of the type,

$$a_{ik} - \delta_{ik} \frac{1}{n_i n_k} = \sum_{m=1}^{6} g_{ik}^{(m)} X_m + \sum_{l=1}^{3} f_{ik}^{(l)} E_l + \sum_{s,t=1}^{3} h_{ik}^{(s,t)} E_s E_t$$

which accounts for the linear changes in a_{ik} with stress and field and the quadratic changes with field. First term on the righthand side of the above equation represents the elasto-optic effect, the second term the linear-optic effect, and the third term the quadratic electro-optic effect. The second and third terms are the optical analogs of the linear piezo effect and of the electro-striction respectively. Actually the matrix for the respective coefficients is identical in form. This analogy goes even deeper since the respective temperature dependences are similar.

The field induced change in lattice parameters is closely related to changes in the optical parameters, since if the crystal is free an applied field causes a mechanical strain due to the piezo-effect which in turn changes the refractive indices because of the elasto-optical effect. This is actually a secondary effect, that due to the absence of mechanical strain for a clamped crystal being known as the

primary effect. The total effect observed in a free crystal, at low frequencies for example, is the sum of the two. At high frequencies the mechanical deformations cannot follow the driving force and the crystal is in a so-called clamped condition.

Above the Curie point there is no linear electro-optical effect (also no piezo effect). Below this the matrix of polarisation constants is

$$\begin{pmatrix} 0 & 0 & 0 & 0 & f_{51} & 0 \\ 0 & 0 & 0 & f_{51} & 0 & 0 \\ f_{13} & f_{13} & f_{33} & 0 & 0 & 0 \end{pmatrix}$$

For an electric field applied along the polar axis ($E_x = E_y = 0$, $E_z \neq 0$) the equation of the indicatrix is now

$$(x^2 + y^2)\left(\frac{1}{n_1^2} + f_{13}E_z\right) + z^2\left(\frac{1}{n_3^2} + f_{33}E_z\right) = 1.$$

Upon application of an electric field E_z, the directions of the axes of the index ellipsoid remain the same but the lengths of the axes change. Thus the crystal remains uniaxial but the value of the spontaneous birefringence changes. The refractive indices become

$$n_1 = n_1(1 + f_{13}E_z n_1^2)^{-\frac{1}{2}}$$

and,
$$n_3 = n_3(1 + f_{33}E_z n_3^2)^{-\frac{1}{2}}$$

and hence the birefringence is

$$\Delta n = n_1' - n_3' = (n_1 - n_3) + \tfrac{1}{2}E_z(f_{33}n_3^3 - f_{13}n_1^3) = \Delta n_o + \delta(\Delta n)$$

where $\Delta n_o = (n_1 - n_3)$ is the spontaneous birefringence ($E = 0$) and $\delta(\Delta n) = \tfrac{1}{2}E_z(f_{33}n_3^3 - f_{13}n_1^3)$ is the change in birefringence due to the electro-optical effect.

The birefringence at room temperature is found to be negative indicating a compression of the indicatrix along the c-axis. This temperature variation terminates abruptly at the Curie point (Forsbergh, 1949). It has also been shown that the birefringence is proportional to the square of the spontaneous polarisation (Merz, 1949), and hence it is the spontaneous polarisation that is responsible for the spontaneous change occurring at the transition temperature in the birefringence.

Measurements of the birefringence as a function of wavelength suggest that there may be an absorption band around 3800 Å (Cross et al, 1950).

The quadratic electro-optical coefficients g_{ijkl} may be defined

$$a_{ij}(P) - a_{ij}(0) = \sum_{k,l} g_{ijkl}P_kP_l$$

where $a_{ij}(P)$ and $a_{ij}(0)$ are the polarising constants with and without lattice polarisation P. The coefficients $(g_{11} - g_{12})$ and g_{44} are practically temperature independent and furthermore the d.c. and 100Mc/s values of the former

are found to be identical. The temperature dependences of both these coefficients are similar to those of the dielectric constant along the 'c' and 'a' axes respectively.

The refractive index also undergoes an anomaly which is strongly temperature dependent and has a maximum value at the Curie point of approximately 2.4.

2.6 THE INFLUENCE OF EXTERNAL STRESSES

2.6.1 Introduction

We have already seen that $BaTiO_3$ exhibits a peak in the dielectric constant at the Curie point. Thus it would be reasonable to suppose that an applied electric field has an important influence on the phase transformation. Also, since the crystal is elastically soft in this temperature region the effect of externally applied mechanical stresses on the nature of the transition would be appreciable.

2.6.2 The influence of electric fields

The early work carried out in investigating the effect of electric fields on the transition, seems to have been for the purpose of confirming Devonshire's assertion of a first order change occurring at the Curie point.

The effect of biasing fields on the dielectric properties is to shift the maximum in the dielectric constant to higher temperatures (Känzig and Maikoff, 1949). The effect of a field induced transition may be demonstrated on an oscilloscope

using the conventional Sawyer-Tower circuit where the effect of a strong a.c. field is seen to produce "double hysteresis" loops above a certain critical field (Merz, 1953). Such field induced transitions may only occur in a narrow temperature range up to about 10°C. above the zero field Curie point, the polarisation then changing continuously above this temperature range no matter how large the field strength applied. It is shown further that on the basis of thermo-dynamic reasoning such double loops may only occur for first order transitions.

Such a field dependent transition has also been investigated optically (Kawabe, 1959). As the transparency is related to the polarisation which in turn is affected by an externally applied field the relationship between the field strength and transition temperature is found to be linear.

2.6.3 The influence of mechanical stresses

The effect of pressure is found to decrease the peak in the dielectric constant which now occurs at slightly higher temperatures. The Curie-Weiss law is obeyed though the extrapolated Curie temperature T_o is decreased, the Curie constant C being unaffected.

Since the onset of spontaneous polarisation corresponds to a change in the lattice parameters then under pressure these parameters occurring at the normal Curie point may be

obtained at different temperatures (Merz, 1950; Forsbergh, 1954; von Hippel, 1951; Jaffe et al., 1957). The shifts in Curie temperature with pressure are found to obey the Clausius-Clapeyron type equation.

2.7 ELECTRICAL PROPERTIES

2.7.1 Introduction

The conductivity of insulating materials is usually of the form

$$\sigma = A(T) \exp-(\phi/kT)$$

where A(T) is a slow changing function of temperature and ϕ, the activation energy may itself also be temperature dependent. In an insulator which is free from impurities and is stoichiometrically balanced, (i.e. the material is intrinsic) the activation energy would be expected to depend upon the energy gap $\Delta E(\phi = \Delta E/2)$ between valence and conduction bands. This gap depends upon the short range forces between neighbouring atoms, and in consequence upon the lattice dimensions. One might expect therefore the activation energy ϕ would change in value with increasing temperature on passing through the Curie point.

When energy levels occur in the forbidden gap, as when impurities or imperfections are present in the lattice, the activation energy is less than the intrinsic value corresponding to stoichiometric balance but would still be

expected to change in value through the Curie point.

The strong elastic deformation of the titanium ion within the oxygen octahedra of $BaTiO_3$ leads one to expect a change in the conducting properties on passing through the Curie point.

2.7.2 Electrical conductivity

Measurements of the electrical conductivity are shown to be well represented by an equation of the above form (Busch et al., 1948). There is a noticeable flattening out of the curve of the log conductivity against reciprocal temperature in the region of the Curie point corresponding to a smaller value of the activation energy. It is known that the conduction band in $BaTiO_3$ suffers displacement with increasing temperature in the tetragonal phase, which is possibly piezoelectric in origin. Others have indicated that electron conductivity may play some part in the process leading to a current decrease in $BaTiO_3$, since a displacement of the conduction band would bring about a change in the carrier activation energy and hence a variation in the carrier density.

3. GROWTH OF BARIUM TITANATE SINGLE CRYSTAL

3.1 INTRODUCTION

Since the first successful growth of Barium Titanate crystals by Blattner et al. in 1947, a considerable amount of work has been done in the past several years on the problem of growing large single crystals, and most of the methods developed for this purpose involve the use of the polycrystalline compound as a starting material.

A more complete study of the phase diagram of the system $BaO-TiO_2$ was carried out by Rase and Roy (1957) which revises the earlier results of Statten (1951). The most important information obtained from this phase diagram is the fact that $BaTiO_3$ transforms from the cubic to a hexagonal phase at 1460°C before melting at 1618°C. This phase change, at 1460°C is apparently very sluggish and the hexagonal phase may be quenched to room temperature by rapid cooling through 1460°C. This probably explains the occurrence of hexagonal crystals in some of the early crystal growing attempts reported and is important when crystals are grown from the melt. The hexagonal modification of $BaTiO_3$ is not ferroelectric and a structure study (Burbank and Evans, 1948) reveals a framework of TiO_6 octahedra which is linked in a different way than in cubic $BaTiO_3$.

3.2 METHOD AND TECHNIQUES

The following methods have been employed for the growth of $BaTiO_3$ crystals:

(i) Growth from the melt (Von Hippel, 1950; and Kremers et al., 1954).

Large single crystals were obtained using both the Stockbarger and flame-fusion process, but the quality was severely limited due to bad twinning and high internal strains.

(ii) Hydro-thermal synthesis (Roy, 1952).

Most attempts to obtain large single crystals under hydro-thermal conditions have not met with any satisfactory degree of success.

(iii) Growth from binary (or ternary) melts which represents to date the most satisfactory method of growth. Several salts have been found to be good solvents for $BaTiO_3$ in their liquid phases, and since some of these salts have a fairly low melting point crystals of $BaTiO_3$ may be obtained from these melts at comparatively low temperatures in much the same way as water soluble crystals are grown from aqueous solutions. Here the solvent is referred to as the "flux" and for this method a knowledge of the phase diagram of the system of $BaTiO_3$ and the flux to be used is essential.

The phase diagram of the system $BaTiO_3$-KF is shown in Fig. 3.1 (Karan and Skinner, 1953; Karan, 1954), from which

it may be seen that crystallisation can take place anywhere along a solid portion of the curve. However, for reasons which will be explained later this is not the only criteria for the formation of $BaTiO_3$ crystals and it is desirable to use only a limited portion of this solid curve.

3.3 CHOICE OF SOLVENT

It is not always possible to predict from a knowledge of the chemical properties of the materials used for the growth of crystals by method (iii) above as to which solvent is the most suitable for a particular substance. An extensive investigation involving $BaTiO_3$ and over 25 different fluxes has been carried out by Sholokhovich and Belyaev (1954). However, the most satisfactory and commonly used solvent has proved to be potassium fluoride. Potassium fluoride (KF) is not unique as a solvent from which crystals are obtained; they have also been obtained from NaF (Egerton et al., 1961; Gorski, 1961), K_2CO_3, PbO, $BaCl_2$(DeVries, 1959), and BaF_2 (Nielsen, 1962).

In choosing a suitable solvent one should bear in mind the following characteristics which should be displayed by the particular choice (White, 1965):

(i) reasonably high solubility for the solute,

(ii) no chemical reaction with the solute,

(iii) low melting point, high boiling point, and low vapour pressure at growth temperatures,

(iv) low viscosity,

(v) high solubility in water or aqueous reagents,

(vi) a common ion with the solute or to consist of ions of such size or charge that they are not readily incorporated in the lattice of the solute crystal.

It has been found that potassium fluoride has proved to be the most satisfactory since it does not attack platinum excessively, is readily leached with warm water, and has a much lower melting point than $BaTiO_3$ which being the heavier sinks to the bottom of the crucible where nucleation occurs.

3.4 GENESIS OF BUTTERFLY TWINS

The technique adopted for the growth of well-formed $BaTiO_3$ crystals is that originally devised by Remeika (1954). In this method a super-saturated solution of $BaTiO_3$ in KF is allowed to cool comparatively rapidly from a soak temperature of 1150-1200°C. to 850-900°C. During this cooling period the $BaTiO_3$ crystallises and before the flux solidifies it is decanted and the crystals allowed to anneal by slowly cooling down to room temperature.

A typical procedure consists in starting from a mixture containing approximately 30 weight per cent. $BaTiO_3$ - 70 weight

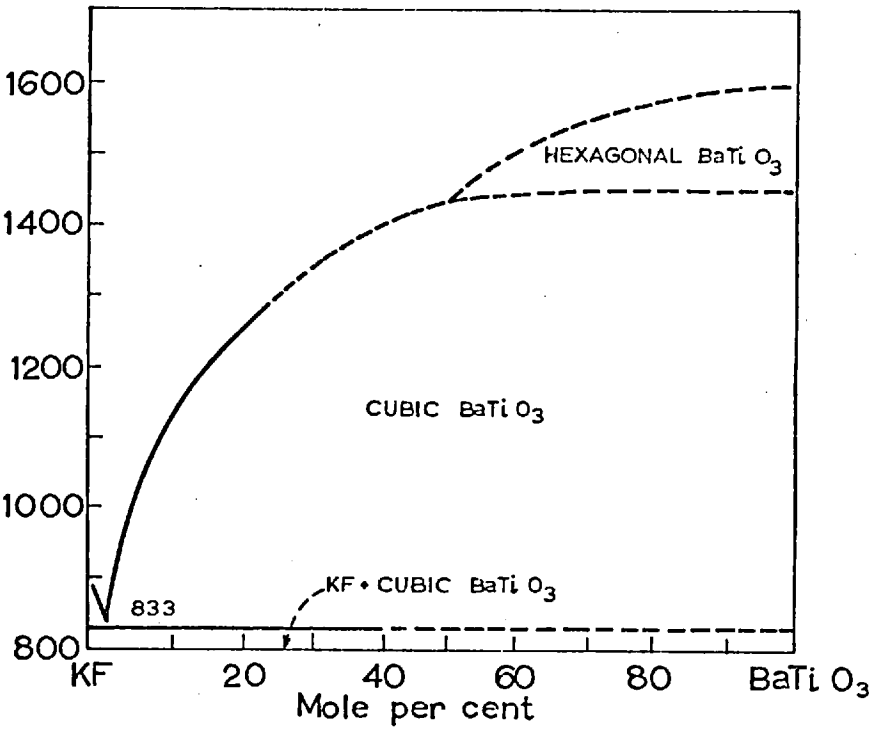

1600
1400
1200
1000
800
HEXAGONAL BaTi O3
CUBIC BaTi O3
KF + CUBIC BaTi O3
833
KF
20
40
60
80
BaTi O3
Mole per cent

Fig. 3.1

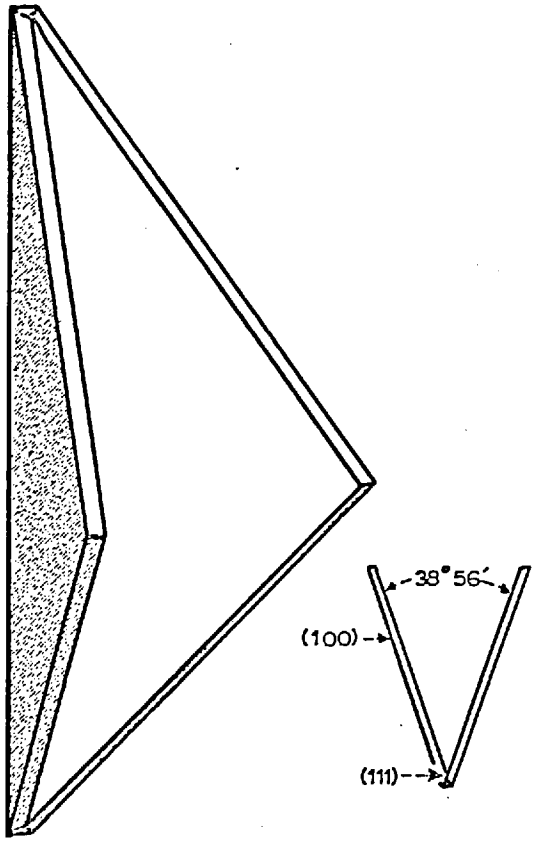

38°56'
(100)
(111)

Fig. 3.2

per cent. KF with about 0.02% Fe_2O_3. The essential points in Remeika's method are the use of potassium fluoride as the flux and the technique involving the decanting of the liquid flux before it solidifies. Indeed, it was the lack of the latter procedure in the early attempts at growing $BaTiO_3$ which was largely responsible for the poor quality of the crystals obtained, being full of internal strains, together with the difficulty in their extraction from the solid flux as the crystals themselves are comparatively brittle. A characteristic feature of the crystals grown by Remeika's method is that they are formed in triangular plates which occur in pairs joined along the common hypotenuse at an acute angle of approximately 39°. This twinning configuration is referred to as "butterfly twins" and usually a narrow well-developed face is present along the junction of the wing plates; this face is a (100) face which is connected to the face plates through two (111) twinning planes, Fig. 3.2. The reasons for the precise occurrence of twins observed is not clear.

It has also been found that the twin yield depends critically on the average particle size of the $BaTiO_3$ used and it is probable that the optimum size of particle for twin formation may be 6 micron or less (Nielsen et al., 1962).

The effect of temperature on the habit of crystals

obtained by Remeika's method was studied by Eustache (1957), whose results show that when crystallisation starts above 1000°C butterfly twins are obtained; when crystallisation starts between 1000°-950°C some square plates are obtained; when crystallisation starts below 950°C one obtains transparent cubes and parallelpipeds (also Novosil'tsev and Khodakov, 1952). In addition to having obtained all three of the above forms in the early attempts at crystal growth, the author has observed dendritic forms (DeVries, 1959).

By stopping the growth at different periods in the region 1160-880°C the growth process of the $BaTiO_3$ butterfly twins was observed. The growth process shows different behaviours above and below 1000°C. Above 1000°C a two-dimensional growth takes place rapidly and below this temperature a thickening growth continuously takes place slowly, the two-dimensional growth now being quite small (Sasaki, 1965). It seems reasonable to attribute the difference of the growth behaviour above and below 1000°C to the difference of temperature coefficient of solubility of $BaTiO_3$ in KF in the two regions. The two-dimensional growth of the crystals forming butterfly twins is probably due to the large degree of super-saturation developing in the $BaTiO_3$-KF system above 1000°C. This does not seem consistent with the $BaTiO_3$-KF phase diagram, since the nucleation of the butterfly twin is related to the ease

of formation of a stacking fault which apparently depends strongly on the size of the ion, and any additive which prevents this stacking fault from forming will sharply decrease the twin yield.

Now it is well known (Faust and John, 1965) that nucleation occurs more easily on a "rough" interface and one would expect that owing to the greater degree of super-saturation at higher temperatures, for a given constant rate of cooling, nucleation on "smooth" surfaces would be the more likely with the formation of cube like crystals. This is in direct contrast to Sasaki's observations. It is probable that the original nucleus is a cube which has been cleaved to reveal a (111) plane, and unless small enough $BaTiO_3$ particles are present to make the probability of exposure of this (111) plane high, the steps necessary for twin nucleation cannot begin.

3.5 APPARATUS

The crystal growth runs were carried out in a furnace of simple design and construction using ordinary fire brick and Morganite crusilite heating elements. Four of these elements were placed on either side of the chamber in which growth was to take place which was isolated from them (Fig. 3.3). This ensured, other things being equal, a longer life since the heating elements were then not in direct contact with fumes from the

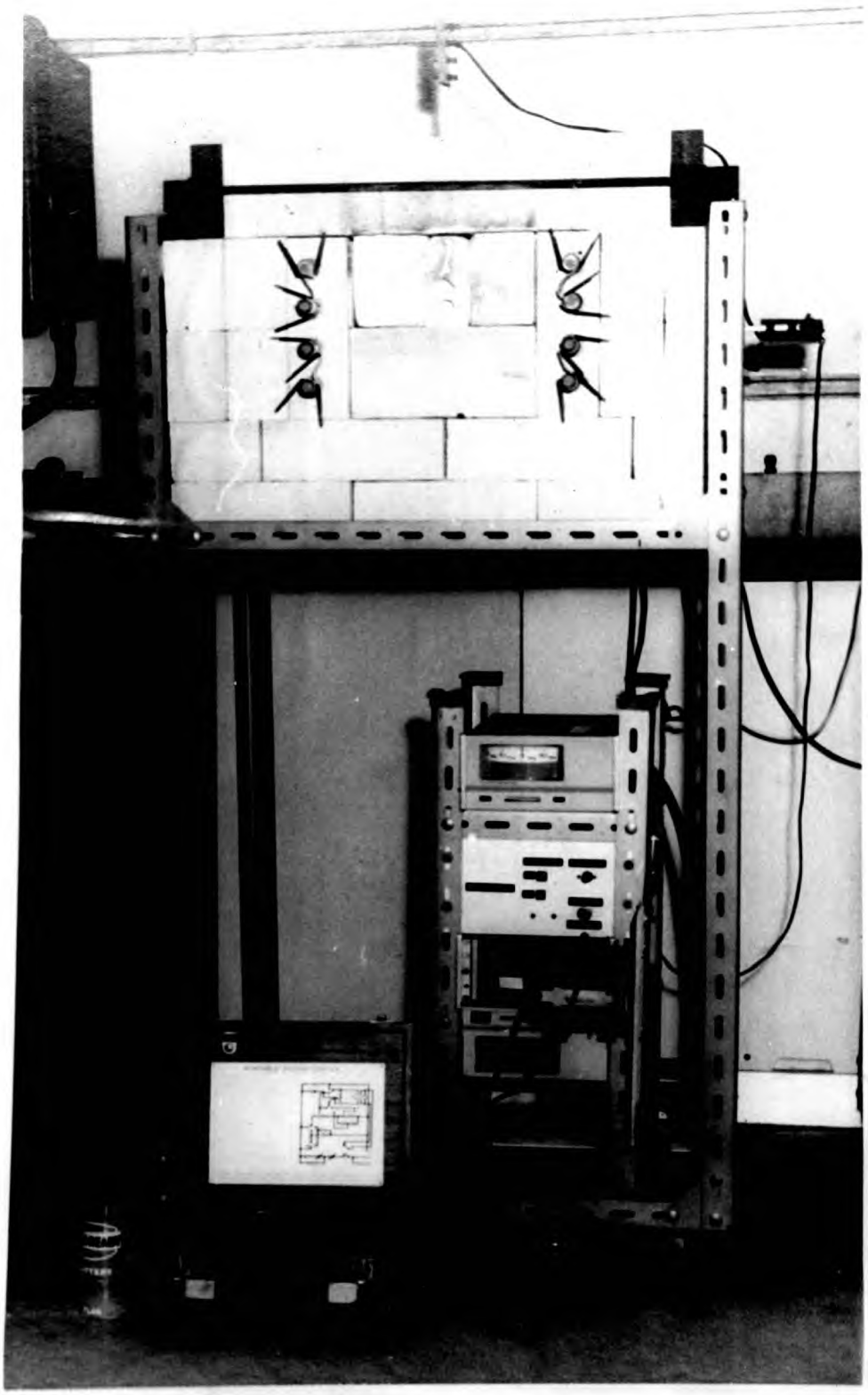


Figure 3.3

growth chamber. The temperature inside the chamber was probed by a Pt-Pt/Rh thermocouple introduced through the roof of the chamber such that the temperature of various parts along the height of the crucible could be monitored. No temperature gradient was observed along the height of the crucible and this was probably due to this height being much less than the total vertical separation of the elements. Any temperature gradients occurring in the chamber occurred along the horizontal only and use was made of this in the experimental method adopted. It was found that placing the crucible to one side in the chamber increased both the yield and quality of the crystals obtained. It is seen that in so placing the crucible, a temperature gradient exists along the horizontal direction which gives rise to thermal stirring thus increasing the amount of $BaTiO_3$ being dissolved in the KF. These findings, though similar to those of Sasaki's (1965) have nevertheless been arrived at quite independently.

In Sasaki's procedure a furnace is used in which the crucible is moved in a vertical direction through a fixed vertical temperature gradient as opposed to the method adopted here where with the crucible stationary and in a thermal gradient, which is allowed to change across the chamber, as cooling takes place. This method possesses the advantage of simplicity and the avoidance of any moving parts at high temperatures.

The rate of cooling was achieved by means of a Eurotherm ramp control which was able to achieve cooling rates of between 1-30°C per hour. Various crystal growth runs were performed at cooling rates between 9-25°C per hour and in all cases over the temperature range of interest desired, a linear rate achieved and this was in no small way a vital factor in the successful performance over several runs. Previous to using this ramp controller, the rate of cooling was achieved by means of mechanical operation on the temperature control using a slowly rotating motor coupled to the control panel via a series of reduction bevel gears. This method proved to be very erratic and even under the best operating conditions did not give a smooth curve but rather a series of unequal discontinuous steps.

3.6 EXPERIMENTAL METHOD

In the literature it is to be noticed that the various percentages by weight of $BaTiO_3$ to KF is always quoted exactly in order that after the soak period and during the cooling period an excess of $BaTiO_3$ remains at the bottom of the crucible which is essential for nucleation to occur and the consequent formation of butterfly twins. It is the opinion of the author that these critical amounts do not constitute the essential factor for a successful run. All that is necessary is that some $BaTiO_3$ is left undissolved and the

factors contributing to this are numerous. An important consideration to take into account is that during the soak period and the cooling period the flux is continuously evaporating so that the molar ratios of the components in the melt change toward lower values of the flux content. It is not necessary as some workers suggest to practically seal the lid on the crucible in order to prevent evaporation of the KF flux, but only to "place" a well-fitting lid over the top to inhibit it somewhat.

Over a period of perhaps in excess of thirty runs it is the opinion of the author that the particular shape of crucible employed is important, together with an intimate knowledge of the thermal behaviour of the furnace employed.

With regard to the crucible shape, two basic shapes were used, one in the form of a right cylinder of 500mm. capacity and the other also of a cylindrical shape but with a tapered base ending in a flat bottom of 200mm. capacity. It was found that keeping other conditions as near equal as possible the quality of the yield in the two cases using the same ratios of starting material was not the same, and also quite reproducible. The results obtained with the regular shaped crucible were always inferior, the two-dimensional growth often not being fully completed owing to the individual platelets not being fully formed.

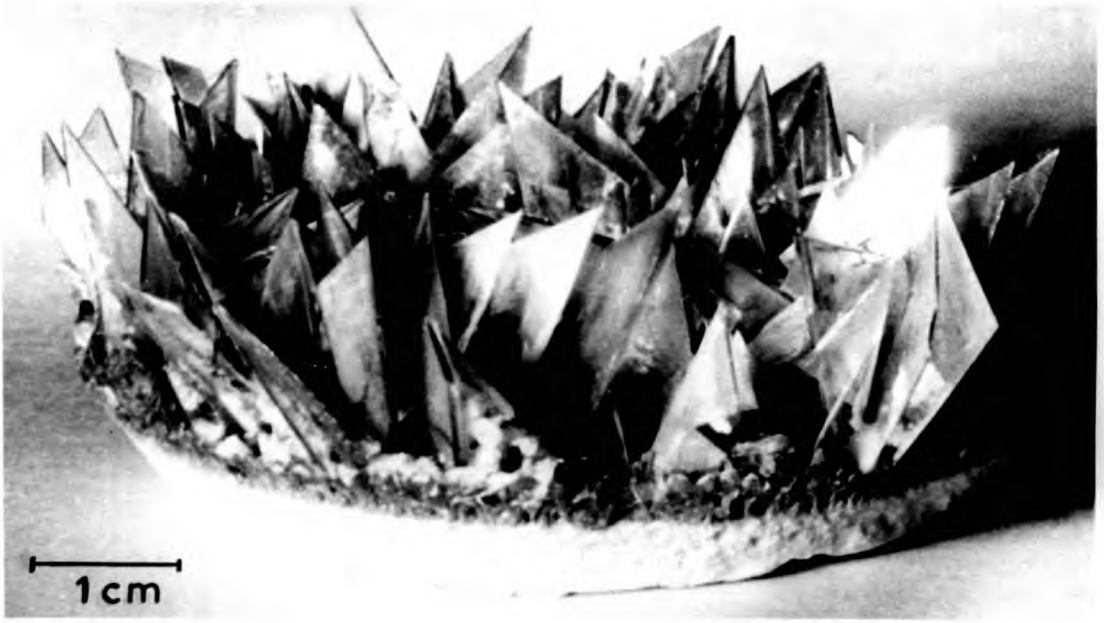
Since an excess of $BaTiO_3$ is necessary for nucleation to occur then it would be expected that the yield would be affected somewhat by the thickness of this excess cake remaining on the bottom of the crucible. Also, the head of liquid KF flux above this cake in which the crystals grow is important. If for a given ratio of the starting materials there is a very thin cake remaining on the bottom of the crucible, together with a not very high head of liquid flux, then the crystal formation would be affected as the temperature was lowered there being a smaller head of flux available for growth to take place in. We see therefore that if a reasonable layer of cake thickness were to be maintained at all times, together with a reasonable head of liquid flux then, other things being equal, a good yield should result. It is clear, therefore, that for a good ratio these two conditions would be different in crucibles of different shape. Consequently the tapered flat bottom crucible would be more suitable for these conditions than the right cylindrical one. We can however restore these conditions somewhat for the second type of crucible by varying the ratios of the starting material to ensure a thick cake of excess $BaTiO_3$ and higher head of flux at all times. The author has found this condition to be satisfied.

Further, the exact ratios of material normally quoted

in the literature is not absolutely necessary, but serves only as an approximate guide. In the present work good quality thin crystals were aimed for which could be easily poled and therefore it was not necessary to produce thick crystals as these were found to contain a higher degree of internal strain and hence could not be so easily poled.

After a few runs and a thorough acquaintance with the thermal behaviour of the furnace one could then estimate quite accurately the amounts of starting material necessary, depending on the crucible used, without recourse to weighing. A typical and reproducible result of such runs is shown in Fig. 3.4, from which it may be seen that the crystals are clearly transparent and well formed.

In a typical run, having charged the crucible with $BaTiO_3$ powder and KF, it was then placed in the furnace at room temperature, which was then switched on and from a knowledge of the time taken to attain a soak temperature of just over 1200°C the cooling run was started overnight by means of an automatic timer, which thus allowed a soak of approximately two hours duration. The liquid flux was quickly decanted inside the furnace at approximately 930°C., the lid left off and the crucible allowed to cool to room temperature after switching off the furnace. The excess KF remaining was leached out with hot water which enabled the





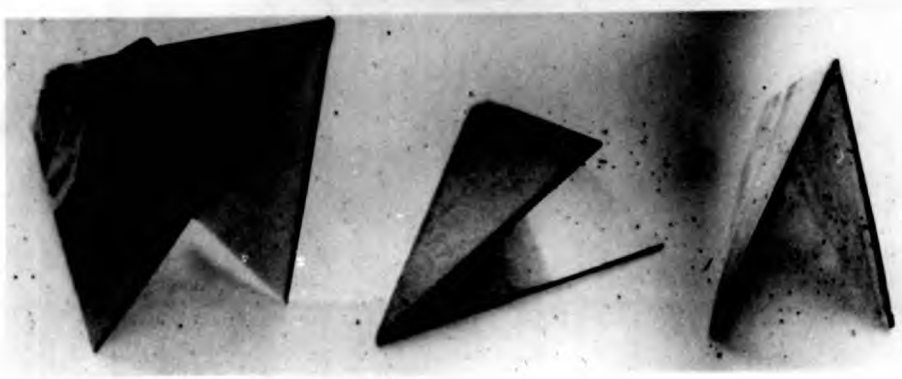


Figure 3.4

cake and the butterfly twins embedded in it to be extracted as a whole.

Throughout all the runs the original crucibles were not used for any other crystal growth attempts in order to reduce the possibility of contamination. In addition, it was not found necessary to clean the crucibles in the normal manner but merely to rinse them under the tap.

The crystals were extracted from the cake and came away clean in most cases. They were then poled, using liquid electrodes of potassium chloride in glycerol and this enabled the characteristics to be observed whilst poling was taking place. Some crystals which retained solidified KF on their surfaces were harder to pole, which was however overcome to a certain extent by etching them in hot phosphoric acid. However, it is the opinion of the author that the poling characteristics are essentially determined during growth and not as a result of any subsequent treatment, since it was found that those crystals whose domains were well-defined poled rather easier than those which were not.

The original $BaTiO_3$ used was of commercial quality supplied by British Drug Houses and was found to be unsuitable for use owing to the large amount of impurities it contained, mainly strontium, which tends to inhibit the formation of platelet twins. The purity of the flux did not appear to

matter since better crystals were obtained using high purity material of smaller average particle size obtained from the Titanium Manufacturing Division of the National Lead Company, U.S.A. Also the colour of the crystals obtained depends on the impurity of the starting material, the more yellow the crystal the greater the degree of impurity. With the National Lead material a very light straw coloured crystal was obtained and subsequent spectrographic analysis on the two types of materials used, confirmed this.

4. THE CRYSTAL STRUCTURE AND ASSOCIATED ATOMIC PROPERTIES

4.1 INTRODUCTION

A knowledge of the crystal structure of $BaTiO_3$, and of the small changes that it undergoes at the transition points, is necessary in order to understand the microscopic processes responsible for its ferroelectric behaviour. The information on the static structure together with some on thermal vibrations has been obtained from X-ray and neutron diffraction measurements.

At the present time not much is known about the configuration of the outer electron shells which would, conceivably, play an important part in the electronic polarisation and chemical bonding. Some information in this direction has been obtained from measurements of optical absorption, while the work in this account provides additional information by means of crystalline field probes using paramagnetic resonance for the electron configuration and the Mössbauer effect for the nucleus.

4.1.1 The Structure in the Cubic Phase

Above 120°C in the cubic phase $BaTiO_3$ has the ideal perovskite structure with the general composition ABO_3 ($BaTiO_3$); the space group is Pm3m, with one formula-unit per unit cell. The simple cubic perovskite cell is shown in Fig. 4.1; placing the origin at an A ion the atomic coordinates are as follows:

A at 0, 0, 0;

B at $\frac{1}{2}$, $\frac{1}{2}$, $\frac{1}{2}$;

3 O's at $\frac{1}{2}$, $\frac{1}{2}$, 0; 0, $\frac{1}{2}$, $\frac{1}{2}$; $\frac{1}{2}$, 0, $\frac{1}{2}$.

Each titanium ion is at the centre of six oxygens, arranged at the corners of a regular octahedron; these octahedra are linked by their corners into a three-dimensional framework enclosing large holes which are occupied by bariums. Each barium has twelve equidistant oxygens; each oxygen is adjacent to two titaniums and four bariums. For convenience this is probably easier to see if the origin is shifted to a titanium site - Fig. 4.2, and in this way the continuity of the structure is better visualised. The barium is shown as the hatched circle, and the titanium ions lie at the corners of the dashed cube, each one being enclosed by an oxygen octahedron. From the crystal chemical point of view the structure is better visualised as a face-centred-cubic close-packed arrangement of Ba^{2+} and O^{2-} ions. There are two types of interstitial positions in such close-packed arrangements which are tetrahedrally and octahedrally coordinated respectively. In the cubic phase every available octahedral hole between six O^{2-} ions is filled with a Ti^{4+} ion and there are no discreet TiO_6 groups.

4.1.2 The Structure in the Tetragonal Phase

With decreasing temperature through the Curie point the

crystal transforms into the polarised phase, the ions being displaced from their original highly symmetric position along one of the (001) axes. The structure becomes tetragonal with the cell dimensions (Reisman et al., 1956),

$$a = 3.992\text{Å}, \quad c = 4.036\text{Å},$$

with space group P4mm and one formula-unit per unit cell. The coordinates of the atoms in these structures can be expressed in terms of three parameters, δz_{Ti}, δz_{01}, δz_{011}, representing the shifts of the atoms from the symmetrical position, thus:

Ba at (0, 0, 0),

Ti at $(\frac{1}{2}, \frac{1}{2}, \frac{1}{2} + \delta z_{Ti})$,

01 at $(\frac{1}{2}, \frac{1}{2}, \delta z_{01})$

2 011 at $(\frac{1}{2}, 0, \frac{1}{2} + \delta z_{011})$; $(0, \frac{1}{2}, \frac{1}{2} + \delta z_{011})$

these coordinates are expressed as fractions of the tetragonal cell edges. For the cubic structure above 120°C all of the δz values are zero. These parameters are indicated in the (010) projection, shown in Fig. 4.3 the oxygen O_{11} superposed upon Ti being omitted. If thermal vibrations are being described then a further nine anisotropic temperature parameters are needed.

The first single-crystal structural study of tetragonal $BaTiO_3$ using X-rays was carried out by Känzig (1956). He assumed that $\delta z O_{11} = 0$, i.e. the oxygens on the faces parallel

to the tetragonal axes have not shifted from their centered position, and hence the shortest distances in the cubic phase between Ba and $\delta z O_{11}$ ions remain equivalent in the tetragonal phase. He also assumed that $\delta z Ti$ and $\delta z O_1$ have opposite sign; their temperature dependence is shown in Fig. 4.4, the actual displacement being with respect to barium. The parameters δz at room temperatures were found to be:

$$\delta z Ti = 0.014 \qquad \delta z O_1 = 0.032$$

$$(\ \delta z O_{11} = 0 \text{ assumed})$$

Evans (1953) avoided the assumption that $\delta z O_{11} = 0$. After extensive study he concluded that the structure could not be solved uniquely by X-ray methods because of the interaction between coordinate and temperature parameters along the tetragonal axis. He found that reasonable assumptions concerning temperature oscillations led to the following coordinate parameters which gave good agreement between observed and calculated intensities:

$$\delta z Ti = +0.012 \qquad \delta z O_1 = -0.026 \qquad \delta z O_{11} = 0$$

His second structure determination gave slightly better agreement in intensities but required rather unreasonable temperature parameters inasmuch that greater amplitudes of vibrations had to be assigned to the heavier ions,

$$\delta z Ti = +0.015 \qquad \delta z O_1 = -0.024 \qquad \delta z O_{11} = -0.020$$

Now in a structure determination by the method of trial

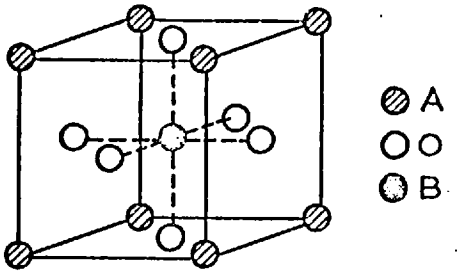


Fig. 4.1

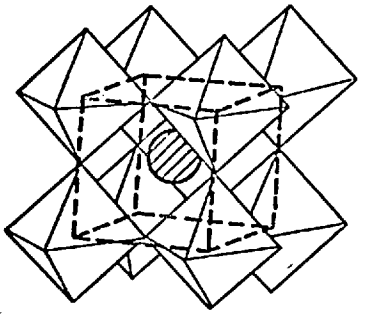


Fig. 4.2

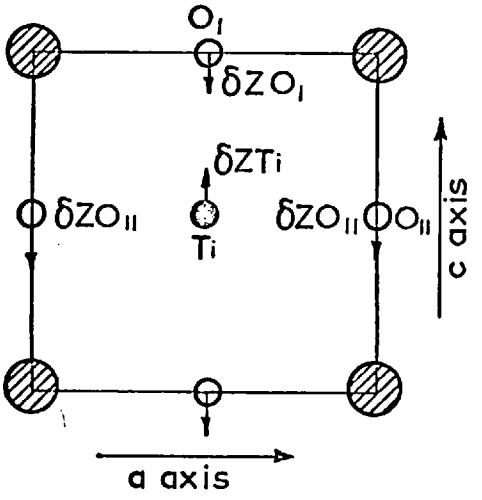


Fig. 4.3

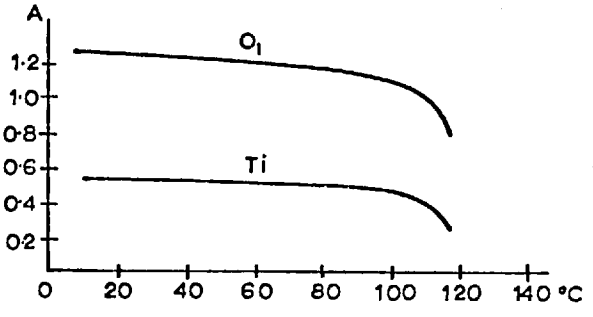


Fig. 4.4

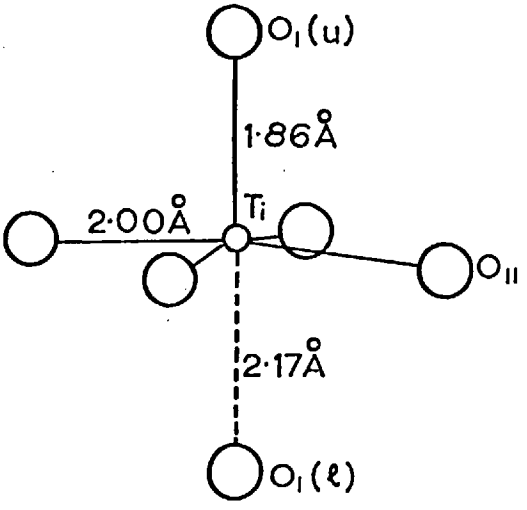


Fig. 4.5

and error, a structure is first postulated and a structure factor can then be calculated from the relation:

$$F_{calc}(hkl) = \sum_{j}^{N} f_j \, e^{2\pi i(hxj + kyj + lzj)} \qquad (1)$$

$$\text{and} \quad f_j = f_j^{o} \, e^{-B_j(\sin\theta/\lambda)^2} \qquad (2)$$

where f_j is the scattering factor of an atom j thermally oscillating, f_j^{o} the scattering factor at rest, and B_j the temperature parameter, which is a function of the mean square displacement of the atom, N the total number of atoms in the cell, $(x_j y_j z_j)$ the coordinates of that atom in the cell, θ the Bragg angle, and λ the X-ray wavelength. The magnitudes of the observed structure factors are given by:

$$F_{obs}(h,k,l) = K\sqrt{I_{obs}(h,k,l)L_p} \qquad (3)$$

where $I_{obs}(h,k,l)$ are the actual observed intensities of the diffraction pattern, K a scale factor and, L_p a factor which depends only on the scattering angle. Thus the agreement between calculated (from 1) and observed (from 3) intensities necessitates a knowledge of the temperature parameters, by (2). Hence, using equation (2) individual temperature corrections for the lattice atoms may be made, and also anisotropic temperature factors deduced.

The chief difficulty in an X-ray analysis lies in the large differences in the ratio of the scattering amplitudes of the individual atoms (Ba: Ti: O_2:: 8.3: 2.7: 0.62) and

in the separation of the small coordinate shifts and temperature oscillations.

However when neutron diffraction is employed the ratio of the scattering amplitudes are more favourable for a structure determination (0.53: -0.38: 0.58). A neutron analysis by Frazer, Danner and Pepinsky (1955) without any assumptions being made concerning $\delta z O_1$ or $\delta z O_{11}$ resulted in the following:

$$\delta z Ti = +0.0139. \quad \delta z O_1 = -0.0230 \quad \delta z O_{11} = -0.0143$$

The high accuracy obtained is reflected in the disagreement or reliability factor,

$$R = \frac{\sum \left| F_{obs} - F_{calc} \right|}{\sum \left| F_{obs} \right|}$$

which is less than 0.03. This work may be taken as giving the most reliable results since some uncertainty exists due to the anisotropic extinction of the X-ray reflections near a phase boundary (Känzig, 1956).

4.1.3 Bond Lengths and Bond Angles

The bond lengths and bond angles in the tetragonal phase based on neutron analysis are tabulated below in Angstrom units:

Ti - O_1	1.86 Å
	2.17 Å
Ti - O_{11}	2.00 Å
Ba - O_1	2.82 Å
Ba - O_2	2.80 Å
	2.89 Å

Angle Ti - O_{11} - Ti $171^{\circ}\ 28^{1}$

The environment of Titanium in the tetragonal phase is shown in Fig. 4.5. It may be seen from these results that the displacement of one set of oxygens with respect to the other is small; thus the distortion of the octahedral framework is slight. Also the displacement of the titanium ion is relatively large (0.31 Å) with respect to the centre of the framework. Because the O_1 and O_{11} displacements are parallel but not equal this brings about a change in the Ti - O_{11} - Ti angle from 180°. From the environment of Ti, depicted schematically in Fig. 4.5, it is seen that the bond length Ti - O_1 is markedly altered by the Ti shift, whereas no large change occurs in the Ba-O bond length. Assuming completely ionic character of the crystal, the positional parameters allow an estimate of the maximum possible contribution of the ionic polarisation. The result is 17 x 10^{-6} C/cm^2, implying that even the minimum contribution of the electronic polarisation (9 x 10^{-6} C/cm^2) is considerable.

4.2 INFRA-RED PROPERTIES

4.2.1 Introduction

A new impetus was given to the study of the infra-red properties by the theory due to Cochran (1960, 1961), which explains ferroelectricity in perovskites on the basis of lattice vibrations.

Considering the normal vibrational modes of the crystal,

it is quite possible that at a certain temperature for one particular mode the short and long range forces almost cancel each other out. The total restoring force along a line of $Ti\text{-}O_1$ chains may be shown to be lowered due to the characteristic 'catastrophy' effect occuring for transverse phonons along this direction, thus rendering the crystal unstable for this particular mode (Parker, 1967). This is the so-called ferroelectric mode which being strongly temperature dependent is responsible for the ferroelectric behaviour of the crystal.

Also, because of the low restoring force it is responsible for an infra-red absorption peak occuring at a frequency ν_F which is much lower than that of the other modes. Theory predicts that this frequency ν_F is temperature-dependent and that because of the Lyddane-Sachs-Teller relation (Lyddane et al., 1941) the dielectric constant reaches a maximum when ν_F reaches a minimum. The temperature at which this occurs is identified by Cochran (1960) as the Curie point of the ferroelectric and he predicts the relation

$$\epsilon = K\nu_F^{-2}$$

where K is a temperature-independent constant. Since the frequency of this ferroelectric mode is far lower than that of the other modes it is found that ν_F corresponds to a frequency in the far infra-red.

4.2.2 Results

On the basis of a Kramers-Kronig analysis it was found that the dispersion spectrum for $BaTiO_3$ could be fairly well represented as a function of the frequency by the following formulae

$$\epsilon' = n^2 - k^2 = \epsilon_\infty + \sum_{j=1}^{3} 4\pi \rho_j \nu_j^2 (\nu_j^2 - \nu) \left[(\nu_j^2 - \nu^2)^2 + \gamma_j^2 \nu^2 \right]^{-1}$$

$$\epsilon'' = 2nk = \sum_{j=1}^{3} 4\pi \rho_j \nu_j^2 \gamma_j \nu \left[(\nu_j^2 - \nu^2)^2 + \gamma_j^2 \nu^2 \right]^{-1}$$

which represent three resonances of damped classical oscillators, where $(n + ik)$ is the complex refractive index, $4\pi\rho_j$ is the strength, γ_j is the width, and ν_j the resonance frequency of the jth resonance. The imaginary part of the dielectric constant of $BaTiO_3$ is plotted versus wavelength and wave-number in Fig. 4.6, and the peak of approximately 296 μm occurs roughly at the wavelength predicted by Cochran and thus provides evidence for the existence of a mode of very low frequency. This low frequency absorption peak may also be shown, from the above analysis, as corresponding to an exceptionally damped resonance.

The measurements of Ballentyne (1964) of the temperature dependence of the far infra-red reflectivity above the Curie point, which have been independently checked by Barker (1966) over the same temperature range, 128-200°C, show that the

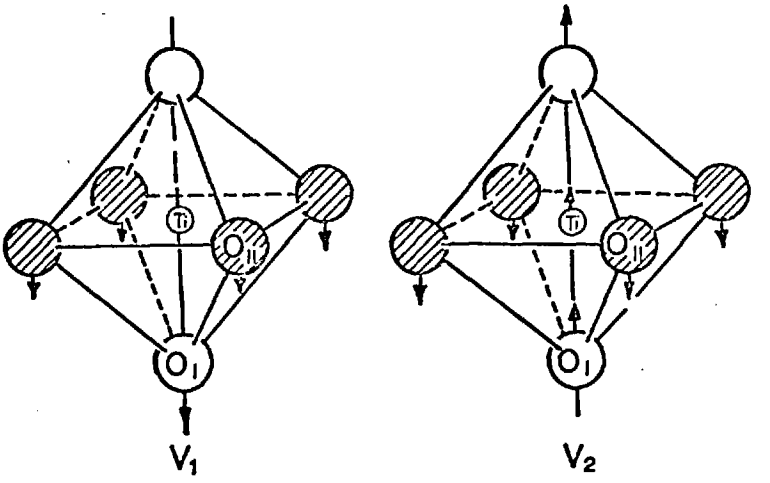

Ti
O II
O I
V1
V2

Fig.4.7.

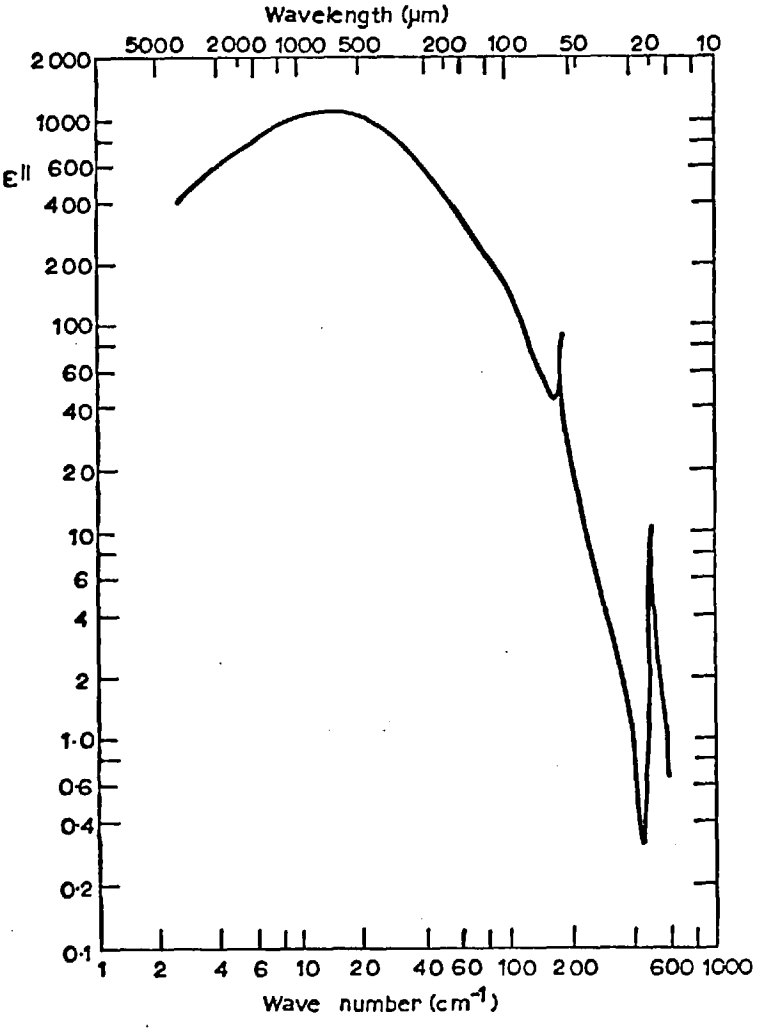

Wavelength (μm)
5000 2000 1000 500 200 100 50 20 10
2000
1000
600
400
200
100
60
40
20
10
6
4
2
1·0
0·6
0·4
0·2
0·1
ε||
1 2 4 6 10 20 40 60 100 200 600 1000
Wave number (cm⁻¹)

Fig. 4.6.

value which must be used for ν_F in Cochran's equation of the previous section is not the frequency at which ϵ'' shows the peak but corresponds to the frequency ν_3 which is the ferroelectric mode (296 μm) predicted by Cochran (Barker, 1966). These two frequencies differ considerably for a very damped resonance.

Unfortunately the reflectivity data show that the resonance is unlike that of a classical oscillator. The reason for the difficulty in the measured reflectivity is because of the large value for the dielectric constant occuring at frequencies just above ν_3.

A much better fit however has been obtained for the infra-red reflectivity data by taking into account the optical mode interactions and details of the higher lying modes (Barker and Hopfield, 1964).

There appears to be disagreement among various authors on the assignment of the modes corresponding to the frequencies ν_1, ν_2, ν_3. The most complete infra-red absorption study is due to Last (1957), who assigned the modes as follows: in discussing the vibrational nature of the TiO_3 group he considers the central Ti atom octahedrally surrounded by six oxygen half atoms to give the group the correct symmetry properties. Fig. 4.7 illustrates the vibrational modes assigned by Last to the frequencies ν_1 and ν_2, from which it is seen that the

mode corresponding to ν_1 is a change in length of the Ti-O_1 bond and is called a 'stretching' vibration; the mode corresponding to ν_2 is a change in the O_{11}-Ti-O_1 bond angle and is called a 'bending' vibration; and the mode corresponding to ν_3 (determined on the basis of specific heat studies) was assigned to the cation-(TiO_3) vibration.

This is not in agreement with the mode assignments of Spitzer et al. (1962). However, the work of Perry et al., (1964, 1965) in which the A cation is substituted by various other cations supports the original mode assignment due to Last.

The above results lead one to conclude that the infra-red measurements on $BaTiO_3$ may be explained on the grounds of crystal symmetry and positions in the cubic phase. No effect is observed which may be related directly to the occurrence of a spontaneous polarisation and ferroelectric activity.

4.3 THE DOMAIN STRUCTURE

4.3.1 Introduction

When a crystal of $BaTiO_3$ undergoes a transition from the cubic to the tetragonal phase, the tetrad axis may be any one of the three original cube edges, and in either direction along the edge. If the crystal is small and perfect it may transform into a single tetragonal crystal. However if it is free from external electrical and mechanical stresses, but

subject to local stresses either from clamping by its neighbours or from local internal imperfections, then it breaks up into domains of such orientations as to reduce stresses to a minimum. The resultant twinning that occurs is influenced by a number of factors. External mechanical stresses would be expected to influence the domain geometry due to the spontaneous strain existing in the individual domains. Also, the application of an externally applied electric field along the ferroelectric axis would favour the formation of a single domain. The simultaneous nucleation of a large number of domains which can occur when the crystal is cooled below the Curie temperature can also lead to a complex domain arrangement.

4.3.2 Experimental evidence for domains

The first papers to appear on the domain structure of $BaTiO_3$ were those of Kay (1948), Blattner et al. (1948), and Mathias and von Hippel (1948). The formation of domains that lead to twinning are of two sorts, the early evidence for which was supported partly from X-ray work and partly from optical studies, using the polarising microscope.

When a single crystal changes to a twin, single spots on the X-ray photograph are replaced by pairs or more complex groups, the relative displacement of the spots in magnitude and direction showing the orientation of the twin components,

and the relative intensities their abundance.

Optical methods however give further information, since if a thin crystal section of tetragonal $BaTiO_3$ is placed between crossed Nicols, it appears dark (extinguishes) when the direction of the polarising or analysing nicol is parallel to a principal vibration direction, i.e. to a symmetry direction; if the section is perpendicular to the tetrad axis it appears dark. The advantage of this method lies in the fact that direct and continuous observation of the domain patterns are possible while subjecting the crystal to varying electrical, mechanical and thermal stresses.

Hooton and Merz (1955) have investigated the domain patterns existing by etching the crystal in concentrated hydrochloric acid for several minutes. They have found that the positive end of a domain in $BaTiO_3$ etches faster than the negative end, and that for etching a domain sidewise is intermediate between the two. This etching rate may however be reduced to a few seconds by using a dilute solution.

More recently Pearson and Feldmann (1959) have used a powder pattern technique for delineating the domain structure. The method consists in employing separate colloidal suspensions of sulphur (yellow) and lead oxide (red) in an insulating organic liquid, hexane. On the hexane evaporating, the charged powder is attracted to domains of opposite sign and

the sulphur is deposited on negative dipole ends and the lead oxide on positive dipole ends. The agreement of this method of rendering of the domain pattern with the etch technique is excellent.

Spivak et al. (1959) have used an "electron reflector" to investigate the domain patterns at room temperature. This method, as opposed to optical methods, would give an image that more nearly represents the electrical properties of the domains since their electric fields would act upon the electrons; the picture quality however is inferior.

In certain cases it is possible, by holding up crystals of $BaTiO_3$ to the light, to be able to observe the presence of domains with the naked eye.

4.3.3 The Domain Geometry of Tetragonal Barium Titanate

Rather complicated domain structures are possible in $BaTiO_3$ because the spontaneous polarisation can occur along several equivalent axes. Hence, there is the possibility for domains polarised perpendicularly to each other (90° twins) as well as for antiparallel domains (180° twins). Accordingly there are two types of walls - 90° walls, and 180° walls. The observations of these structures is rendered possible by the large spontaneous birefringence. The literature on this subject is rather abundant; the early outstanding work being due to Kay and Vousden (1949), Kay (1948), Forsbergh (1949),

Merz (1952, 1954, and 1955), and Little (1954). We now consider each type of twin separately.

4.3.4 180° Domains

In general 180° domains are cylinders parallel to the tetragonal axis, two individuals being related by rotation about the normal to a face of the form (100) which is the composition plane. The tetrad axes are thus at 180° to each other. Since the spontaneous strain depends quadratically upon the polarisation it is the same for "up" and "down" domains, and hence this configuration being compatible with the spontaneous strain does not lead to internal stresses in the crystal. Optically, the "up" and "down" domains are indistinguishable, though if an electric field is applied perpendicular to the tetrad axis they become visible between crossed nicols due to the opposite torques on the dipoles in the individual domains. A mechanical stress has the same effect because the piezoelectric effect is of opposite sign (Hooton and Merz, 1955). The 180° twin boundaries may also be made visible with careful illumination, in the absence of external mechanical and electrical stress, showing up as thin white lines on a dark background. This is caused by local differences of refractive index, possibly due to boundary strain.

4.3.5 90° Domains

These are correlated in a different way, two individuals being related by twinning on faces of the form (011), and (101), which serve as the domain walls, the condition of no charge on the walls being fulfilled. Now in the tetragonal phase we have seen already that careful measurements have revealed a deviation of the axial ratio c/a from unity. More exactly the angle between individual twins is given by $2 \tan^{-1} c/a$ which for c/a = 1.011, is $90^{\circ}\ 38'$; hence the difference in the angle from 90° between them for this axial ratio is $38'$. Various values for this difference have been reported varying from $32'$ to $46'$, which is found to decrease to zero as the temperature approaches the Curie point. This may only be investigated using the methods of multiple beam interferometry (Bhide and Bhapat, 1961) and not the polarising microscope, since the difference in the refractive index of the individual twins near the Curie point is practically zero. From the above discussion it follows that domain configurations in which different 90° walls meet or intersect inside the crystal give rise to internal stresses.

Very often, twinning is repeated on the same plane giving rise to a series of lamellae, and with larger crystals, different regions use different planes of the same form as twin planes, giving sets of lamellae at right angles to each

other. This latter configuration has been very extensively investigated by Forsbergh (1949) who observed the continued appearance and disappearance of the resulting square net patterns on cooling and heating through the Curie point respectively. This seems to suggest a predetermined regularity in the factors which give rise to twinning, of an origin as yet not fully understood.

The microtopography for both the above types of twinning has been investigated by Bhide and Bhapat (1961) using Fizeau fringes (see R.S. Longhurst - Geometrical and Physical Optics, p.134). Their results clearly show the step ladder appearance of the surface for laminar twinning, that for laminar intersection being rather more complicated. Their work also clearly indicates the deformation suffered by the crystal when 90° wedge domains appear. An interesting aspect of their interferograms reveal that for a wedge shaped domain the tip of the wedge is at zero depth from the surface, and increases towards the base. Also, their growth is noted to be temperature dependent, though this dependence is not specified. These workers have attributed the growth mechanism of these domains to the marrying of a left-handed and right-handed screw dislocation resulting in their annihilation to form a wedge shaped domain. The nature of the interferograms was such as to conclude that the dipoles

were coupled in a head to tail fashion, which appeared to be a general rule for $BaTiO_3$, though head to head, and head to tail coupling also occurred.

Usually both 180° and 90° walls are present simultaneously. Of particular interest are the "domain reflections" revealed by the etch technique. To the extreme left of Fig. 4.8 there appears a distinct region (a) of inverted polarisation. To the right of the two very narrowly spaced sharp lines (two 90° walls) the mirror image (b) of this region is observed. The two sharp lines represent the boundaries of the wedge shaped (a) domain through which the reflection of the oppositely polarised region takes place. This arrangement shows the coupling of the dipoles in the forward direction. Also shown is a similar polarised region (c) reflected through a wide 'a'-domain to the right side of the figure at (d).

4.3.6 The Domain Walls

The essential geometrical difference between a 180° wall and a 90° wall with respect to domain orientation has already been mentioned. However, other characteristics exist which determine their physical differences.

4.3.7 180° Walls

The 180° wall appears to have a very simple structure. In calculating the energy of such a wall Merz (1954) represents the wall energy per unit volume by an expression of the form:

$$E_{wall} = AN + B/N$$

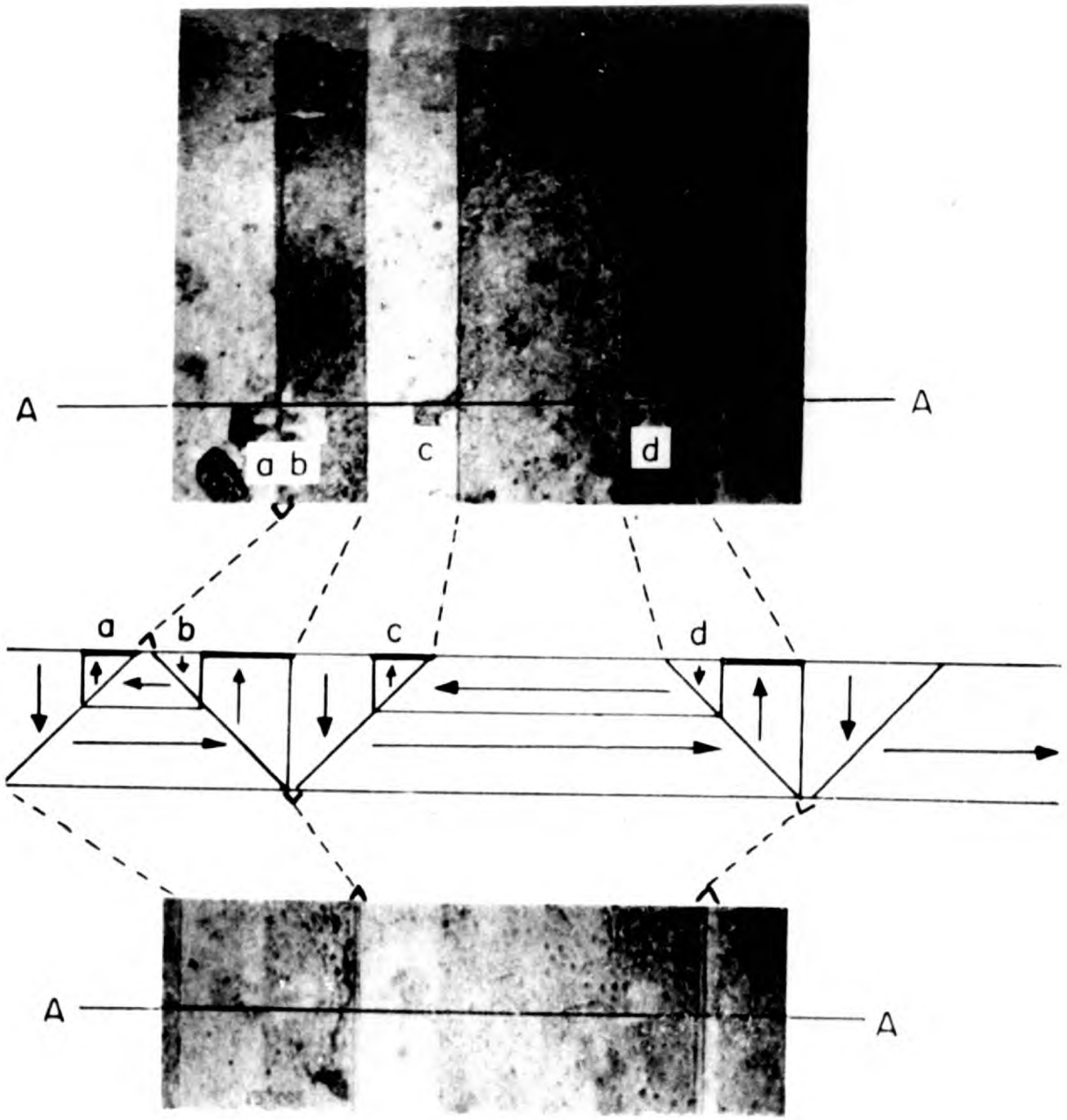


Figure 4.8

where B/N is the contribution due to dipole-dipole interaction, and AN is the contribution from anisotropy. N in both terms is the wall thickness in atomic separations, whilst A and B are constants. In substituting a value for B, the dipole energy was roughly estimated from calculations of dipolar interactions. The constant B in the anisotropy term, which is the elastic energy stored in the wall due to the spontaneous deformation, embodies the elastic constant C_{33} and the spontaneous strain along the ferroelectric axis, which on substitution of room temperature values, and minimising the above expression, lead to a wall thickness of one lattice unit. Substitution of this value of N leads to a wall energy of 7 erg cms^{-2}.

However Kinase and Takahasi (1957) contend that the B/N term involving dipole interaction is made up of two parts: (i) an interaction in a direction parallel to the polarisation, and (ii) perpendicular to the polarisation. It is this latter contribution, rather than the total contribution, as Merz assumes, that contributes to the wall energy. Their calculations result in the value 1.40 erg cms^{-2} for the wall energy, using a model of the wall accompanied by an abrupt change in the direction of polarisation.

4.3.8 <u>90° Walls</u>

These have a much more complicated interface, which for

geometrical reasons contain unit cells with anomalous strain. Kite shaped cells are contained in the wall and these contribute to the elastic energy. Little (1954) assumes two contributions to the wall energy. The first is given by a linear and continuous variation of the angle between the dipoles within the wall (c.f. Bloch wall in the ferromagnetic case); and the second is given by a term whose microscopic origins are not specified but which is postulated as being inversely proportional to the wall thickness. In this way she obtains for the wall energy, 65 erg cms^{-2}, and for the wall thickness 4000A or about 1000 lattice units. This value for the wall thickness has been verified optically. It may be noted that the wall thickness and wall energy for 90° walls is greater than that for 180° walls.

5. THEORIES FOR BARIUM TITANATE

5.1 GENERAL REMARKS

We may distinguish between two types of theory, the phenomenological theory and the model thoery, their approaches and purposes being different.

A phenomenological theory takes as its starting point an expression connecting all the properties of the material which are relevant to the purpose. Assumptions are then made as to which of the coefficients in the expression change during the process being considered, and which remain constant, this being based partly on experimental evidence and partly on judgment. Then with the help of thermodynamical laws, mathematical relations are established between these various quantities, which if some are known experimentally, enable others to be calculated. A phenomenological theory has the advantage in being independent of any particular model, but does not account for the mechanism responsible in altering the properties of a material; it is thus very general in its scope.

A model theory on the other hand begins by postulating a certain mechanism in the structure which is likely to explain some of the properties, which may be tested experimentally, and then goes on to deduce others, which may also be tested experimentally. A model theory is not used to predict

experimental behaviour outside the range of properties it is devised to fit.

5.1.1 Phenomenological Theory and Thermodynamics of the Transition

A phenomenological theory of $BaTiO_3$ due to Devonshire (1949, 1951, 1954) has been quite successful in accounting for the change in the properties of $BaTiO_3$ through the Curie point. He assumes that the tetragonal phase of the crystal is merely a strained form of the cubic phase, and considers the same expression in the cubic and tetragonal phases, for its free energy as a function of stress and polarisation. For a stress-free crystal the free energy is expanded in increasing powers of polarisation thus:

$$G-G_o = \tfrac{1}{2}\chi^x(P_x^2+P_y^2+P_z^2) + \tfrac{1}{4}\xi_{11}{}^x(P_x^4+P_y^4+P_z^4) + \tfrac{1}{2}\xi_{12}{}^x(P_y^2P_z^2+P_z^2P_x^2+P_x^2P_y^2) + \tfrac{1}{6}\zeta^x(P_x^6+P_y^6+P_z^6) + \ldots \quad (1)$$

where the superscript x indicates that the quantity is to be taken at constant stress, P_x, P_y, P_z are the components of polarisation along the x,y and z directions, and χ^x, $\xi_{11}{}^x$, $\xi_{12}{}^x$ and ζ^x are coefficients which strictly speaking depend on temperature. G_o, the zero point of free energy, is taken to be that of the unpolarised, unstressed crystal. Since the stress free case is being considered the free energy function is given by the elastic Gibbs function. In order to account

satisfactorily for the transition Devonshire found it necessary to consider terms up to P^6.

Now in the tetragonal phase the crystal is ferroelectric and is polarised along the c axis; thus $P_x = P_y = o$, and writing $P_z = P$, equation (1) reduces to:

$$G-G_o = \tfrac{1}{2}\chi^x P^2 + \tfrac{1}{4}\xi^x P^4 + \tfrac{1}{6}\zeta^x P^6 \qquad (2)$$

It may be shown from thermodynamics that the applied electric field and polarisation are related by:

$$E = \partial G/\partial P = \chi^x P + \xi^x P^3 + \zeta^x P^5 \qquad (3)$$

$$\text{hence } \partial E/\partial P = \partial^2 G/\partial P^2 = \chi^x + 3\xi^x P^2 + 5\zeta^x P^4 \qquad (4)$$

$$(\partial E/\partial P)\, P = o = \chi^x \qquad (5)$$

Hence χ^x is the dielectric stiffness (reciprocal susceptibility) for zero polarisation, and since it is large it is effectively equal to $\epsilon/4\pi$ whence $\chi^x = 4\pi/\epsilon$ for the unpolarised crystal; equation (4) gives the value of the dielectric stiffness for the polarised crystal, and hence the dielectric constant would depend on ξ^x and ζ^x.

The onset of spontaneous polarisation may be explained by considering the effect of the coefficients in equation (2) on a plot of $G-G_o$ against P. Devonshire assumed that χ^x changed continuously with decreasing temperature through zero, to assume negative values. The experimental evidence for this

comes from the Curie-Weiss law, where a plot of $\frac{1}{\epsilon}$ against T gives a straight line, the same graph establishing the value of T_o, the extrapolated Curie temperature. He assumed further that ξ^x is negative and ζ^x positive, "in order to account for the observed facts", and also temperature independent. The assumption of negative ξ^x means that the transition is of the first order, though decisive evidence for this was not forthcoming for a few years yet, until Roberts (1952) detected the latent heat of the transition. Now by inspection of equation (2), for P = 0, $G-G_o = 0$ and the curve of $G-G_o$ always goes through the origin. For χ^x positive the $G-G_o$ curve first goes through a maximum, for finite values of the polarisation, decreases through a minimum, and then increases again with increasing polarisation. This is repeated for negative values of the polarisation, since equation (2) is symmetrical in P. Further the curve changes from a minimum to a maximum at the origin according as χ^x is positive or negative, as may be seen from equation (3). There is a certain temperature range in which there are three minima and one particular temperature at which they are all of equal depth. This is the transition temperature, which corresponds to a stable state for both zero and finite values ($\pm$) of the polarisation.

Now since $G-G_o = 0$ for P = 0, and in this case also for $P = P_s$ since this also represents a stable state, and since

$\partial G/\partial P = 0$ at a maximum then we have from equations (2) and (3) respectively:

$$\tfrac{1}{2}\chi^x P_s^2 + \tfrac{1}{4}\xi^x P_s^4 + \tfrac{1}{6}\zeta^x P_s^6 = 0 \qquad (6)$$

and $$\chi^x P_s + \xi^x P_s^3 + \zeta P_s^5 = 0 \qquad (7)$$

hence: $$P_s^2 = \tfrac{3}{4}(-\xi^x/\zeta^x) \qquad (8)$$

and $$\chi^x = \frac{3}{16}(\xi^x)^2/\zeta^x \qquad (9)$$

Now on one side of the transition P is zero; on the other it jumps suddenly to a finite value, P_s - i.e. it changes discontinuously. At the transition χ^x is not zero but positive, and the dielectric stiffness given by equation (4) changes discontinuously since the polarisation does so; hence the dielectric constant changes discontinuously as well.

The free energy in the region of the Curie point is shown plotted against the polarisation with the absolute temperature as the parameter, Fig. 5.1 (Drougard, Landauer and Young, 1955). It may be noted that the temperature hysteresis occurring for measurements on the dielectric constant, (see earlier chapter) is because of the potential hump between the polarised and the unpolarised state.

Equations (8) and (9) permit determination of the coefficients ξ^x and ζ^x since they may be re-written:

$$\xi^x = \frac{-4\chi^x}{P_s^2} \qquad (10)$$

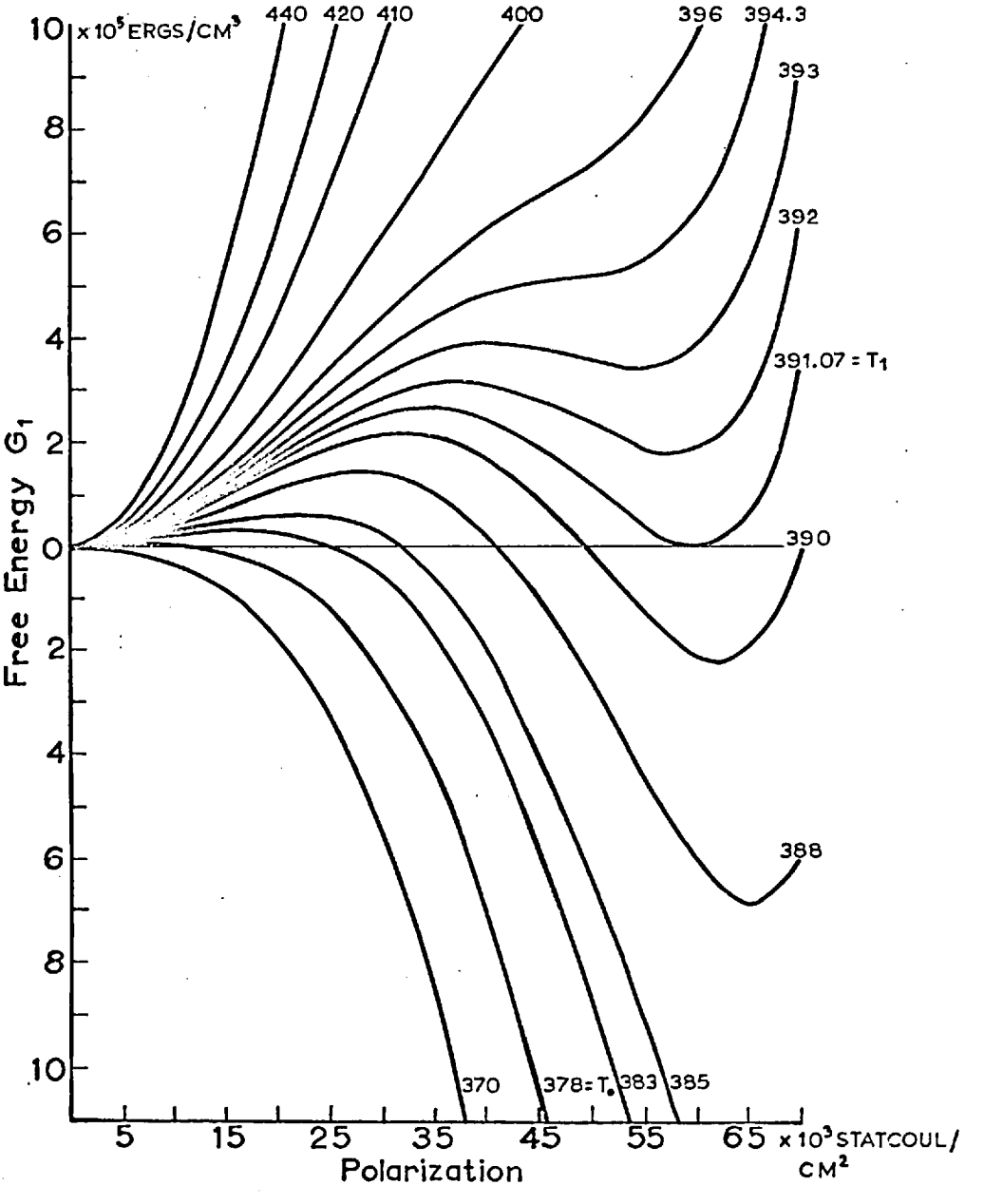

10
x 10⁵ ERGS/CM³
440
420
410
400
396
394.3
393
392
391.07 = T₁
390
388
370
378 = T₀
383
385
8
6
4
2
0
2
4
6
8
10
Free Energy G₁
5
15
25
35
45
55
65
x 10³ STATCOUL/CM²
Polarization

Fig. 5.1.

and $$\zeta^x = \frac{3\chi^x}{P_s 4} \qquad (11)$$

where χ^x is the value of the susceptibility at the Curie point. Since $\chi^x \simeq \frac{\epsilon}{4\pi}$, it is thus equal $\frac{4\pi}{C}(T_1 - T_o)$. The right hand side of equations (10) and (11) are in terms of measurable quantities.

The values of these coefficients obtained by various workers are tabulated below. The values in brackets beside Merz are more reliable values on better crystals by direct observation of hysteresis loops. Devonshire's values are those calculated using the rather low values at the transition temperature of P_s due to Hulm, i.e. $10\mu C\ cms^{-2}$, as opposed to later determinations of $18\mu C\ cms^{-2}$ which since it is raised to the second and fourth powers in the denominator has a considerable effect on the final result

	$\xi^x(T_1)$ cgs	ζ^x cgs
Merz (1953)	-6.8×10^{-13} (-10.8)	2.28×10^{-22}
Devonshire (1949)	-44×10^{-13}	37.0×10^{-22}
Drougard et al (1955)	-10.8×10^{-13}	

Direct measurement of ξ^x (Drougard et al, 1955) in the paraelectric region has shown that it is not temperature-independent, as assumed by Devonshire, but that it decreases by about 50% in 30^oC above the Curie point - Fig. 5.2. No temperature variation of ζ^x was detected in this region.

Now from equation (4) we can write for the dielectric constant

$$\frac{4\pi}{\epsilon} \simeq \frac{\partial E}{\partial P} = \chi^x + 3\xi^x P^2 + 5\zeta^x P^4 \qquad (12)$$

and knowing the coefficients in the free energy expansion, the spontaneous polarisation is obtained by solving equation (7), and the dielectric constant from equation (12); the resulting theoretical curves obtained by Devonshire though qualitatively in good agreement with the experimental curves, are not quantiatively exact.

Devonshire also considered the effect of stress on the crystal, and expanded the free energy as a function of the polarisation and the strain, extra terms being added involving the strains, the elastic coefficients and piezoelectric coefficients. The relevant free energy function in this case is the Helmholtz free energy, the expansion being:

$$A-A_o=\tfrac{1}{2}\chi^x(P_x^2+P_y^2+P_z^2)+\tfrac{1}{4}\xi^x_{11}(P_x^4+P_y^4+P_z^4)+\tfrac{1}{2}\xi^x_{12}(P_y^2P_z^2+P_z^2P_x^2+P_x^2P_y^2)$$

$$+ \ldots\ldots + \text{terms in } (C_i, \varkappa_i) + \text{terms in } (g_j \varkappa_j P_j) + \ldots. \qquad (13)$$

where A_o is the zero of the free energy corresponding to the unpolarised, unstrained state, the C_i's are elastic coefficients, the g_j's piezoelectric coefficients, the $\varkappa_i$'s and $\varkappa_j$'s components of the linear strains, and P_j's components of the polarisation. No differentiation of A with respect to each of the components of strain gives the corresponding stress, i.e. $X_i = \left(\frac{\partial A}{\partial \varkappa}\right)_x$ which

if assumed zero then gives a set of equations of the strain in terms of the polarisation, from which it is seen that the strains are proportional to the square of the polarisation. The numerical factors in this proportionality bring in the elastic constants, which are evaluated by calculating the theoretical value of each kind of strain at a given temperature and equating it to a value derived from determinations of the cell dimensions at that temperature. Once these numerical factors are known the variation of strains with temperature was deduced. Again, agreement between theory and experiment is only quantitative, and not exact. This is probably due to the fact that the above constants were evaluated in terms of the early known quantities at room temperature only, which later work has shown to be erroneous.

Devonshire (1954), in a later paper, discusses the effect of clamping on the nature of the transition. Just as the magnitudes and signs of the coefficients χ^x, ξ^x, ζ^x have an important bearing on the stress-free transition, so also are χ^x, ξ^x, ζ^x important for the strain-free condition. It turns out that by comparing coefficients for components of the field for the stress-free and strain-free conditions that $\chi^x = \chi^x$. Also, it turns out that whereas ξ^x was negative, ξ^x is positive. This means that the transition for the clamped crystal is of the second order.

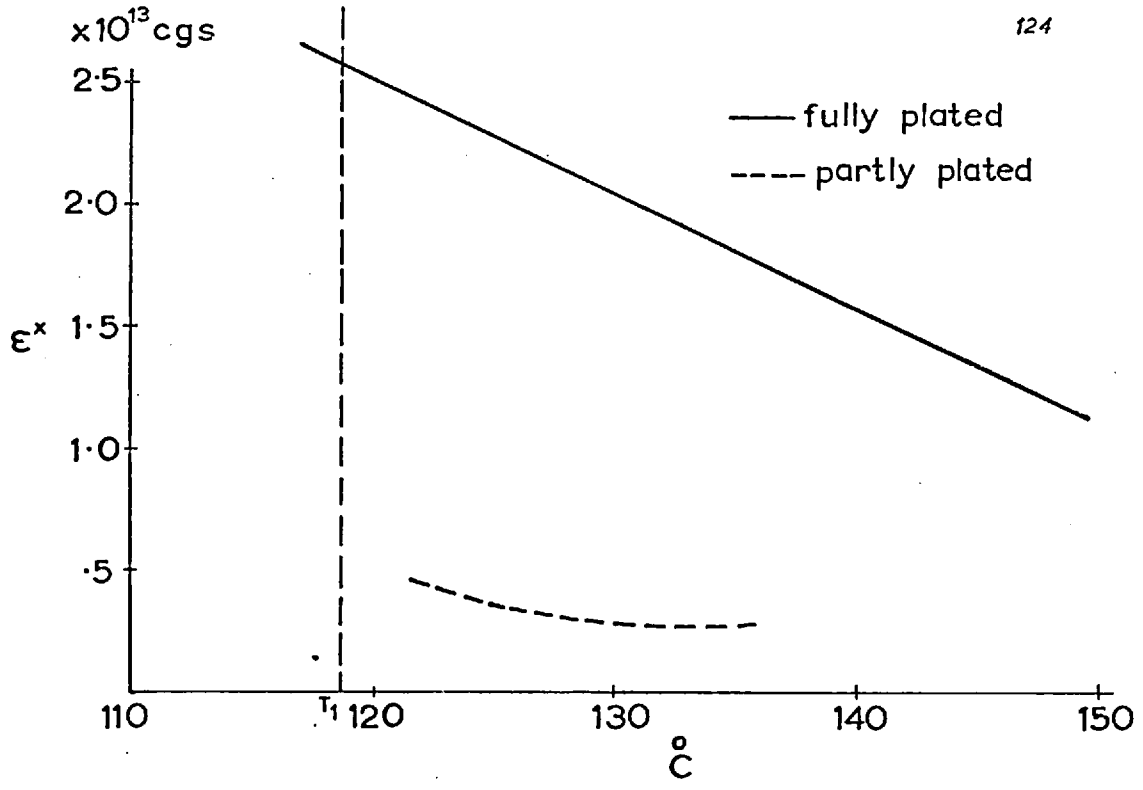

x10^13 cgs
2·5
2·0
ε^x 1·5
1·0
·5
fully plated
partly plated
110
T1
120
130
140
150
°C

Fig. 5.2

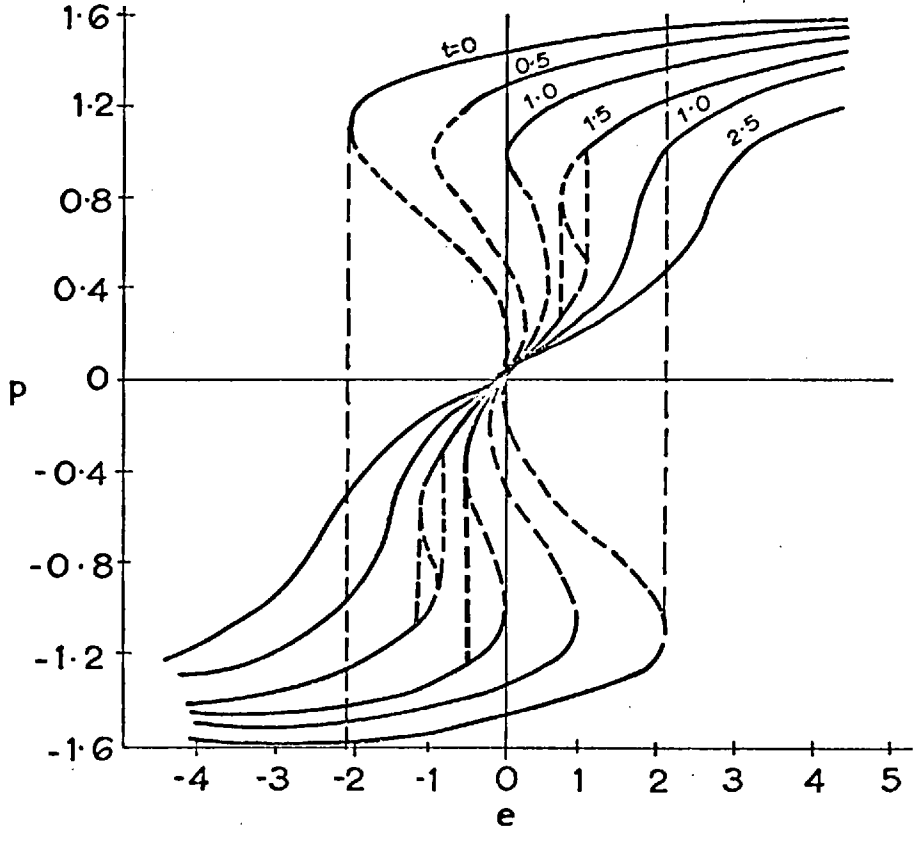

1·6
1·2
0·8
0·4
0
-0·4
-0·8
-1·2
-1·6
p
t=0
0·5
1·0
1·5
1·0
2·5
-4
-3
-2
-1
0
1
2
3
4
5
e

Fig. 5.3.

Merz (1953) has shown how Devonshire's theory accounts for the double hysteresis loops characteristic of an induced transition just above the Curie point. He expresses Devonshire's relations in the form:

$$\chi^x = 2A(T-T_o) \qquad (a)$$
$$\xi^x = -4 \qquad (b)$$
$$\zeta^x = 6C \qquad (c) \qquad (14)$$

and goes on to define new dimensionless parameters thus:

$$p = (3C/B)^{\frac{1}{2}} \qquad (a)$$
$$e = 1/B\ (3C/B) \qquad (b)$$
$$t = A/B\ (3C/B)(T-T_o) \qquad (c) \qquad (15)$$

hence equation (3) can now be written in the form:

$$e = 2pt - 4p^3 + 2p^5 \qquad (16)$$

and is shown plotted in Fig. 5.3 for different values of t. This figure, which represents the reduced curves of polarisation versus field at different temperatures, explains the existence of hysteresis loops, since regions in which $\partial e/\partial p$ is negative represent unstable states and the crystal switches over to a state with positive $\partial e/\partial p$ and the same e, as shown by the vertical dashed lines. The existence of forced dielectric hysteresis brought about by large fields at temperatures just above the normal transition temperature is also explainable. For example at t = 1.5, there is only one stable state for e = 0, but for e = 1 there are two states for p, at approximately

0.4 and 1.0. Dielectric hysteresis loops are formed in this region, and in the corresponding region near e = -1, the curve joining them being nearly a straight line.

Now the existence of these forced loops depends on the negative value of ξ^x, since if ζ^x is positive and constant, then $\partial^2 e/\partial p^2$ always has the same sign as p, as may be seen from equation (3) and hence $\partial e/\partial p$ cannot change sign twice in a region where p does not change sign, as would be needed to make a forced hysteresis loop. Hence forced loops may only be obtained for first order transitions.

Merz has checked the experimental curves of P versus E against the theoretical curves of p versus e by finding the scaling constants P/p and E/e for a few points on the curve, and found satisfactory agreement. This confirms the assumptions made about the constant χ, ξ, ζ, in the free energy expansion. However the temperature dependence of ξ^x in the paraelectric state contradicts the theory (Drougard et al, 1955). It is possible that closer quantitative agreement between theory and experiment may be obtained by investigating the behaviour of this coefficient through the Curie point, more thoroughly.

The entropy of polarisation which may be calculated from Devonshire's free energy expansion, is given by the relation

$$S = -\left(\frac{\partial G}{\partial T}\right)_{P,X} \qquad (17)$$

and hence the change in entropy at the transition is given by:

$$\Delta S = S - S_o = \tfrac{1}{2}P_s^2 \frac{d\chi^x}{dT} - \tfrac{1}{4}P_s^4 \frac{d\xi^x}{dT} - \cdots\cdots \qquad (18)$$

where S_o is the entropy for zero polarisation,

$$\Delta S \approx -\tfrac{1}{2}P_s^2 \frac{d\chi^x}{dT} = -\tfrac{1}{2}P_s^2\left(\frac{4\pi}{C}\right) \qquad (19)$$

if one assumes higher order terms of the polarisation are negligible. Since all the terms in equation (19) are known it is possible to test its validity, and observed and calculated entropy changes are in fact in satisfactory agreement.

A criticism of Devonshire's theory is the use of the same expression for the free energy above and below the transition implying a continuity of the constants across the Curie point, while a first order transition is essentially discontinuous (Jaynes, 1952). The objection, though valid, does not answer the fact that the same set of constants predicts with reasonable accuracy the values experimentally observed in the two temperature ranges. Further, in order to treat the transition as first order, it is necessary to look on it as being caused by the more or less accidental crossing of two entirely different free energy functions representing the two phases, each of which can persist a short distance into the temperature range where the other is the

stable form. A first order phase change does indeed imply a discontinuity in the spontaneous polarisation and a discontinuous change in the lattice parameters, together with the existence of a latent heat at the transition. However there does not appear to be any limitation on the smallness of the discontinuities. In practise it is very difficult to distinguish between really discontinuous changes and very sharp but continuous changes. This is especially important for the case of $BaTiO_3$ where internal strains, render the change sluggish. Perhaps the argument may best be treated as an example of the difficulty in attempting a satisfactory definition of first and second order transitions.

5.2 MODEL THEORIES

5.2.1 Introduction

The account of the various individual model theories given below includes the basic assumptions put into the theories and the results that can be drawn from them. The detailed mathematical treatment is not included.

In the construction of a model theory, some feature of the unit structure is considered which can give rise to two different states having slightly different energies. In the earlier theories, the experimentally observed properties were explained, more or less, in terms of the dipolar interaction contained between the various unit structures. Here the

emphasis was placed on the long-range forces where the state of each unit is independent of its neighbours except through the effect of the internal field. This effect, which involves assumptions about the field-factor of the internal field is used to calculate the possible energy states of each unit.

However it is by no means obvious that short-range forces, not electrostatic in origin, are of no consequence. With these forces the state of each unit is affected by the state of its neighbours. These forces may be presumed to exist if only to provide finite limitations on the bulk compressibility of the solid.

Before reviewing the various theories of the ferroelectric behaviour in $BaTiO_3$ a brief discussion of some aspects of dielectric theory in general is given for linear behaviour in the paraelectric region.

5.2.2 Polarisation and Susceptibility

Consider an array of dipoles, n per unit volume, each of moment μ (or if permanent dipoles, a moment with average vector component μ), then the net polarisation due to this array is defined thus:

$$P = n\mu \qquad (1)$$

The local field acting on each dipole due to the whole array

may be expressed as a power series in P;

$$E_{loc} = \beta P - \xi^{x} P^{3} - \zeta^{x} P^{5} \qquad (2)$$

the restriction to odd powers ensuring that E_{loc} changes sign but not magnitude when P changes sign. If now an external field E is applied, then for small P the effective field acting on the dipoles is F,

$$F = E + P\beta \qquad (3)$$

Assuming that the net dipole moment is proportional to the effective field inducing it, their ratio is defined as the macroscopic polarisability per unit volume α_m/v where v is the volume of the unit cell

$$P = \frac{\alpha_m}{v} F \qquad (4)$$

since the polarisation is the dipole moment per unit volume. Combining equations (3) and (4)

$$P = E/\left(\frac{v}{\alpha_m} - \beta\right) \qquad (5)$$

and the susceptibility χ defined as (P/ E) is given by:

$$\chi = 1\left(\frac{v}{\alpha_m} - \beta\right) = \frac{\alpha_m/v}{1 - \beta\alpha_m} \qquad (6)$$

If β is taken to be constant, and $^{v}/_{\alpha_m}$ is temperature dependent, then at some temperature $^{v}/_{\alpha_m}$ equals β , and the susceptibility χ and hence also the dielectric constant becomes infinite. This temperature may be denoted by T_o.

5.2.3 The Internal Field

In an early treatment of the internal field it was shown that a randomly-placed array of point dipoles in parallel orientation gave a field factor of $4\pi/3$, as also did an array of similar dipoles on a simple cubic lattice (Lorentz, 1916). The condition of parallel orientation does not hold for models with permanent dipoles since these are misoriented due to thermal motions. Onsager (1936) put forward an alternative theory when he postulated that the neighbours of any misoriented dipole at a given instant were in equilibrium with it by following its movements without any time lag. In Lorentz's theory they remained unaffected by it. Actually, Devonshire (1954) suggested something between the two was the more likely. Onsager's theory gives the value of the internal field as βP where β is not constant but dependent on the dielectric constant ϵ .

For dipoles of fixed direction it appears that the Lorentz field is applicable provided that the array is either random or on special positions on the triad axis of a cubic structure. This condition however is not fulfilled in the case of $BaTiO_3$. In this case the variation in the internal field from point to point inside the unit cell has to be taken into account. Now in each unit cell there are several independent dipoles, each of which is repeated

throughout the lattice to give a set characterised by its own internal field. The field due to a set i which acts in a given direction at a vector distance r_i from the dipole in the same unit cell is calculated and expressed in terms of a scaler constant β_r. If the polarisation of this set of dipoles is P_i then its contribution to the internal field is $\beta_r P_i$ and hence the total internal field at any point is the sum of such contributions, the β_r's being worked out for the vector distances of the various dipoles from the point. This method has been used by Slater (1950).

5.2.4 Polarisability

Now from equation (6) the polarisability may be rewritten thus,

$$\frac{\alpha_m}{v} = \frac{\chi}{1+\beta\chi} \qquad (7)$$

where v is the volume of a unit cell, and since $\epsilon = 1 + 4\pi\chi$, and using the value $4\pi/3$ for β

becomes $$\frac{4\pi}{3}\frac{\alpha_m}{v} = \frac{\epsilon - 1}{\epsilon + 2} \qquad (8)$$

This is known as the Clausius-Mosotti relation, and serves to define α_m in terms of the measurable ϵ. Strictly, this relation holds only for those crystals where the Lorentz theory is applicable.

Suppose a structure contains two different kinds of dipoles which give rise to polarisations P_1 and P_2, then

the resultant polarisation is the sum of the two individual polarisations and they both give contributions to the internal field at a given point, though not necessarily having the same field factor. Hence the equation in this case corresponding to (3) is,

$$F = E + \beta_1 P_1 + \beta_2 P_2 \qquad (9)$$

It is then possible to express the dielectric constant (assumed independent of E) as a function of one of the polarisations.

Let the first set of dipoles have a polarisability $\gamma_1 v$ where γ_1 is defined by,

$$P_1 = \gamma_1 F \qquad (10)$$

$$\text{then} \qquad F = \frac{E + \beta_2 P_2}{1 - \beta_1 \gamma_1} \qquad (11)$$

$$\text{and} \qquad P = \frac{\gamma_1 E}{1 - \beta_1 \gamma_1} + P_2 \left[\frac{1 + \beta_2 \gamma_1}{1 - \beta_1 \gamma_1} \right] \qquad (12)$$

and since $\epsilon = 1 + 4\pi P/E$ then,

$$\epsilon = 1 + \frac{4\pi\gamma_1}{1 - \beta_1\gamma_1} + \frac{4\pi P_2}{E} \frac{(1+\beta_2\gamma_1)}{1 - \beta_1\gamma_1} \qquad (13)$$

5.2.5 The Mason-Mathias Theory

Mason and Mathias (1948) have put forward a theory which is essentially one of permanent dipoles capable of taking up anyone of six positions. At high temperatures all positions are equally probable, but at low temperatures an ordered

arrangement results. The dipole is assumed to be a result of the displacement of the titanium ion to an off-centre position, towards one of the six oxygen ions which surround it in the form of an octahedron. The double potential energy wells separating two oxygen ions on either side of a titanium ion have a barrier between them of height Δu. The dipole moment is proportional to δ, "the displacement of the titanium ion from its mid position of the unit cell" but there may also be some added contribution "if the oxygen moves in towards the titanium". The polarisation consists of two parts; a part P_d due to dipole polarisation, and a part P_a due to all other effects other than the Ti displacements. Both these contribute to the internal field, the field factor of $4\pi/3$ being used for both. Application of an external field along an axis would change the energy of the dipoles associated with the two wells, along that axis, that of the other four remaining unaltered.

They obtain the following expression for the polarisation due to these titanium dipoles:

$$P' = \frac{\sinh\left[a\,(P' + \frac{E}{\beta n\mu})\right]}{2 + \cosh\left[a\,(P' + E/\beta n\mu)\right]} \qquad (14)$$

where the quantity $a = \frac{n\mu 2\beta}{kT(1-4\pi\gamma/3)}$, and $P' = P_z/n\mu$.

The condition for spontaneous polarisation is that P' has

non-zero values for E = 0; this turns out to be that;

$$a \geqslant 3 \tag{15}$$

at the Curie point therefore,

$$T_o = \frac{\beta n \mu^2}{3k(1-4\pi\gamma/3} \tag{16}$$

The expression for the Curie constant obtained is

$$C = \frac{4\pi aT}{3\beta}\left(1 + \frac{\beta\gamma}{1-4\pi\gamma/3}\right) \tag{17}$$

Equations (16) and (17) allow the evaluation of β and μ since they are given in terms of experimental parameters. They found the value of β to be 0.142, this small value indicating strong shielding of the dipoles, and μ to be 1.56×10^{-18} cgs units. From these numerical values, those calculated for the spontaneous polarisation and dielectric constant in the tetragonal phase gave good agreement with experiment.

Jaynes (1952), in criticizing the theory has pointed out that because of the six possible positions of the dipole it would predict an entropy change of $k \log_e 6$ per unit cell, i.e. 3.6 cal mol^{-1} deg^{-1} whereas the observed value is 0.12 cal mol^{-1} deg^{-1}.

In Mason's (1951) second form of the theory β is made an adjustable parameter; this gives closer agreement with experiment, but the discrepancy in the entropy remains. This would suggest perhaps that the answer to this particular theory is not to be sought in trying to improve on values for

the internal field.

5.2.6 Devonshire's Model Theory

Devonshire (1949) regards $BaTiO_3$ as an ionic crystal and unlike the previous theory, the dipole moment of an atom vibrating in the field of its neighbours not of constant magnitude, but dependent on the displacement r from the equilibrium position. The potential energy of an ion is assumed to be of the form $ar^2 + br^4$, which is seen to change more rapidly than it would for a harmonic oscillator. The values of 'a' and 'b' are different for the different ions and were evaluated from the force constants of the structure using the Born-Mayer postulate, namely that each pair of ions with charges e_1 and e_2 separated by a distance r, has a potential energy of the form,

$$\frac{e_1 e_2}{r} - \frac{\phi}{r^6} + \frac{\nu}{r^9} \qquad (18)$$

The dipole moment is proportional to the displacement r and to a quantity z which represents the charge.

Devonshire derived the coefficients in his free energy expansion $\chi^x \xi^x \zeta^x$ in terms of a, b, z and β, which was assigned the Lorentz value $4\pi/3$. He made numerical estimates of quantities derived from these, which agreed with the experimental observations. His analysis showed, and experiment on the temperature coefficient of polarisability confirmed, that an anharmonic term was required for the potential energy of the

atomic vibrations. The use of the value $4\pi/3$ for the field factor is doubtful.

5.2.7 Slater's Theory

Slater (1950) has modified Devonshire's model theory and introduces two new features which are dealt with below. His model was that of Megaw who suggested that the titanium ion could move rather freely in the comparatively large volume available to it within the oxygen octahedron.

The first new feature of Slater's theory is the emphasis on the physical meaning of the polarisabilities where each atom is assumed to have an electronic polarisation and only the movement of titanium ion an ionic polarisation. These may be denoted by α_j and β_i. From equation (6) we have seen that the condition of an infinite dielectric constant is that $\beta\alpha_m/v = 1$, which becomes on replacing α_m by the sum of the separate polarisabilities, and β by the Lorentz factor $4\pi/3$,

$$\frac{4\pi}{3}\left[\sum\left(\frac{\alpha_j}{v}\right) + \frac{\alpha_i}{v}\right] = 1 \qquad (19)$$

Now the values of α_i/v are known experimentally for barium and titanium, but uncertainty exists in assigning a value to oxygen since it varies from compound to compound. He chose a value for oxygen such that the electronic polarisability of the crystal as a whole was correct. The electronic polarisability α_e is defined by an equation analagous to equation (8) where α_m is replaced by α_e and the dielectric

constant by the square of the refractive index, n. Slater finds that ferroelectricity occurs when

$$\frac{4\pi}{3} \quad \frac{(\alpha_i)Ti}{v} \quad = 0.39 \qquad (20)$$

The second new feature of Slater's theory involves a recalculation of the field constant β which is based on the actual arrangements of the ions themselves rather than on the assumption of a Lorentz factor $4\pi/3$.

Consider a simple cubic lattice Fig. 5.4 of side 'a', containing point dipoles at the origin of coordinates A, the dipole direction being AA'. According to the Lorentz treatment the field factor is $4\pi/3$ at other lattice points such as A' and A'' but not at B,C,D etc. However it is possible to evaluate the field at all these intermediate points (Luttinger and Tisza, 1946; 1947). The results show a very large value of the factor at points midway between dipoles, in the direction of their dipole moment. Slater on this information, then derives a set of equations giving the effective field acting on each ion which takes the form

$$F_x = E + \sum \beta_y P_z \qquad (21)$$

where the subscripts x and z refer to the type of ion, and y to the lattice site. Since the polarisation of each atom is known in terms of its polarisability and the field acting on it given by a set of equations such as

$$P_x = \left(\frac{\alpha_j}{v} + \frac{\alpha_i}{v}\right) F_x \qquad (22)$$

where F_x is given by equation (21), then the set of equations (22) may be solved to give the separate polarisation of each atom and the dielectric constant of the whole crystal.

If the electronic polarisabilities are all zero then,

$$\frac{4\pi}{3} \frac{\alpha_i}{v} = 1 \qquad (23)$$

and if the ionic polarisability is that due to titanium movement alone the calculation reveals,

$$\frac{4\pi}{3} \cdot \frac{\alpha_i}{v} = 0.06 \qquad (24)$$

Equation (24) shows that the ionic polarisability of titanium is about 1/16 of what it would need to be in the absence of electronic polarisability, and 1/6 if the field factor $4\pi/3$ is applied throughout (c.f. equation (20)). The theory shows that a small ionic polarisation is greatly enhanced due to a large electronic polarisability as a result of the particular factors which in turn is due to the arrangement of the atoms in rows of alternating titanium and oxygen.

In criticising Slater's theory it has been pointed out that since the internal field acts on the displaced atoms then the assigned β values ought to be those at these displaced positions and not as Slater assumed, those for special positions with all coordinates 0 or $\frac{1}{2}$. Also, it was found that nothing in the theory which favours parallel displacement of the titanium - oxygen chain; it is rather an antiparallel

displacement that is favoured (Cohen, 1951).

Further there seems to be no real justification for assigning the whole ionic polarisation to titanium alone; this seems to have been done because the large volume available to it suggested a looseness of binding. The occurrence of spontaneous polarisation in the direction of the titanium - oxygen chains which is predicted very naturally does not appear to hold for the two lower phases where the direction of the spontaneous polarisation does not coincide with the titanium - oxygen chains.

5.2.8 Oxygen Displacement Theory (Jaynes)

This theory has been put forward by Jaynes (1952) who argues that if $BaTiO_3$ is considered an ionic crystal then any picture based on the concept of rather freely movable ions must consider motions of the oxygen ion to be as important as that of the titanium ion. Actually his model, in which the atoms are treated as rigid spheres, considers the oxygen displacement as the active cause of ferroelectricity and is capable of explaining in a simple intuitive manner the existence of the three phase transitions.

Now since each unit cell has three oxygen ions O_x, O_y, O_z which are considered free to move in the x,y,z directions respectively, then as the crystal is cooled the mismatch of ionic sizes successively causes the O_z then the O_y and then

the O_x ions to be squeezed out of their planes of barium ions thus causing spontaneous polarisation along a cube edge, then a face diagonal, and then a body diagonal as is observed experimentally. Using a simple geometrical argument based on hard spheres in contact he obtains the following relationship between the strain and the oxygen dipole polarisation,

$$-\frac{\Delta a}{a} = 3.8 \times 10^{-12} P_d^2$$

where P_d is in $\mu C\ cm^{-2}$ (25)

Now $-\Delta a/a$ is found to be proportional to the square of the polarisation with a coefficient of 1.2×10^{-12} (Merz, 1949), and Jaynes then concludes from this that the transverse contraction is given correctly if P_d represents just over half the total polarisation.

Though the approach is interesting and unusual, because predictions of the model may be seen qualitatively by simple physical reasoning without mathematical analysis, it is difficult to draw any serious conclusions from it, in view of the rather circular arguments proposed, also, though the oxygen ion undergoes displacement as verified by X-ray and neutron diffraction, considerable doubt is expressed concerning the true ionic nature of $BaTiO_3$.

5.2.9 Electronic Theory

The abnormally high polarisability of oxygen in the presence of titanium as compared in other oxides (Shockley,

1948), and the fact that all substances are ferroelectric in which an atom or ion with a closed shell structure is surrounded by an octahedron of oxygen ions in the manner of the structure of $BaTiO_3$ (Mathias, Wood and Holden, 1949), led Jaynes to adopt the view that $BaTiO_3$ is not a strongly ionic crystal and that the electronic structure is such that the oxygen octahedron must be thought of as a single unit rather than as a structure of several independent parts. It was this structure, rather than the presence of any specific positive ion, that was considered the necessary element for producing ferroelectricity.

He assumes further that each octahedron possesses an internal electronic quantum state independent of the state existing in adjacent cells, and due to its central symmetry each of these cells has a definite parity. Spontaneous polarisation and an internal electric field may then arise if there is interaction between octahedra possessing two states of opposite parity which lie close together in energy so that the combination has a non-zero dipole moment.

The electronic model is able to explain the Curie-Weiss law, the observed dielectric constant at high temperatures and the magnitude of the polarisation at low temperatures. Jaynes finds that the theoretical entropy change agrees with that observed. This is a consequence of the energy difference

between two states of the octahedron being $4kT_o$ where k is Boltzmann's constant and T_o is the extrapolated Curie temperature.

Jaynes cites as evidence for the electronic theory the case with which the polarity of $BaTiO_3$ may be flipped in contrast to that of other pyroelectric substances such as tourmaline where there is little doubt that the movement of ions is the cause of polarisation. However this is merely a qualitative argument. The theory predicts further an infra-red absorption line at about 10 microns corresponding to the initial level separation $4kT_o$. This, however, has so far not been experimentally observed.

5.2.10 Megaw's Theory

In contrast to the long range forces of dipole interaction embodied in the above models, Megaw (1952, 1954) approaches the problem in another way. She considers the transition as being associated with a change of the type of chemical bonding rather than a change in the dipole structure. The importance of the homopolar character of the bond is emphasised and the bond angles of the O_{11} ions with the Ti were considered an essential factor for the tetragonal structure. Her treatment is based entirely on these short range forces though they are not considered to provide the driving force which induces the ferroelectric transition.

5.3 LATTICE DYNAMICS THEORY

5.3.1 Introduction

The ferroelectric properties of a cubic crystal with the perovskite structure depend on macroscopic displacements of the atoms comprising the crystal in response to changes in temperature. It would seem therefore that such crystals are natural objects of study for the dynamical theory of crystal lattices which is concerned with the microscopic displacements of the atoms in the crystal in response to local temperature fluctuations, i.e., the normal modes of vibration of the crystal.

The condition that a crystal should be stable for all small deformations is that all the normal modes should have real frequencies (Born and Huang, 1954). The limit of stability against a particular mode of vibration is approached as the corresponding frequency approaches zero. In an harmonic crystal any displacement of the ions may be expressed as a sum of the normal modes of vibration, and the whole crystal is stable provided each normal mode is stable independently. When anharmonic interactions are present the energy required to distort the crystal can no longer be obtained as a sum of normal mode displacements.

5.3.2 Theory of Ferroelectricity (Cochran)

For a diatomic cubic crystal the frequencies of the

transverse optic (T.O.) and longitudinal optic (L.O.) modes of wave vector q ($q = 2\pi/\lambda$) zero is given by (Cochran, 1959)

$$\mu\omega_T^2 = R_o' - 4\pi(\epsilon + 2)(Z'e)^2/9v \qquad (1)$$

$$\mu\omega_L^2 = R_o' + 8\pi(\epsilon + 2)(Z'e)^2/9v\epsilon \qquad (2)$$

where μ is the reduced mass of the ions, ϵ the high frequency dielectric constant (square of the optical refractive index), and v the volume of the unit cell. $Z'e$ is the effective ionic charge, while $R_o'\vec{u}$ is the restoring short-range force on any one atom when the two lattices carrying nuclei of different type are displaced a small relative distance $\vec{u}$. R_o' arises from the short-range interaction while the other expression on the right-hand side in the above equations is due to the Coulomb interaction. Consider the situation that would arise if their difference approached zero. It is found from the theory (Woods et al, 1959) that ω_T may approach zero without the crystal necessarily becoming unstable against other vibration modes. The quantities which appear on the right of equation (1) may be temperature dependent since the lattice vibrations are in practice not completely harmonic so that near $T = T_c$ it is postulated

$$\frac{\mu\omega_T^2}{R_o'} = 1 - \frac{4\pi(\epsilon + 2)(Z'e)^2}{9vR_o'} = \gamma(T - T_c) \qquad (3)$$

where γ is a temperature coefficient and T_c is the temperature

at which the crystal becomes unstable. Now by the Lyddane-Sachs-Teller relation

$$\omega_L^2/\omega_T^2 = \epsilon_o/\epsilon \qquad (4)$$

where ϵ_o is the static dielectric constant. Combining these equations gives,

$$\frac{\epsilon_o - 1}{4\pi} \simeq \frac{\epsilon_o - \epsilon}{4\pi} \simeq \frac{(\epsilon + 2)^2(Z'e)^2}{9vR_o'\gamma(T - T_c)} \qquad (5)$$

so that a Curie-Weiss law is followed with a Curie constant

$$C = (\epsilon + 2)^2(Z'e)^2/9vR_o'\gamma \simeq (\epsilon + 2)/4\pi\gamma \qquad (6)$$

the condition $\epsilon_o \to \infty$ corresponds to $\omega_T^2 \to 0$. The ionic polarisability of one unit cell is found to be given by

$$\alpha_i = (Z'e)^2/R_o' \qquad (7)$$

while the electronic polarisation is given by

$$4\pi\alpha_e/3v = (\epsilon - 1)/(\epsilon + 2) \qquad (8)$$

The condition $\omega_T^2 = 0$ is the same as

$$(4\pi/3v)(\alpha_i + \alpha_e) = 1 \qquad (9)$$

so that the terms "instability" and "polarisability catastrophe" are synonymous in this case.

If the short-range potential between the two lattices is not exactly harmonic or isotropic for comparatively large displacements then the crystal may become spontaneously polarised without becoming completely unstable, and instead

it makes a transition to another phase.

The Lyddane-Sachs-Teller formula above, equation (4), may be generalised for the case when there are N atoms per unit cell (Cochran, 1959) and is given by

$$\frac{\epsilon_o}{\epsilon} = \prod_{j=2}^{n} \frac{\omega_j^2{}_L}{\omega_j^2{}_T} \qquad (10)$$

This relation is open to criticism in that it is assumed that the short-range interaction between ions is independent of their state of polarisation and conversely. However, it has been shown by Woods et al. (1959) that the ions may be treated as charged cores coupled isotropically to massless charged shells which represent the outer electrons (Dick and Overhauser, 1958).

Now it is known (Leibfried, 1955) that one effect of the anharmonicity of the lattice vibrations is to make parameters such as R_o' linearly temperature dependent and hence terms such as equation (7) above are expected to vary linearly with temperature. A quantumn mechanical study of anharmonic interactions between the normal modes of vibration (Cowley, 1965) has made it possible to relate the anharmonic terms to the temperature dependence of the modes and to the linear expansion coefficient. It may be shown that in the harmonic approximation the crystal would be unstable against vibrations of the low frequency or ferroelectric mode, and it would

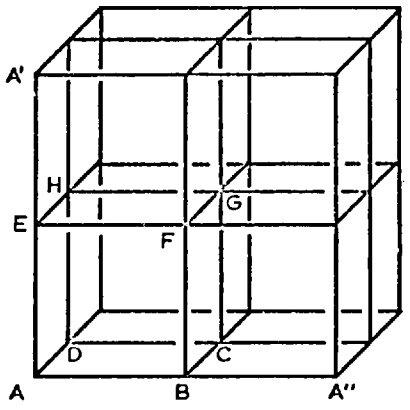


Figure 5.4

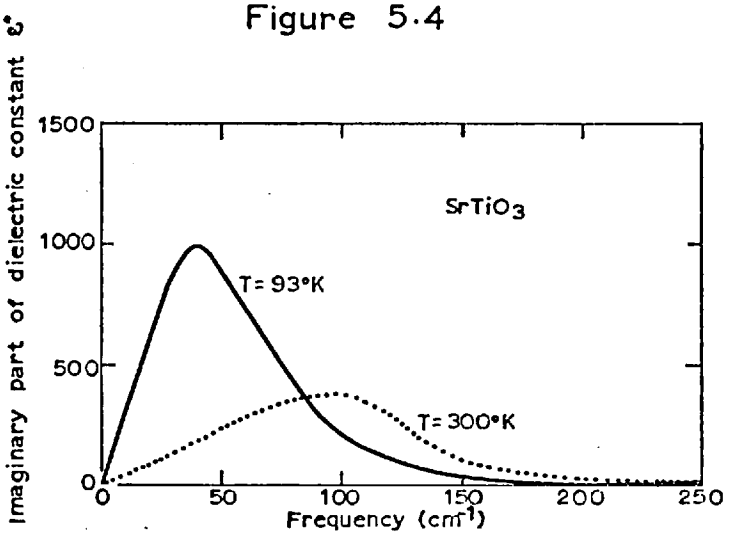


Figure 5.5

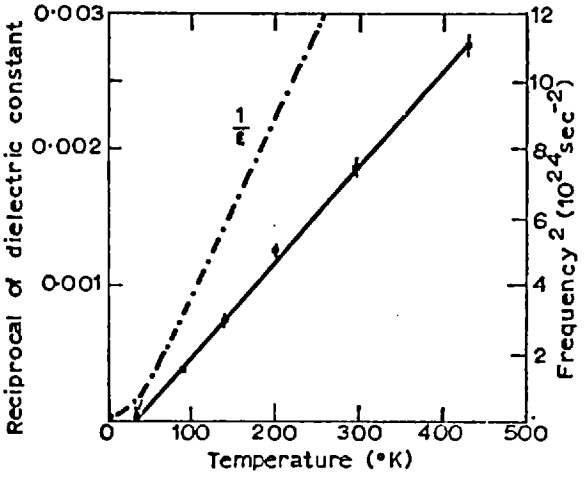


Figure 5.6

disrupt at temperatures just below T_c unless the transition to another structure occurring at or above T_c raises the frequency of the ferroelectric mode. This transition would take place if the short-range forces are not exactly harmonic but possess a small anharmonic component.

That low frequency transverse optical modes do occur in ferroelectric perovskite has been demonstrated experimentally. Barker and Tinham (1962) found a very strong peak in the frequency dependence of the imaginary part of the dielectric constant of $SrTiO_3$ at 100 cm^{-1} at room temperature which shifts downward to 40 cm^{-1} at 93°K (Fig. 5.5). Similarly, Spitzer et al (1962) measured the reflectivity of $SrTiO_3$ and $BaTiO_3$ at room temperature and from classical dispersion analysis of the data for $BaTiO_3$ they deduced a value of 33.8 cm^{-1} for the frequency of the lowest peak in the imaginary part of the dielectric constant. However, the most striking demonstration of the temperature dependence of a low frequency transverse optical mode in a crystal of the perovskite structure is due to Cowley (1962) who studied the temperature dependence of the lowest frequency transverse optical branch along the (100) direction in $SrTiO_3$ by neutron spectroscopy, which shows that the frequencies of these modes are strongly temperature dependent at long wave-lengths.

In Fig. 5.6 Cowley's results for the temperature

dependence of the lowest frequency transverse optical mode of infinite wave-length are reproduced from which it is seen that the square of this frequency is a linear function of temperature which may be extrapolated to zero at a value of $T_c = 32 \pm 5^{\circ}K$. Also shown is a plot of the reciprocal dielectric constant as a function of temperature (Mitsui and Westphal, 1961), and from its values above about $70^{\circ}K$ a Curie temperature of $28^{\circ}K$ is predicted. This should be compared with a value of T_c of $37^{\circ}K$ obtained from microwave loss measurements carried out by Bell and Rupprecht (1962).

Thus there seems no doubt that strongly temperature dependent transverse optical modes of infinite wave-length corresponding to structural instability occur in crystals of the perovskite structure. However, the difficult question to answer is what is the microscopic origin of the cancellation between the Coulomb and short-range contributions to the lowest frequency transverse optical mode of infinite wave-length and, in addition, why the other two infra-red active modes do not display a similarly strong temperature dependence even if they do not become unstable. The answers to this probably await quantumn mechanical calculations of the inter-ionic forces in these crystals from first principles, and it would appear that such calculations represent one of the most challenging problems of the theory of ferroelectricity.

6. ELECTRON PARAMAGNETIC RESONANCE (EPR).

6.1 INTRODUCTION

The paramagnetic resonance method (EPR) is used to investigate the lowest electronic energy levels of paramagnetic ions in crystals. In principle the method is simple. A steady magnetic field is applied to the paramagnetic ions, and the electronic energy levels undergo Zeeman splittings. Simultaneously a small radiofrequency magnetic field is also applied, and the splittings can be measured directly and very accurately by finding the frequencies which induce transitions between the Zeeman levels. If the ground state of the ion contains a number of levels which are separated in zero applied magnetic field (within a few cms^{-1}) then these separations may also be determined accurately.

Under certain conditions the data obtained from paramagnetic resonance may be used to interpret bulk properties of crystals especially at low temperatures when such properties depend only on the energy levels within a few centimeters of the ground level, i.e., on those levels measured by resonance methods. Since the resonance spectrum arises from electronic transitions then information on the nucleus of the paramagnetic ion can be obtained if there is hyperfine structure which arises from the interaction between electrons and nucleus.

The lowest electronic energy levels and hence the resonance spectrum are extremely sensitive to the environment of the paramagnetic ion in the crystal and the spectrum thus provides information about the symmetry of the environment of the ion and about the nature and strength of the binding of the ion and its immediate diamagnetic neighbours.

The widths of the absorption lines in a fully resolved spectrum depend on a number of factors which include the rates at which microwave energy absorbed by the electron spins is transferred into thermal (lattice vibration) energy, i.e. on a spin-lattice relaxation time, the magnetic dipole interaction between neighbouring paramagnetic ions, and the exchange interaction between neighbours. In practice the absorption extends over a range of fields centered at the resonance value H_o and extending a finite amount on either side. The two most commonly considered line-shape functions are the Lorentzian and Gaussian. Often in practice line-shapes lie somewhere between, as there may be several factors of comparable magnitude which contribute to the line width. Line broadening may be 'homogeneous' or 'inhomogeneous'. The former arises from the finite lifetime of the upper state involved in a resonance experiment (lifetime broadening); the latter is really an envelope of a number of narrower but unresolved lines. Any interaction between the magnetic ion and its

surroundings may broaden the line if it results in energy being transferred from the ion following excitation by the radio frequency field. Two common sources of homogeneous broadening are spin-lattice relaxation (the lifetime being characterised by a time T_1) and spin-spin interaction between similar magnetic ions in the crystal (characterised by T_2). In the former mechanism energy is transferred from the excited ion to the crystal lattice, while in the latter case it is exchanged between two ions.

6.2 THE RESONANCE PHENOMENON

The first successful application to the study of Zeeman levels in the centimeter and millimeter range in paramagnetic substances was made by Zavoisky (1945). Very soon afterward experiments were reported by Cummerow and Halliday (1946) and by Bleaney and Penrose (1946).

The phenomenon is shown in its simplest form by a set of non-interacting paramagnetic ions each possessing a single unpaired electron and a 'spin only' magnetic dipole moment of $\frac{1}{2}g_s\beta$ where β is the Bohr Magneton and $g_s = 2.0023$ and is called the electron g factor. In a steady magnetic field H, each dipole can orient itself parallel or anti-parallel to H, with energies $-\frac{1}{2}g_s\beta H$ and $+\frac{1}{2}g_s\beta H$. Magnetic dipole transitions are induced between these two energy levels by applying a high frequency magnetic field polarised perpendicular to H and with

frequency ν such that the quantum of high frequency energy equals the separation between the levels, i.e. $h\nu = g_s\beta H$. Resonance absorption occurs corresponding to the dipoles being flipped from the parallel to the anti-parallel state, and there is induced emission corresponding to the reverse process. For a system in thermal equilibrium more spins are in the parallel state because of its lower energy and there is thus a net absorption of high frequency power.

In a paramagnetic resonance experiment this absorption may be measured by placing the specimen in a wave guide or cavity resonator and detecting a drop in the microwave power at resonance. Normally one uses a fixed frequency ν and a variable field H such that if H is steadily increased an absorption line(s) will be found at $H = \frac{h\nu}{g_s\beta}$. Using an X-band spectrometer operating at about 3cm wavelength with ν = 9,500 mc/s the field for resonance of a free electron would be about 3,400 gauss.

6.3 THE CRYSTAL FIELD

6.3.1 Introduction

The lowest and excited energy levels of an ion situated in a crystal of a given symmetry are modified by the crystalline surroundings and the problem of understanding their properties consists in calculating the allowed energy states of the ion usually in the presence of a magnetic field. This is a

formidable task in the majority of cases but in practice it is only necessary to know the energies of those states which are populated at or below room temperature, since it is these which take part in a resonance experiment. The populations follow a Boltzmann distribution provided they are restricted to levels within about 100 cm^{-1} of the ground state.

The problem is considered in two parts; the calculation of the energy for a free ion, and the way in which this is modified by the surrounding crystal.

6.4 THE FREE ION

For any particular ion the electrons nearly always occur in a single shell and have energies appropriate to it. Each electron is characterised by an orbital angular momentum quantumn number ℓ ($\ell = 2$ for d electrons) and a spin quantumn number s ($s = \frac{1}{2}$). For each electron there are $(2\ell + 1)$ possible orbital states available to it each characterised by a magnetic quantumn number m_ℓ, and for each of these states there are $(2s+1)$ spin states characterised similarly by m_s. Thus the total number of allowed states is $(2s+1)(2\ell+1)$, that is $2(2\ell+1)$, and by the exclusion principle is the maximum number of electrons allowed in a shell.

The most important interaction in an atom is given by the Coulomb term (V_F) which consists of the interaction of the electrons with the nuclear charge and the mutual repulsion

of the electrons. The next most important interaction is a magnetic interaction (V_{LS}) between the electron spins and the orbital momentum. Confining attention to states of definite L and S of the same configuration (Russell-Saunders coupling) the spin-orbit interaction may be written $\lambda L.S$ where λ is the spin-orbit constant for a given ion. There is also the much weaker spin-spin interaction V_{SS} (Pryce, 1950), that is a magnetic coupling between the magnetic moments of the electron and nucleus which is entirely analogous to the dipolar coupling between two bar magnets. These are the dominant terms for the free ion.

If the nucleus has a spin I and a quadrupole moment Q there are two additional interactions V_N and V_Q. The first term V_N describes the dipole-dipole interaction between the nuclear moment and the magnetic moments of the electron. The second term denotes the anomalous interaction of the s-electrons with the nuclear spin, see Chapter 7 (Fermi, 1930). V_Q describes the electrostatic interaction with the quadrupole moment Q of the nucleus. The interaction with the external magnetic field H is given by V_H and the direct interaction of the nucleus with the external field is V_h. The general Hamiltonian of the free ion is then given by the sum of all the above terms V_F and V_h and the range of orders of magnitude involved in these interactions varies from $V_F \sim 10^5 cm^{-1}$ through to $V_Q \sim 10^{-3} cm^{-1}$.

6.4.1 Effect of a Static Crystalline Field

The behaviour of the magnetic electrons responsible for the above interactions is modified somewhat by the crystalline environment which exerts strong electric fields on the electrons. The simplifying concept which makes it possible to understand many of the paramagnetic resonance spectra is the static 'crystal field' or 'ligand field'. Kramers (1929), and later on in more detail Van Vleck (1932) and Penney and Schlapp (1932 and 1932) in the explanation of magnetic phenomena regard the surrounding ions as point charges or point dipoles placed at approximate lattice points. The problem then resolves itself into finding the energy levels in a Stark field of certain strength and symmetry determined by the static charges. Experimental observations of these Stark splittings in the optical spectra of crystals reveals that the strengths of the various crystalline fields fall into three categories:

(a) Strong crystalline fields

These occur in ions in which there is considerable chemical bonding with the ligands where the crystal field interaction is so large as to break-down the coupling between individual electrons. This is most common in ions of the platinum and palladium groups.

(b) Intermediate crystal fields in which the interaction of the Stark splittings is stronger than the coupling

between spin-orbital motion and we may regard the orbital motion as 'clamped' by the crystal field so it is unable to respond to an applied magnetic field. The orbital contribution is said to be quenched and the magnetic properties are due almost entirely to spin which is coupled only weakly to the crystal field by means of spin-orbit coupling. The effective g-factor is close to the free ion spin value of 2.0023 and is quite different from the free ion Landé factor. To distinguish the two the term 'spectroscopic splitting factor' is used and it is this which is implied whenever we use the phrase 'g-factor'. It is seen that the behaviour of Fe^{3+} in BaTiO follows closely the description given here.

(c) Weak crystal field

Here the crystal field interaction is weaker than the spin-orbit coupling so, to a first approximation the free ion calculation is valid. However, the crystal field must be considered before the effect of an external magnetic field since, depending on the spin configuration of the ion involved, it is responsible for the arrangement of the degeneracy of the spin states.

6.5 ENERGY LEVELS OF THE d ELECTRONS

6.5.1 Qualitative outline

Provided the symmetry of the site of the paramagnetic ion

is known group theory gives a detailed qualitative account of the way in which the orbital degeneracy of a magnetic ion is lifted by a magnetic field and the mathematical problem of representing the crystal field potential arising from all the other ions at the place of the paramagnetic ion is not very difficult (Ballhausen, 1962; Low, 1966). The surrounding ions are regarded as point charges which do not overlap the paramagnetic ion and the electrostatic potential is therefore supposed to obey Laplace's equation $\nabla V=0$, the solutions to which are the generalised Legendre polynomials.

We may regard the total Hamiltonian of the ion as being made up of a static part (that of the free ion) on which is superimposed a perturbation due to the ligands which determines the electronic motions and term values of the metal ion in the complex. It is convenient to expand the potential in terms of the polynomials,

$$V = \sum_n \sum_{m=n}^{-n} \sum_k A_n^m r^n Y_n^m(\theta_k \phi_k) = \sum_n \sum_m V_n^m$$

where the summation k is over all the electrons. The normalised harmonics Y_n^m are defined as

$$Y_n^m(\theta,\phi) = (-1)^n \left[\frac{1}{4\pi} \frac{(2n+1)(n-m)}{(n+m)}\right]^{\frac{1}{2}} P_n^m(\cos\theta) e^{im\phi}.$$

The symmetry of the ligands around the metal ion has to be known because V must transform as the total symmetric

representation in the symmetry group of the molecule. This is due to the fact that the Hamiltonian for the molecule must remain totally symmetric under all symmetry operations. Symmetry arguments will reduce the number of terms in this expansion considerably. For instance, when only d electrons are involved, all potentials after the fourth-order terms (n=4) exert no influence because the direct product of two d-orbital sets spans no representations of the rotation group of the order higher than four. The reason for this is that the wave function of the electrons can also be expanded in harmonic functions $\psi_\ell^i \sim R(r_i) Y_\ell^i(\Theta_i \phi_i)$ where $R(r_i)$ refers to the radial part of the wave function. Also all terms with odd n must vanish. The reason for this lies in the fact that the product $\psi_\ell^i \psi_\ell^i$ is unchanged by inversion symmetry, (i.e. $x \to -x$, $y \to -y$, $z \to -z$) whereas in the potential $V = \sum_{n,m} V_{2p+1}^m = -V$, $(2p+1 = n)$ changes sign. The term n=0 in the expansion is a constant and merely shifts all the levels of a given configuration by the same amount. Therefore it has no significance as far as the magnetic and optical properties of crystals are concerned.

Low has worked out complete potential functions for the various crystalline symmetries and has expressed the results using Stevens' method of operator equivalents (1952), also Elliott (1953) and Judd (1955).

6.5.2 d-orbital splitting

We are principally interested in this work in the s-state ions of the first long series, namely, Mn^{2+} and Fe^{3+} whose paramagnetism is due to the $3d^5$ electrons and although they possess 4s electrons the positive charges on them make the d-orbitals relatively more stable.

The five d-orbitals of a free ion have precisely the same energy and may be classified according to their orbital angular momenta L^2 and L_z. However, if we consider an octahedral complex in which the metal ion is surrounded by six negative ions, or other groups which forms bonds with it, then these ligands introduce the so-called 'ligand-field splitting' of the d-orbitals which removes their degeneracy and mixes together orbitals with different L_z quantumn numbers. Now for electrons in a d shell $\ell = 2$ and there are five d-orbits corresponding to the $(2\ell+1)$-fold orbital degeneracy and the associated wave functions can be expressed as a function of the radius r multiplied by functions with angular variation of the form $\frac{xy}{r^2}$, $\frac{yz}{r^2}$, $\frac{zx}{r^2}$, $(\frac{x^2-y^2}{r^2})$ and $(\frac{2z^2-x^2-y^2}{r^2})$ respectively. These five orbitals may be represented diagramatically by the charge cloud distribution in Fig. 6.1 where the dots represent the attached negative ions. The ligands affect the d-orbitals in two distinct ways; one is through the electrostatic field of the negative charges and the other is by covalent bonding

with the ligand orbitals. Both these effects alter the energies of the d-orbitals in approximately the same manner. The d-electrons try to keep in orbits such that the negative charge cloud avoids the attached negative ions. Hence, the orbitals xy, yz and zx, usually called $d\varepsilon$ -orbitals, have lower electrostatic energy than the $d\gamma$ - orbitals (x^2-y^2, $2z^2-x^2-y^2$). The energy gap between the two types of orbitals is called the ligand field splitting Δ , and is the origin of the crystal field splitting of the ground term which leads to quenching of the orbital magnetic moment. The effects of covalent bonding, which may be pictured simply as the sharing of the metal ion and ligand orbits thereby evening out the charge distribution, leads to an increased splitting between the $d\varepsilon$ triplet and the $d\gamma$ doublet. This ligand field splitting is generally of the order of about 20,000 cm^{-1} as obtained by optical spectra.

Two distinct situations are possible depending on the size of Δ . If Δ is much smaller than the Coulomb and exchange energies of the electrons in the free ion then the electron configuration of Fe^{3+} in octahedral cubic coordination is five unpaired d-electrons with a total spin $S=\frac{5}{2}$, and the configuration is $(d\varepsilon)^3(d\gamma)^2$. This is known as the high spin case where the exchange energies predominate since the electrons prefer to go into the configuration with the largest number of parallel spins and the highest exchange energy. On the other

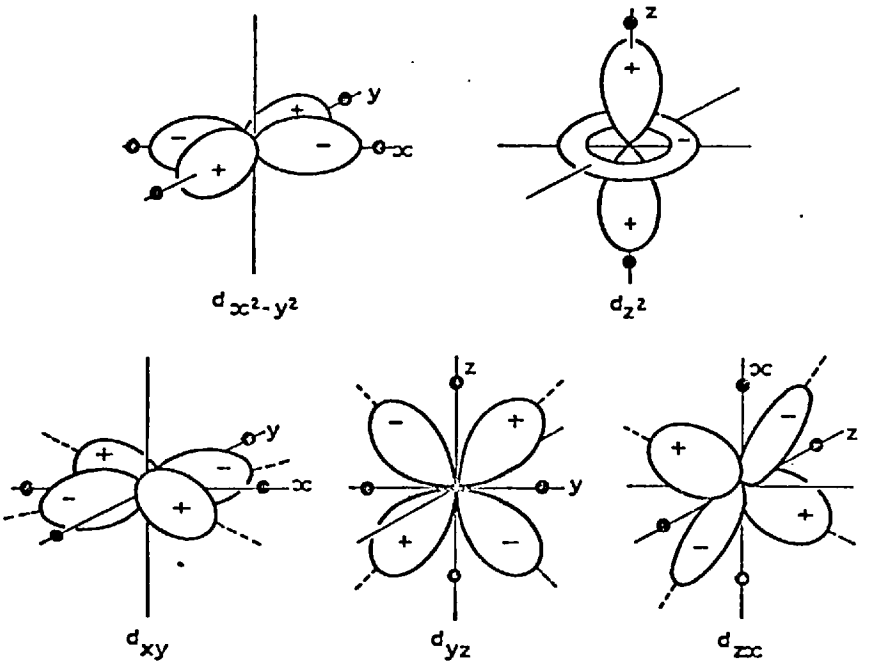


Figure 6.1

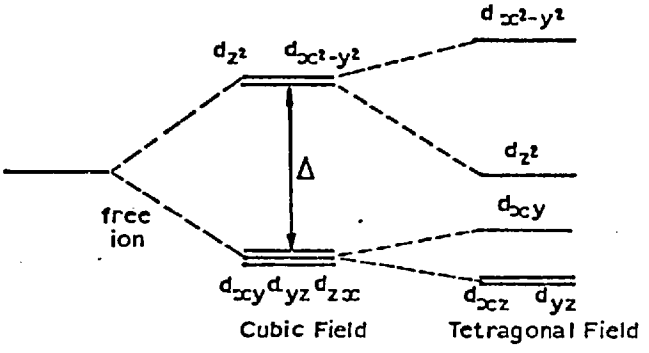


Figure 6.2

hand, if Δ is very large, as it is in the cyanides for instance, the electrons first fill-up the $d\varepsilon$ levels, two per level according to Pauli's principle and thus Fe^{3+} in this case would only have spin $\frac{1}{2}$.

Experimental evidence has shown that in the temperature range of interest concerned with this work Δ belongs to the former category. If there is distortion of the octahedron surrounding the metal ion along the axis (i.e. tetragonal distortion) the degeneracy of these orbitals is further lifted and the effect is to produce further splitting of these ground state levels. There may be additional splitting due to the effect of spin orbit coupling of the order of a few 100-1000 cm^{-1} and approximately 1 cm^{-1} when there is spin degeneracy only. The complete scheme is shown in Fig. 6.2.

6.5.3 Kramers' Theorem

In some cases the degeneracy is never completely removed by the crystal field alone and according to a theorem due to Kramers (1930) which states that in the absence of an external magnetic field the electronic states of any molecule with an odd number of electrons are at least doubly degenerate. Thus in the case of Fe^{3+} and Mn^{2+} one obtains three 'Kramers doublets'. This is important because paramagnetic resonance absorption can be observed only if the transition between two levels is permitted or if the separation of the levels is not

larger than the applied microwave field and we may look upon Kramers' theorem as being responsible for resonance absorption for spin systems containing an odd number of electrons. It is one of the purposes of the work in this section to monitor the change in the relative displacement of these Kramers' doublets with change in temperature thus seeing how the effect of the crystal field (at the titanium site) changes with temperature. This is done by evaluating the relevant parameters in the spin Hamiltonian as a function of temperature.

6.6 THE SPIN HAMILTONIAN

6.6.1 Introduction

The lowest group of energy levels, between which microwave transitions are induced, and which lie typically some hundreds or thousands of wave numbers below all others, depend in a rather complicated way on the particular ion and the symmetry and strength of the crystal field (outlined above), and also on the spin-orbit coupling, and on other effects such as the hyperfine interaction between electrons and nucleus, etc. These ground state levels are regarded as an isolated set whose properties may be described without reference to other levels. Frequently only two are involved and the number rarely exceeds eight; in this work six levels are involved comprising three Kramers' doublets.

The energy levels and the associated experimental resonance

data is described by the use of the so-called 'spin Hamiltonian' in a fairly simple way requiring no detailed knowledge of the above effects.

Even though each electronic state is characterised by a single quantumn number S' it is really a complicated mixture of the spin and orbital wave functions of the free ion (Abragam and Pryce, 1951). S' is the effective or fictitious spin of the system and is obtained by equating the number of levels in the ground state (the ground state multiplicity) to (2S'+1). It is assumed that S' represents these ground state levels, and that each level is characterised by a quantumn number M_s which corresponds to the M_J used in describing the free ion ground state. In some cases S' equals the free ion spin S, but for the case of an ion with an odd number of electrons the effect of the crystal field and spin-orbit coupling is to leave a Kramers doubtlet well below all the other electronic levels and thus $S'=\frac{1}{2}$. For the case considered here of Fe^{3+} substituting for Ti^{4+} in the octahedron of O^{2-} ions the separation of the Kramers doublets due to effects other than an applied magnetic field, though slightly greater than the quantumn of microwave radiation, permits us to equate S' with $S=\frac{5}{2}$.

The use of an effective spin means that the paramagnetic ion is treated like a magnetic dipole which has 2S'+1 allowed

orientations in an applied magnetic field. The dipole may not be treated as free since in addition to the above interaction, energy terms must also be added which describe, for instance, electrostatic interaction between the unpaired electrons and the crystal field (which give Stark splittings if $S>\frac{1}{2}$) and the additional interactions mentioned above.

Now the sum of all terms written as a sum of energy operators to be applied to the effective spin states, constitutes the spin Hamiltonian H for the system. The actual energies are the eigenvalues E_o which satisfy the operator equation $H\psi = E_o\psi$ where ψ represents the wave functions of the effective spin states which can be, though not always, admixtures between the various states.

The advantage of the above method is that it enables the experimental results to be expressed comparatively simply in terms of a small number of parameters and the wide range of possible effects mentioned above is thus reduced to a neat standard form. Without this it would be necessary to give complicated formulae and diagrams of how energy levels diverge in a magnetic field as was done in the earlier work. The technique of the 'spin Hamiltonian' is due originally to Abragam and Pryce (1951) and Pryce (1950). Each term considered alone is fairly simple and is now discussed in more detail.

6.6.2 The spectroscopic splitting factor-g.

The g-value may be defined in terms of experimentally observed splittings $g\beta H$ produced by a magnetic field between the effective spin levels. The magnetic dipole moment associated with the effective spin S (dropping S') has (2S+1) allowed orientations in a magnetic field H corresponding to quantumn numbers M_s = S, S-1, ... -S, the relative energies being $g\beta HM_s$. The 2S allowed transitions ($\Delta M_s = \pm 1$) between the (2S+1) equally spaced levels occur at the same field $H = h\nu/g\beta$. If the paramagnetic ion is in a crystal then because of additional energy terms the splittings of the levels when H = 0 will not all occur at the same field.

This spectroscopic splitting factor is analogous to the Landé splitting g_J for the free ion (if effective spin equals free ion spin) but in general has different values for an ion in a crystal due to modification of the orbital part of the magnetic moment. If the orbital moment is greatly reduced by the crystal field then g lies close to g_s (2.0023). Quenching of the orbital moment by the crystal field would then mean a g-value for the ion of 2.0023 and this is practically the case for Fe^{3+} in $BaTiO_3$ (see Fig. 6.6).

The total g-value (spin plus orbit) may be anisotropic depending on the amount of orbital contribution and asymmetry in the crystal field. The electronic Zeeman interaction may be

represented in the spin Hamiltonian by the term $H = \beta H.g.S$ where g is a tensor which may be anisotropic. This anisotropy is represented by three principle values g_x, g_y, g_z, which are mutually perpendicular. For a generalised applied H in the spin Hamiltonian the splitting of the effective spin levels is represented by the energy operators $H = \beta(g_z H_z S_z + g_x H_x S_x + g_y H_y S_y)$. If H is parallel to Z then the Hamiltonian reduces to $H_z = g_z \beta H_z S_z$ and the eigenstates can be represented by the magnetic quantumn numbers $M_s = S, S-1, \ldots\ldots -S$, and the eigenvalues by $g_z \beta H M_s$.

6.6.3 Fine Structure

Often, in the absence of an applied magnetic field (i.e. H = 0) there are initial splittings of the effective spin levels although there is always at least two-fold degeneracy if the free ion spin is half integral (Kramers theorem). The most important cause of these splittings is the Stark effect arising from an asymmetrical crystalline electric field, and hence we would expect to have some anisotropic terms in the spin Hamiltonian to represent this zero-field splitting, and these cannot involve H.

The above effects may be demonstrated by considering the effects of the spin-orbit interaction represented by $\lambda L.S$, where λ is the spin-orbit coupling constant, and the other by the perturbing interaction of the magnetic field H on both the

spin and orbital contribution which is of the form $\beta H.(L+2S)$. Pryce (1957) has shown in a general way the kind of terms to be obtained on carrying out a full second-order calculation to terms of order λ^2 as well as the λH terms. If the effects of nuclear moment interactions are neglected the resultant Hamiltonian may be written,

$$H = \sum_{i,j=1}^{3} \beta g(\delta_{ij} - 2\lambda\Lambda_{ij})S_{ij}H_j - \lambda^2\Lambda_{ij}S_iS_j \quad + \text{diamagnetic terms in } H_iH_j$$

where Λ_{ij} is defined with respect to the ground state(o), and excited state ($n > o$) as

$$\Lambda_{ij} = \sum_{n \neq o} \frac{\langle o|L_i|n\rangle \langle n|L_j|o\rangle}{E_n - E_o}$$

a tensor, which when referred to the principal axes of a crystal possessing axial symmetry, is diagonal with $\Lambda_{zz} = \Lambda_{\parallel}$, and $\Lambda_{xx} = \Lambda_{yy} = \Lambda_{\perp}$. The term $-\lambda^2\Lambda_{ij}S_iS_j$ is responsible for splitting the spin multiplet even in the absence of an external field, and the spin Hamiltonian is now,

$$H = -\lambda^2\Lambda_{ij}S_iS_j$$

By using the identity

$$S_x^2 + S_y^2 = S(S+1) - S_z^2$$

$-\lambda^2\Lambda_{ij}S_iS_j$ simplifies to

$$\lambda^2(\Lambda_{\perp} - \Lambda_{\parallel})S_z^2 - S(S+1)\lambda^2\Lambda_{\perp}$$

which is normally written as

$$-\tfrac{1}{3}S(S+1)\lambda^2(\Lambda_{\parallel}+2\Lambda_{\perp}) + D(S_z^2-\tfrac{1}{3}S(S+1))$$

where

$$D = \lambda^2(\Lambda_{\perp}-\Lambda_{\parallel})$$

The first term in the previous equation represents a constant shift down of all the levels of the lowest spin-multiplet, and the second corresponds to a splitting of these levels. Now since S_z has eigenvalues $M_s = S, S-1, \ldots -S$ then the eigenvalues from this equation are DM_s^2 + constant, and we can see from this therefore that a zero-field splitting occurs only if $S>1$. Thus the effect of an axial crystalline field may be represented in the spin Hamiltonian by the operator DS_z^2, and any fields of lower symmetry than axial (e.g. orthorhombic), which may give additional splittings, by $E(S_x^2-S_y^2)$.

6.6.4 Magnetic hyperfine structure

The occurrence of hyperfine structure in EPR is due essentially to two principle causes: (a) isotropic hyperfine coupling, (b) dipolar interaction.

In (a) the magnetic moments of the electrons and nucleus are coupled via the so-called Fermi contact interaction which represents the energy of the nuclear moment in the magnetic field produced at the nucleus by the electrons. The interaction Hamiltonian for this is given by,

$$H_1 = \frac{8\pi}{3} g\beta g_N\beta_N\delta(r)\mathbf{I}.\mathbf{S}$$

where g_N and β_N are the nuclear g-factor and Bohr magneton respectively and I the nuclear spin.

In (b) there is magnetic coupling between the magnetic moments of the electron and nucleus which is analogous to the classical dipolar coupling between two bar magnets and the interaction Hamiltonian is

$$H_2 = -g\beta g_N \beta_N \left[\frac{I.S}{r^3} - \frac{3(I.r)(S.r)}{r^5} \right]$$

The complete Hamiltonian is given by the operator AS.I. In general A is anisotropic if g is, and the hyperfine operator now takes the form $A_z S_z I_z + A_x S_x I_x + A_y S_y I_y$.

Since the nuclear moment has 2I+1 allowed values, each proportional to the nuclear magnetic quantumn number m (=I,I-1,..... -I), in the magnetic field arising from each of the 2S+1 orientations of the electronic moment, then each electronic energy level is subdivided into 2I+1 components. The microwave field has a negligible effect on the nuclear moment and so the selection rules for transitions are $\Delta M = \pm 1$, $\Delta m = 0$. Since all nuclear orientations are equally probable, at normal temperatures, then the lines are of equal intensity, unlike those due to fine structure. The spacing of the hyperfine lines is however not quite equal as was found for the case of Mn^{2+} doped crystals of $BaTiO_3$, and the reason for this is given below.

6.6.5 Quadrupole Interaction

The nucleus of a paramagnetic ion will possess an electrical quadrupole moment Q, if $I>\frac{1}{2}$, and some orientations will be energetically more favourable than others if it is in an electric field gradient, the greatest contribution to which, at the nucleus comes mostly from unpaired electrons. The contribution to the field gradient from the crystal field is comparatively small and though not detectable using EPR on S-state ions (e.g. Mn^{2+}) in $BaTiO_3$ is readily detectable as a quadrupole splitting using the Mössbauer effect (see Chapter 7 for more detailed discussion).

The energies of the electronic levels are modified somewhat by the electrostatic interaction between electrons and nucleus, and this is represented by operators such as $P\left[I_z^2-\frac{1}{3}I(I+1)\right]$ in the spin Hamiltonian, and it may be seen for instance that the eigenvalues corresponding to this operator for $I = \frac{3}{2}$ will be $P(m^2-\frac{5}{4})$, is here $m^2 = (\pm\frac{3}{2})^2$ and $(\pm\frac{1}{2})^2$ thus splitting each electronic level into two components with spacing 2P, each pair of levels having the same energy. If the electric field gradient departs from axial symmetry then an additional term $P'(I_x^2-I_y^2)$ must be added to the spin Hamiltonian.

The effect of quadrupole interaction on the resonance spectrum is usually to destroy the equivalent spacing in the

hyperfine splitting and the result is that for a general direction of H the intensities and spacings of the usual 2I+1 hyperfine lines corresponding to $\Delta m = 0$ are modified by P, the spacings increasing with increasing field, and there may be additional lines corresponding to normally forbidden transitions with $\Delta m = \pm 1, \pm 2$. It was in fact this unequal spacing in the hyperfine splittings of Mn^{2+} in $BaTiO_3$ indicating quadrupole interaction, which led to an investigation of the temperature effects of this splitting.

6.6.6 Nuclear interaction with the external field.

The nuclear magnetic moment μ_N may interact directly with the applied field H, the operator in the spin Hamiltonian being $-g_N\beta_N H.I$. The measurable effect on the spectrum is usually very small or negligible compared with the previous two effects above and in any case does not affect the spacing of the $\Delta m = 0$ transitions which are the ones normally observed.

6.6.7 S-state Ions.

The above terms in a spin Hamiltonian do not take into account what happens when the orbital state of the free ion has no degeneracy, and assuming Hund's rule this happens whenever the unfilled shell is half filled, which is the case for Fe^{3+} giving $3d^5\ {}^6S$ configuration. Application of the crystal field on the orbital state does not result in splitting, as there is no orbital degeneracy, and the only way in which

splittings may be obtained is to include coupling between spins and orbits and regard the ground level as having six-fold degeneracy.

This problem was first considered by Van Vleck and Penney (1934) who showed that by using spin-orbit interactions and the crystal field it was necessary to go to a higher order in the perturbation theory before any splittings were obtained. This work shows that the resonance spectrum of Fe^{3+} in $BaTiO_3$ above the Curie point may only be explained by the inclusion of such higher order terms in the spin Hamiltonian. Abragam and Pryce (1951) concluded that these splittings were too big to be explained by the above process and suggested that the combined action of an electric field gradient and spin-spin interaction was to distort the charge cloud from a perfect sphere to an ellipsoid which would then vary the dipole-dipole energy of the spins with their orientation. Following these ideas Watanabe (1957) estimates higher order processes involving crystalline potential, spin-orbit coupling, and spin-spin interaction within the ion which are supposed to be dominant in the ground level splitting. However Powell, Gabriel and Johnston (1960) have shown terms in addition to those calculated by Watanabe must be considered in order to explain the cubic field parameter "a" of the conventional spin Hamiltonian.

By a consideration of the expressions needed to span a

general expression in S_x, S_y and S_z when $S = \frac{5}{2}$ in the iron group only Bleaney and Stevens (1953) have shown that in the absence of a magnetic field and in cubic symmetry the additional contribution to the spin Hamiltonian is

$$\frac{1}{6}a\left[S_x^4 + S_y^4 + S_z^4 - \frac{1}{5}S(S+1)\,(3S^2 + 3S - 1)\right]$$

which is further modified by a tetragonal distortion to separate S_z^4 from S_x^4 and S_y^4 with an additional coefficient b. (Bowers and Owen, 1955).

6.7 DERIVATION OF ENERGY LEVELS FROM THE SPIN HAMILTONIAN.

6.7.1 Introduction

We will only outline the procedure necessary for making these calculations. A more rigorous and detailed account of particular aspects of the theory and also for a derivation of the spin Hamiltonian may be obtained by referring to Pryce (1950), Abragam and Pryce (1951), Stevens (1952), and for a more general theoretical background to Van Vleck (1932).

6.7.2 The Matrix Representation.

The problem here is to find the energy eigenvalues E_n which satisfy $H\psi_n = E_n\psi_n$ where ψ_n represents the energy eigenfunctions of the effective spin states. We will assume for the present that I = 0, i.e. no nuclear interaction terms. The advantage of the matrix representation is that the problem is set out fully in a neat and compact form, which lends itself to fairly easy solution. In addition one may deduce by

inspection certain of the physical properties associated with the problem.

Suppose the eigenfunctions ψ_n and eigenvalues λ_n of the operator α are unknown, and ϕ_k are a set of orthogonal functions which are not eigenfunctions of the operator α. Further assume the integrals

$$A_{lk} = \int \phi_l \alpha \phi_k d\tau \qquad \text{may be calculated.}$$

Now ψ_n may be expressed as a linear combination of the ϕ_k,

$$\psi_n = \sum_k a_{kn} \phi_k$$

The eigenvalue equation for α may be written

$$\sum_k a_{kn} \alpha \phi_k = \lambda_n \sum_k a_{kn} \phi_k$$

multiplying from the left by ϕ_l^* and integrating gives

$$\sum_k a_{kn} A_{lk} = \sum_k a_{kn} \lambda_n \delta_{lk}$$

since $\int \psi_n^* \psi_m d\tau = \delta_{nm}$

i.e. $\sum_k a_{kn} (A_{lk} - \lambda_n \delta_{lk}) = 0$ for all l, n.

This equation represents a set of simultaneous equations in the constants a_{kn}. Such a set of homogeneous equations has non-trivial solutions only if the determinant of the coefficients vanishes:

$$\det | A_{lk} - \lambda_n \delta_{lk} | = 0.$$

The solution of this secular equation gives the eigenvalues λ_n of α in terms of the assumed known A_{lk}, and for a particular λ_n it is then possible to solve the above set of equations for the appropriate a's, but this is not necessary for our purpose.

The solution of an eigenvalue problem consists of two parts; calculation of the matrix elements, and solution of the matrix equation to obtain the eigenvalues and corresponding eigenvectors a_n. We now consider this.

6.7.3 Angular Momentum Operators (Dirac notation)

In evaluating the matrix elements H_{lk} it is convenient to consider the properties of the angular momentum operators and the so-called spin operators in particular.

In a magnetic field H any degeneracy, of an effective spin level S having a multiplicity (2S+1), is raised and the component of S along H, i.e. S_z, takes values M ranging from -S to S in integral steps, and these are the eigenstates of the operator S_z, which are used to define the basic vectors. Having defined the basic states in terms of components of angular momentum, then introduction of the appropriate angular momentum operators allows the required matrix elements to be computed, i.e.

$$H_{lk} = \langle M_l | H | M_k \rangle \equiv \int \phi_l^* H \phi_k \, d\tau$$

It may be shown using the commutation relations

$$[S_x, S_y] = iS_z; \quad [S_y, S_z] = iS_x; \quad [S_z, S_x] = iS_y,$$

that the operators $S^2(=S_x^2+S_y^2+S_z^2)$ and S_z commute and this implies that they both can be represented as diagonal matrices, and further that no two of S_x, S_y and S_z commute, which means that S_x and S_y must be represented by non-diagonal matrices. Now in a representation where S^2 and S_z are diagonal it may be shown that the operators S^2, S_z, S_x and S_y have the following properties: (Rosè, 1957),

$$S^2|M\rangle = S(S+1)|M\rangle$$

$$S_z|M\rangle = M|M\rangle$$

$$S_+|M\rangle = S(S+1) - M(M+1)^{\frac{1}{2}}|M+1\rangle$$

$$S_-|M\rangle = S(S+1) - M(M-1)^{\frac{1}{2}}|M-1\rangle$$

where $S_+ = S_x+iS_y$ and $S_- = S_x-iS_y$ are the shift operators. These operator equations are used to "set up" the Pauli spin matrices for the various S's. Thus the matrix element for the operator S_z between the states $\langle M_l|$ and $|M_k\rangle$ is $\langle M_l|S_z|M_k\rangle = M_k\langle M_l|M_k\rangle = M_k\delta_{ik}$ showing S_z is diagonal.

Choosing as basic states the functions $|M\rangle$, where M has the values S,(S-1) ..... -S, the energies of the various ground state levels are then obtained as the eigenvalues E_n of the Hamiltonian operator H_s operating only on the spin states $|M\rangle$ thus:

$$H_s|\psi_n\rangle = E_n|\psi_n\rangle \qquad n = 1, 2, \ldots(2S+1)$$

where the eigenfunctions of H_s are given by:

$$|\psi_n\rangle = \sum_i a_{ni}|M_i\rangle$$

and the calculation of the matrix elements $\langle M_j | H_s | M_i \rangle$ will depend on the form of the spin Hamiltonian. The Pauli spin matrices appropriate to the spin Hamiltonian used for Fe^{3+} are shown evaluated in Appendix A.

6.8 THE SPECTROMETER SYSTEM

The Varian X-band spectrometer used was a V4502-15 system operating at about 9.3Gc/s using either 100kc/s field modulation or superheterodyne detection at 30Mc/s. This system uses a 12 inch magnet, rotatable about a vertical axis, supplied by a solid state power supply. The field produced by the magnet is regulated by a "Fieldial" regulator enabling the field to be set with an accuracy of ± 2 gauss. Two different field modulation supplies are available at 100kc/s and a variable modulation up to 400c/s. Using a dual cavity, therefore, two samples, the unknown and the reference, may be examined at the same time and the results displayed simultaneously on both tracks of a dual pen recorder.

This Varian reflection electron spin resonance spectrometer can operate in one of two modes, homodyne or superheterodyne. A block diagram of the microwave circuit is given in Fig. 6.3. The most noticeable points about this spectrometer are firstly, that it employs a 3dB directional coupler instead of the more normal "magic T". The properties of a "magic T" are that if power is fed down any one of its four arms the power is split

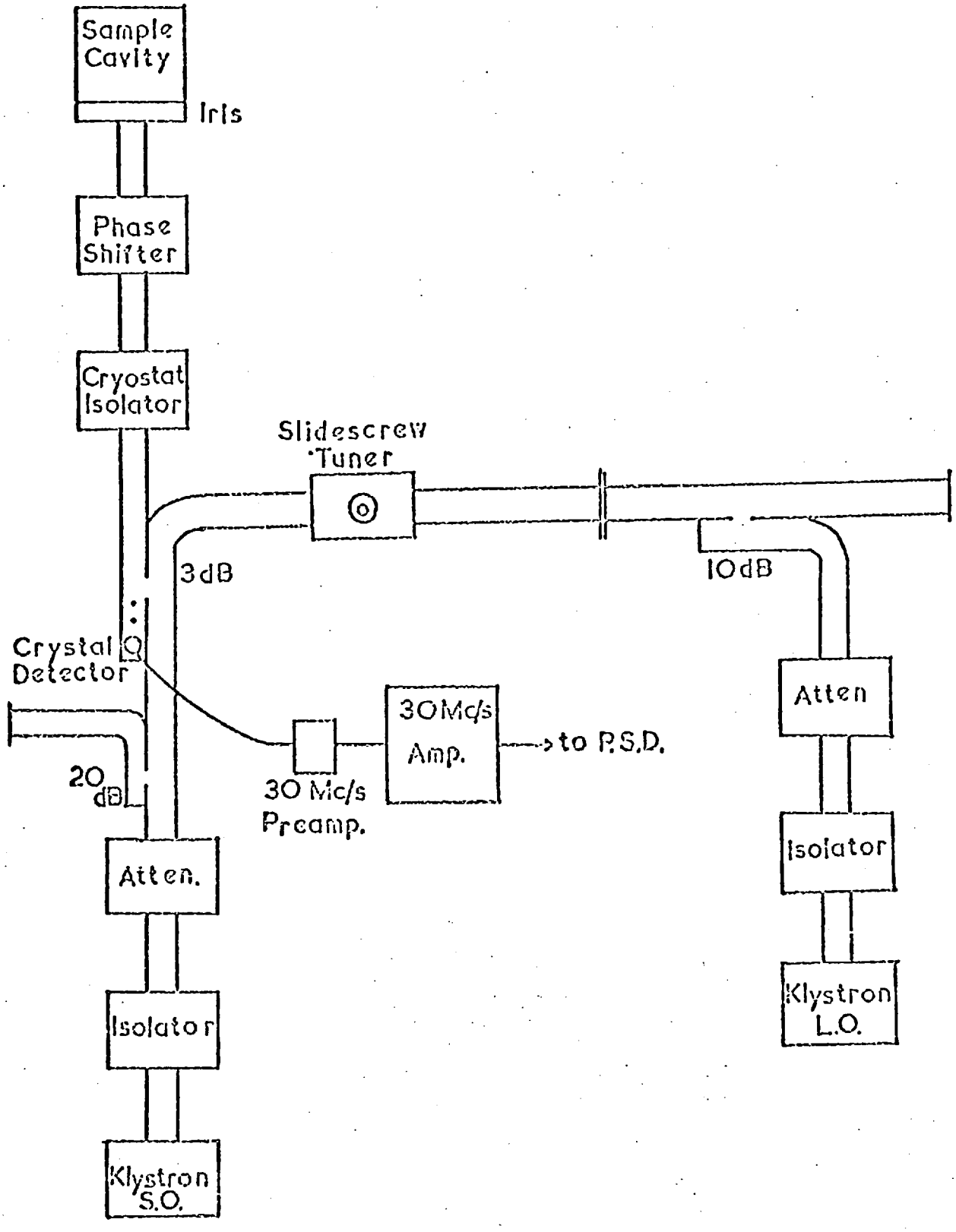


FIG. 6.3 Varian V 4502 E.S.R. Spectrometer.

equally into two parts which emerge from two of the other arms. No power is coupled into the fourth arm of the "T". The 3dB coupler used in this apparatus acts in the same way although, in general, directional couplers do not have as good a directivity as a "magic T". The second noticeable feature of this apparatus is the cryostat isolator in the sample cavity arm. This is a ferrite device which will strongly attenuate to the desired amount in the forward direction but has virtually no attenuation in the reverse direction. The attenuation is frequency dependent; calibration against frequency being required before use.

The principle of operation in the homodyne system is that microwave power (about 300mW) from a Varian V153C klystron is split equally into two parts by the directional coupler, half being fed into the sample cavity arm and half to the dummy arm. Half the power reflected from the sample cavity arm and half that reflected from the dummy arm are mixed in the directional coupler and fed into the detector arm onto a crystal detector. The reflected power from the sample cavity is amplitude modulated at 100kc/s when a sample is undergoing resonance and this is detected at the crystal. After amplification and phase sensitive detection this signal is fed to the recorder. There may also be a signal at 400c/s from the reference cavity and this is fed to the other channel of the recorder. Automatic

frequency control (A.F.C.) is applied to the klystron to lock its frequency to the sample cavity resonance frequency whilst the measurement is taking place. This is done by applying a 10kc/s signal to the klystron reflector to frequency modulate the microwaves; the detected output at 10kc/s from the crystal is then dependent in amplitude and phase on the deviation between the klystron frequency and the cavity resonant frequency. This is then applied via a suitable network to the klystron reflector as an error voltage to correct the microwave frequency.

If superheterodyne detection is used a local oscillator signal, the frequency of which is 30Mc/s away from the signal oscillator although it is not locked, is coupled into the dummy arm and this is mixed with the reflection from the sample cavity arm in the 3dB directional coupler and the resulting 30Mc/s signal fed to the crystal arm where it is detected. After amplification and phase sensitive detection as before this signal is fed to the recorder.

Many accessories have been used with this equipment. A Varian computer of average transients (C.A.T.) has been used for some of the applications and is useful where the signal to noise ratio of the spectrum cannot be enhanced by other methods (e.g. higher concentration of paramagnetic species, higher microwave power, lower temperature or higher 100kc/s modulation amplitude). This device will enhance the

sensitivity since the electron spin resonance signal is coherent whilst the noise is incoherent.

Another indispensable accessory is the nitrogen gas flow, the temperature of which is regulated by a small heater and temperature sensor in the gas stream just before it enters the cavity. The sensor is a platinum resistance which is in one arm of a Wheatstone bridge, the control arm of which can be set so that the temperature of a sample is any desired value from -200 to +300°C, the accuracy of which was shown to be $\pm 1^{\circ}C$ by calibration with a copper/constantin thermocouple.

The standard general purpose cavity in use with this equipment is one operating in the rectangular H_{102} mode with modulation coils of several hundred turns embedded in resin behind the sidewalls of the cavity. For all the experiments in which this apparatus was used a dual sample cavity was in use which consists of two standard cavities bolted together forming an H_{104} cavity. This enables two samples to be studied at once. The 100kc/s modulation frequency was normally used on the cavity containing the sample to be studied and the other cavity contained the reference sample, usually 0.01% Mn in MgO fused under hydrogen at 1100°C and containing a small quantity of α:α diphenyl β picryl hydrazyl used as a field marker and calibrant, with 400c/s modulation frequency being

applied to it. The signals from these two samples can then be displayed on a dual channel recorder at the same time. A disadvantage of this cavity for some applications is that, as the cavity is twice the size of the standard one, the microwave field at any point, and consequently the sensitivity, is only half that of the single cavity.

6.9 THE CRYSTAL GONIOMETER

The magnet of the above spectrometer, though freely rotatable through an angle of approximately 200°, could not be utilised in this way because the modulation coils were attached to the sides of the rectangular cavity and any movement of the magnet out of 'true' with the field produced by the modulation coils would then result in a decrease in the signal intensity. This would also have the added effect of changing the selection rules for the transitions. In order to overcome this the two axis goniometer shown in Fig. 6.4 was constructed, and it was estimated that alignment of the 'c' axis of the crystal with the magnet field could be effected to within half a degree.

The twin axis mount on which the crystal was mounted was so dimensioned that it was able to fit into a specially constructed spectrosil insert through which was passed nitrogen gas whose temperature was varied in the manner described in the preceding section. By placing a thermocouple in contact with the crystal its temperature was verified to be that of the heated gas.

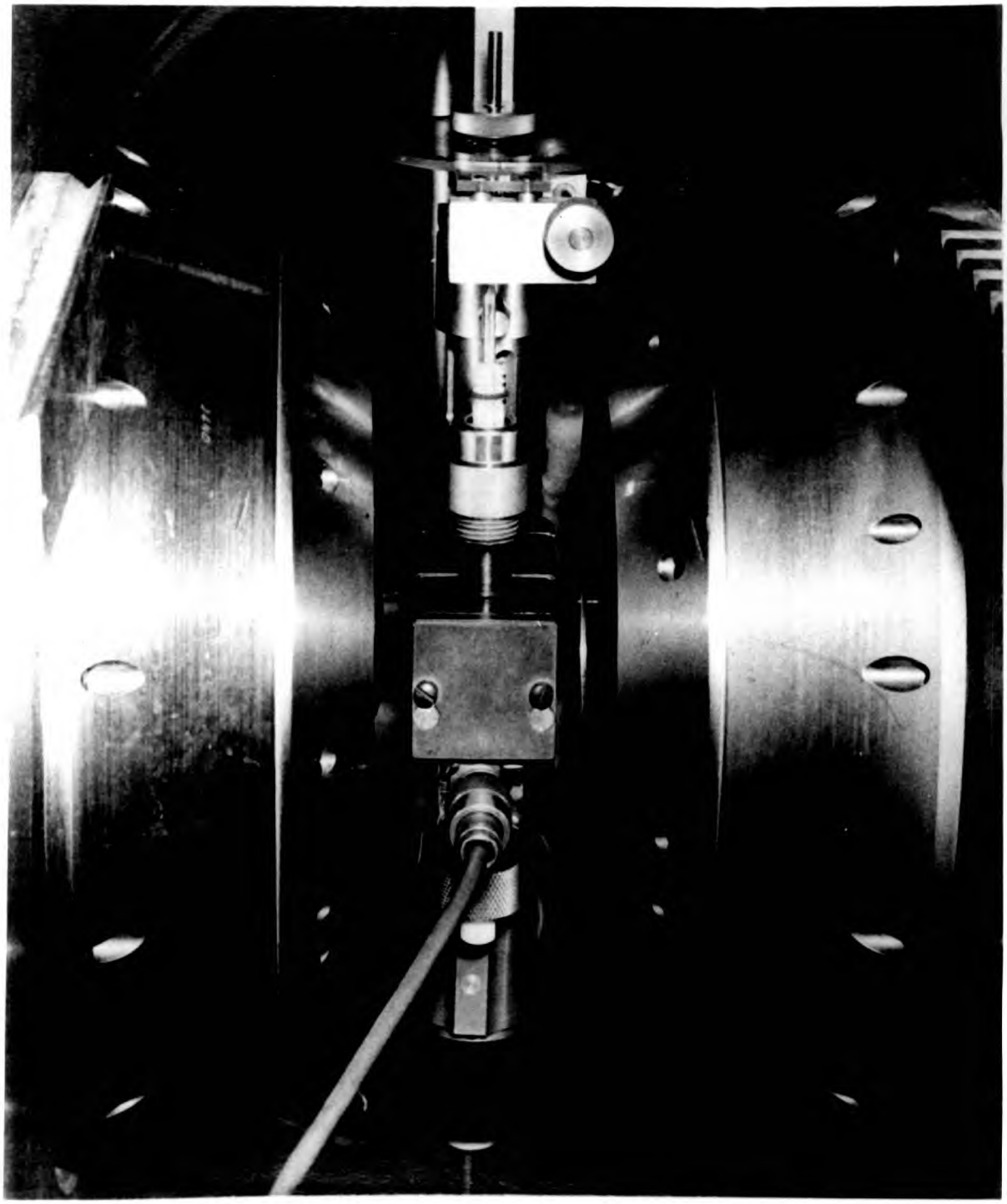


Figure 6.4 (a)

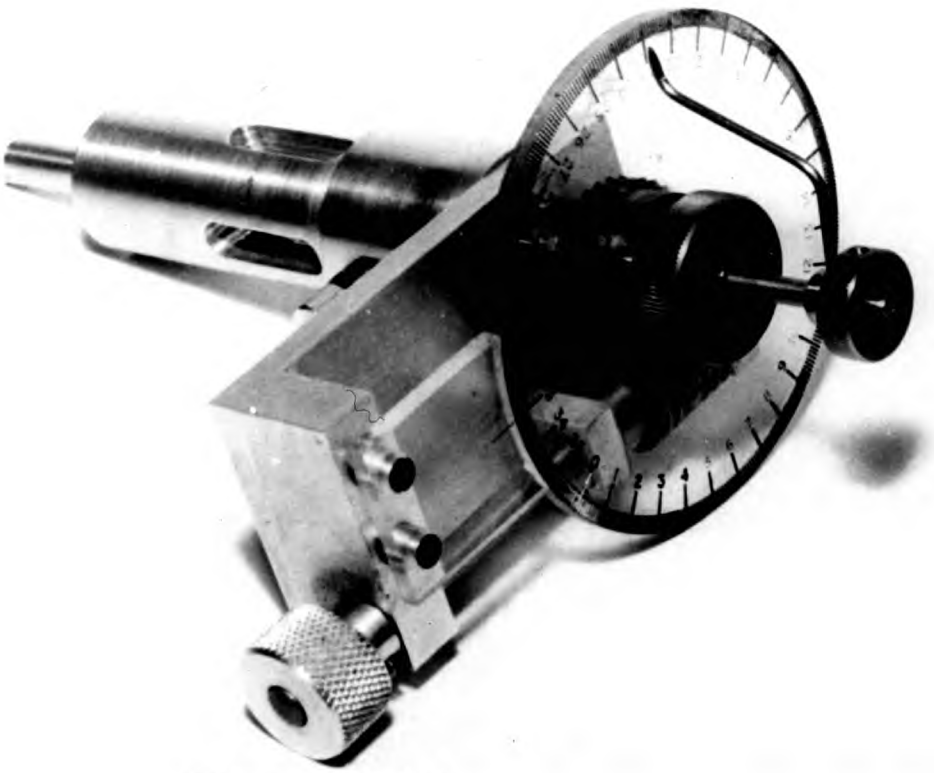


Figure 6.4 (b)

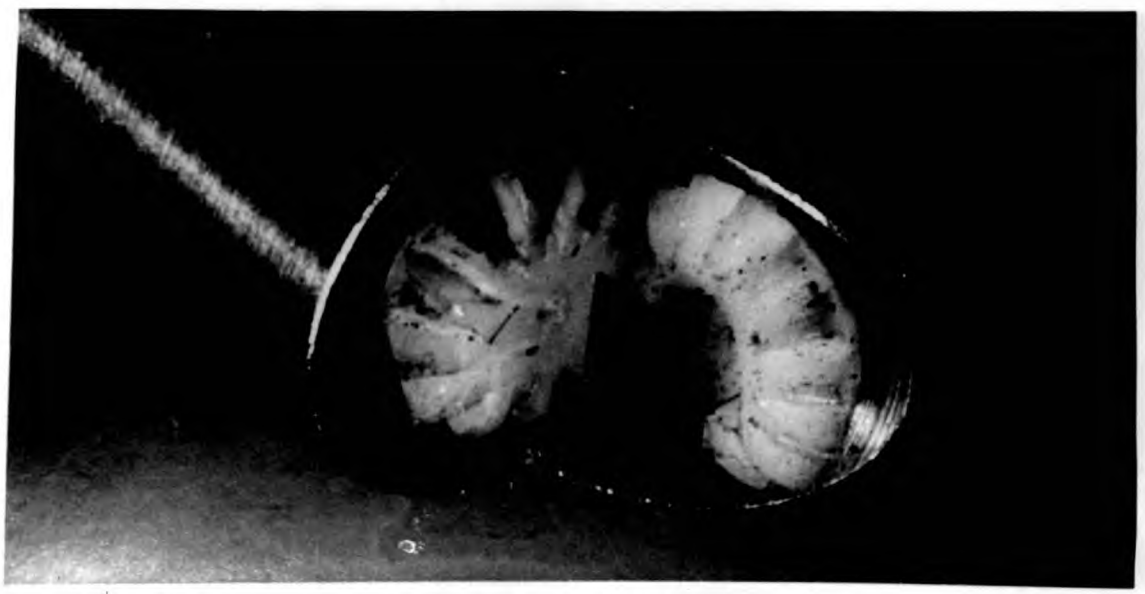


Figure 6.4 (c)

6.10 Fe^{3+} EXPERIMENTAL

6.10.1 The Room Temperature Resonance Spectrum

Since Fe^{3+} is always present in $BaTiO_3$ even in the 'purest' crystals it was not unnatural then that most of the early magnetic resonance investigations of $BaTiO_3$ should have been directed to explaining the origin of the spectral lines so obtained. Hornig et al (1954) though identifying some of the lines, did not identify them all, and some of them incorrectly in both phases (tetragonal and cubic). The earlier work of Low and Shaltiel (1958) and Hornig et al. (1954) finally identified a primary five line spectrum as stemming from Fe^{3+} (Hornig et al. 1959). The present work confirms this spectrum with the addition of the line γ which is shown in Fig. 6.5, the five lines concerned being shown; those marked α, β and γ are discussed later.

6.10.2 Rotation of the crystal (spectrum)

This was effected by means of the goniometer already described such that the value of θ could be varied without changing the angle between the microwave field H_1 and the d.c. magnetic field H. Changing the angle between H_1 and H in addition to affecting the intensity of the lines would alter the selection rules. We have found that rotation of the sample affects the electrical properties of the cavity hardly at all since it does not need retuning over an appreciable

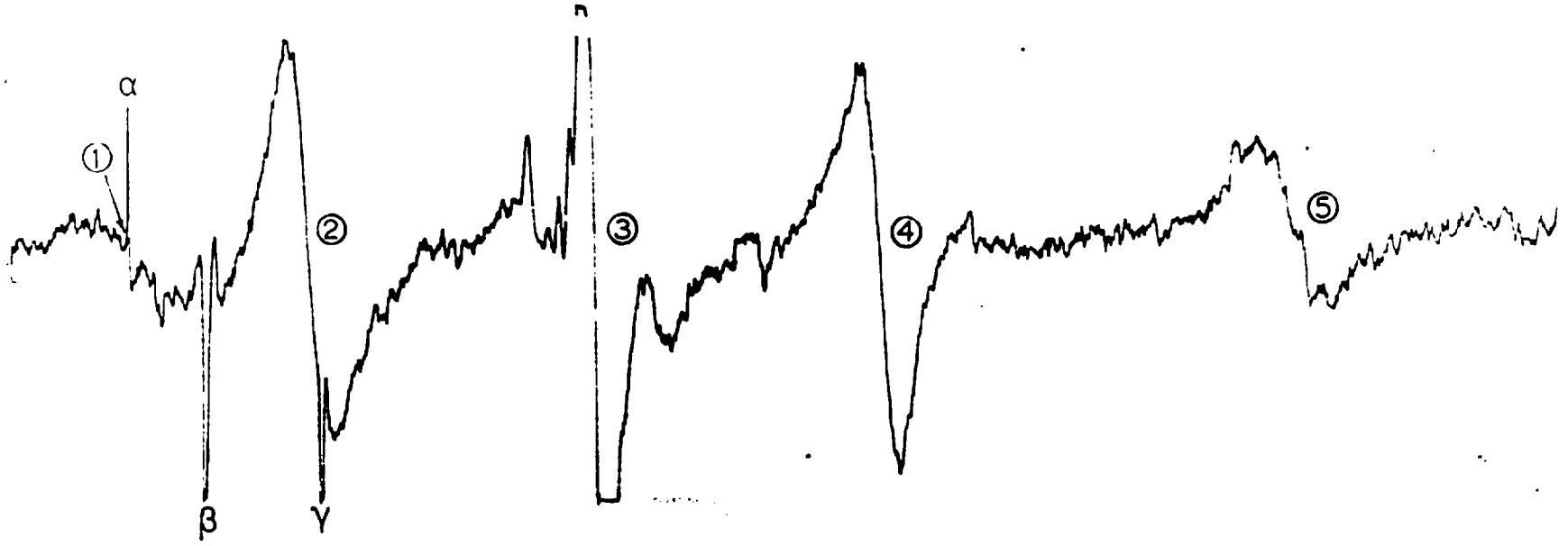


Figure 6.5

angle of rotation - approximately 80°.

The results of rotation on the room temperature spectrum are shown in Fig. 6.6 from which it is seen that the angular behaviour of the various transitions does not follow a typical $3(g_{\prime\prime}/g)^2\cos^2\theta-1$ law as would be expected if $h\nu$ at X-band were large compared to the zero field splitting (Bleaney, 1951). The large separation at $\theta = 0^{\circ}$ also supports this conolusion. However it is clear from the angular behaviour that there are basically five relatively intense transitions.

6.10.3 Temperature dependence

The behaviour of the resonant magnetic fields of the five lines as the temperature is varied from room temperature to above the Curie point is shown in Fig. 6.7, the transitions between those energy levels shown which is responsible for a particular line being derived from the energy level diagram. Immediately apparent is the rather large variation of crystal field splittings and it's sudden 'collapse' at $129^{\circ}C$. The shaded region extending up to $129^{\circ}C$ shows the range over which the resonant fields were measured at increments of $1^{\circ}C$; this region was quite reproducible using the same crystal after repoling.

6.11 THEORY OF Fe^{3+} IN BARIUM TITANATE

6.11.1 Introduction

The form of the spin Hamiltonian which describes adequately

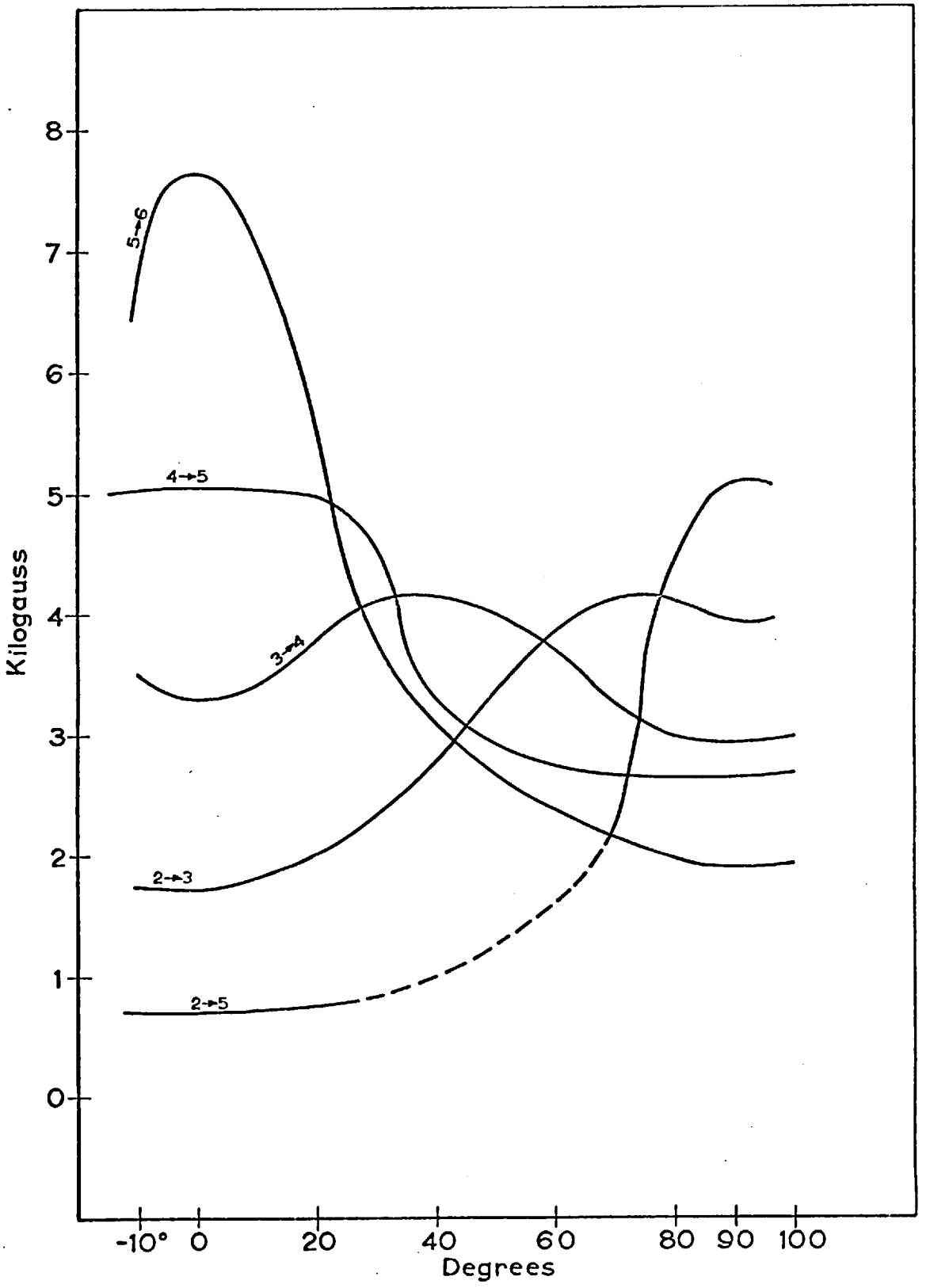

8
7
6
5
4
3
2
1
0
Kilogauss
5→6
4→5
3→4
2→3
2→5
-10°
0
20
40
60
80
90
100
Degrees

Figure 6.6

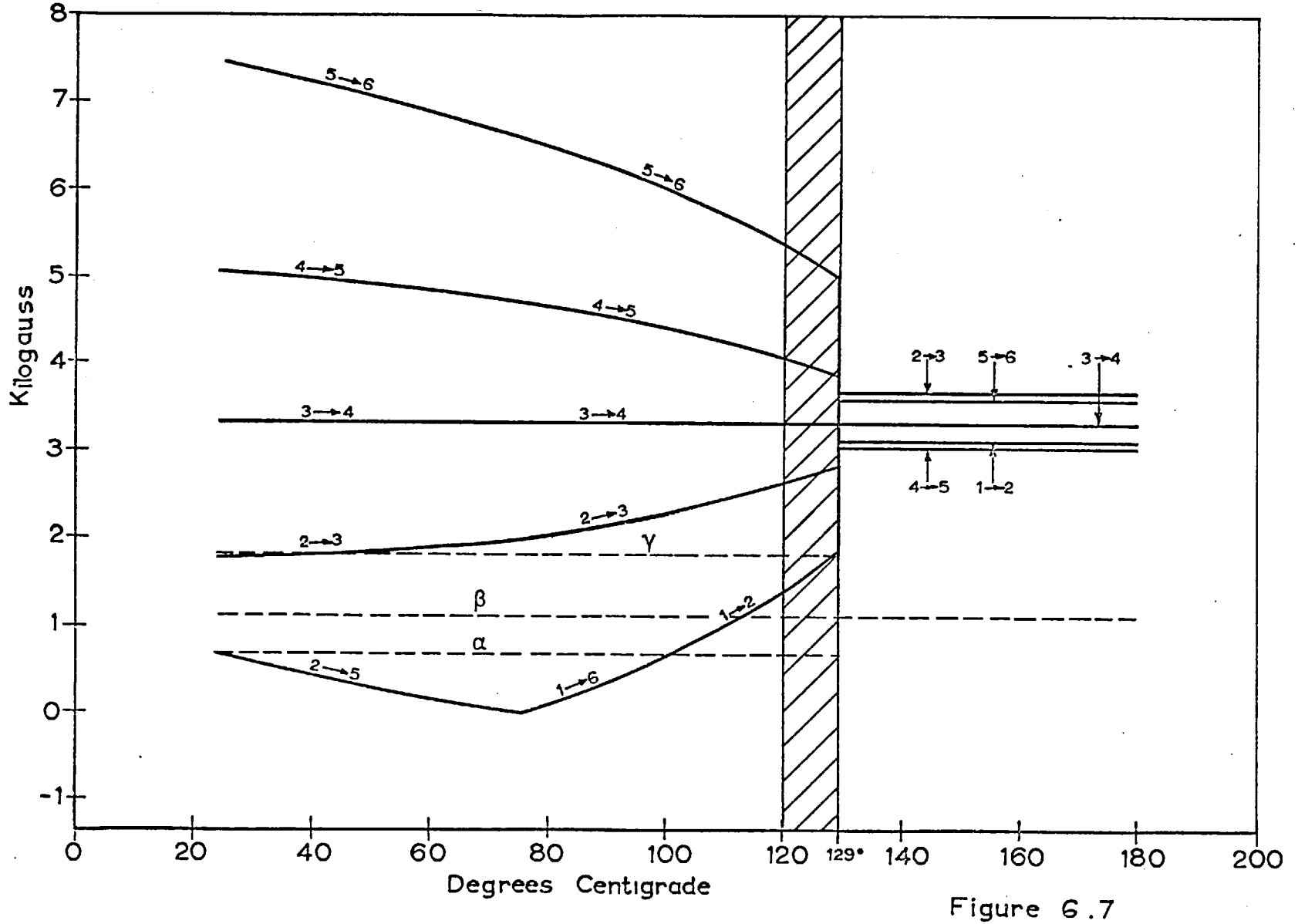

Kilogauss
8
7
6
5
4
3
2
1
0
-1
0
20
40
60
80
100
120
129°
140
160
180
200
Degrees Centigrade
5→6
5→6
4→5
4→5
3→4
3→4
2→3
2→3
γ
β
α
1→2
2→5
1→6
2→3
5→6
3→4
4→5
1→2

Figure 6.7

the energy levels of a $^6S_{5/2}Fe^{3+}$ ion in a tetragonal crystalline electric field and an external magnetic field is given by:

$$H = \beta H.g.S + DS_z^2 + aS_z^4 + b(S_x^4 + S_y^4)$$

The first term is the Zeeman term common to all spin Hamiltonians, the term in DS_z^2 describes the effect of axial distortion, there being no term in $E(S_x^2 - S_y^2)$ as the axial symmetry is not further lowered. The final fourth order terms represents, as we have already seen, the effect of the cubic crystalline field on the degeneracy of S-state ions. Since there is no nuclear spin associated with Fe^{3+}, then there will be no terms representing hyperfine interaction, quadrupole interaction, or direct interaction with the external magnetic field.

6.11.2 The Matrix Elements

Owing to the form of the Zeeman term $\beta(H.g.S)$ the effect of crystal orientation on the Hamiltonian matrix is of prime importance in determining the necessary parameters once the energy eigenvalues are known.

Consider the action of a magnetic field H at general angles θ and ϕ to the 'c' axis as shown in Fig. 6.8.

Now the components of H are given by,

$$H_x = H \sin\theta \cos\phi$$

$$H_y = H \sin\theta \sin\phi$$

$$H_z = H \cos\theta$$

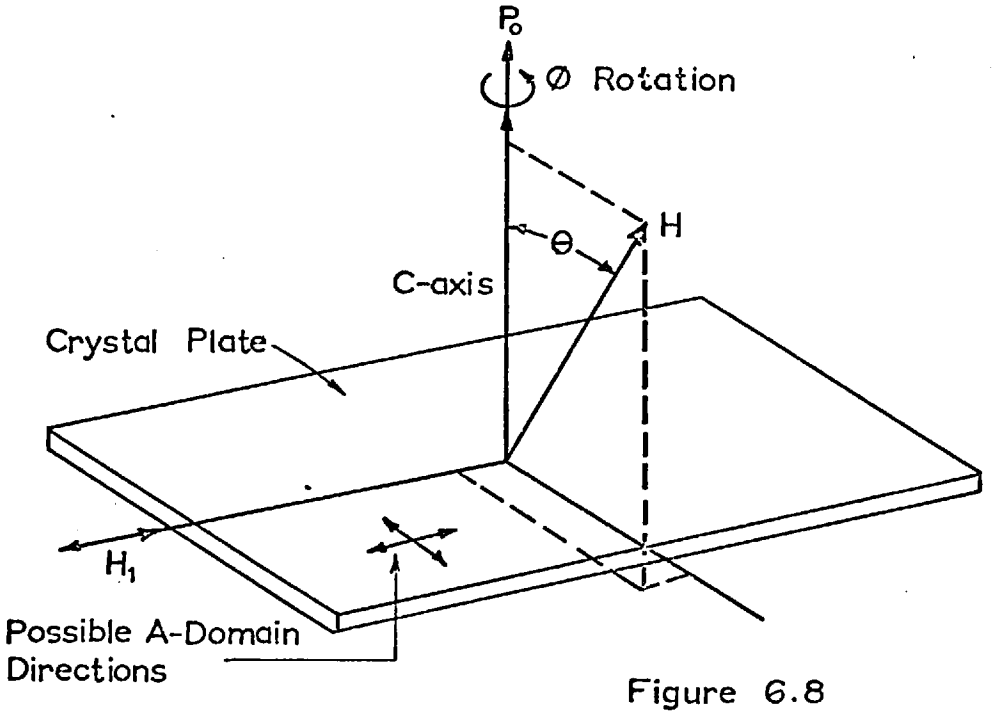


Figure 6.8

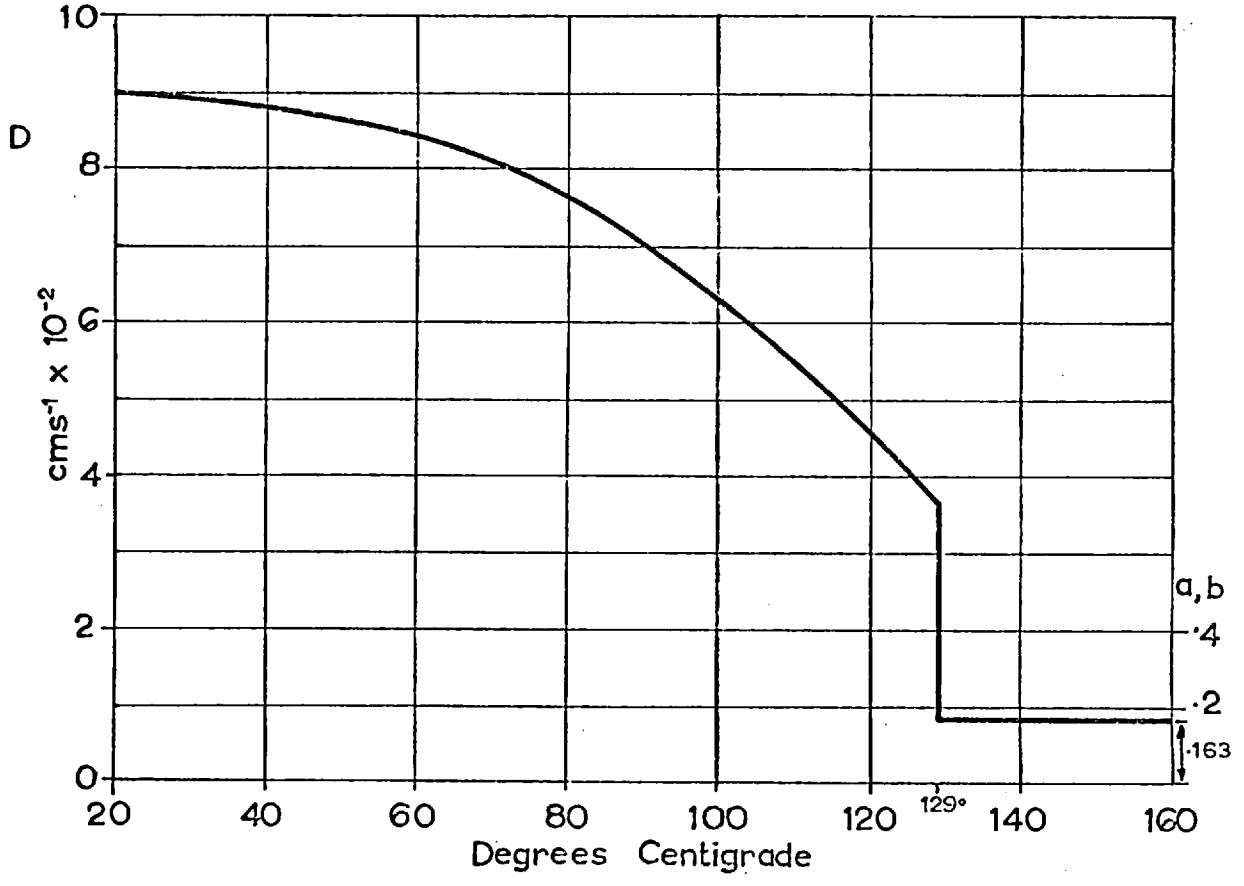


Figure 6.9

$$\beta(H.g.S) = \beta\left[H\sin\theta\cos\phi.g_{\perp}.S_x + H\sin\theta\sin\phi.g_{\perp}.S_y + H\cos\theta.g_{\parallel}.S_z\right]$$

where $g^2(\theta) = g_{\parallel}^2\cos^2\theta + g_{\perp}^2\sin^2\theta$

and we obtain from the shift operators,

$$S_x = \frac{S_+ + S_-}{2}, \qquad S_y = -\frac{i}{2}(S_+ - S_-)$$

hence $$\beta(H.g.S) = Hg_{\perp}\sin\theta\left[\frac{(S_+ + S_-)}{2}\cos\phi - \frac{i}{2}(S_+ - S_-)\sin\phi\right] + Hg_{\parallel}\cos\theta S_z$$

$$= qS_+ + q^*S_- + pS_z$$

where $$q = \tfrac{1}{2}\beta Hg_{\perp}\sin\theta(\cos\phi - i\sin\phi) = \tfrac{1}{2}Hg_{\perp}\sin\theta e^{-i\phi}$$

$$q^* = \tfrac{1}{2}\beta Hg_{\perp}\sin\theta e^{i\phi}$$

$$p = \beta Hg_{\parallel}\cos\theta$$

With the general orientation the spin Hamiltonian is now of the form,

$$H = \beta(qS_+ + q^*S_- + pS_z) + DS_z^2 + aS_z^4 + b(S_x^4 + S_y^4)$$

Using the Pauli spin matrices we may now 'fill in' the elements of the Hamiltonian matrix which then takes the form shown below:

	$\|5/2\rangle$	$\|3/2\rangle$	$\|1/2\rangle$	$\|-1/2\rangle$	$\|-3/2\rangle$	$\|-5/2\rangle$
$\langle 5/2\|$	$5/2p+\xi$	$5q$	0	0	$3\sqrt{5}b$	0
$\langle 3/2\|$	$5q^*$	$3/2p+\eta$	$2\,2q^*$	0	0	$3\sqrt{5}b$
$\langle 1/2\|$	0	$2\,2q^*$	$1/2p+\zeta$	$3q$	0	0
$\langle -1/2\|$	0	0	$3q^*$	$-1/2p+\zeta$	$2\,2q$	0
$\langle -3/2\|$	$3\sqrt{5}b$	0	0	$2\,2q^*$	$-3/2p+\eta$	$5q$
$\langle -5/2\|$	0	$3\sqrt{5}b$	0	0	$5q^*$	$-5/2p+\xi$

where we have written

$$\frac{25}{4}D + \frac{625}{16}a + \frac{65}{8}b = \xi$$

$$\frac{9}{4}D + \frac{81}{16}a + \frac{241}{8}b = \eta$$

$$\frac{1}{4}D + \frac{1}{16}a + \frac{401}{8}b = \zeta$$

The solutions of this Hamiltonian matrix are the eigenenergies of the system which, when compared with experiment, enable us to determine the five parameters $g_{\parallel}$, $g_{\perp}$, a, b and D. However the Hamiltonian matrix in its present form does not lend itself to a convenient solution, and noting that if the 'c' axis is aligned parallel with the d.c. magnetic field then $\theta = 0$ which makes $q = q^* = 0$, the only off diagonal terms are the $3\sqrt{5}b$ ones which since they are derived from fourth order terms in the spin Hamiltonian are very much smaller than the D and Zeeman terms. Redundancy of terms in q and q^* enables us to put the Hamiltonian matrix into the workable form using the techniques of matrix algebra as shown below:

	$\|5/2\rangle$	$\|-3/2\rangle$	$\|1/2\rangle$	$\|-1/2\rangle$	$\|3/2\rangle$	$\|-5/2\rangle$
$\langle 5/2\|$	$5/2p+\xi$	$3\sqrt{5}b$	0	0	0	0
$\langle -3/2\|$	$3\sqrt{5}b$	$-3/2p+\eta$	0	0	0	0
$\langle 1/2\|$	0	0	$1/2p+\zeta$	0	0	0
$\langle -1/2\|$	0	0	0	$-1/2p+\zeta$	0	0
$\langle 3/2\|$	0	0	0	0	$3/2p+\eta$	$3\sqrt{5}b$
$\langle -5/2\|$	0	0	0	0	$3\sqrt{5}b$	$-5/2p+\xi$

The solution of the eigenenergies is now particularly simple and is given as:

$$E_{3,4} = \pm \frac{p}{2} + \zeta$$

$$E_{1,5} = \tfrac{1}{2}(p+\xi+\eta) \pm (2p+\xi-\eta)^2 + 4.45b^2\,{}^{\frac{1}{2}}$$

$$E_{2,6} = \tfrac{1}{2}(-p+\xi+\eta) \pm (-2p+\xi-\eta)^2 + 45b^2\,{}^{\frac{1}{2}}$$

These then are the six eigenvalues corresponding to the spin Hamiltonian operator for the ${}^6S_{5/2}d^5$ Fe^{3+} ion in an axially distorted field. The variation of these eigenenergies with magnetic field for a given temperature (energy level diagram) may then be obtained once the constants in the spin Hamiltonian have been evaluated.

6.12 EVALUATION OF THE PARAMETERS OF THE SPIN HAMILTONIAN FROM DATA AT $\theta = 0$.

The resonance spectrum of five lines is obtained as a result of transitions stimulated between the above six energy levels by the microwave field. These transitions are given by:

$$E_{1-2} = h\nu = g\beta H_{12} + \sqrt{[(\Delta+2g\beta H_{12})^2 + 45b^2]} - \sqrt{[(\Delta-2g\beta H_{12})^2 + 45b^2]} \qquad (1)$$

$$E_{2-3} = h\nu = -g\beta H_{23} + 2\Delta - 12a - 9b - \sqrt{[(\Delta-2g\beta H_{23})^2 + 45b^2]} \qquad (2)$$

$$E_{3-4} = h\nu = g\beta H_{34} \qquad (3)$$

$$E_{4-5} = h\nu = -g\beta H_{45} - 2\Delta + 12a + 9b + \sqrt{[(\Delta+2g\beta H_{45})^2 + 45b^2]} \qquad (4)$$

$$E_{5-6} = h\nu = g\beta H_{56} + \sqrt{[(\Delta-2g\beta H_{56})^2 + 45b^2]} - \sqrt{[(\Delta+2g\beta H_{56})^2 + 45b^2]} \qquad (5)$$

where we have made the substitution

$$\Delta = 2D + 17a - 11b = \frac{\xi - \eta}{2}$$

6.12.1 (i) g - tensor

Now from equation (3) we can get a value for $g_{\parallel}$ and since this line was found to coincide exactly with that for the free radical DPPH then $g_{\parallel} = g_{\perp} = g = 2.003$ and we may conclude that the g tensor is isotropic and also from Fig.6.7 that it is independent of temperature.

(ii) D, a, b

Evaluation of these constants involves solution of simultaneous non-linear equations. Using computer programs for the solution of matrices by an iterative process it was not possible to iterate to zero because the matrix of the above constants was found to be unstable.

Because of this we may without appreciable error ignore the off diagonal components $3\sqrt{5}b$ when the eigenvalues are then given straight away by the diagonal terms, from which a set of linear equations is obtained similar to those above. If we assume that a = b at room temperature (as it does above 129°C) then insertion of the values for the resonance field give the following values:

$$|D| = 0.0900 \pm 0.002 \text{ cms}^{-1}$$

$$|a| = |b| = 0.00163 \pm 0.001 \text{ cms}^{-1}$$

By setting H = 0 we obtain the magnitude of the zero field splittings (separation of Kramers doublets) as 0.391 cms^{-1} between the $\pm$ 5/2 and $\pm$ 3/2 level and 0.160 cms^{-1} between the $\pm$ 3/2 and $\pm$ 1/2 levels. Also for H = 0 in the expressions for the eigenvalues we see that the separation between the upper level (states 1 and 2) and the intermediate level (states 5 and 6) is $2\sqrt{[(\frac{\xi-\eta}{2})^2 + 45b^2]}$ and the zero field splitting between the intermediate level and the lower level (states 3 and 4) is $\xi - \eta - 12a - 9b - \sqrt{[(\frac{\xi-\eta}{2})^2 + 45b^2]}$. Substitution of the values obtained for D, a, b into these expressions gives the separations quoted above.

The variation of D, and 'a' and 'b' with temperature is shown in Fig. 6.9 from which the rather dramatic change in D is noticeable, the cubic field parameters remaining constant.

6.13 THE ENERGY LEVEL DIAGRAM

Because of the rather large effect of the crystalline electric field relative to the Zeeman interaction it was somewhat difficult at first to positively identify the various transitions without a detailed knowledge of the energy level diagram. However, due to the occurrence of off-diagonal terms in the Hamiltonian matrix, reflection of the wave functions at low magnetic fields will occur and transitions may take place between non-adjacent levels. Also at these low fields the Zeeman term is small and decreasing in magnitude since it is

linearly dependent on H and in this region the crystal field terms will predominate. This may be seen quite easily by straight-forward use of second order perturbation theory, but will not be included here.

Working with the two highest field lines, values for D, a, b, were obtained which were then substituted back into the eigenvalues together with the value previously obtained for g. The eigenvalues were then numerically evaluated for varying H//z and the energy level diagram of Fig. 6.10 at room temperature was plotted. The two lower field transitions were then identified and values for D, a, b, were obtained which agreed with those found from the two high field lines.

With H//x, the eigenvalues are obtained immediately from those for H//z by replacing g_z (= $g_{\parallel}$) by g_x (= $g_{\perp}$), D by $\frac{1}{2}(3E - D)$. This can be seen if, using the relation $S_x^2 + S_y^2 + S_z^2 = S(S + 1)$, one rewrites the axial crystal field operator in the form $D_x S_x^2 + D_y S_y^2 + D_z S_z^2, (D_x + D_y + D_z = 0)$ where $D = 3/2 D_z$. It follows then that for H//x, D is replaced by $3/2 D_x = -\frac{1}{2}D$. These transformation rules are independent of the value of S, and by their substitution into the eigenvalues of the Hamiltonian matrix and their subsequent evaluation for increasing magnetic field enables the energy level diagram for the case H//x to be constructed - see Fig. 6.11.

Owing to the sudden collapse of the axial field at 129°C

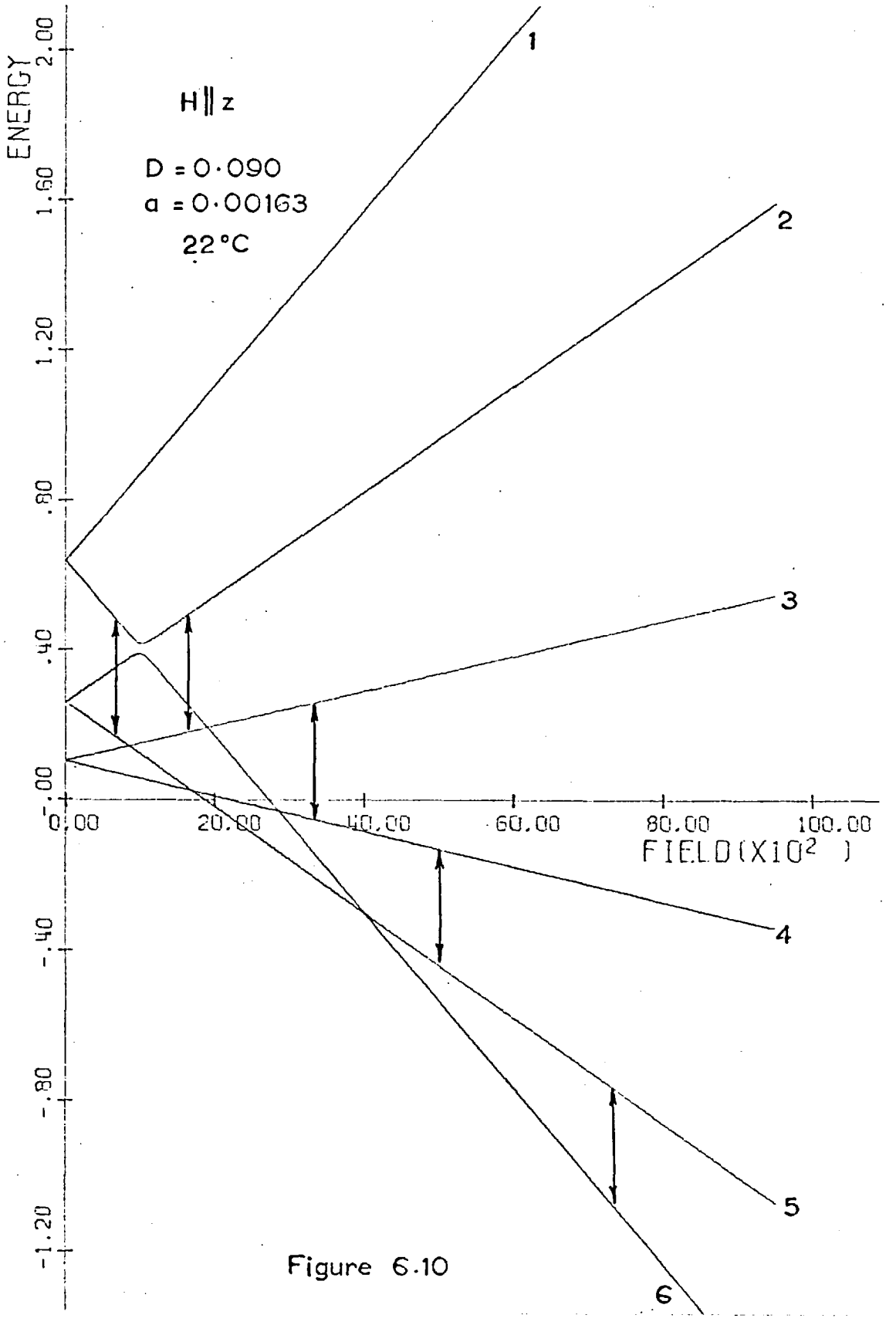

ENERGY
2.00
1.60
1.20
.80
.40
.00
-.40
-.80
-1.20
H || z
D = 0·090
a = 0·00163
22°C
1
2
3
4
5
6
0.00
20.00
40.00
60.00
80.00
100.00
FIELD (X10²)

Figure 6.10

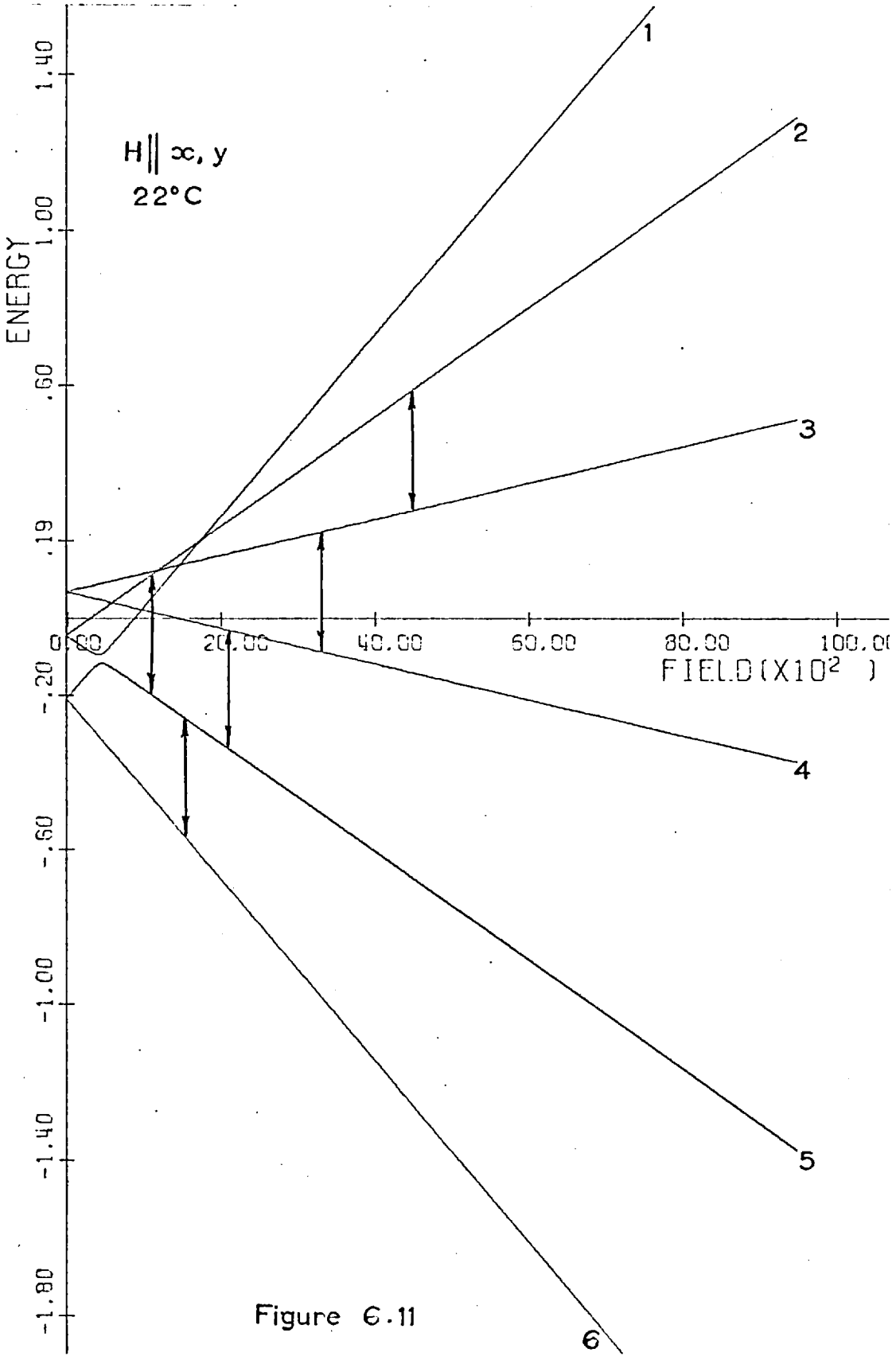

H∥ x, y
22°C
ENERGY
1.40
1.00
.60
.19
-.20
-.60
-1.00
-1.40
-1.80
0.00
20.00
40.00
60.00
80.00
100.00
FIELD(X10²)
1
2
3
4
5
6

Figure 6.11

(see Fig. 6.7), the axial field parameter (D) thus goes to zero and only the cubic field terms are then responsible for the splitting of the paramagnetic spectrum in the cubic phase. It is found that this is accounted for by assigning the same value to 'a' (which now equals b) as that found in the tetragonal phase. This then shows that the cubic field parameters undergo no change in crossing the Curie point. The spectrum obtained in the cubic phase is shown in Fig. 6.12, from which we see how the central line is undeviated, together with two unresolved lines on either side. This is more clearly seen from the resultant energy level diagram (Fig. 6.13) which is here calculated for the case D = 0.

We may, since there is some inaccuracy in deciding on the exact value of the transition field for a particular line other than of course the centre line which coincides with that for DPPH, insert suitable values for D, a (= b) then evaluate the eigenenergies as a function of increasing magnetic field and fit our transitions accurately by means of the resulting energy level diagram. It was found that the transitions, and hence the resulting energy level diagram, were extremely sensitive to variations in D (third decimal place), but notso to the cubic field parameters.

In addition, a computer program was written which searches for transitions by equating the difference between any two

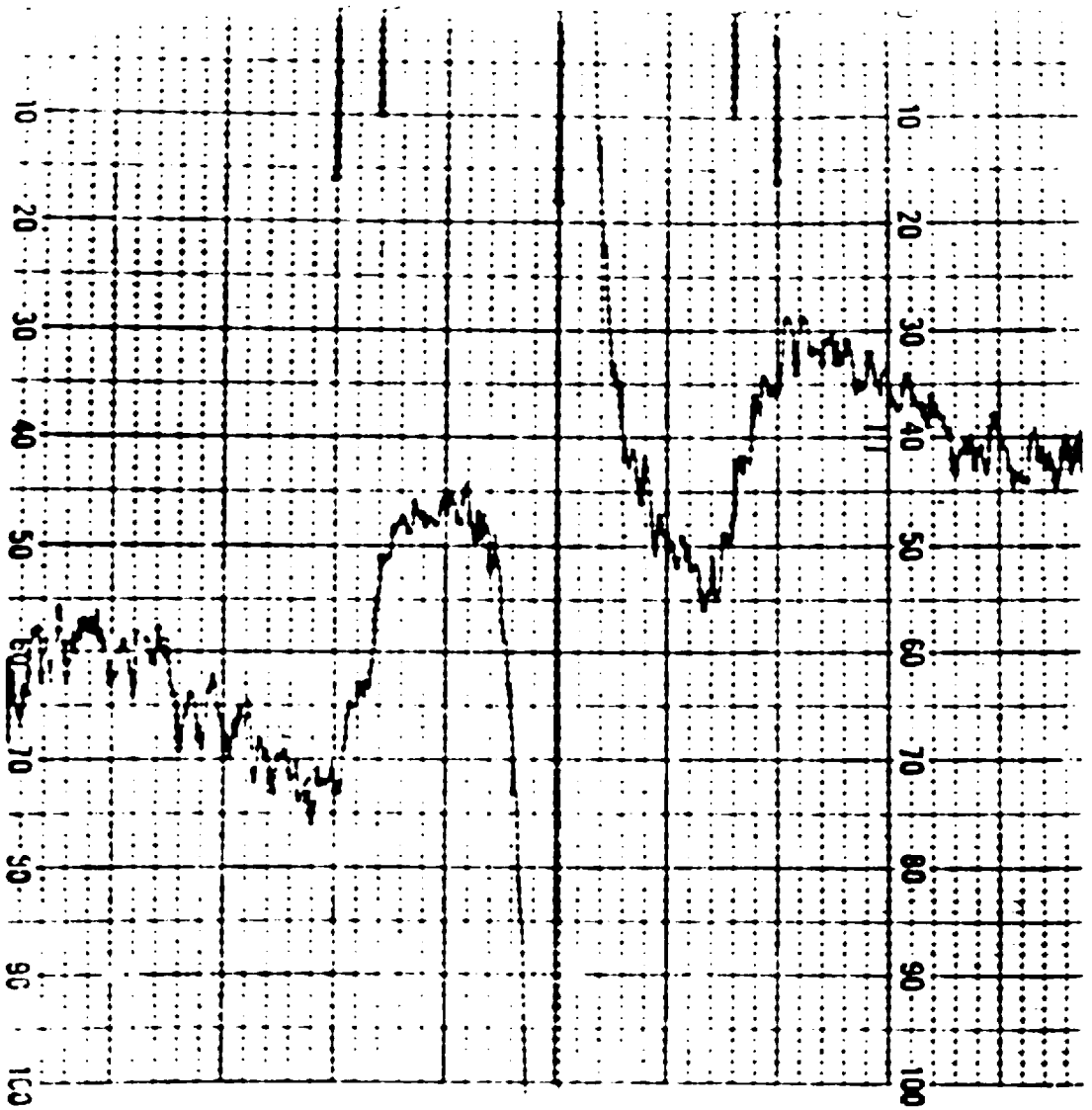


Figure 6.12

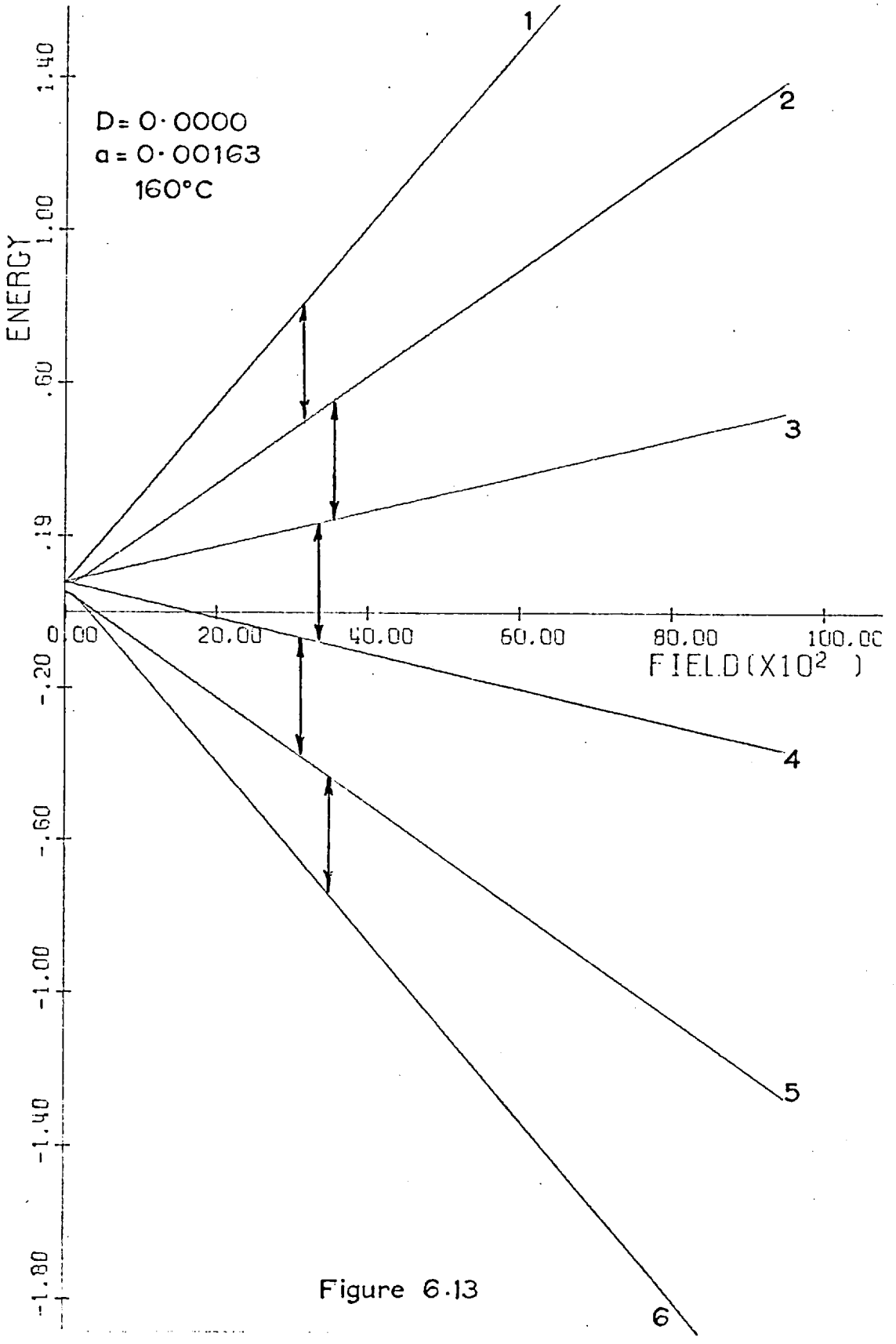

D= 0·0000
a = 0·00163
160°C
ENERGY
1.40
1.00
.60
.19
-.20
-.60
-1.00
-1.40
-1.80
0.00
20.00
40.00
60.00
80.00
100.00
FIELD (X10²)
1
2
3
4
5
6

Figure 6.13

eigenenergies to the quantumn of microwave radiation concerned. It should be noted that in this procedure the program will identify so-called 'forbidden' transitions, i.e. $\Delta M_s \geq \pm 2$. This is an added check to our evaluation of the Hamiltonian matrix and was done over the temperature range of interest concerned. Having decided by this procedure on a suitable value for D, a (= b) for a given temperature then the computerised eigenenergies were fed into the CALCOMP routine and the resulting energy level diagram automatically plotted. This plotting routine was found to be far more accurate than other direct computer plots because of it's superior resolution. All direct computer plots employed were not sufficiently resolved to enable positive identification of the low field transitions. The whole of the above process was then repeated over the complete temperature range and in this way a 'best fit' of the variation of D,'a' with temperature was achieved. Two resulting energy level diagrams at intermediate temperatures are shown in Figs. 6.14; 6.15.

Having established the nature of the energy level diagram, the transitions associated with their movement could be followed. This was particularly important for the low field line where we see that in different temperature ranges there are three different transitions responsible for it which may be seen from the above series of energy level diagrams with increasing temperature.

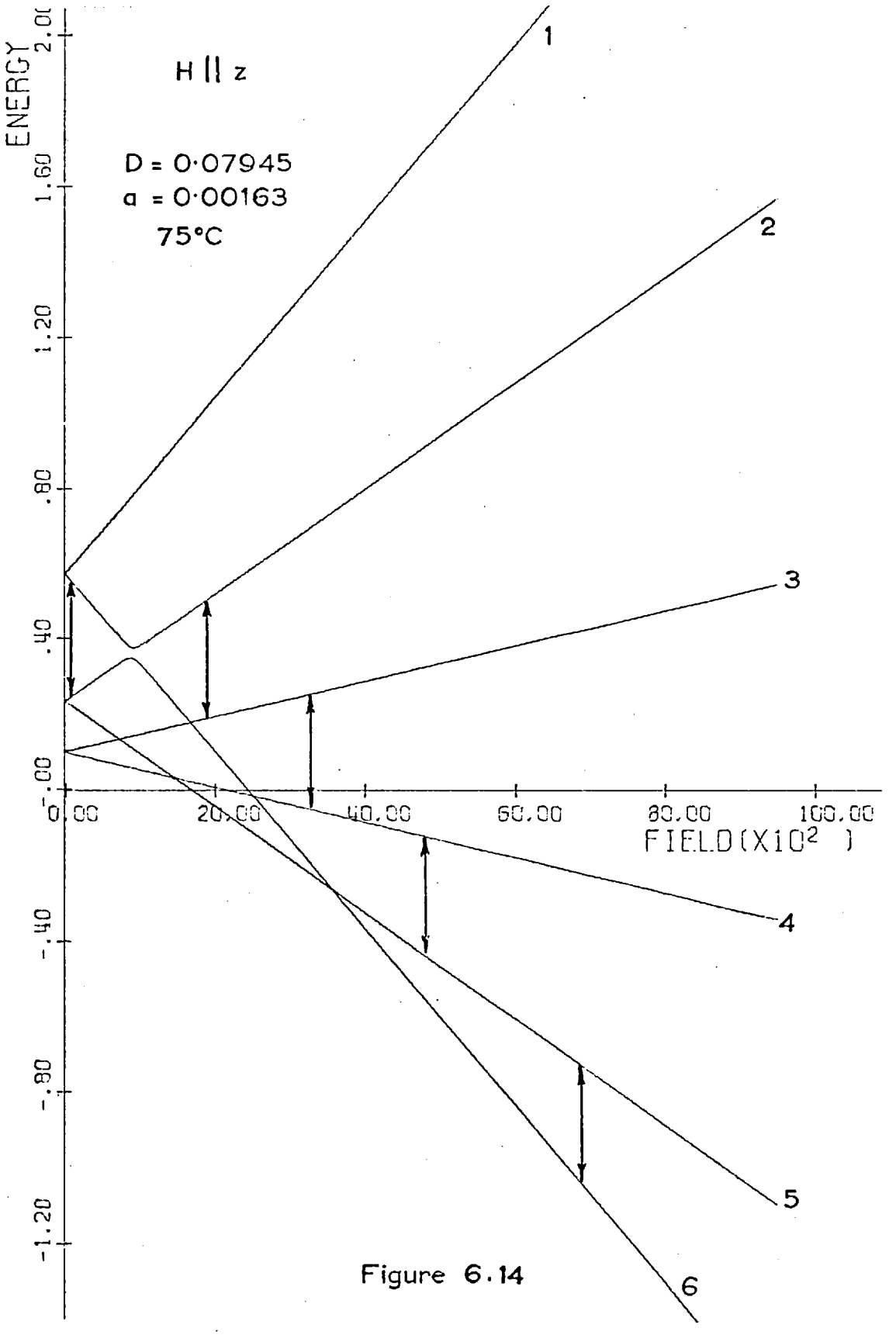

H || z
D = 0·07945
a = 0·00163
75°C
ENERGY
2.00
1.60
1.20
.80
.40
.00
-.40
-.80
-1.20
0.00
20.00
40.00
60.00
80.00
100.00
FIELD (X10²)
1
2
3
4
5
6

Figure 6.14

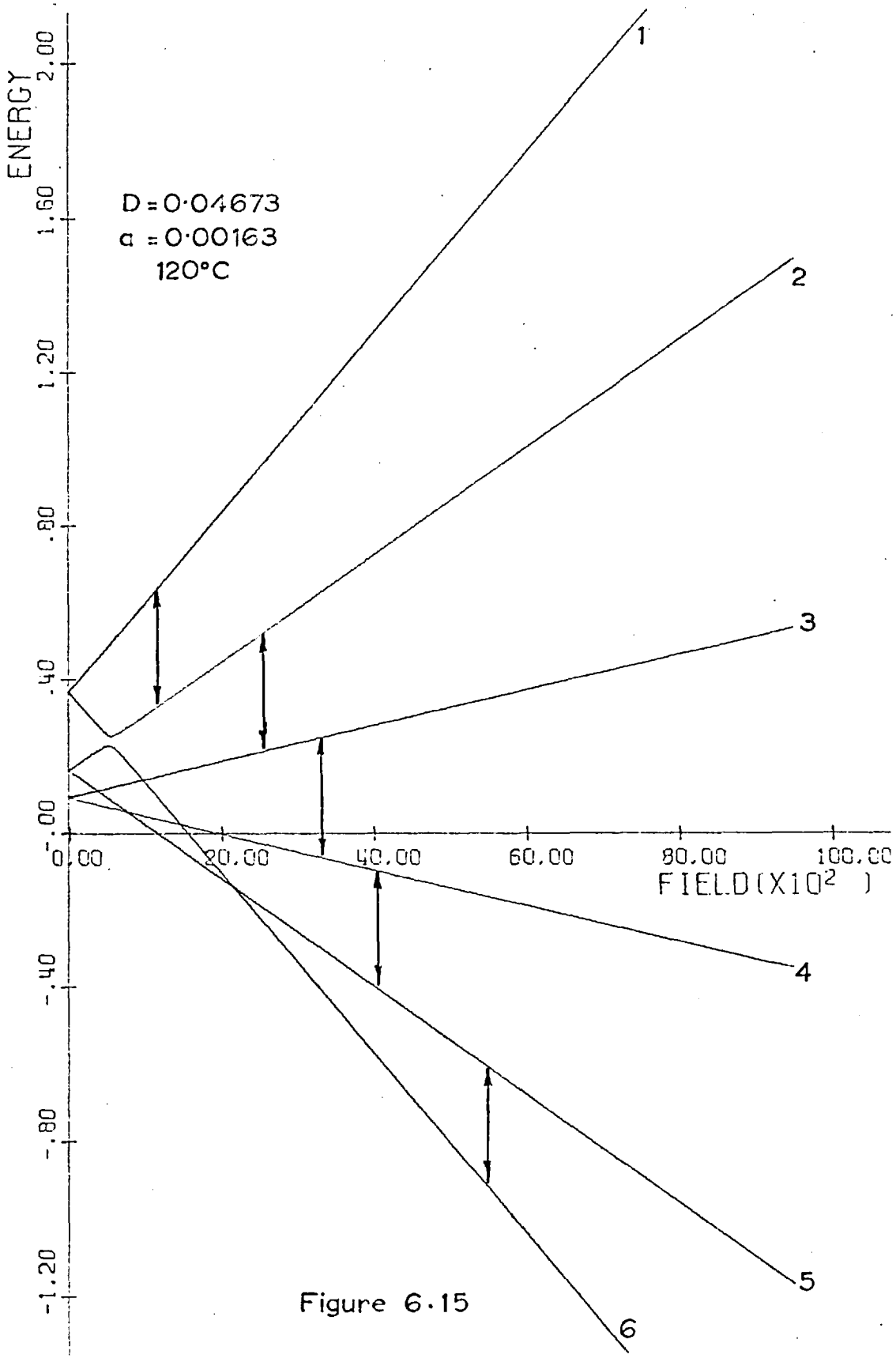

ENERGY
2.00
1.60
1.20
.80
.40
-.00
-.40
-.80
-1.20
D = 0·04673
a = 0·00163
120°C
1
2
3
4
5
6
0.00
20.00
40.00
60.00
80.00
100.00
FIELD (X10²)

Figure 6.15

6.14 Mn^{2+} - EXPERIMENTAL

6.14.1 Introduction

Since single crystal doped with Mn^{2+} (approximately 0.01%), was successfully grown and preliminary experiments revealed a six-line spectrum, then because Mn^{2+} has $I = \frac{5}{2}$ and $S = \frac{5}{2}$ it was hoped that it would be possible to monitor the nuclear properties as a function of their interaction with the crystal field (since $S = \frac{5}{2}$, d^5 is spherically symmetric) and of temperature. The main interaction here would be the additional splitting of the hyperfine spectrum due to the quadrupole interaction of the Mn^{2+} nucleus with the O^{2-} ligands.

The paramagnetic resonance spectrum of Mn^{2+} ions in $BaTiO_3$ was studied by Low (1960), Odehnal (1963), and Ikushima and Hayakawa (1964). The above workers made their studies on powdered samples of $BaTiO_3$ and, with the exception of the last worker mentioned, confined their attention to liquid nitrogen temperatures. Odehnal studied forbidden transitions $\Delta m \neq 0$ where m denotes the nuclear magnetic quantumn number and a number of other workers have also been engaged in investigating similar 'forbidden' transitions in crystals of similar structure (Bleaney and Ingram, 1951; Herd, Sachs and Hershberger, 1954; Sierro, Lacroix and Müller, 1959; and Folen, 1962). However, it will be seen from the following discussion that any measurements involving temperature variation would have to be made

using single crystals.

6.14.2 Experimental

Bleaney and Rubins (1961) give the following expression for the ratio of the intensity of a first order forbidden transition to that of an allowed transition as

$$\left(\frac{3D}{4g\beta H}\right)^2 \sin^2 2\theta \left[1 + \frac{S(S+1)}{3M(M-1)}\right]^2 x \left[I(I+1) - m^2 + m\right]$$

where $g^2 = g_{\parallel}{}^2\cos^2\theta + g_{\perp}{}^2\sin^2\theta$ and θ is the angle the 'c'-axis makes with the magnetic field and the other symbols have their usual meaning. This enables a value of D, the zero field splitting parameter to be evaluated, where an allowed transition is of the type $M,m \rightarrow M-1,m$ and the forbidden transition is of the type $M,m \rightarrow M-1,m-1$ or $M,m-1 \rightarrow M-1,m$. It has been shown (Vessela et al. 1965) that the variation of D^2 with temperature is linear up to the Curie point but that no forbidden transitions occur in the cubic phase. No hyperfine parameters may be evaluated by this method. The value of D so found agrees with that of Ikushima (1966) also using single crystal, but in this case by direct substitution into the appropriate spin Hamiltonian. These workers however only get the thirty line spectrum at an angle of 50° to the magnetic field with the intensity of the six lines of the lowest lying doublet being very much greater than all the others. The value of the quadrupole moment was substituted into this spin Hamiltonian

using a room temperature value found previously by Ikushima and Hayakawa (1965), who calculated to third order perturbation theory the splittings of the 'forbidden' doublets.

Even by careful experimentation it has not been possible to obtain for $\Delta m = 0$, the thirty lines which should be exhibited by Mn^{2+} in the tetragonal phase in $BaTiO_3$ but only six hyperfine lines corresponding to transitions between the lowest pair of Kramers doublets, i.e. $+\frac{1}{2} \rightarrow -\frac{1}{2}$, the separations of which do not vary with temperature. We have observed first order forbidden transitions and second order transitions as well (see Fig. 6.16), the ratio of intensities of which vary with temperature. However, contrary to the findings of Vessela et al. (1965) the forbidden transitions do not disappear in the cubic phase. This then would imply that D does not go to zero and the explanation for this is not clear.

6.14.3 ENDOR-Electron nuclear double resonance.

The ENDOR experiment provides an alternative but far more accurate method of measuring the hyperfine splittings than a conventional EPR experiment. In this experiment one 'sits' on a particular resonance line in a conventional EPR experiment occurring between a given pair of nuclear levels and then increases the power until saturation occurs and the line almost disappears. If now a strong rf pulse is applied which reverses the nuclear spins completely and interchanges the populations of

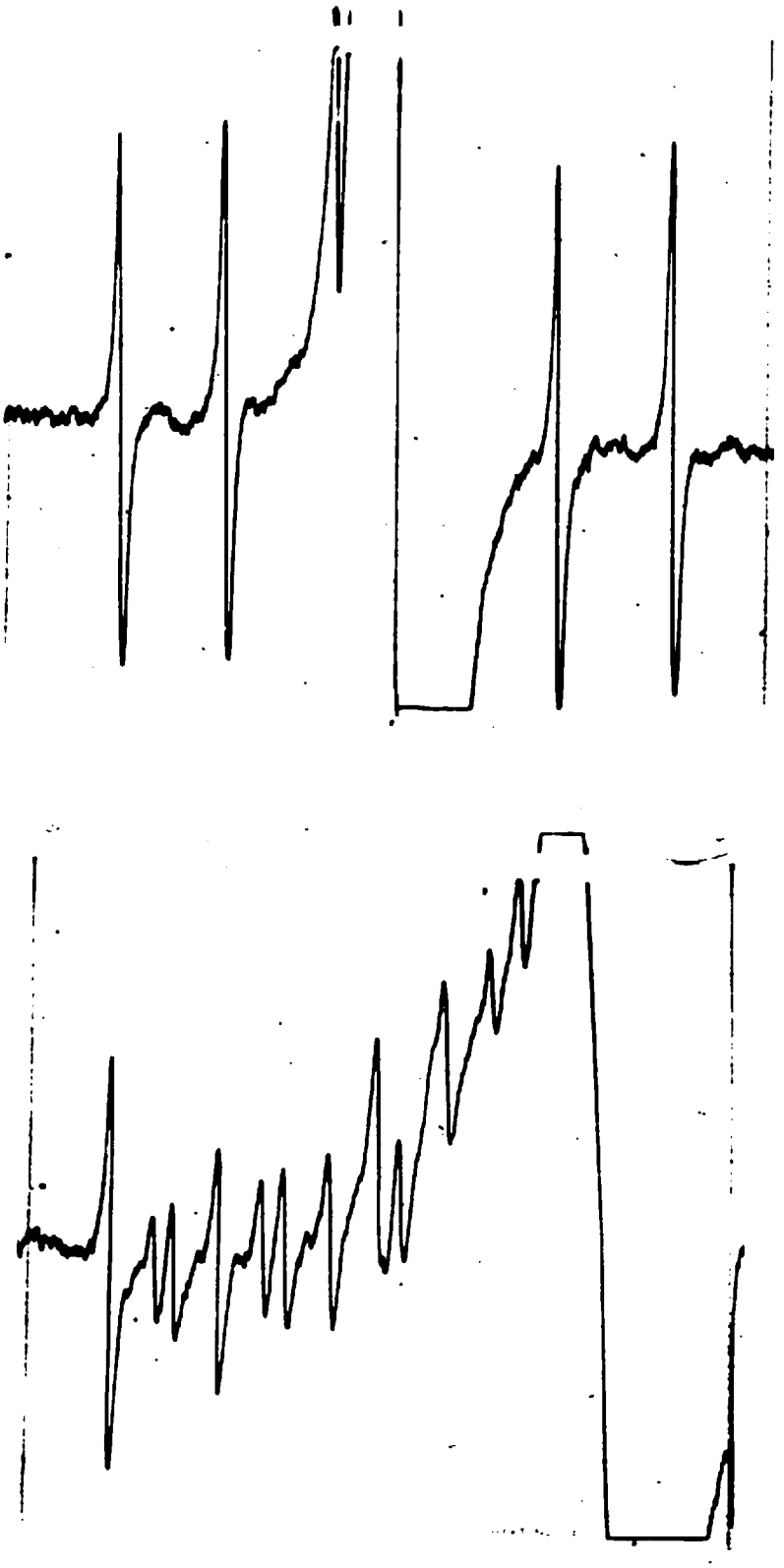


Figure 6.16

the two states then these will no longer have equal populations and the electron resonance signal suddenly ceases to be saturated and the absorption rises temporarily. In this way one may measure the frequency separation of the lines occurring in a hyperfine spectrum and thus determine if quadrupole interaction is present by their unequal spacing.

Preliminary measurements on the Varian V4502 spectrometer used indicated that saturation for an electron resonance signal was possible since a decrease in the line intensities was obtained when the microwave power was increased. However, experiments conducted in conjunction with Dr. A.J. Cooke at the National Physical Laboratory on specially constructed ENDOR apparatus produced negative results. This was almost certainly due to the relatively low abundance of nuclear spins, since any successful NMR experiment would require an almost 100% abundance. It was primarily for this reason that experiments using the Mössbauer effect were decided on due to the extreme sensitivity of the nuclear levels on their surroundings and the added facility of being able to accumulate data over a period of several hours. This is achieved by storing the number of counts and reproducing them by means of a 'kicksorter'.

7. THE MOSSBAUER EFFECT

7.1 FUNDAMENTAL FEATURES

7.1.1 Introduction

The recoil-free emission and resonant absorption between the nuclear ground and excited states of electromagnetic radiation (gamma rays) in solids was discovered by Mössbauer during graduate work at Heidelberg in 1957. The discovery rests on the realisation that some of the energies associated with nuclear events are not necessarily larger than those of chemical binding 1 - 10 eV, or even those characteristic of lattice vibrations, 10^{-2} - 10^{-1} eV. The energies in question are those associated with the recoil imparted to a nucleus by the emission of a low-energy gamma ray.

Prior to the work of Mössbauer the analysis of gamma-ray emission was usually carried out for the case of a free atom. This was based on the fundamentally sound precept that the energies involved in nuclear reactions are much larger than the energies of chemical binding and that the atom may well be thought of as a free atom when analysing nuclear events.

Since atomic resonance radiation depends on the existence of quantised energy levels, which are also present in nuclei, the possibility of observing nuclear resonance fluorescence (absorption) was obvious, and the search was started in 1929 (Kuhn, 1929). However, even though problems in atomic and

nuclear resonance seem very similar, there are marked differences which make nuclear experiments much more difficult. The difficulties associated with the resonance fluorescence process are outlined in greater detail in the following discussion on the emission of gamma rays by nuclei.

7.1.2 Emission of Gamma Rays by Nuclei

Consider a free atomic or nuclear system of mass M, with two energy levels A and B separated by an energy E_r. If the system decays from B to A by emission of a photon of energy E_γ, then the conservation of the momentum p of the photon and of the momentum P of the recoiling system must be equal and opposite. The recoiling system receives an energy R, given by

$$R = \frac{P^2}{2M} = \frac{p^2}{2M} = \frac{E_\gamma{}^2}{2Mc^2} \qquad (1)$$

(It is assumed that the recoiling system may be treated non-relativistically - an assumption satisfied in atomic and nuclear spectroscopy). Actually, all gamma rays involved in atomic and nuclear fluorescence have energies small compared to the rest energy Mc^2 of the emitting atomic or nuclear system. The recoil energy is thus very small compared to the gamma ray energy, and by energy conservation

$$E_r = E_\gamma + R \qquad (2)$$

Since R is very small compared to E_γ, then E_γ may be replaced

by E_r in equation (1):

$$R \cong E_r^2/2Mc^2 \qquad (1')$$

and the fraction of the available energy which is lost to the recoiling atom is small; for a gamma ray of 100 keV and nucleus of mass number 100 it is only 5 parts in 10^7. Before Mössbauer's work it was impossible to measure the energy of a gamma ray with sufficient precision to detect such small energy differences. The recoil energy R is plotted in Fig. 7.1 as a function of the transition energy E_r for a quantumn system of mass number 100.

However the energy loss does become significant when it is compared with the inherent width of the gamma ray, i.e. the nucleus. The finite width arises from the finite time which the nucleus spends in the excited state B, and is a result of the uncertainty principle of energy and time. If the uncertainty in the energy of the state B corresponds to the width, Γ, the linewidth of the gamma ray, and the uncertainty in time corresponds to the mean life against decay τ, then according to the Heisenberg uncertainty principle the energy of state B is given by

$$\tau . \Gamma = \hbar \qquad (3)$$

Perturbation theory shows that the decaying state B is not characterised by one well-defined energy E_r only, but that

the energy E of the state is distributed about the centre energy E_r as shown in Fig. 7.2(a) (Heitler, 1949). The energy of the stable ground state A is sharp according to equation (3). Photons emitted in the transition from B to A thus show a distribution in energy E_γ, centered around $E_r - R$ displaying a natural line shape of width Γ, Fig. 7.2(b), and that corresponding to a mean life $\tau = 10^{-8}$ sec. is shown in Fig. 7.1. Such a mean life is typical for atomic states and not unreasonable for low-lying nuclear levels.

Now when a photon of energy E_γ and momentum p strikes a target of mass M, initially at rest, the entire momentum p is transferred to the target, which recoils with energy of recoil R again given by equations (1) or (1'). This energy is supplied by the gamma ray, and only an energy $E_r - R$ is available for excitation of internal degrees of freedom, Fig. 7.2(b), and in order to excite a level of energy E_r the incoming gamma ray must have energy $E_r + R$ as shown in Fig. 7.2(c). Hence resonance fluorescence can occur only if some of the incoming photons possess enough energy to "reach" state B and at the same time provide energy R to the recoiling system. Thus only the overlapping part of the spectra, Figs. 7.2(b) and 7.2(c), is responsible for resonance fluorescence, Fig. 7.2(d). The condition for overlap is

$$2R \lesssim \Gamma \qquad (4)$$

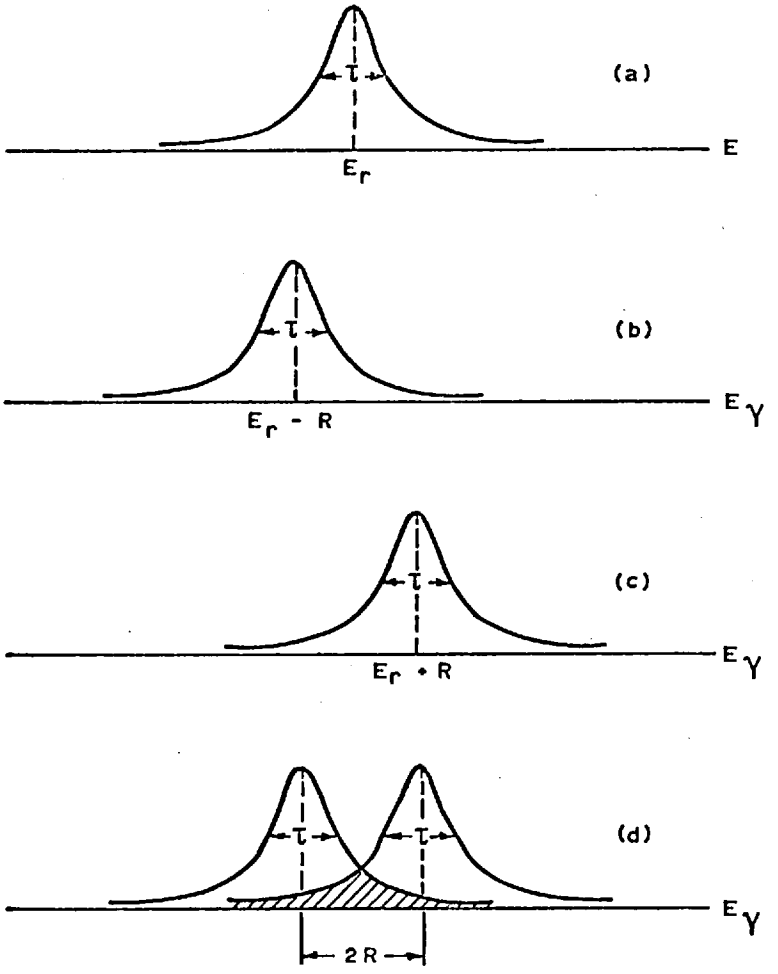


Figure 7.2

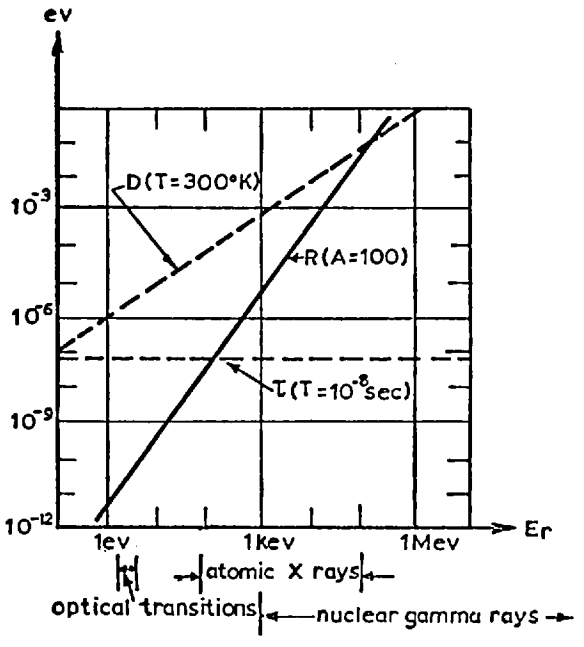


Figure 7.1

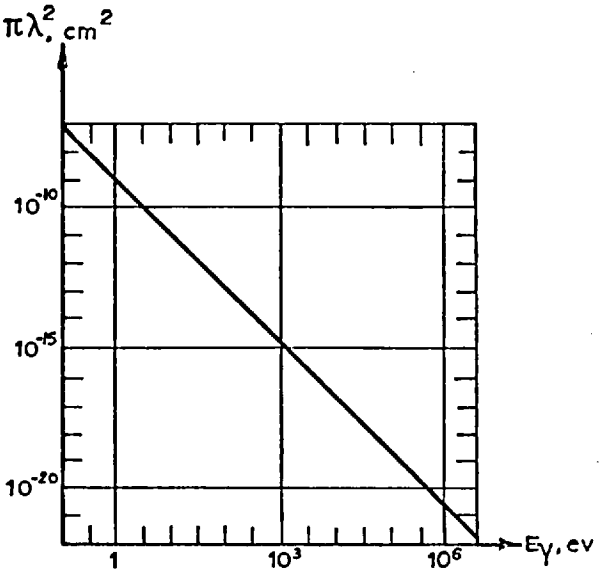


Figure 7.3

Fig. 7.1 shows that optical transitions fulfil condition (4) but not nuclear transitions.

7.1.3 Doppler Broadening

In the discussion above, the emitting and absorbing system is assumed to be at rest. Actually the atoms in both systems are in thermal motion which introduces an additional widening of the emission and absorption lines, called Doppler broadening.

For a source with initial momentum P_i, which emits a photon of momentum p, the momentum of the source after emission is $P_i - p$. The energy gained by the source and lost by the gamma ray is (assuming no mass change):

$$R' = \frac{(P_i-p)^2}{2M} - \frac{P_i^2}{2M} = \frac{p^2}{2M} - \frac{p.P_i}{2M} \qquad (5)$$

The first term is R of equation (1) for the initially stationary system; the second term represents Doppler broadening. If the kinetic energy of the quantumn system before photon emission is $K = P_i^2/2M$ and a 'Doppler energy'

$$D = 2(KR)^{\frac{1}{2}} \qquad (6)$$

this second term may be written $D\cos\phi$, where ϕ is the angle between p and P_i. The photon energy then becomes

$$E_\gamma = E_r - R' = E_r - R + D\cos\phi \qquad (7)$$

Since ϕ varies from 0 to 2π, the Doppler term causes a spread in photon energy of the order of D, and for a source

whose velocities of the individual emitters are directionally isotropic and Maxwellian in magnitude this additional broadening is of the order

$$\bar{D} = 2(\bar{K}R)^{\frac{1}{2}} \qquad (8)$$

where $\bar{K}$ is the average value of the kinetic energy of the emitters. Curve D, Fig. 7.1, shows such a Doppler broadening for a gaseous source at room temperature. Fig. 7.1 also shows that the natural line width Γ is not always the dominant feature in resonance fluorescence. We see also that the conditions for resonance fluorescence are readily satisfied for optical transitions, but for nuclear gamma rays $R \lesssim D$ and the conditions for resonance fluorescence depend on the cross section under various conditions.

7.1.4 Cross Section for Resonance Fluorescence

Resonance experiments with gamma rays involve either measuring the scattered intensity (resonance fluorescence or scattering) or by determining the attenuation of a beam due to resonant absorption. The cross sections for these processes for an incident gamma ray of energy E and wavelength $2\pi\lambda^2$, for thin absorbers is given by (Heitler, 1949; Jackson, 1955)

$$\sigma_{scatt}(E) = \sigma_o \frac{\Gamma^2}{4(E-E_r)^2 + \Gamma^2} \qquad (9)$$

$$\sigma_{abs}(E) = \sigma_o \frac{\Gamma\Gamma_\gamma}{4(E-E_r)^2 + \Gamma^2} \qquad (10)$$

where Γ is the total width of the absorption line, Γ_γ its gamma ray width, and σ_o the maximum resonance cross section given by

$$\sigma_o = \frac{2I_B + 1}{2I_A + 1} 2\pi\lambda^2 \qquad (11)$$

where I_A and I_B are the spins of the nuclear ground and excited states respectively.

Scattering and absorption cross sections given by equations (9) and (10) show a Briet-Wigner or Lorentz energy dependence of the form

$$I(E) = \frac{\Gamma}{2\pi} \frac{1}{(E-E_r)^2 + (\Gamma/2)^2} \qquad (12)$$

where Γ is the full width of the line at half maximum, and is normalised to

$$\int_0^\infty I(E)dE = 1 \qquad (12')$$

Expressions (9) and (10) are derived under the following assumptions:

a. Only one absorbing or scattering level exists. If more than one level exists, at or close to E_r, or if E_r is split into sublevels by a strong magnetic field equations (9) and (10) must be modified (Margulies, 1961).

b. The width of the level is given entirely by decay processes, the two competing modes for which in nuclei are internal conversion and gamma ray emissions. Total width and

gamma ray width are related by

$$\Gamma_\gamma = \frac{1}{1+\alpha}\,\Gamma \qquad (13)$$

where α is the coefficient of internal conversion.

c. The incoming photon is monoenergetic. However actual sources possess an energy spectrum I(E), where I(E)dE denotes the number of gamma rays emitted with energies between E and E + dE. Scattering and absorption cross sections then become

$$\sigma_{eff} = \frac{\int_0^\infty \sigma(E)I(E)dE}{\int_0^\infty I(E)dE} \qquad (14)$$

For an incoming gamma ray possessing an energy spectrum I(E) described by a Lorentz shape (equation 12), of width Γ identical to the absorbing state, and energy centered at E_r, then from equations (10), (12) and (14) the maximum cross section for resonance absorption is

$$\sigma_{eff\ abs} = \sigma_o \frac{\Gamma_\gamma}{2\Gamma} = \frac{\sigma_o}{2(1+\alpha)} = \frac{\lambda^2}{2\pi}\,\frac{2I_B+1}{2I_A+1}\cdot\frac{1}{1+\alpha} \qquad (15)$$

In Fe^{57}, $\sigma_{eff\ abs} = 2.2 \times 10^{-18}$ cm.^{2}, which is about 200 times greater than photoelectric absorption, the next most important process, and hence resonant absorption can dominate even when the resonant isotope is a minor constituent.

Equation (15) describes resonance absorption under the following ideal conditions:

(i) emission and absorption line possess the natural line width

(ii) emissions and absorption line are centered at the same energy, and if (i) and (ii) are satisfied, and α is small then the cross section for resonance absorption is large. The effective maximum resonance cross section is shown plotted against photon energy in Fig. 7.3. The effective absorption cross section in the presence of Doppler broadening is

$$\sigma_{abs}^{D} \simeq \sigma_o \frac{\Gamma_\gamma}{D} \qquad (16)$$

and the maximum cross section is reduced by a factor of Γ_γ/D. For optical transitions, since $\alpha = 0$, and $\Gamma_\gamma = \Gamma$, the maximum resonance cross section is reduced, on consulting Fig. 7.1, by one or two orders of magnitude, which renders optical transitions feasible. However Γ_γ/D is much smaller for nuclear than for optical transitions, and we may see from Fig. 7.1 that the maximum cross section for these transitions is decreased by many orders of magnitude.

7.1.5 Applications of the Mössbauer effect to Barium Titanate

It is well known that the ferroelectric behaviour in $BaTiO_3$ is closely associated with (a) intense electric field at the B lattice site, (b) temperature-dependent homogeneous transverse optical mode, (c) nature of the B-O bond, and (d) displacement of the B ion in the surrounding oxygen octahedra. These effects would manifest themselves, depending on the charge state of the Mössbauer probe, in measured values of the isomer shift and quadrupole coupling, at the Ti^{4+} site.

The nuclear quadrupole resonance studies of Nb^{3+} in $KNbO_3$, which has the same perovskite structure as $BaTiO_3$ with Nb at the B site, have shown that the Nb ion is subjected to a strong electric field gradient (Hewitt, 1961). Unfortunately the quadrupole resonance of Ti in $BaTiO_3$ is not possible owing to the low abundance of Ti^{47} and Ti^{49} as well as their small magnetic moment. However, X-ray investigations have, as we have already seen, shown that the Ti bond is partially ionic.

Since the Mössbauer effect is essentially a property of the nucleus, then any effect the lattice may have on the nucleus would be of interest from the point of view of the lattice vibrations.

7.2 LATTICE VIBRATIONS

7.2.1 Introduction

The role played by the lattice vibrations in the emission of gamma rays from nuclei bound in solids is a fundamental one. We have seen that, according to Cochran, the lattice vibrational temperature-dependent transverse optical mode plays a key role in bringing about ferroelectric behaviour in $BaTiO_3$. Consequently it would seem reasonable to suppose that any peculiarities which occur in the lattice vibrations, such as a 'softening' of the optical mode in the region of the transition, would have an effect on the emission of the gamma rays.

We may perhaps see this more clearly by considering the case of an Einstein solid (i.e. 3N vibrational modes, of the same frequency ω, where N is the number of atoms in the solid) where the recoil energy is less than the phonon energy. Since the lattice is a quantised system, which may not be excited in an arbitrary fashion, then the only possible changes in its state correspond to the absorption or emission of quanta of energy $\hbar\omega$. The emission of a gamma ray is accompanied by the transfer of integral multiples of this phonon energy $\hbar\omega$ to the lattice. Only those fractions of the above events, f, which take place without lattice excitation, provided the recoil energy is less than $\hbar\omega$, give rise to the Mössbauer effect.

Consider the transfer of momentum to the lattice which makes these zero-phonon events possible. Now the velocity with which momentum travels through the lattice is the velocity of sound, and the time available is the decay time of the damped oscillator representing the radiating nucleus. The velocity of sound in solids is typically 10^5 cms. sec^{-1}, so that during the 1.4×10^{-7} sec. lifetime of Fe^{57} the impulse travels 1.4×10^{-2} cms. But we already know (Chapter 2) that the velocity of sound undergoes an anomaly at the Curie point, which means that the distance the impulse travels should undergo a change at the transition and as a consequence the

number of nearby atoms which are involved in the recoil free process will be altered. Hence we would expect the recoil free fraction to undergo an anomaly in this temperature region as well.

7.2.2 Probability of a recoil-free emission (absorption)

The probability for a transition, in which the nucleus decays from an excited state N_i to the ground state N_f, while the lattice simultaneously goes from its initial state L_i to its final state L_f, is proportional to the square of the matrix element connecting the two states involved in the transition:

$$W(N_i \rightarrow N_f,\ L_i \rightarrow L_f) = \text{const} |\langle f | H_{int.} | i \rangle|^2 \qquad (1)$$

where $|i\rangle$ and $|f\rangle$ denote the initial and final state of the whole system including the lattice, and $H_{int.}$ is the interaction Hamiltonian. This may be factored into a nuclear and a lattice matrix element (Lamb, 1939) thus:

$$\langle f | H_{int} | i \rangle = \langle L_f | e^{i\underline{k}.\underline{X}} | L_i \rangle \langle N \rangle \qquad (2)$$

The term on the right-hand side is the matrix element for a momentum $\hbar\underline{k}$ transfer to the lattice by the decaying nucleus; where $k = p/\hbar$ is the wave vector of the emitted gamma ray, and X the coordinate vector of the centre of mass of the decaying nucleus. The Hamiltonian of a charged particle moving with a momentum $\underline{p}$ in an electromagnetic field given by a vector

potential $\underline{A}$ is:

$$\langle f|H_{int}|i\rangle = \text{const.}\ \langle f|\exp.(i\underline{k}.\underline{X})p_A|i\rangle \qquad (3)$$

where p_A is the gradient operator. Since the nuclear forces are of short range then the nuclear decay may be approximated as being uninfluenced by the state of the lattice, and the state functions $|i\rangle$ and $\langle f|$ may be written as products $|N_i\rangle|L_i\rangle$ and $\langle L_f|\langle N_f|$, of nuclear and lattice state functions with $\langle L_f|L_i\rangle = \delta_{fi}$ and $\langle N_f|N_i\rangle = \delta_{fi}$. Introducing internal nuclear coordinates:

$$x = X + \rho$$

where X is the coordinate vector of the centre of mass of the decaying nucleus (Fig. 7.4) and splitting up the momentum operator into its internal, and centre of mass, nuclear coordinates gives

$$p_A = p_X + p_\rho \qquad (5)$$

Substitution of equations (5) and (4) into (3) allows the matrix element to be separated into two parts consisting of a product of a nuclear and lattice matrix element:

$$\langle f|H_{int}|i\rangle = \text{const}\ \langle N_f|e^{ik.\ p}|N_i\rangle\langle L_f|e^{ik.X}|L_i\rangle + \langle N_f|e^{ik.\ }|N_i\rangle\langle L_f|e^{ik.X}p_X|L_i\rangle \qquad (6)$$

By the use of the closure relation (Feynman, 1961)

$$\sum_{n'}|n'\rangle\langle n'| = 1 \qquad (7)$$

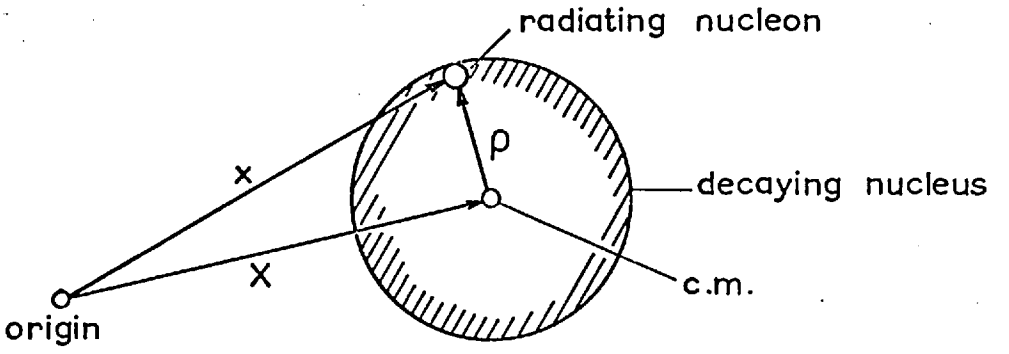


Figure 7.4

Properties of Fe^{57} [a]

	Ground state	First excited state
Energy (keV)	0	14.36
Spin and parity	$\frac{1}{2}^-$	$\frac{3}{2}^-$
Magnetic moment (nm)	0.0903	-0.153
Quadruple moment (barns)	0	0.29
Mean life (sec)	Stable	1.4×10^{-7}

[a] Internal conversion coefficient: 9.7 ± 0.2

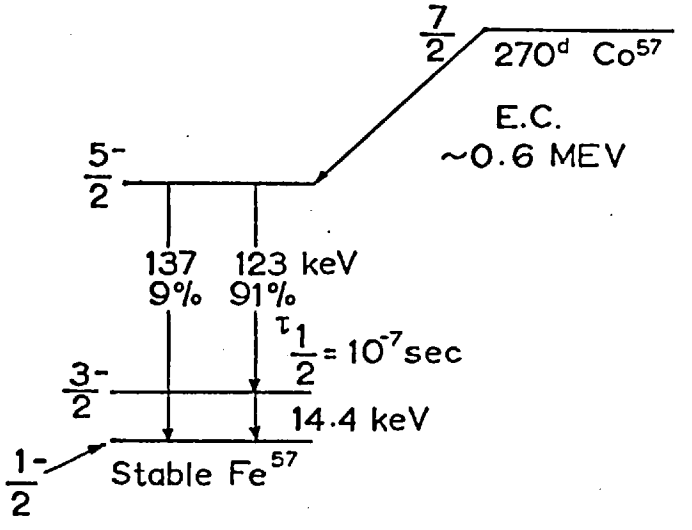


Figure 7.5

it may be shown that the first term in equation (6) is much larger than the second, the ratio being 10^5 or larger. Hence we may use equation (2) to calculate the fraction f of gamma rays emitted without energy loss to the lattice ($L_i \rightarrow L_i$):

$$f = \frac{|\langle L_i | e^{ik.X} | L_i \rangle|^2}{\sum_{L_f} |\langle L_f | e^{ik.X} | L_i \rangle|^2} \qquad (8)$$

By the use of equation (7) the denominator may be shown to be one,

$$\sum_{L_f} |\langle L_f | e^{ik.X} | L_i \rangle|^2 = \sum_{L_f} \langle L_i | e^{-ik.X} | L_f \rangle \langle L_f | e^{ik.X} | L_i \rangle$$

$$= \langle L_i | e^{-ik.X} | L_i \rangle = 1$$

Hence $$f = |\langle L_i | e^{ik.X} | L_i \rangle|^2 \qquad (9)$$

is the fraction of gamma rays emitted or absorbed without energy loss. f is known as the Lamb-Mössbauer factor. The complete decay scheme for Co^{57} to the stable ground state of Fe^{57} via the intermediate excited nuclear levels is shown in Fig. 7.5. It is the 14.4 keV gamma ray resulting from a transition between the 3/2 to 1/2 nuclear levels which is used for measuring the isomer shift and quadrupole splitting.

7.2.3 The Debye Solid

If we assume $BaTiO_3$ to be a Debye solid, that is one in which the individual atoms possess a range of frequencies up

to a cut-off frequency, then the probability f may be shown to be (Visscher, 1960; Lipkin, 1960)

$$f = e^{-2W} \tag{10}$$

where $$W = \frac{R}{3\theta_D}\left[\frac{1}{4} + \left(\frac{T}{\theta_D}\right)^2 \int_0^{\theta/T} \frac{x}{e^x - 1}\, dx\right] \tag{11}$$

Equation (11) was arrived at by introducing a density of vibrational states $\rho(\omega)$, assuming a partition function of the form $1/(1 - e^{(-\hbar\omega/kT)})$.

In considering the temperature dependence of the recoil free fraction f for a Debye crystal possessing both acoustic and optical modes, it is found that a limit exists on the propagation of an acoustic mode up to a maximum frequency whose wavelength is shorter than the periodicity of the lattice. In the transverse optical mode the light and heavy masses move out of phase with a definite frequency. Introducing the proper vibrational spectrum corresponding to an optical mode having a single characteristic frequency which may be represented by a delta function of the form (Wertheim, 1965)

$$\rho(\omega) = 3N\delta(\omega - \omega_o) \tag{12}$$

the recoil free fraction is now

$$f = \exp\left[-\frac{E_R}{\hbar\omega_o} \coth\left(\frac{\hbar\omega_o}{2kT}\right)\right] \tag{13}$$

which shows the temperature dependence of the recoil free fraction.

Now since the transverse optical mode, according to Cochran, undergoes a temperature anomally at the Curie point, then this should effect the recoil free fraction which would manifest itself as a change in the intensity of the Mössbauer absorption line. This then should provide a good test of the Cochran model, under these ideal conditions.

7.3 THE ISOMER SHIFT (IS)

7.3.1 Introduction

The isomeric or chemical shift arises out of small variations in the energy differences between the ground and first excited states due to the environment of the nucleus. This splitting in the nuclear energy levels is due to the electrostatic interaction of the assumed uniformly charged spherical nucleus with it's surrounding electronic charge. A change in the s-electron density will result in an altered Coulombic interaction which shifts the nuclear levels.

7.3.2 Isomer Shift

The difference in the electrostatic interaction between the electronic charge density ρ with a hypothetical point nucleus and one of actual radius R, both having the same charge, may be shown to be

$$\delta E = -\frac{2}{5}\pi Ze\rho R^2 = \frac{2}{5}\pi Ze^2|\psi(o)|^2R^2 \qquad (1)$$

where $-e|\psi(o)|^2$ is an alternate expression for the electronic charge density ρ. The gamma ray energy represents the

difference of two such terms for the nucleus in the ground and excited states:

$$\delta E_{ex} - \delta E_{gd} = \frac{2\pi}{5} Ze^2 \left[|\psi(o)|^2 \right] (R_{ex}^2 - R_{gd}^2) \qquad (2)$$

This energy difference is vanishingly small for realisable changes in $|\psi(o)|^2$ and is beyond the limit of detectability of the most sensitive instruments, but it is measurable in a Mössbauer experiment because the nuclear transition energy in a source is being compared with that in an absorber, i.e. the nuclei are being tuned to one another, by Doppler perturbing one of them. The shift relative to some standard substance is merely the difference of two such equations and may be written:

$$\text{I.S.} = \frac{2\pi Ze^2}{5} (R_{ex}^2 - R_{gd}^2) \left[|\psi(o)|^2_{abs} - |\psi(o)|^2_{source} \right] \qquad (3)$$

$$\text{I.S.} = \underset{\text{nuclear}}{\frac{4\pi}{5} Ze^2 R^2 \left(\frac{\delta R}{R}\right)} \underset{\text{atomic}}{\left[|\psi(o)|^2 - |\psi(o)|^2 \right]} \qquad (4)$$

where $\delta R = R_{ex} - R_{gd}$. This equation consists of two terms; the first consists of nuclear parameters which are constant, the second contains the atomic parameters of the total s-electron density at the nucleus. Hence the isomer shift is due to the total s-electron density at the nucleus and any causes affecting a change in this will result in a different isomer shift.

A systematic behaviour of the isomer shift was demonstrated for Mössbauer experiments done with common salts of iron (De Benedetti, Lang and Ingalls, 1961; Bodmer, 1953; 1958; 1960). We have seen from above that the electronic contribution to the isomer shift is given by the total s-electron density at the nucleus, the main contribution coming from the filled inner s-electron orbitals, that from the bonding contributing only a very small part.

Now the results of Hartree-Fock wave calculations by Watson (1959, 1960), which were done on multiply ionised free iron ions for various d^n configurations, showed that the total s-electron density differed for the various d^n configurations, the differences being essentially due to changes in 3s density. The importance of these results has been interpreted by Walker et al. (1961) as a consequence of the shielding of the 3s orbitals by the 3d orbitals. The results of these calculations yields a value for δR in equation (4), and since only relative values of $\psi_s^2(o)$ can be derived from measured isomer shifts, it is necessary to calibrate the calculated total s-electron density with measured isomer shifts. This has been done by Walker et al., and is shown in Fig. 7.6 which is a comparison between measured isomer shifts and electronic charge density, all

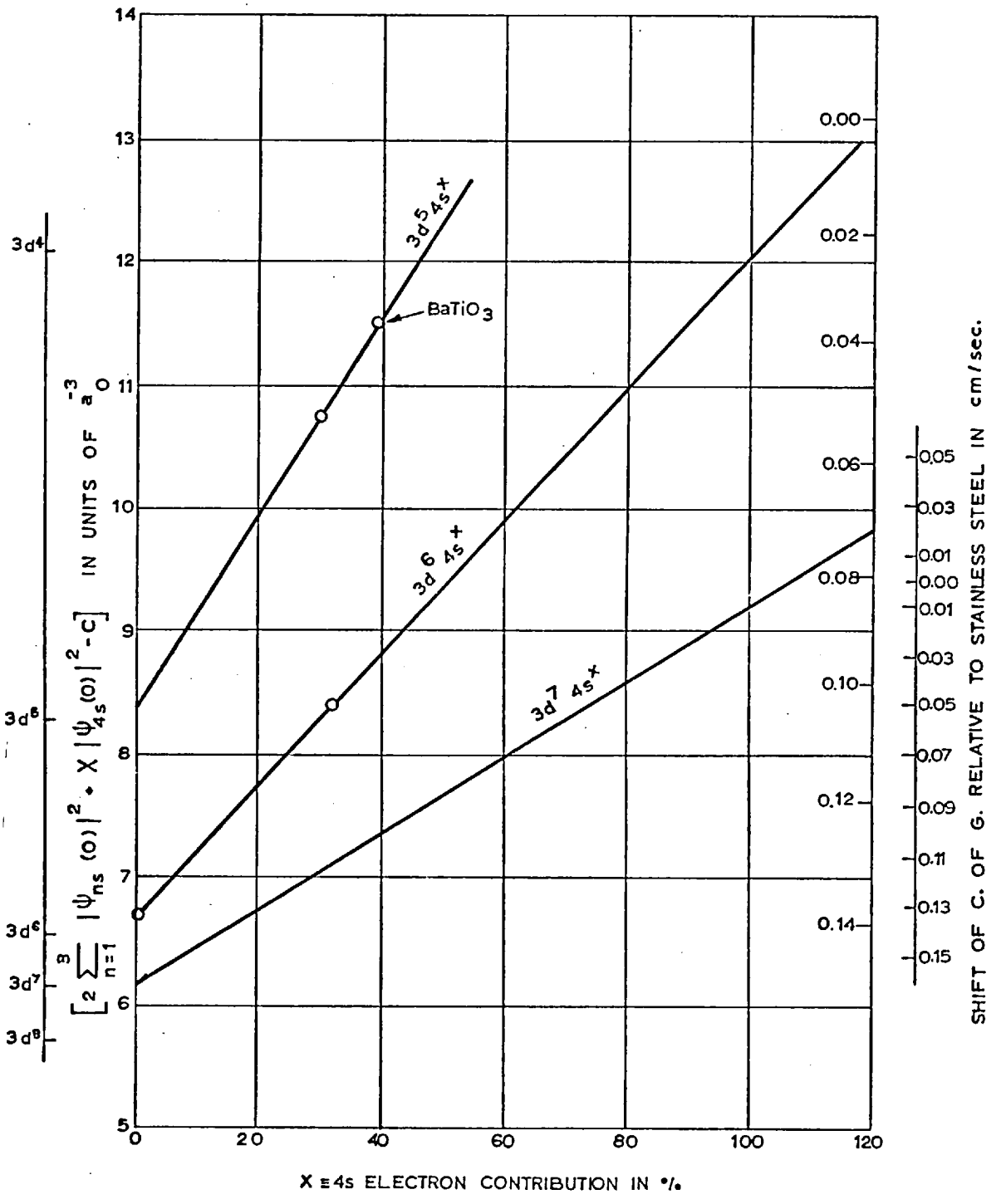

14
13
12
11
10
9
8
7
6
5
0
20
40
60
80
100
120
3d⁴
3d⁶
3d⁶
3d⁷
3d⁸
3d⁵4s⁺
BaTiO₃
3d⁶4s⁺
3d⁷4s⁺
0.00
0.02
0.04
0.06
0.08
0.10
0.12
0.14
0.05
0.03
0.01
0.00
0.01
0.03
0.05
0.07
0.09
0.11
0.13
0.15
[2 Σ n=1 to 3 |ψns(0)|² + X|ψ4s(0)|² - C] IN UNITS OF a₀⁻³
X ≡ 4s ELECTRON CONTRIBUTION IN %
SHIFT OF C. OF G. RELATIVE TO STAINLESS STEEL IN cm/sec.

Figure 7.6

shifts are at room temperature and with respect to stainless steel. Along the left-hand ordinate are the charge densities corresponding to the free-ion 3d configurations according to the Hartree-Fock calculations, the measured shifts for ionic di- and tri-valent compounds determine the right-hand ordinate.

Now the possible mechanisms that can modify the isomer shift have been stated by Shulman and Sugano (1965) summarising the conclusions of previous authors as:

(a) Contribution from 4s bonding.

(b) Indirect contribution from 3d bonding which can be as follows:

(i) Covalency effects between d electrons and filled ligand orbits which increases the number of d electrons on the metal. This tends to compensate the effect of s-bonding on the isomer shift.

(ii) Bonding of d electrons with empty ligand orbitals, decreasing the d-electron density at the metal ion because of 'back donation'. This tends to decrease the isomer shift by increasing $\psi_s^2(o)$.

To account for the 4s contribution Walker et al. add a fraction of 4s density, $x\,\psi_{4s}^2(o)$ to the contribution of the inner s orbitals, the values of $\psi_{4s}^2(o)$ being calculated from the Fermi-Segre-Goudsmit formula for hyperfine contact (Fermi

and Segre, 1933; Goudsmit, 1933). This simple addition does not really account for the possible shielding of the inner s-electron by the 4s, but the assumption was justified somewhat, by the results of Watson above which showed a negligible difference in the wave functions for the $3d^n4s^2$ and $3d^n$ configurations.

The effect of 4s-electrons is shown in Fig. 7.6 by the solid lines, the abscissa gives the fraction of 4s-electrons, and a compound whose isomer shift has been measured is plotted on this graph along a horizontal line. Now the above calibration has been made assuming the measured values of the isomer shift of the more ionic complexes to be the same as those for the free ion, which means then that one neglects the 4s-orbital occupation in the more ionic complexes.

On the basis of experimental data, mainly on the work of effective charge measurements in complexes by X-ray absorption spectra (Goldanski, 1963), the above approximation cannot be accepted. However by using the methods of effective electronegativity equalisation of atoms in molecules (Danon, 1964) an order of magnitude for the 4s-orbital occupation has been derived and the discrepancies observed with the above calibration are removed to a large extent. Both these calibrations are shown in Fig. 7.6, the inner calibration due to Danon and the outer due to Walker et al. The outcome

of this is to show that the 3d shell maintains its free ion behaviour, which we have already seen from our results with electron spin resonance.

7.4 QUADRUPOLE COUPLING

7.4.1 Introduction

In the preceding section we were concerned with the effect of the electrostatic interaction between nuclear and electronic charge on the "position" of nuclear levels, and the isomer shift equation was derived assuming the nucleus to be spherical and the charge density uniform. If these conditions are relaxed, other effects appear which are higher order terms in the multipole expansion of the electrostatic interaction. These terms do not shift the nuclear levels, they split them, i.e. they lift all or part of their (2I+1) fold degeneracy (I is the nuclear-spin quantumn number).

The second non-vanishing term of the electrostatic interaction of a nucleus with it's surrounding electronic charge is the quadrupole coupling, which results from the interaction of the nuclear quadrupole moment Q, with the gradient of the electric field due to other charges in the crystal. The nuclear quadrupole moment reflects the deviation of the nucleus from spherical symmetry, an oblate (flattened) nucleus has a negative quadrupole moment while a prolate (elongated) one has a positive moment. Nuclei whose

spin is 0 or $\frac{1}{2}$ are spherically symmetric and have zero quadrupole moment; thus the ground state of ^{57}Fe, with $I = \frac{1}{2}$ cannot exhibit quadrupole splitting.

The use of nuclear moments as probes of internal electromagnetic fields does not require an understanding of the origins of the moments, so long as the parameters characteristic of that nucleus are unaffected in magnitude by outside influences. This is not so for magnetic dipole interactions with an externally applied field and hence their moments may be determined with considerable accuracy. On the other hand, the nuclear quadrupole moment interacts with an electrostatic field gradient, and since no appreciable gradient can be produced by direct external means, a significant gradient is always the result of internal fields. Such internal fields being produced by electric charges close to the nucleus can be quite large and sensitive to the charge distribution responsible for them. Even if the electrostatic field gradient (EFG) at the atomic site were known accurately, a small distortion of the ionic core may modify the value of the field gradient at the nuclear site appreciably, and hence its calculation, effective in nuclear quadrupole interaction is a difficult problem (see antishielding factor). Thus even though the nuclear quadrupole moment serves as a very sensitive probe of internal electric fields in solids, it is often

difficult to interpret observations in quantitative terms.

7.4.2 The Quadrupole Hamiltonian

The interaction energy E of a charge distribution of density ρ with a potential V due to external sources may be expressed classically as

$$E = \int \rho(r) V(r) d\tau \qquad (1)$$

Expanding V(r) in a Taylor's series about the origin:

$$V(r) = V(o) + \left(\sum_{\alpha} x_{\alpha} \frac{\partial V}{\partial x_{\alpha}} \right)_{r=o} + \frac{1}{2!} \left(\sum_{\alpha\beta} x_{\alpha} x_{\beta} \frac{\partial^2 V}{\partial x_{\alpha} \partial x_{\beta}} \right)_{r=o} + \cdots \qquad (2)$$

where x_{α} (α=1,2,3) stands for x,y,z respectively. Defining

$$V_{\alpha} \equiv \left(\frac{\partial V}{\partial x_{\alpha}} \right)_{r=o} \qquad (3)$$

$$V_{\alpha\beta} \equiv \left(\frac{\partial^2 V}{\partial x_{\alpha} \partial x_{\beta}} \right)_{r=o}$$

we have

$$E = V(o) \int \rho d\tau + \sum_{\alpha} V_{\alpha} \int x_{\alpha} \rho d\tau + \frac{1}{2!} \sum \int x_{\alpha} x_{\beta} \rho d\tau \ \ldots\ldots \qquad (4)$$

Choosing the origin as the mass centre of the nucleus, the first term represents the electrostatic energy of a point nucleus; it is independent of nuclear size, shape or orientation, and is of no interest here. The second term represents the electric dipole moment which vanishes because the nuclear ground state wave function ψ_{Im} has a definite parity so that $\psi_{Im}\,\psi_{Im'}$ is unchanged if the sign of all nuclear coordinates are reversed. Here m and m' are the magnetic quantumn numbers of the ground and excited state,

labelling the orientation of the nuclear spin I (Ramsey, 1953; Townes et al. 1955).

The third term is the so-called electrical quadrupole term. An identical argument shows that in breaking off the expansions (2) after the quadrupole term, the first term omitted (electric octupole term) would also vanish, so that the following (electric 16-pole or hexadecapole) term constitutes the next higher order correction to the interaction energy.

Considering the orders of magnitude of successive terms in the expansion (2) $V_o \sim \frac{e}{r_e}$ where r_e is of atomic dimension, say 10^{-8}cm. The leading term in (2) is the electrostatic energy $Ze^2/r_e \sim 10^5 cm^{-1}$ corresponding to an ultraviolet frequency. The next term $er_n^2(e/r_e^3) = eV_o(r_n/r_e)^2$ where $r_n \sim 10^{-12}$cm is the nuclear radius. Hence the quadrupole interaction is of the order of 10^{-8} times the electrostatic energy, i.e. of the order of 10^{-3} or 30 Mc, which is comparable to the magnetic dipole interaction of a nucleus with an externally applied field. Similarly the hexadecapole term is of the order $(r_n/r_e)^2 \sim 10^{-8}$ of the quadrupole term, i.e. of the order of a cycle per second. This is ordinarily quite outside the range of experimental detectability. Therefore we shall neglect the hexadecapole interaction.

One can always find principal axes of the potential V

such that

$$V_{\alpha\beta} = 0 \quad \text{if } \alpha \neq \beta \tag{5}$$

must satisfy Laplaces equation:

$$\nabla^2 V = 0 \tag{6}$$

which evaluated at the origin gives,

$$\sum_{\alpha} V_{\alpha\alpha} = 0 \tag{7}$$

Considering quantities $Q_{\alpha\beta}$ defined as

$$Q_{\alpha\beta} = \int \left[3x_\alpha x_\beta - \delta_{\alpha\beta} r^2 \right] \rho \, d\tau \tag{8}$$

we then have

$$\int x_\alpha x_\beta \, d\tau = \tfrac{1}{3} \left[Q_{\alpha\beta} + \int \delta_{\alpha\beta} r^2 \rho \, d\tau \right] \tag{9}$$

and hence for the quadrupole energy

$$E^{(2)} = \frac{1}{6} \sum_{\alpha\beta} V_{\alpha\beta} \tag{10}$$

which by (7) gives

$$E^{(2)} = \frac{1}{6} \sum_{\alpha\beta} V_{\alpha\beta} Q_{\alpha\beta} \tag{11}$$

Replacing classical ρ by its quantumn mechanical operator $\rho^{(op)}$ given by

$$\rho^{(op)}(r) = \sum_k q_k \delta(r - r_k)$$

i.e.

$$= e \sum_{\text{protons}} \delta(r - r_k) \tag{12}$$

Substitution of (12) into (8) gives for the quadrupole operator $Q_{\alpha\beta}^{(op)}$

$$Q_{\alpha\beta}^{(op)} = e \sum_{\text{protons}} (3x_{\alpha k} x_{\beta k} - \delta_{\alpha\beta} r_k^2)$$

and a quadrupole term for the Hamiltonian H_Q is given by

$$H_Q = \frac{1}{6}\sum_{\alpha\beta} V_{\alpha\beta} Q_{\alpha\beta}^{(op)} \tag{13}$$

By use of the Wigner-Eckhart theorem (Slichter, 1964; Cohen and Reif, 1957) equation (13) reduces to

$$H_Q = \frac{eQ}{6I(2I-1)}\sum_{\alpha\beta} V_{\alpha\beta}\left[\frac{3}{2}(I_\alpha I_\beta + I_\beta I_\alpha) - \delta_{\alpha\beta} I^2\right] \tag{14}$$

where Q is the quadrupole moment of the nucleus.

This effective quadrupole interaction (equation (14)) applies for an arbitary orientation of the rectangular coordinates $\alpha = x,y,z$. The tensor coupling to the symmetric (in x,y,z) tensor may be simplified by choosing principal axes relative to which $V_{\alpha\beta} = 0$ for $\alpha \neq \beta$. In terms of these axes and using Laplace's equation $\sum_\alpha V_{\alpha\beta} = 0$ the above expression may be rewritten

$$H_Q = \frac{eQ}{6I(2I-1)}\left[V_{zz}(3I_z^2 - I^2) + (V_{xx} - V_{yy})(I_z^2 - I_y^2)\right] \tag{15}$$

Defining the asymmetry parameter and field gradient by

$$eq = V_{zz} \tag{16}$$

$$\eta = \frac{V_{xx} - V_{yy}}{V_{zz}} \tag{17}$$

For the case of $BaTiO_3$ in its room temperature phase $\eta = 0$ and the interaction Hamiltonian is now

$$H = \frac{e^2 q Q}{4I(2I-1)}(3I_2^2 - I) \tag{18}$$

showing that the quadrupole splitting is a result of the crystal symmetry. In the cubic phase $V_{zz} = V_{xx} = 0$ and hence the quadrupole splitting should vanish. Since I^2 and I_z commute with H giving the quantumn numbers I and m respectively the eigenenergies of the above interaction Hamiltonian are given by

$$E = \frac{e^2 q Q}{4I(2I - 1)} \left[3m^2 - I(I + 1) \right] \qquad (19)$$

In general when $I = (n + \frac{1}{2})$ where n is an integer the energy levels are doubly degenerate in the absence of a magnetic field, but that for integral spin, the degeneracy may be completely removed with the $m = 0$ state. This is another example of Kramer's degeneracy which has already been mentioned in connection with electron spin. This situation, taking into account the isomer shift and quadrupole splitting, is shown in Fig. 7.7. The mechanism responsible for producing quadrupole splitting of Fe^{57} in $BaTiO_3$ is discussed below.

7.5 THE ELECTRIC FIELD GRADIENT (EFG)

The two fundamental sources contributing to the EFG are the charges on distant ions and the electrons in incompletely filled shells of the atom itself. Distant ions contribute if their symmetry is lower than cubic. For a known crystal structure the value of the EFG at the atomic site may be obtained for a straight-forward electrostatic

calculation. This is not the EFG at the nuclear site. This EFG is normally appreciably modified by the atom's own electrons, whose wave functions are distorted by interaction with the external EFG, thus creating an EFG of their own (Sternheimer, 1950, 1951, 1952, 1954, 1957; Sternheimer and Foley, 1953). This normally serves to amplify the EFG due to distant charges and the phenomenon is known as antishielding which is amenable to calculation. The EFG due to partially filled non-spherical shells tends to be larger than that due to distant charges. This field gradient is also subject to shielding or antishielding corrections. We are thus able to write the field gradient in terms of the EFG due to distant charges, q' and the antishielding factor $(1 - \gamma_\infty)$ thus

$$q = q'(1 - \gamma_\infty) \qquad (20)$$

In the case of Fe^{57} two different situations appear. For the case of divalent iron the electronic configuration of $Fe^{2+} 3d^6$ in a crystal field where Hund's rule is obeyed is $^5D_4$, i.e. there is one d-electron outside a half-filled spherically symmetric shell and the entire field gradient arises from this sixth 3d-electron.

The second case, which is of direct interest in this work, is that of trivalent iron ($3d^5$) where smaller quadrupole splittings are found. Since the five 3d-electrons are in a half-filled shell with spherical symmetry, which does not

contribute to the field gradient, then the observed quadrupole splitting must arise from the field gradient due to other ions in the crystal. For the case of $BaTiO_3$ with Co^{57} substituted for the titanium ion the observed quadrupole splitting would be due to the axial distortion of the surrounding oxygen octahedra, and hence as the temperature of the crystal is raised this distortion decreases finally becoming zero as the temperature passes through the Curie point and the crystal goes cubic. One would expect, as a result of this, a gradual decrease in the quadrupole splitting with increasing temperature which should then vanish in the cubic phase. From equation (19) for $I = 3/2$ and for the two allowed values of m, $1/2$ and $3/2$ the quadrupole splitting taking into account the antishielding factor (equation (20)) is

$$\Delta E_Q = E_Q(3/2, 3/2) - E_Q(3/2, 1/2) = 1/2\, e^2 q' Q (1 - \gamma_\infty)$$

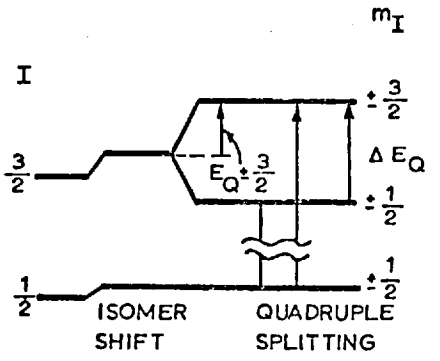
This difference is the experimentally measured quadrupole splitting.

The z-component of the EFG is given by,

$$q_{zz} = \frac{3\cos^2\theta - 1}{r^3}$$

$$= \frac{2z^2 - x^2 - y^2}{(x^2 + y^2 + z^2)^{5/2}}$$

from which one can see that in the cubic phase no field gradient exists but does so for the case of axial symmetry. The main



$$E_Q(m_I = eqQ\left[\frac{3m_I^2 - I(I+1)}{4I(2I-1)}\right]$$

$$\Delta E_Q = E\left(\frac{3}{2}\right) - E_Q\left(\frac{1}{2}\right) = \frac{eqQ}{2}$$

Figure 7.7

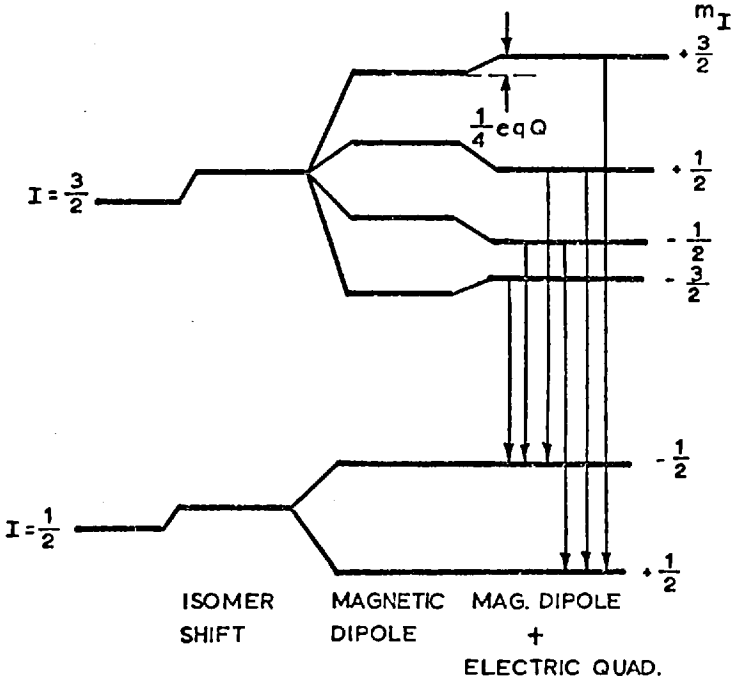


Figure 7.8

difficulties associated in computing the EFG are (i) the crystal may not be assumed to be structurally ionic so it is not clear what charge to associate with a lattice point or if the point charge approximation is not valid; (ii) if the lattice sum is very sensitive to small changes in the position of the ions which fall within the limits of error of the structure determinations.

Additional information may be obtained from the intensity of the quadrupole split pair, where it may be shown (see section on Hyperfine Splitting) that the intensity of the quadrupole split pair is equal. However, the product of the angular dependence of quadrupole splitting and the angular dependence of the recoil-free fraction (Gol'danskii et al., 1963) is given by

$$\pm \tfrac{3}{2} \rightarrow \pm \tfrac{1}{2} \qquad \tfrac{3}{2}(1 + \cos^2\theta)f(\theta)$$

$$\pm \tfrac{1}{2} \rightarrow \pm \tfrac{1}{2} \qquad (1 + \tfrac{3}{2}\sin^2\theta)f(\theta)$$

which if averaged over a sphere will in general be different for the two transitions. This effect seems to be noticeably absent in the literature.

7.6 MAGNETIC HYPERFINE STRUCTURE (hfs)

7.6.1 Introduction

The magnetic hyperfine structure arises from the interaction

of the nuclear magnetic dipole moment μ , with the magnetic field H, due to the atoms' own electrons. (There is no magnetic hfs for nuclear levels of zero spin since for this case μ is zero).

The interaction Hamiltonian is given by,

$$H_m = - \mu.H = -g \mu_n I.H \qquad (1)$$

and the energy levels are

$$E_m = - \mu H m_I / I = -g \mu_n H m$$

$$m = I, I-1, ... -I \qquad (2)$$

where μ_n is the nuclear magneton, and g the gyromagnetic ratio or nuclear g-factor. According to equation (2) there are (2I + 1) equally spaced levels; the splitting between adjacent levels is $g\mu_n H$, and the splitting between the lowest and highest level is $2g\mu_n HI$. This case applies to Fe^{57}.

The emitted gamma ray corresponds to a transition from a particular magnetic sublevel of an excited nuclear state to a sublevel of the ground state, the selection rule depending on the multipolarity of the radiation. In normal nuclear magnetic resonance experiments one observes transitions between adjacent magnetic sublevels.

When magnetic hfs is present, the individual transitions between magnetic sublevels may be resolved and the individual transitions identified with the appropriate sublevels.

7.6.2 The Transition Probabilities

The transition probabilities between the Zeeman levels have been determined from the general theory of multipole radiation (Fagg and Hanna, 1959). The angular intensity distribution, $I_m(\theta)$ for dipole radiation is shown to be

$$I_m(\theta)=\sum_m |\langle I_e\ M-m,m|I_e 1 I_g M\rangle|^2 x \left[1+\tfrac{1}{4}(3m^2-2)(3\cos^2-1)\right] \quad (3)$$

Here θ is measured about the axis of quantisation, and the Wigner or Clebsch-Gordon coefficients $\langle I_e 1\ M-m,m|I_e 1\ I_g M\rangle$ are known constants. The relative intensities from the ground to the first excited state are given below for Fe^{57}:

Excited State $\|M-m\rangle$	Ground State $\|M\rangle$	Relative Intensities
$\pm 3/2$	$\pm 1/2$	$3/4\,(\cos^2\theta + 1)$
$\pm 1/2$	$\pm 1/2$	$\sin^2\theta$
$\mp 1/2$	$\pm 1/2$	$1/4\,(\cos^2\theta + 1)$

When the emitting nucleus interacts with magnetic and electric fields the gamma ray absorption spectrum splits into a six line spectrum provided the absorber has a single line resonance.

In the absence of a magnetic field at the nucleus, but only an electric field gradient, the six line spectrum would collapse into a doublet of equal intensity.

7.6.3 The Internal (Magnetic) Field

This is a misleading term since the field does not exist everywhere inside the solid but is the result of the interaction of the nucleus with its own electrons.

The direct coupling between the nucleus and an s-electron is called the Fermi contact interaction which may be written

$$H_s = -\frac{16\pi}{3}\beta\langle\sum(s_\uparrow - s_\downarrow)\rangle \qquad (4)$$

where $s_\uparrow$ and $s_\downarrow$ are s-electron spin densities at the nucleus for spin up and spin down respectively (Marshall and Johnson, 1962), and β is the Bohr magneton. The exchange interaction of the 3d-shell electrons with the s-electrons is such as to differentiate between the radial parts of the two s-electron wave functions so that the spin densities at the nucleus no longer cancel and a Fermi contact interaction field is observed.

Other mechanisms which can give rise to a magnetic field at the nucleus are due to the orbital magnetic moment, but from the results of electron spin resonance (see Chapter 6) we see that this mechanism provides a null contribution due to quenching, as manifested by a free ion g value, in both phases of the material. A further contribution arises from the interaction between the electron and nuclear spins and the electron angular momentum. This, dipolar term, is much smaller than the Fermi contact term (Golding, Mol. Phys. in press). Hence the field that have been observed in compounds

of trivalent iron are almost entirely via the Fermi contact interaction from the d-shell spin-moment.

Usually, for this internal magnetic field to be observed the material concerned must be magnetically ordered, as in a ferromagnetic complex when the six-line spectrum is observed.

However, there seems to be no reason, in principle, why hfs cannot be obtained in a paramagnetically dilute material, as is the case here, of sufficient dilution such that there is no spin-spin interaction, but several conditions must be met which make Mössbauer experiments more difficult.

Firstly, the crystal field states should not be split in such a way as to leave one of the states much lower than the rest since it will then be exclusively populated. This fortunately does not apply to Fe^{3+} in $BaTiO_3$.

Secondly, for the nuclear spin to couple with the internal field, the electron spin-lattice relaxation time T_1 must be shorter than the Larmor frequency of the nucleus, because then the time-averaged value of the internal magnetic field affecting the nucleus is different from zero, being sufficiently long to present a stationary magnetic field at the nucleus.

In conclusion the effect of combined magnetic and electric hyperfine coupling is shown in Fig. 7.8; the effect is to displace all four magnetic sublevels by the same amount due to the quadrupolar interaction.

7.7 EXPERIMENTAL

7.7.1 Introduction

In order to render a Mössbauer experiment feasible the following conditions, as we have seen, must be obeyed:

1) the emitting and absorbing nuclei must be in the solid state to avoid effects of recoil and thermal broadening;

2) the gamma ray energy must be fairly low (10^4-10^5eV) to obtain an appreciable number of recoil free events;

3) the half-life of the nuclear excited state should be in the range 10^{-6}-10^{-11} sec. as longer lived species give lines too narrow for detection, and lines which are very broad and become lost in the background noise;

4) the internal conversion coefficient should be as small as possible (0-20) to ensure that an appreciable number of gamma transitions result in gamma ray photons and not as conversion electrons.

Now in an actual resonance fluorescence experiment, if the gamma ray from an excited nucleus is incident on an identical nucleus in its ground state it will be re-absorbed and the intensity of the gamma ray beam will diminish; if the absorbing nucleus is not in precisely the same chemical-

physical environment as the emitter then there will be no resonance fluorescence and the count-rate will be unaltered. In order to overcome this the source (or absorber) is Doppler perturbed by placing the source on a vibrator that moves relative to the absorber, in order that the energy of the gamma rays sweeps through the resonance energy and a change in the count rate is observed by the detector. We can estimate the velocity, V, required to shift the gamma ray energy, E_γ, by the half-width of a line Γ. Thus $V/c = \Gamma/E$, and since $\Gamma \simeq 10^{-2} E_\gamma$ then $V \simeq 10^{-12} c$, i.e. 10^{-12} of the velocity of light $\simeq 0.3$mm sec^{-1}. These velocities are easily realisable in practice.

7.7.2 The Mössbauer Spectrometer

In Fig. 7.9 is shown a block diagram of the system used, the modulation technique employed the Doppler effect which is provided by a transducer, on which the source is mounted, and is based on a velocity controlled electro-mechanical feedback system which in essence are two coupled loudspeaker coils. The purpose is to provide energy modulation permitting examination of the region of the absorption spectrum near the unperturbed energy of the gamma ray.

In the system used here the transducer executes a saw toothed waveform which sweeps repeatedly through the range of velocities of interest, storing the instantaneous counting

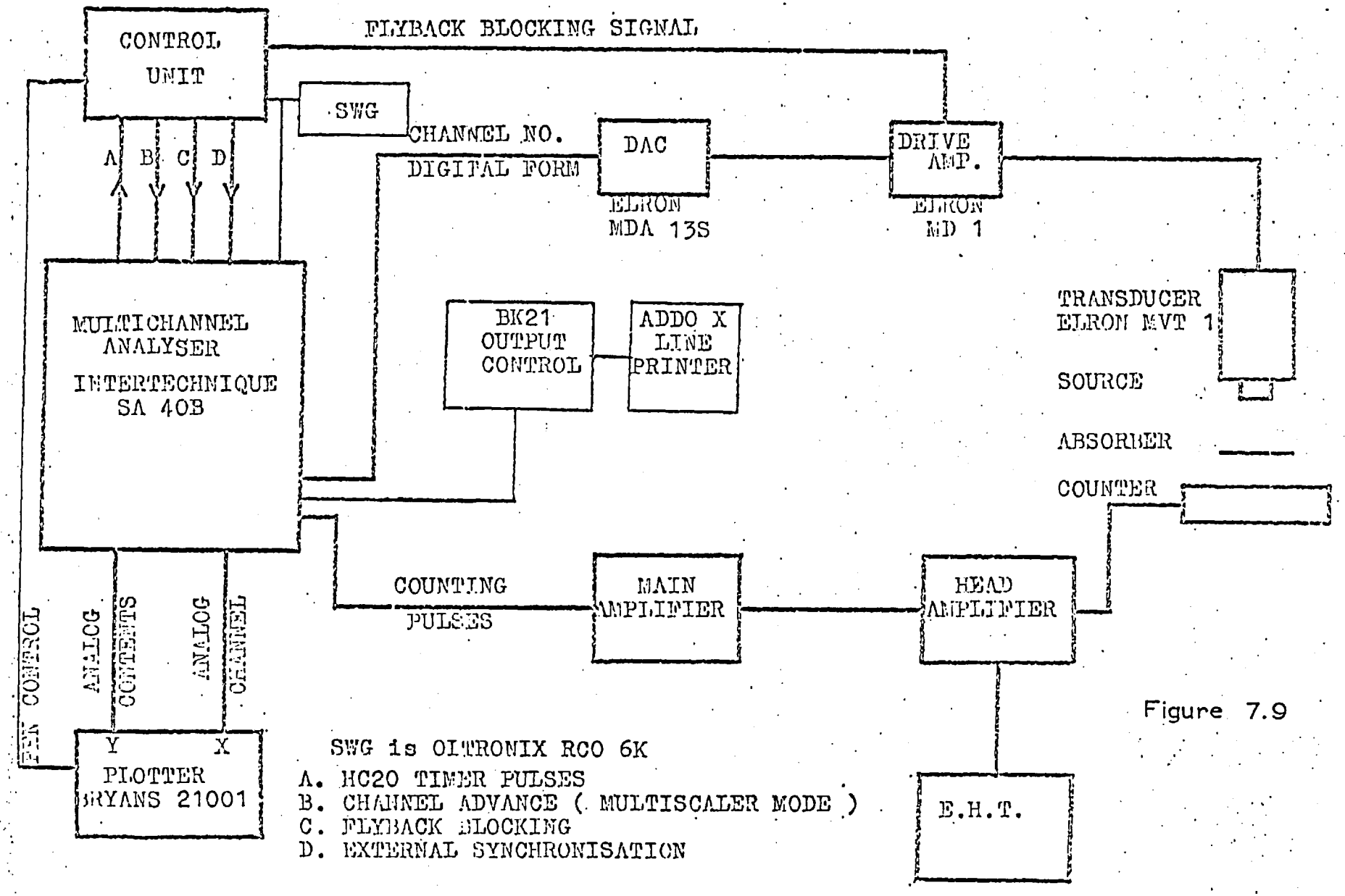


Figure 7.9

SWG is OLTRONIX RCO 6K

A. HC20 TIMER PULSES
B. CHANNEL ADVANCE (MULTISCALER MODE)
C. FLYBACK BLOCKING
D. EXTERNAL SYNCHRONISATION

information in a large number of scalers. Since equal velocity increments in equal lengths of time are necessary to ensure a saw tooth output this then is equivalent to constant acceleration, which is equivalent to sweeping through a range of velocities.

With each cycle over a range of velocities the complete spectrum of interest is swept out and the counts are stored in a multichannel analyser (Intertechnique). As yet, we do not know the connection between the velocity and the count rate. However, as may be seen from the block diagram, the multichannel anaylser steps through its channels at a clock controlled rate, and synchronism between the mechanical motion of the transducer and the analyser is obtained by using the analyser as the waveform generator. This means that the waveform is not continuous but is a series of discrete steps, there being 400 in all corresponding to the total number of channels in the analyser. It is not absolutely necessary to know what channel number corresponds to zero velocity as the isomer shift of a given sample may be obtained in the manner we have already indicated (see Transition Probabilities).

Since the energy of recoil free gamma rays encountered is from a few keV to about 150 keV then it is necessary to select a desirable gamma ray from a complicated spectrum. Because of its comparatively low energy a scintillation

counter with a crystal of the right thickness for the 14.4 keV of Fe^{57} was used as supplied by the manufacturers (Elron).

7.7.3 Temperature Variation

The temperature variation for increasing temperatures was achieved by the construction of a mini-oven capable of producing temperatures up to approximately 200°C. On a brass cylinder of 2" length and $1\frac{1}{4}$" diameter was doubly wound 30 gauge flexi-glass coated manganin wire. On top of this was wound asbestos string. The whole was then held between two shaped halves of firebrick by alumina paste when solidified. The temperature inside the 'mini-oven' could be controlled to ± 1°C. Both the control and monitor thermocouples were of the finest gauge available and were of iron/constantan. The power supply was controlled via an Ether 0-200°C temperature controller.

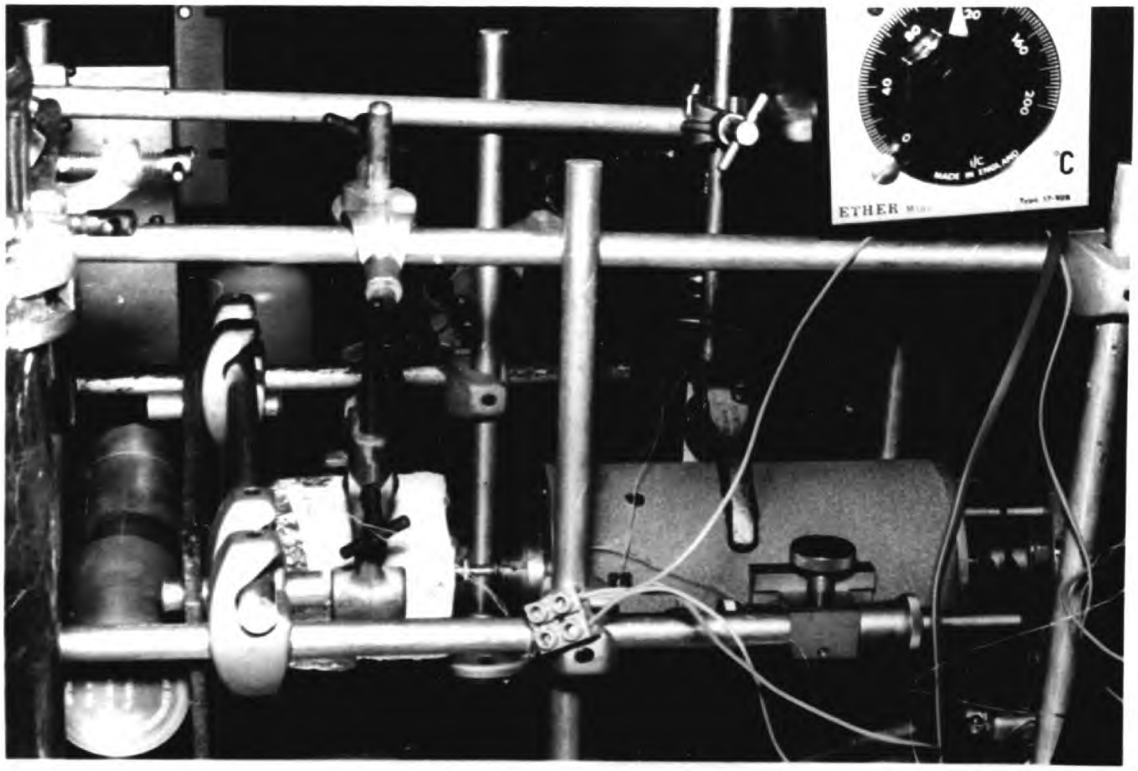
In order to vibrate the source while varying its temperature, a mount was constructed whose base was fixed to the transducer head, the crystal being stuck on the opposite end which protruded into the oven through a hole bored into a removable asbestos stopper forming an end wall. The gamma rays were brought out of the other end through a mica or thin aluminum foil window, though mica was usually adopted since one was then able to view directly into the oven as a check before commencing the counts. This is shown

as set up for the counting procedure with temperature variation in Fig. 7.10.

In order to lower the temperature of the source, the crystal was stuck onto the cold face of a 'frigistor' but owing to it's weight it is not possible to vibrate this mass as it would destroy the output waveform of the transducer. Hence a 'cage' of duralumin rods was constructed one end of which was stuck to the head of the transducer, and the absorber was stuck onto the other end. Inside the cage, but not in contact with it, and held firmly from outside, was the frigistor with the crystal on its face. The whole weight of the cage plus absorber - 3.8gm was well within the specified limits for the transducer, - 10gm.

7.7.4 Sample Preparation

The crystals used were from the same batch as those employed for the ESR studies, and were chosen for their well shaped faces and surface smoothness. It has been shown that $BaTiO_3$ does not act as a good absorber, since a doping level sufficient to give a strong enough absorption signal would result, due to the addition of iron, in distortion of the lattice from tetragonal to hexagonal at room temperature and we should then be destroying the effect that it is intended to measure. This change in the lattice structure together with a weakening in the ferroelectric action is achieved with



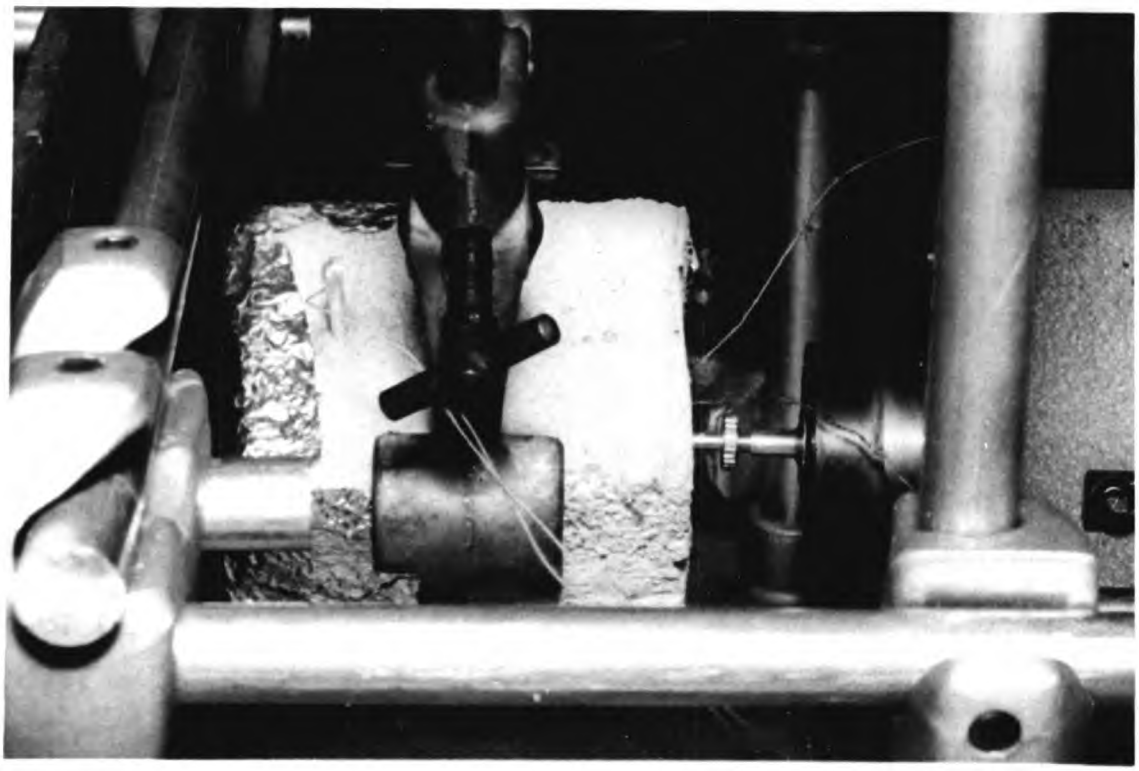


Figure 7.10

the addition of 5-mole per cent of iron (Nishioka, Sekikowa and Owaki, 1957). Addition of one mole per cent of Fe^{57} gives a very weak absorption spectrum against a Co^{57}-copper source, its absorption being comparable to the background noise (Bhide and Multani, 1965; Nicholson and Burns, 1963). Because of this, the Mössbauer effect study of the $BaTiO_3$ lattice as a host for absorbing nuclei is quite limited. There is also the question of the practical difficulties involved in the use of radioactive constituents at high temperatures when these have to be incorporated into the crystal growth process. Consequently it is preferable to first obtain crystals of fairly good quality in the conventional manner and then incorporate the Mössbauer probes into the lattice, since any mishap which might possibly occur during a crystal growing run would then result in the total loss of the Co^{57}.

Fairly large crystal plates were selected. These plates were etched in hot orthophosphoric acid at about 250°C for approximately 20-30 seconds to expose fresh surfaces. Drops of Co^{57} solution in 0.1 normal HCl were deposited on the surface of the crystal plate which was then warmed under an infra-red lamp until the aqueous solution evaporated from the surface. This procedure was repeated a number of times until the desired amount of activity was left residing on the surface. This was estimated from the total amount of carrier free Co^{57}

solution contained in one m-Curie of activity purchased from the Radiochemical Centre, Amersham. The active residue remaining on the crystal was then diffused for about an hour in a hydrogen atmosphere at approximately 850°C. The reducing atmosphere produced a slight darkening of the crystal which is normally associated with oxygen vacancies. The hydrogen atmosphere combines with the chlorine leaving behind cobalt metal. The crystals were then heated in air at 1150°C for between two to three hours when the Co^{57} diffuses into the crystal. After this length of time the crystals, which were held in an alumina boat, were quickly withdrawn from the furnace and cool air from a hair dryer played over them. This near quenching from a high temperature is aimed at providing the Co^{57} with a substitutional site rather than an interstial site. After the above procedure all the crystals treated were observed to have regained their original light straw colour.

Owing to unexpected results in the Mössbauer measurements several crystals were so treated varying in activity from 0.7-0.3 mCi.

7.7.5 Location and Charge State of the Mössbauer Probe

There is extensive evidence existing which leads to definite conclusions on the location and charge state of cobalt and iron impurities in $BaTiO_3$. Studies on the magnetic susceptibility of cobalt-doped $BaTiO_3$ show that cobalt enters

the lattice substitutionally as a divalent ion (Hurd et al. 1959). Size considerations (Co^{2+}, 0.77Å; Ti^{4+}, 0.64Å; Ba^{2+}, 1.38Å) would also favour Ti replacement. The results on the dielectric properties and optical absorption conclusively establish such a substitution (Kudzins, 1962).

Also, from electron spin resonance of Fe^{3+} in $BaTiO_3$ in this work and elsewhere (Hornig et al. 1959), iron impurities are known to occupy Ti sites as Fe^{3+}, in the other perovskites $SrTiO_4$ (Kirkpatrick et al. 1964) and $PbTiO_3$ (Gainon, 1964) as well.

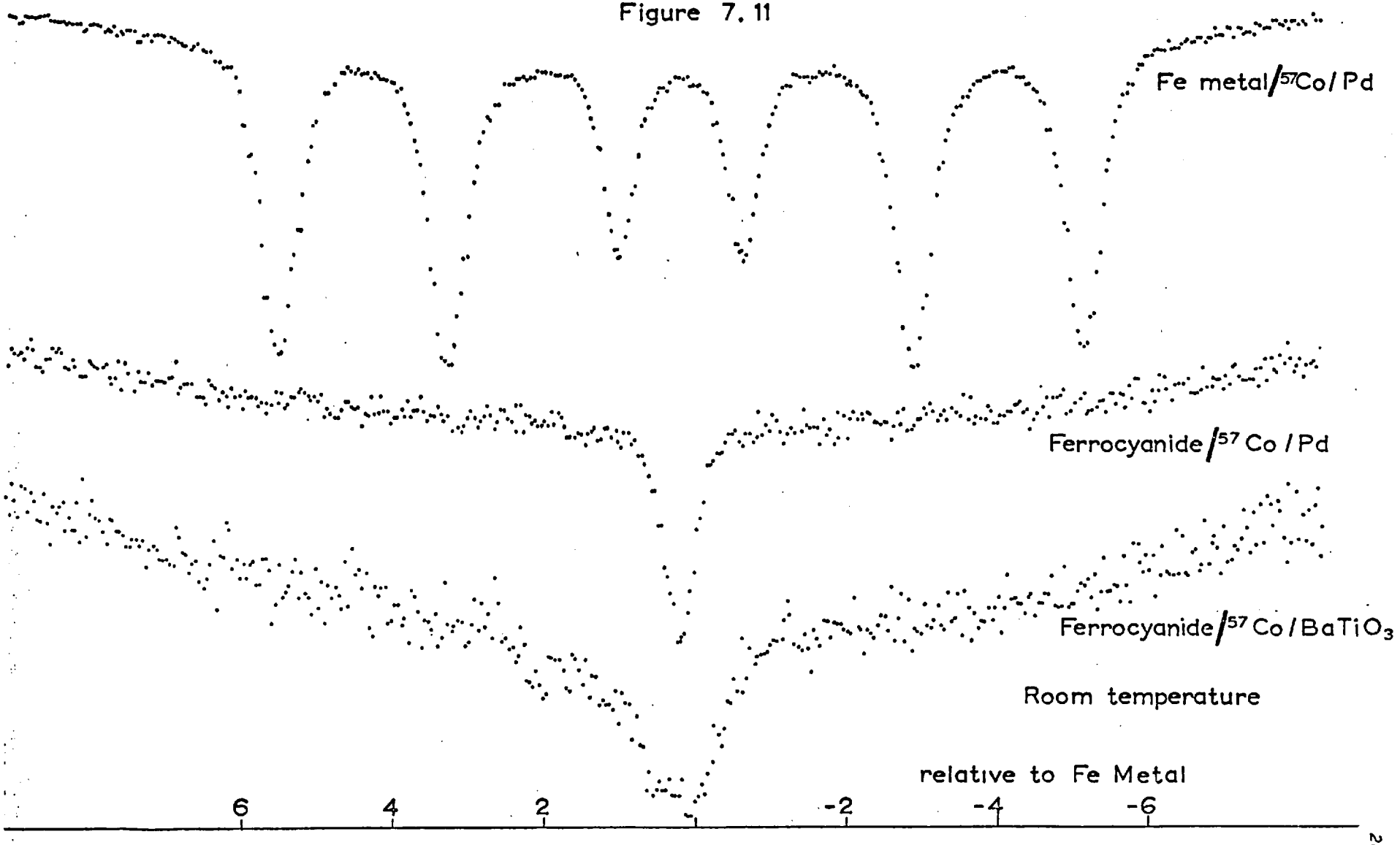
In the light of this, if we assume a perfect local environment for the Mössbauer probe, then any change in this should reflect itself in changing values of the isomer shift and the quadrupole splitting.

7.7.6 Measurements and Results

The spectrum obtained by Fe^{57} in iron metal and the separation of the hyperfine lines which is known accurately is used to calibrate the velocity scale with respect to channel number in determining the isomer shift and quadrupole splitting of Co^{57} in $BaTiO_3$, in conjunction with the known isomer shift of Co^{57} in palladium. The six line hfs of Fe metal, the isomer shift of Co^{57}/Pd and of $BaTiO_3$ are shown in Fig. 7.11 for comparison.

Better resolution for the spectrum of $BaTiO_3$ only is

Figure 7.11


Fe metal/57Co/Pd
Ferrocyanide/57Co/Pd
Ferrocyanide/57Co/BaTiO3
Room temperature
relative to Fe Metal
6
4
2
-2
-4
-6

shown on the expanded scale of Fig. 7.12, where the quadrupole splitting is now evident. We have measured the isomer shift to be 0.39 $mm.sec^{-1}$ and the quadrupole splitting is found to be 0.45 $mm.sec^{-1}$.

We have applied an electric field of about 8000 $Vcms^{-1}$ to the crystal to see if there was any alteration in the intensity of either of the quadrupole split pair, but the results have proved negative.

On varying the temperature well into the cubic phase we have been unable to obtain any difference in the quadrupole splitting as is evident from the results shown in Fig. 7.13. These spectra were obtained relative to sodium nitroprusside since any closing up of the quadrupole splitting would necessitate the need for better resolved lines. We have also extended the results to well into the orthorhombic phase and from Fig. 7.14 we see that there is a difference in the quadrupole splitting.

These results indicate that the surroundings of the impurity probe atom are very different from the normal Ti^{4+} site and it would appear that the splitting seen is produced not entirely by distortions of the lattice but rather perhaps by a neighbouring oxygen vacancy, since these must be present in the crystal in order to maintain overall charge neutrality.

One further point should be mentioned in connection with

Figure 7.12

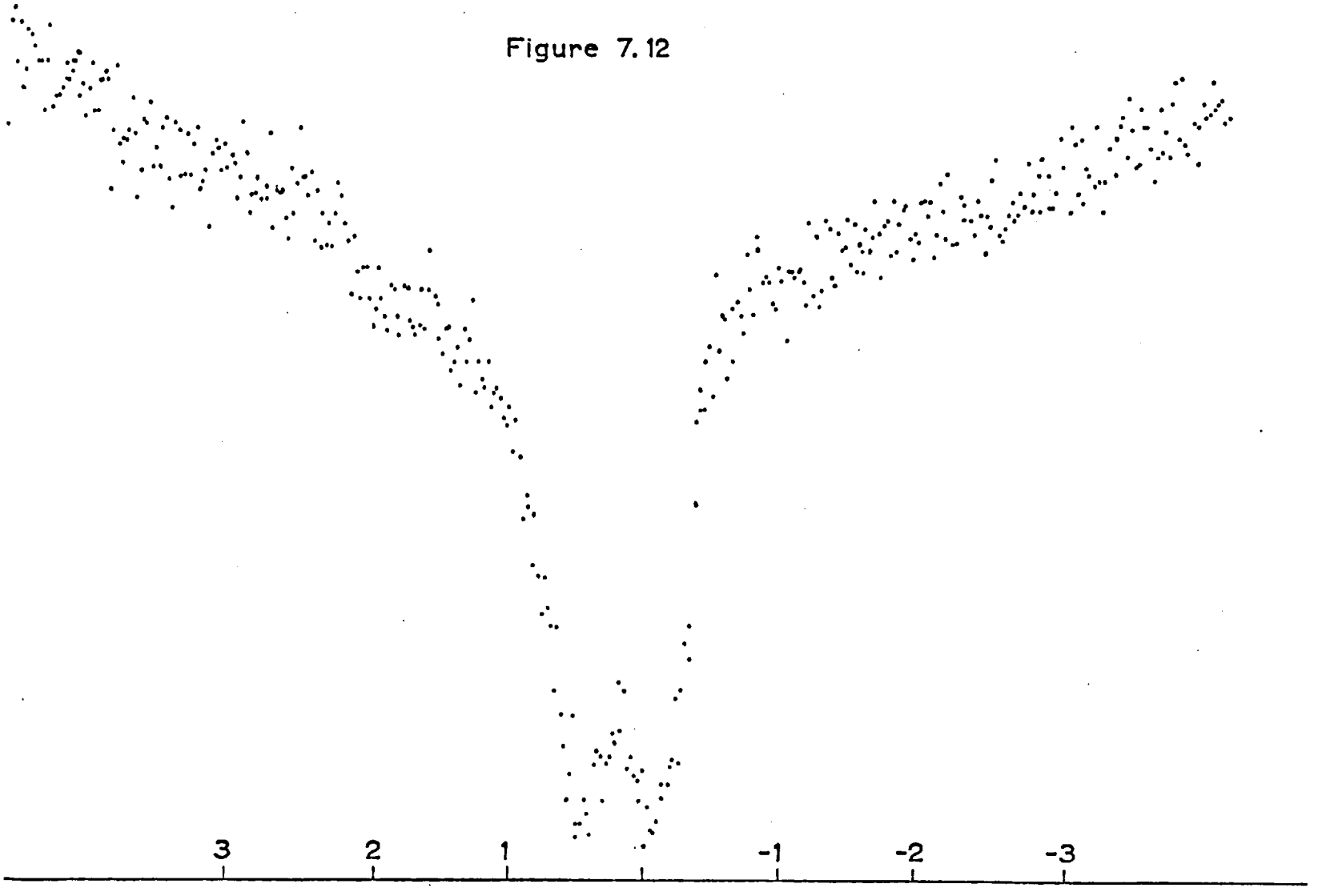
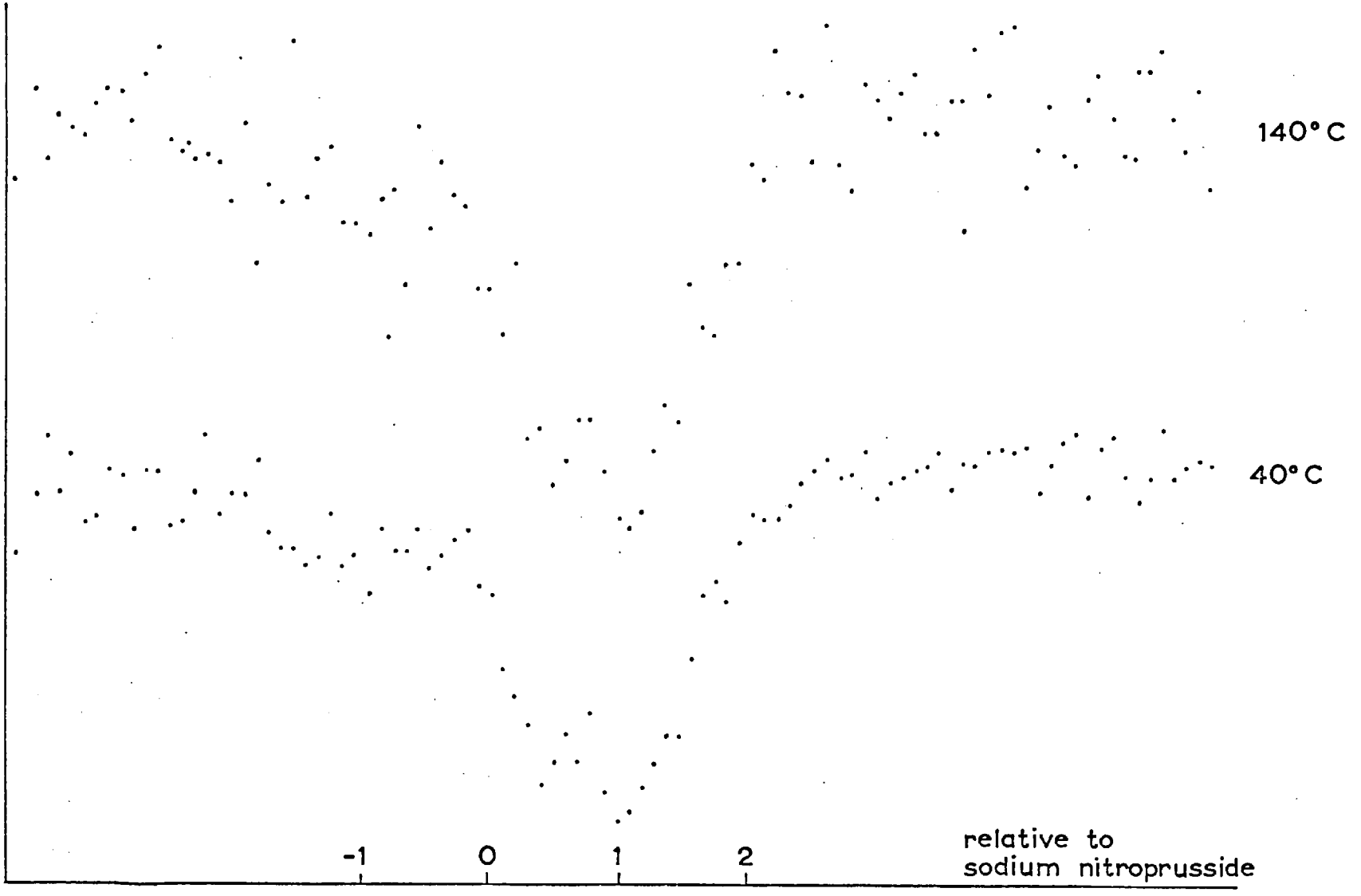


Figure 7.13



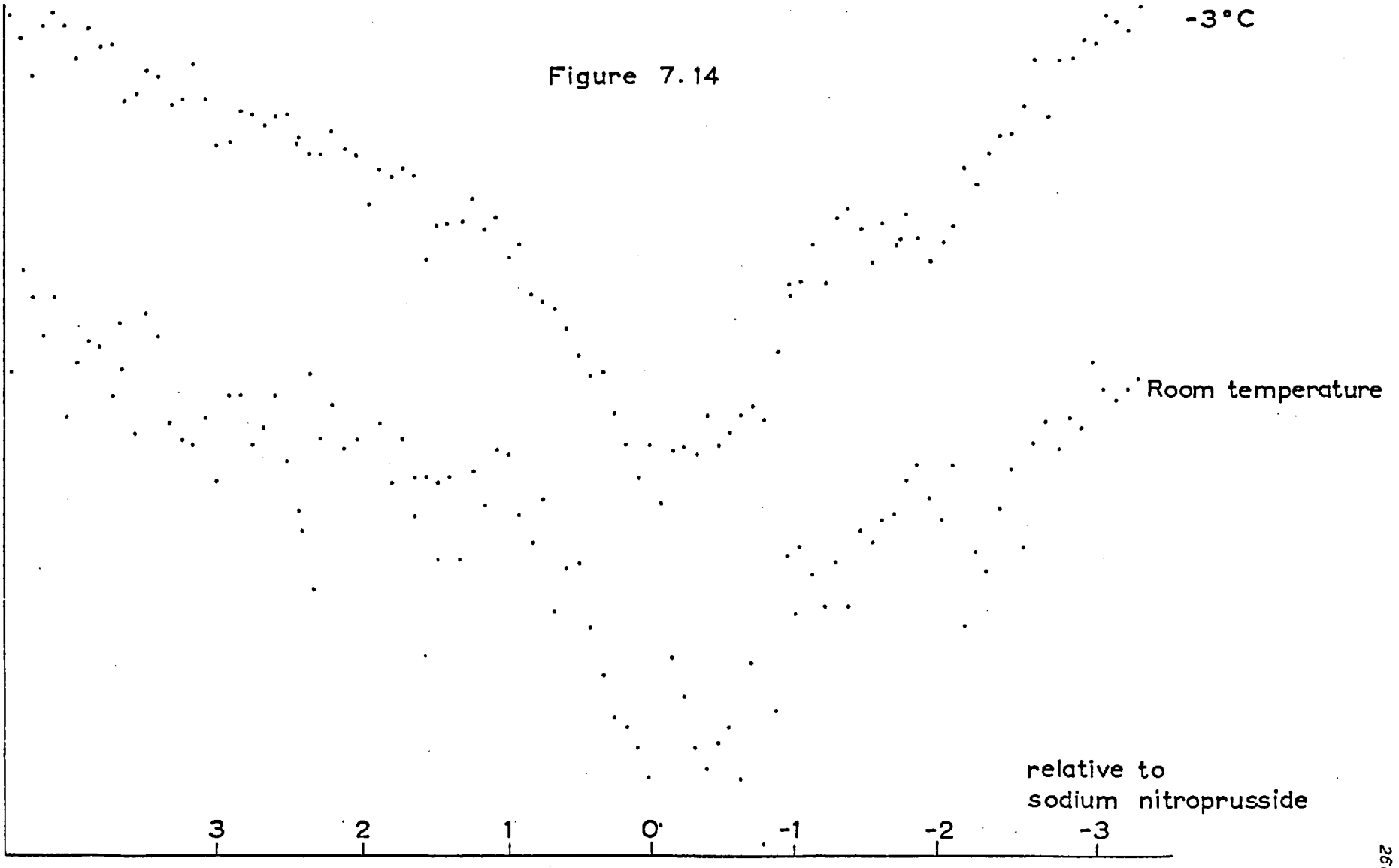

-3°C
Room temperature
relative to
sodium nitroprusside
3
2
1
0
-1
-2
-3

Figure 7.14

the spectra obtained in the cubic phase, i.e. at 140°C. That a phase transition does occur was seen to be the case in placing the actual crystal used with the incorporated Mössbauer probe on the hot stage of a microscope and viewed between crossed polaroids which clearly showed the disappearance of domains on raising the temperature of the crystal to about 135°C.

We are also unable to detect hfs of Fe^{3+} in $BaTiO_3$ at room temperature and at -3°C which implies an insufficiently long T_1 despite the ion being an S-state ion. The above results have been computer synthesised by the Mössbauer group at Harwell using programs specially written to search for lines of comparable magnitude to the background noise, with negative results. It is possible that hfs may occur in $BaTiO_3$ if cooled to low enough temperatures, as has been observed in the non-magnetically aligned matrix of Fe^{3+} in corundum at 78°K (Wertheim and Remeika, 1964), but this is outside the temperature range of interest in this investigation.

However, the spin-lattice relaxation times of the S-state ions Mn^{2+} and Fe^{3+} in MgO, which are similarly oxygen-octahedrally coordinated to $BaTiO_3$, have a spin-lattice relaxation, T_1, of 10^{-6} - 10^{-5} secs., (Low, 1965), which is 10-100 times longer than the nuclear lifetime of Fe^{57}. As far as the author is aware no work has been done on determining

T_1 for S-state ions in $BaTiO_3$ and it would be interesting to see the results of any future work on T_1 in the light of the present lack of hfs at room temperatures and above. Consequently we are not able to learn anything about the change in the phonon modes since we cannot even detect, by this mechanism, the lifetime of the spin-phonon coupling.

8. DISCUSSION

8.1 INTRODUCTION

It is probably fairly accurate to say that up to the present time the majority of the work which has gone into investigating the phase changes occurring in ferroelectric perovskitc with a view to elucidating the mechanisms responsible for bringing about the cooperative effect of ferroelectricity, have utilised in the main, macroscopic techniques.

While these have certainly contributed to a better understanding of the properties exhibited by this class of materials, for which numerous and profitable applications have been found, it has because of this inhibited somewhat a deeper and fundamental understanding of the microscopic processes involved. This situation is now fortunately changing and more industrial laboratories have now recognised the usefulness of such techniques.

8.2 ELECTRON SPIN RESONANCE STUDIES

These we have found to be of fundamental importance despite the lack of fulfilment of some of the results which were sought.

The importance that one may attach to the effect of the crystalline field on the site occupied by the cation which is responsible for ferroelectric behaviour as the temperature is

varied is clear. We see first of all that magnetic resonance shows quite clearly a discontinuity in the phase change, the evidence providing an unambiguous assignment to a first order phase change. This is more striking than the results provided by thermal methods - e.g. specific heat and latent heat determinations. The variation of the crystal field with temperature as manifested in the rather dramatic change of the zero field splitting parameter D is most noticeable.

In regard to the spectrum obtained of Fe^{3+} in $BaTiO_3$, we may draw several conclusions from this. The basic five line spectrum has unambiguously been identified and the associated transitions shown in Fig. 6.10. The line widths of the individual transitions are strongly angularly dependent and are only relatively sharp when they are parallel to one of the cubic axes. This may possibly be taken as an indication that various domains are not quite parallel, the axes of which do not really meet the surfaces of the crystal at right angles.

The variation of the individual line widths probably has an explanation in inhomogenity broadening which stems from lattice defects and because of these the individual paramagnetic ions would see differing crystalline electric fields. The result of this, as we have seen, is to give a distribution of values to the parameters D, a, b, and may also introduce other terms in the spin Hamiltonian arising from lack of complete

tetragonal symmetry.

In addition to the five line spectrum there are the three lines α , β , γ . The transitions associated with the line α have been identified from a series of temperature dependent energy level diagrams as being between levels 1 and 2 up to about 100°C and thence up to the transition temperature (129°C) as between levels 1 and 6. The line we have denoted as β is of greater interest and provides a possible explanation for the incompleteness of our Mössbauer results. We have found that β , which occurs at 1100 gauss, is independent of temperature throughout the range of interest. The fact that it occurs at a value of g = 6 would lead us to suppose that it is associated with a different site to that of the normal five line spectrum.

Now we know that if Fe^{3+} substitutes for Ti^{4+} then overall charge neutrality within the crystal is maintained if there are oxygen vacancies (O^{2-}). These, by virtue of the growth process, are randomly distributed throughout the crystal but it is not unreasonable to suppose that they will also constitute nearest-neighbours to a substitutional Fe^{3+}. This then will create a greater electric field gradient at the Ti^{4+} site and would involve a larger D value. Gibson and Dowsing (1967) (unpublished) have calculated for S state ions the transitions expected for various D values in a spin Hamiltonian of the form similar to that used here, but excluding fourth order terms, and these

results indicate that a transition would be expected at around 1100 gauss for values of $D \geq 2.5$ cm^{-1}. This is the strongest indication that the line β is that due to a nearest-neighbour oxygen vacancy, the field gradient of which is so intense that the transition is observed in both phases, and is due to the lowest lying Kramers doublet.

We are unable to identify the origin of the line δ, which was originally thought to be, at room temperature, the emissive part of the normal absorption line 2 associated with the transition between levels 2 and 3. However, as line 2 moves away from δ with increasing temperature we cannot associate one with the other even in the nature of a forbidden transition. Consequently we are unable to draw any conclusions about line δ, which as we have mentioned earlier is an additional line to that observed by previous workers.

In Fig. 8.1 we see that a plot of D^2 vs T^oC is not linear and this would indicate that the spontaneous polarisation is not wholly electronic in origin since we should then have a linear relationship (Merz, 1953). These findings do not agree with those of the other S state ion Mn^{2+} where D^2 is found to be linearly related to T^oC (Vesela et al., 1965). However, the method of determination in their work is inherently inaccurate as measurement of line intensity is involved and it is possible that more careful experimentation may reveal a linear relationship between

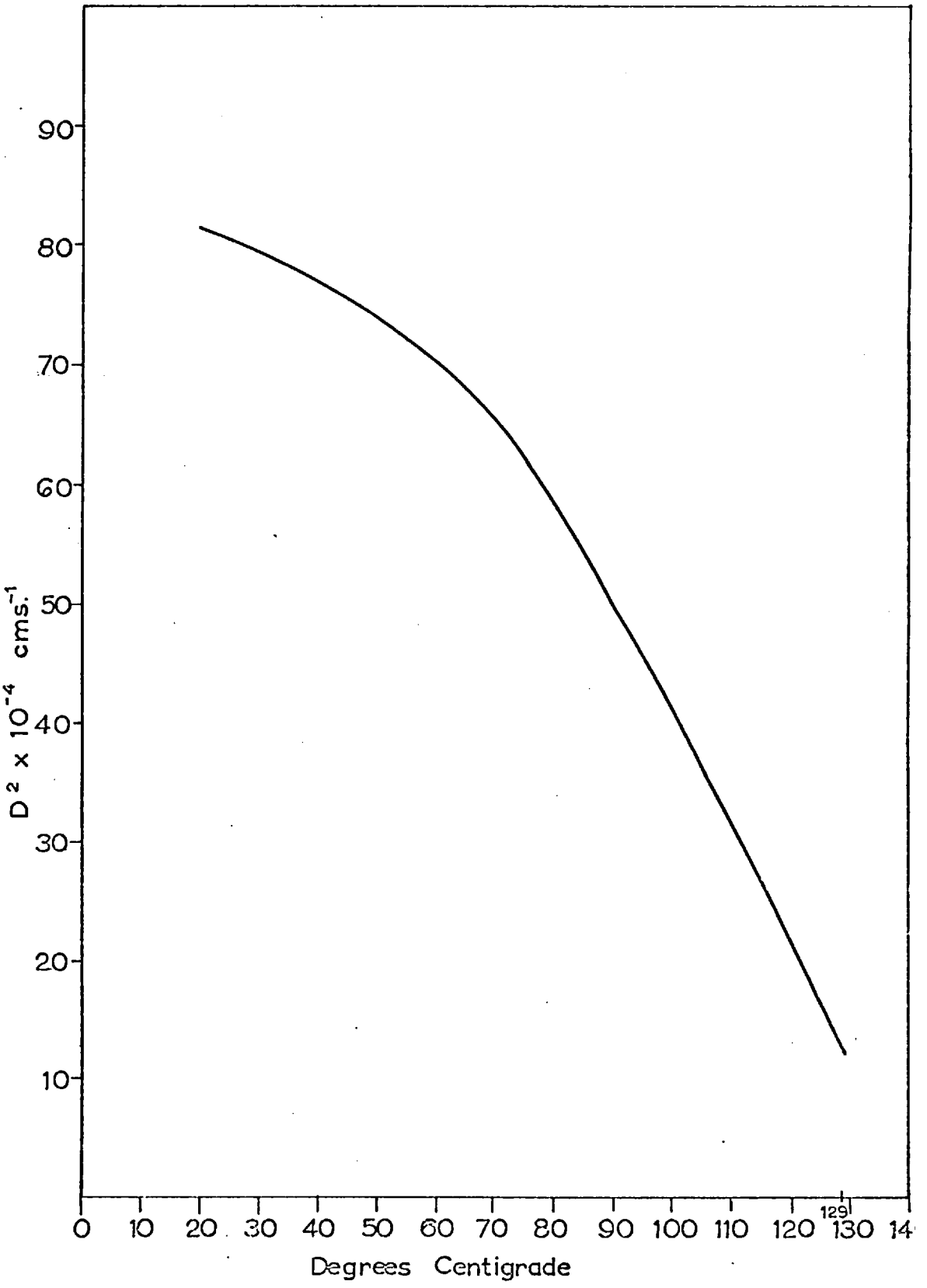

90
80
70
60
50
40
30
20
10
$D^2 \times 10^{-4}$ cms.$^{-1}$
0 10 20 30 40 50 60 70 80 90 100 110 120 129 130 14
Degrees Centigrade

Figure 8.1.

these two quantities. It is unfortunate that the results obtained using Mn^{2+} were not sufficiently sensitive to enable us to measure simultaneously at the same site and in the same crystal field values for D the zero field splitting, and Q the quadrupole splitting. However, its presence is noticeable by the very nature of the spectra obtained.

8.3 MOSSBUAER STUDIES.

The results we have obtained on the Mössbauer measurements have not been as complete as we would have wished. We see from Fig.7.13 that the quadrupole splitting does not disappear in the cubic phase and the origin of this is perhaps due to the method of sample preparation adopted. Now it is known that at elevated temperatures oxygen is extremely mobile whilst titanium is not so. Hence we would expect the incorporation of Co^{57} into the lattice to occur along a line of oxygen vacancies. This also is the only way in which titanium may diffuse out. Consequently on quenching the crystal with a view to substitutional incorporation of Co^{57} into the lattice, and in view of charge neutrality conditions, the occurrence of nearest-neighbour oxygen vacancies is not unreasonable and this would account for the same quadrupole splitting in both phases. We have tried to restore these conditions somewhat by cooling the crystal in an oxygen enriched environment at 70 atmospheres from $1100^{\circ}C$ to room temperature, but without success.

Assuming the presence of a nearest-neighbour oxygen vacancy, then even in the cubic phase there would still be present, an electric field gradient which is responsible for the quadrupole splitting. This field gradient would vary hardly at all in the two phases since the atomic displacements are in any case only very slight. However, on lowering the temperature the crystal symmetry is lowered from tetragonal and we would expect therefore, because of this, a change of the field gradient in the presence of this oxygen vacancy. This, as we have seen, is indeed the case.

One factor to emerge from our room temperature measurements of the quadrupole splitting is a determination of the ionicity of the substituted ion in $BaTiO_3$ which we see to be approximately 60%. This value is in close agreement with that infered by Kinase and Takahasi (1955) and Treibwasser (1957). Because of the presence of the nearest-neighbour oxygen vacancy we have been unable to measure the variation in quadrupole splitting with temperature and to thus determine its relation, if any, to the variation in spontaneous polarisation with temperature. It would have been an added advantage to have determined this variation of quadrupole splitting with temperature in order to compare it with the variation of the parameter D in the spin Hamiltonian of Fe^{3+}, interest in which has been awakened recently by Watanabe (1957). Nicholson and Burns (1963) tried to

correlate the variation of D with quadrupole splitting measured in different host crystals of the same environment but their attempts were unsuccessful. It would appear more useful to attempt a correlation using the same ion in the same crystal for both types of measurement.

8.4 CONCLUSION

We see that one of the major outcomes of this work is to demonstrate the unique role played by the microscopic techniques adopted as probes of the crystalline field at a particular site and the importance that may be attached to the sample preparation processes. We have in the main body of the text drawn conclusions resulting from our measurements but it should be stressed that these techniques do not in any way tell us whether a material is ferroelectric or not, even though measurements may provide strong evidence for this.

We conclude by remarking that perhaps one of the most convincing demonstrations of the Cochran model awaits measurements of the spin lattice relaxation time, T_1, over the temperature range of interest and as a function of orientation.

REFERENCES

ABRAGAM, A. and PRYCE, M.H.L., Proc. Roy. Soc. A, 205, 135, 1951.

ALLSOP, H. and GIBBS, D., Phil. Mag.(8) 4, 359, 1959.

ANLIKER, M., BRUGGER, H.R. and KANZIG, W., Helv. Phys. Acta. 27, 99, 1954.

BALLANTYNE, J.M., Phys. Rev. 136, A429, 1964.

BALLHAUSEN, C.J., Introduction to Ligand Field Theory, McGraw Hill, 1962.

BARKER, A.S. Jr., Phys. Rev. 145, 391, 1966.

BARKER, A.S. Jr., and HOPFIELD, J.J., Phys. Rev. 135, A 1732, 1964.

BARKER, A.S. Jr., and TINKHAM, M., Phys. Rev. 125, 1527, 1962.

BELL, R.O. and RUPPRECHT, G., Phys. Rev. 125, 1915, 1962.

BENEDICT, T. and DURRAND, M., Phys. Rev. 109, 1091, 1958.

BERSUKER, I.B., Phys. Lett. 20, 589, 1966.

BHIDE, V.G. and BHAPAT, N., Physics (Netherlands), Vol.27, No.16, 531, 1961.

BHIDE, V.G. and MULTANI, M.S., Phys. Rev. 139, 6A, A 1983, 1965.

BJORKSTOM, J.L. and OETTEL, R.E., Proc. Int. Meeting on Ferroelectricity, Prague, Vol. 2, p.91, 1966.

BLATTNER, H., KANZIG, W., and MERZ, W., Helv. Phys. Acta. 20, 225, 1947.

BLATTNER, H., KANZIG, W., MERZ, W. and SUTTER, H., Helv. Phys. Acta. 21, 207, 1948.

BLATTNER, H., KANZIG, W., and MERZ, W., Helv. Phys. Acta. 22, 35, 1949.

BLEANEY, B., Phil. Mag. 42, 441, 1951.

BLEANEY, B. and INGRAM, D.J.E., Proc. Roy. Soc. A205, 336, 1951.

BLEANEY, B. and PENROSE, R.P., Nature 157, 339, 1946.

BLEANEY, B. and RUBINS, R.S., Proc. Phys. Soc. (London) 77, 103, 1961.

BLEANEY, B. and STEVENS, K.W.H., Rep. Prog. Phys. 16, 108, 1953.

BLINC, R. and SVETINA, S., Phys. Rev. 147, 430, 1966; Phys. Rev. 147, 423, 1966.

BODMER, A.R., Proc. Phys. Soc. (London) A66, 1041, 1953.

BODMER, A.R., Nucl. Phys. 9, 371, 1958.

BODMER, A.R., Nucl. Phys. 21, 347, 1960.

BORN, M. and HUANG, K., Dynamical Theory of Crystal Lattices (Clarendon Press, Oxford), p.153, 1954.

BOTTCHER, C.J.F., Theory of Electric Polarisation, Elsevier, Amsterdam, 1952.

BOWERS, K.D. and OWEN, J., Repr. Prog. Phys. 18, 304, 1955.

BROUT, R., MULLER, K.A. and THOMAS, H., Solid State Comm. 4, 507, 1966.

BURBANK, R.D. and EVANS, H.T., Acta. Cryst. 1, 330, 1948.

BUSCH, G., FLURY, H. and MERZ, W., Helv. Phys. Acta. 21, 212, 1948.

CHYNOWETH, A.G., J. Appl. Phys. 27, 78, 1956.

CHYNOWETH, A.G., Phys. Rev. 102, 705, 1956.

COCHRAN, W., Z. Krist. 112, 465, 1959.

COCHRAN, W., Phil. Mag. Suppl. 9, 387, 1960.

COCHRAN, W., Advan. Phys. 10, 401, 1961.

COHEN, M., Phys. Rev. 84, 368, 1951.

COHEN, M.H. and REIF, F., Solid State Physics, Vol.5, Academic Press, 1957.

COWLEY, R.A., Phil. Mag. 11, 673, 1965.

CROSS, L., Phil. Mag.(7), 44, 1161, 1953.

CROSS, L.E., NICHOLSON, M.M. and WHIDDINGTON, R., Nature 165, 440, 1950.

CUMMEROW, R.L. and HALLIDAY, D., Phys. Rev. 70, 433, 1946.

DANON, J., Proc. 8th Int. Cong. on Coord. Chem., Springer Verlag, Vienna, 1964.

DE BENEDETTI, S., LANG, G. and INGALLS, R., Phys. Rev. Letters, 6, 60, 1961.

DE GENNES, P.G., Solid State Comm. 1, 132, 1963.

DE VRIES, R.C., J. Am. Ceram. Soc. 42 (11), 547, 1959.

DEVONSHIRE, A.F., Phil. Mag.(7) 40, 1040, 1949.

DEVONSHIRE, A.F., Phil. Mag.(7) 42, 1065, 1951.

DEVONSHIRE, A.F., Advances in Physics, 3, 85, 1954.

DICK, B.G. and OVERHAUSER, A.W., Phys. Rev. 112, 90, 1958.

DROUGARD, M. and YOUNG, D., Phys. Rev. 95, 1152, 1954.

DROUGARD, M., YOUNG, D. and HUIBREGTSE, E., Phys. Rev. 98, 1562, 1955.

DROUGARD, M., LANDAUER, R. and YOUNG, D.R., Phys. Rev. 98, 1010, 1955.

EGERTON, L. and VAN UITERT, L.G., J. Appl. Phys. 32, 959, 1961.

ELLIOTT, R.J. and STEVENS, K.W.H., Proc. Roy. Soc. A 218, 553, 1953.

ENSTACHE, H., Compt. Rend. 244, 1029, 1957.

EVANS, H., Mass. Inst. Technol. Lab. Insultn. Res. Tech. Rept. No. 58, 1953.

FAGG, S. and HANNA, R., Rev. Mod. Phys. 31, 711, 1959.

FAUST, J.W. and JOHN, H.F., Trans. A.I.M.E., 233, 230, 1965.

FERMI, E., Z. Physik 60, 320, 1930.

FERMI, E. and SEGRE, E., 2. Physik 32, 729, 1933.

FEYNMAN, R.P., Quantumn Electrodynamics, W.A. Benjamin Inc., N.Y., p.8, 1961.

FOLEN, J., Phys. Rev. 125, 1581, 1962.

FORSBERGH, P., Phys. Rev. 76, 1187, 1949.

FORSBERGH, P., Phys. Rev. 93, 686, 1954.

FORSBERGH (Jr.) P.W., "Piezoelectricity, electrostriction and ferroelectricity". Hand Buch der Physik, Vol.17, pp. 264-392, Springer-Verlag, Berlin, 1956.

FRAZER, B., DANNER, H. and PEPINSKY, R., Phys. Rev. 100, 745, 1955.

GAINON, D.J.A., Phys. Rev. 134, A1300, 1964.

GIBSON, J.F. and DOWSING, R.G., (unpublished) 1967.

GOL'DANSKI, V.I., G.E.C. Atomic Energy Rev. 1, 3, 1963.

GOL'DANSKI, V.I., MAKAROV, E.F. and KHRAPOV, V.V., Zh. Eksperim. i Teor. Fiz. 44, 752; 1963; Soviet Physics, JETP 17, 508, 1963; see also Phys. Letters 3, 344, 1963.

GOLDING, R.M., Mol. Phys. in press.

GORSKI, G., Private communication, Harshaw Chemical Co., 1961.

GOUDSMIT, S.A., Phys. Rev. 43, 636, 1933.

HEITLER, W., Quantumn Theory of Radiation, O.U.P., 1949.

HERD, K.F., SACHS, M. and HERSHBERGER, W.D., Phys. Rev. 93, 373, 1954.

HEWITT, R.R., Phys. Rev. 121, 45, 1961.

HOOTON, J. and MERZ, W., Phys. Rev. 98, 409, 1955.

HORNIG, A.W., JAYNES, E.T., and WEAVER, H.E., Phys. Rev. 96, No.6, 1703, 1954.

HORNIG, A.W., JAYNES, E.T., and WEAVER, H.E., Phys. Rev. Letters 1, No.8, 1954.

HORNIG, A.W., REMPEL, R.C. and WEAVER, H.E., J. Phys. Chem. Solids, 10, 1, 1959.

HUIBREGTSE, E., BESSEY, W. and DROUGARD, M., J. Appl. Phys. 30, 899, 1959.

HULM, J.K., Nature 160, 126, 1947.

HURD, J.D., SIMPSON, A.W. and TREDGOLD, R.H., Proc. Phys. Soc. (Lond.) 73, 448, 1959.

IKUSHIMA, H., J. Phys. Soc. Japan Vol. 21, No. 10, 1866, 1966.

IKUSHIMA, H. and HAYAKAWA, S., J. Phys. Soc. Japan 20, 1517, 1965.

IKUSHIMA, H. and HAYAKAWA, S., J. Phys. Soc. Japan, 1986, 1964.

JACKSON, J.D., Can. J. Phys. 33, 575, 1955.

JAFFE, H., BERLINCOURT, D. and McKEE, J., Phys. Rev. 105, 57, 1957.

JAYNES, E., "Ferroelectricity", Princeton, 1952.

JOHNSON, V.J., VALENTA, M.W., DOUGHERTY, J.E., DOUGLASS, R.M., and MEADOWS, J.W., J. Phys. Chem. Solids 24, 85, 1963.

JONA, F. and SHIRANE, G., "Ferroelectric Crystals", Pergamon Press, Oxford, 1962.

JUDD, B.R., Proc. Roy. Soc. A227, 552, 1955.

KANZIG, W., Phys. Rev. 98, 549, 1955.

KANZIG, W., Helv. Phys. Acta. 24, 131, 1956.

KANZIG, W., "Ferroelectrics and Antiferroelectrics", Solid State Physics, Vol. 4, pp.1-197, Academic Press, New York, 1957.

KANZIG, W. and MAIKOFF, N., Helv. Phys. Acta. 22, 395, 1949.

KANZIG, W. and MEIER, R., Helv. Phys. Acta. 21, 585, 1949.

KARAN, C., J. Chem. Phys. 22, 957, 1954.

KARAN, C. and SKINNER, B.J., J. Chem. Phys. 21, 2225, 1953.

KAWABE, K., J. Phys. Soc. Japan, Vol.14, No.12, 1755, 1959.

KAY, H., Acta. Crysta. 1, 229, 1948.

KAY, H.F. and VOUSDEN, P., Phil. Mag.(7) 40, 1019, 1949.

KINASE, W. and TAKAHASI, H.J., J. Phys. Soc. Japan 10, 942, 1955.

KINASE, W. and TAKAHASI, H.J., J. Phys. Soc. Japan 12, No.5, 464, 1957.

KIRKPATRICK, E.S., MULLER, K.A., and RUBINS, R.S., Phys. Rev. 135, A86, 1964.

KRAMERS, H., Proc. Amsterdam Acad. Sci., 32, 1176, 1929.

KRAMERS, H., Proc. Amsterdam Acad. Sci., 33, 959, 1930.

KREMERS, H.C., WILLIAMS, H.D. and HACSKAYLO, M., Harshaw Chem. Co., Contract No.DA-36-039-sc-15493 Final Report, 1954.

KUDZINS, A.Y., Kristallografiya 7, 799, 1962.

KUHN, W., Phil. Mag. 8, 625, 1929.

LAMB, W.E., Phys. Rev. 55, 190, 1939.

LANDAUER, R., YOUNG, D.R. and DROUGARD, M.E., J. Appl. Phys. 27, 752, 1956.

LAST, J.T., Phys. Rev. 105, 1740, 1957.

LEIBFRIED, G., Encyclopaedia of Physics 7, Pt.1, Springer-Verlag, Berlin, 1955.

LIPAOVA, N. and SHARANI, G., Sov. Phys. Solid State, Vol.2, No. 3, 1960.

LIPKIN, H.J., Annals of Physics 9, 332, 1960.

LITTLE, E., Mass. Inst. Technol. Lab. Insultn. Res. Tech. Rpt. No.87, 1954.

LORENZ, H., "Theory of Electrons", Teubner, Leipzig, 1916.

LOW, W., Paramagnetic Resonance in Solids, Academic Press N.Y., 1960.

LOW, W., Paramagnetic Resonance, Benjamin & Co., N.Y., 1965.

LOW, W., Solid State Physics, Supplement 2, (Paramagnetic resonance), 1966.

LOW, W. and SHALTIEL, D., Phys. Rev. Letters, 1, No. 2, 1958; Phys. Rev. Letters, 1, No.8, 1958.

LUTTINGER, J. and TISZA, L., Phys. Rev. 70, 954, 1946.

LUTTINGER, J. and TISZA, L., Phys. Rev. 72, 257, 1947.

LYDDANE, R.H., SACHS, R.G., and TELLER, E., Phys. Rev. 59, 673, 1941.

MARGULIES, S., The Mössbauer effect in Fe^{57} (unpublished Thesis, Univ. Illinois, 1961.

MARSHALL, W. and JOHNSON, C.E., J. Phys. Radium 23, 733, 1962.

MASON, W.P., "Piezoelectric Crystals and their application to ultrasonics", D. van Nostrand, 1951.

MASON, W.P. and MATHIAS, B., Phys. Rev. 74, 1622, 1948.

MATHIAS, B., WOOD, E. and HOLDEN, A., Phys. Rev. 76, 175, 1949.

MATHIAS, B. and VON HIPPEL, A., Phys. Rev. 73, 1378, 1948.

MEGAW, H.D., Proc. Roy. Soc. A189, 261, 1947.

MEGAW, H.D., "Ferroelectricity in crystals", Methuen, 1957.

MEGAW, H.D., Acta. Crysta. 5, 739, 1952.

MEGAW, H.D., Acta. Crysta. 7, 187, 1954.

MERZ, W.J., Phys. Rev. 76, 1221, 1949.

MERZ, W.J., Phys. Rev. 78, 52, 1950.

MERZ, W.J., Phys. Rev. 88, 421, 1952.

MERZ, W.J., Phys. Rev. 95, 690, 1954.

MERZ, W.J., Phys. Rev. 91, 1513, 1953.

MERZ, W.J. and CASPARI, M., Phys. Rev. 80, 1082, 1950.

MITSUI, T. and WESTPHAL, W.B., Phys. Rev. 124, 1354, 1961.

NICHOLSON, W.G. and BURNS, G., Phys. Rev. 129, 21, 90, 191, 1963.

NIELSEN, J.W., LINARES, R.C. and KOONCE, S.E., J. Am. Ceram. Soc. 45(1), 12, 1962.

NISHIOKA, A., SEKIKOWA, K., and OWAKI, M., J. Phys. Soc. Japan, 11, 181, 1957.

NOVOSIL'TSEV, N.S. and KHODAKOV, A.L., Doklady Akad. Nauk. S.S.S.R. 85, 1263, 1952.

NYE, J.F., "Physical properties of crystals", p. 189, O.U.P., 1957.

ODEHNAL, M., Czech. J. Phys. 13, 566, 1963.

ONSAGER, L., J. Amer. Chem. Soc. 58, 1486, 1936.

PARKER, A.S.(Jun.), Symposium on Ferroelectricity, General Motors Research Labs., 1967.

PEARSON, G. and FELDMANN, W., J. Phys. Chem. Solids Vol.9, No.1, 28, 1959.

PENNEY, W.G. and SCHLAPP, R., Phys. Rev. 41, 194, 1932; Phys. Rev. 42, 666, 1932.

PERRY, C.H., KHANNA, B.N. and RUPPRECHT, G., Phys. Rev. 135, A408, 1964.

PERRY, C.H., McCARTHY, D.J. and RUPPRECHT, G., Phys. Rev. 138, A1537, 1965.

PICKARA, A. and PAJAK, A., Acta. Phys. Polon. 11, 256, 1952.

POWELL, M.J.D., GABRIEL, J.R. and JOHNSTON, D.F., Phys. Rev. Letters 5, 145, 1960.

POWLES, J. and JACKSON, W., Proc. Inst. Elec. Engrs. 96, 383, 1949.

PRYCE, M.H.L., Phys. Rev. 80, 1107, 1950.

PRYCE, M.H., Proc. Phys. Soc. A. 63, 25, 1950b.

PRYCE, M.H., Nuovo Cimento 6 (Supplemento) 817, 1957.

RAMSEY, N.F., "Nuclear Moments", p. 23, Wiley, N.Y., 1953.

RASE, D.E. and ROY, R.J., J. Phys. Chem. 61, 747, 1957.

REISMAN, A., HOLTZBERG, F., TRIEBWASSER, S. and BERKENBLIT, M., J. Amer. Chem. Soc. 78, 719, 1956.

REMEIKA, J.P., J. Am. Chem. Soc. 76 (3), 940, 1954.

ROBERTS, S., Phys. Rev. 85, 925, 1952.

ROSE, M.E., Elementary Theory of Angular Momentum, Wiley, N.Y., Ch.2, 1957.

ROY, R., Qtly Rpt. Penn. State Univ., 1952.

RZHANOV, A., J. Exp. Theor. Phys. (U.S.S.R.) 19, 502, 1960.

SASAKI, H. and KUROKAWA, E., J. Am. Ceram. Soc. Vol. 48, (3), 171, 1965.

SAWYER, C. and TOWER, C., Phys. Rev. 35, 269, 1930.

SCHMITT, G., Zeit. Phys. 145, 534, 1956.

SCHMITT, G., Z. Angen. Physik Vol. 9, No. 3, 107, 1957.

SHIRANE, G. and TAKEDA, A., J. Phys. Soc. Japan 7, 1, 1952.

SHOCKLEY, W., Phys. Rev. 73, 1273, 1948.

SHOLOKHOVICH, H.L. and BELYAEV, I.N., Zhur. Obschei Khim. 24, 218, 1954.

SHULMAN, R.G. and SUGANO, S.J., J. Chem. Phys. 12, 39, 1965.

SHUVALOV, L.A., Soviet Physics - Crystallography, Vol.8, No. 4, Jan-Feb. 1964.

SIERRO, J., LACROIX, R. and MULLER, K.A., Helv. Phys. Acta. 32, 286, 1959.

SLATER, J., Phys. Rev. 78, 748, 1950.

SLICHTER, C.P., Principles of Magnetic Resonance, Harper and Row, 1964.

SPITZER, W.G., MILLER, R.C., KLEINMAN, D.A. and HOWARTH, L.E., Phys. Rev. 126, 1710, 1962.

SPIVAK, G., IGROSS, E., PHYMKOVA, I. and ZHELUDEV, I., Kristallografiya Vol.4, No.1, 123, 1959.

STATTON, W.O., J. Chem. Phys. 19, 33, 1951.

STERN, W. and LURIO, M., Phys. Rev. 123, 117, 1961.

STERNHEIMER, R.M., Phys. Rev. 80, 102, 1950.

STERNHEIMER, R.M., Phys. Rev. 84, 244, 1951.

STERNHEIMER, R.M., Phys. Rev. 86, 316, 1952.

STERNHEIMER, R.M., Phys. Rev. 95, 736, 1954.

STERNHEIMER, R.M., Phys. Rev. 105, 158, 1957.

STERNHEIMER, R.M. and FOLEY, H.M., Phys. Rev. 92, 1460, 1953.

STEVENS, K.W.H., Proc. Phys. Soc. A, 65, 209, 1952.

TODD, S. and LORENSEN, R., J. Amer. Chem. Soc. 74, 2043, 1952.

TOWNES, C.H. and SCHAWLOW, A.L., "Microwave Spectroscopy", p.132, McGraw Hill, N.Y., 1955.

TRIEBWASSER, S.J., J. Phys. Chem. Solids 3, 53, 1957.

VAN VLECK, J.H., Phys. Rev. 41, 208, 1932.

VAN VLECK, J.H., Theory of Electric & Magnetic Susceptibilities, O.U.P., 1932.

VAN VLECK, J.H. and PENNEY, W.G., Phil. Mag. 17, 961, 1934.

VESSELA, J., BROUBEK, Z. and ZDANSKY, K., Phys. Stat. Sol. 10, K99, 1965.

VISSCHER, W.M., Annals of Physics, 9, 194, 1960.

VOLGER, J., Philips Research Reports, 7, 21, 1952.

VON HIPPEL, A.H., Revs. Modern Phys. 22, 221, 1950.

VON HIPPEL, A.H., Revs. Modern Phys. 22, 221, 1951.

WALKER, L.R., WERTHEIM, G.K. and JACCARINO, V., Phys. Rev. Letters 6, 98, 1961.

WATANABE, H.W., Pragr. Theoret. Phys. (Kyoto) 18, 405, 1957.

WATSON, R.E., Solid State & Molecular Theory Group, Techn. Rpt., No. 12, M.I.T., 1959.

WATSON, R.E., Phys. Rev. 119, 1934, 1960.

WEIDER, H.H., J. Appl. Phys., 26, 1479, 1955.

WERTHEIM, G.K., Mössbauer Effect, p. 45, Academic Press, 1965.

WERTHEIM, G.K. and REMEIKA, J.P., Phys. Rev. Letters, 10, 14, 1964.

WESTPHAL, A., Dielectrics and Waves, von Hippel, Wiley, 1954.

WHITE, E.A.D., Technique of Inorganic Chemistry, Interscience Vol. 4, 31, 1965.

WOODS, A.D.B., COCHRAN, W. and BROCKHOUSE, B.N., Phys. Rev. 119, 980, 1960.

ZAVOISKY, E.J., J. Phys. (U.S.S.R.) 9, 211, 1954.

APPENDIX A

We wish to calculate the matrix elements appropriate to the form of the spin Hamiltonian used (see Chapter 6). These, as we have seen, are given by the three following operator relationships:

$$\langle M_s | S_z | M_s \rangle = M_s$$

$$\langle M_s+1 | S_+ | M_s \rangle = \left[S(S+1) - M_s(M_s+1)\right]^{\frac{1}{2}}$$

$$\langle M_s-1 | S_- | M_s \rangle = \left[S(S+1) - M_s(M_s-1)\right]^{\frac{1}{2}}$$

Using the shift operators $S_+ = S_x + iS_y$ and $S_- = S_x - iS_y$ we can then obtain the following:

$$S_x = \tfrac{1}{2}(S_+ + S_-)$$

and

$$S_y = \frac{1}{2i}(S_+ - S_-)$$

The matrices for spins 1, 3/2, and 5/2 have been calculated and are shown on the following pages.

NOTE

The above matrices are identical to those for nuclear spins, in which case read I for S.

S=1

S_z

	$\|1\rangle$	$\|0\rangle$	$\|-1\rangle$
$\langle 1\|$	1	0	0
$\langle 0\|$	0	0	0
$\langle -1\|$	0	0	-1

S_+

	$\|1\rangle$	$\|0\rangle$	$\|-1\rangle$
$\langle 1\|$	0	$\sqrt{2}$	0
$\langle 0\|$	0	0	$\sqrt{2}$
$\langle -1\|$	0	0	0

S_-

	$\|1\rangle$	$\|0\rangle$	$\|-1\rangle$
$\langle 1\|$	0	0	0
$\langle 0\|$	$\sqrt{2}$	0	0
$\langle -1\|$	0	$\sqrt{2}$	0

S_x

	$\|1\rangle$	$\|0\rangle$	$\|-1\rangle$
$\langle 1\|$	0	$1/\sqrt{2}$	0
$\langle 0\|$	$1/\sqrt{2}$	0	$1/\sqrt{2}$
$\langle -1\|$	0	$1/\sqrt{2}$	0

S_y

	$\|1\rangle$	$\|0\rangle$	$\|-1\rangle$
$\langle 1\|$	0	$-i/\sqrt{2}$	0
$\langle 0\|$	$i/\sqrt{2}$	0	$-i/\sqrt{2}$
$\langle -1\|$	0	$i/\sqrt{2}$	0

S_x^2

	$\|1\rangle$	$\|0\rangle$	$\|-1\rangle$
$\langle 1\|$	1/2	0	1/2
$\langle 0\|$	0	1	0
$\langle -1\|$	1/2	0	1/2

S=1

S_y^2

	$\|1\rangle$	$\|0\rangle$	$\|-1\rangle$
$\langle 1\|$	1/2	0	-1/2
$\langle 0\|$	0	1	0
$\langle -1\|$	-1/2	0	1/2

$S_x^2 - S_y^2$

	$\|1\rangle$	$\|0\rangle$	$\|-1\rangle$
$\langle 1\|$	0	0	1
$\langle 0\|$	0	0	0
$\langle -1\|$	1	0	0

S_z^2

	$\|1\rangle$	$\|0\rangle$	$\|-1\rangle$
$\langle 1\|$	1	0	0
$\langle 0\|$	0	0	0
$\langle -1\|$	0	0	1

S_+^2

	$\|1\rangle$	$\|0\rangle$	$\|-1\rangle$
$\langle 1\|$	0	0	2
$\langle 0\|$	0	0	0
$\langle -1\|$	0	0	0

S_-^2

	$\|1\rangle$	$\|0\rangle$	$\|-1\rangle$
$\langle 1\|$	0	0	0
$\langle 0\|$	0	0	0
$\langle -1\|$	2	0	0

$S_+^2 + S_-^2$

	$\|1\rangle$	$\|0\rangle$	$\|-1\rangle$
$\langle 1\|$	0	0	2
$\langle 0\|$	0	0	0
$\langle -1\|$	2	0	0

$S = 3/2$

S_z

	$\|3/2\rangle$	$\|1/2\rangle$	$\|-1/2\rangle$	$\|-3/2\rangle$
$\langle 3/2\|$	3/2	0	0	0
$\langle 1/2\|$	0	1/2	0	0
$\langle -1/2\|$	0	0	-1/2	0
$\langle -3/2\|$	0	0	0	-3/2

S_+

	$\|3/2\rangle$	$\|1/2\rangle$	$\|-1/2\rangle$	$\|-3/2\rangle$
$\langle 3/2\|$	0	$\sqrt{3}$	0	0
$\langle 1/2\|$	0	0	2	0
$\langle -1/2\|$	0	0	0	$\sqrt{3}$
$\langle -3/2\|$	0	0	0	0

S_-

	$\|3/2\rangle$	$\|1/2\rangle$	$\|-1/2\rangle$	$\|-3/2\rangle$
$\langle 3/2\|$	0	0	0	0
$\langle 1/2\|$	$\sqrt{3}$	0	0	0
$\langle -1/2\|$	0	2	0	0
$\langle -3/2\|$	0	0	$\sqrt{3}$	0

$S = 3/2$

S_x

	$\|3/2\rangle$	$\|1/2\rangle$	$\|-1/2\rangle$	$\|-3/2\rangle$
$\langle 3/2\|$	0	$\sqrt{3}/2$	0	0
$\langle 1/2\|$	$\sqrt{3}/2$	0	1	0
$\langle -1/2\|$	0	1	0	$\sqrt{3}/2$
$\langle -3/2\|$	0	0	$\sqrt{3}/2$	0

S_y

	$\|3/2\rangle$	$\|1/2\rangle$	$\|-1/2\rangle$	$\|-3/2\rangle$
$\langle 3/2\|$	0	$-i\sqrt{3}/2$	0	0
$\langle 1/2\|$	$i\sqrt{3}/2$	0	$-i$	0
$\langle -1/2\|$	0	i	0	$-i\sqrt{3}/2$
$\langle -3/2\|$	0	0	$i\sqrt{3}/2$	0

S_x^2

	$\|3/2\rangle$	$\|1/2\rangle$	$\|-1/2\rangle$	$\|-3/2\rangle$
$\langle 3/2\|$	3/4	0	$\sqrt{3}/2$	0
$\langle 1/2\|$	0	7/4	0	$\sqrt{3}/2$
$\langle -1/2\|$	$\sqrt{3}/2$	0	7/4	0
$\langle -3/2\|$	0	$\sqrt{3}/2$	0	3/4

$S = 3/2$

S_y^2

	$\|3/2\rangle$	$\|1/2\rangle$	$\|-1/2\rangle$	$\|-3/2\rangle$
$\langle 3/2\|$	3/4	0	$-\sqrt{3}/2$	0
$\langle 1/2\|$	0	7/4	0	$-\sqrt{3}/2$
$\langle -1/2\|$	$-\sqrt{3}/2$	0	7/4	0
$\langle -3/2\|$	0	$-\sqrt{3}/2$	0	3/4

$S_x^2 - S_y^2$

	$\|3/2\rangle$	$\|1/2\rangle$	$\|-1/2\rangle$	$\|-3/2\rangle$
$\langle 3/2\|$	0	0	$\sqrt{3}$	0
$\langle 1/2\|$	0	0	0	$\sqrt{3}$
$\langle -1/2\|$	$\sqrt{3}$	0	0	0
$\langle -3/2\|$	0	$\sqrt{3}$	0	0

S_z^2

	$\|3/2\rangle$	$\|1/2\rangle$	$\|-1/2\rangle$	$\|-3/2\rangle$
$\langle 3/2\|$	9/4	0	0	0
$\langle 1/2\|$	0	1/4	0	0
$\langle -1/2\|$	0	0	1/4	0
$\langle -3/2\|$	0	0	0	9/4

$S = 3/2$

S_+^2

	$\|3/2\rangle$	$\|1/2\rangle$	$\|-1/2\rangle$	$\|-3/2\rangle$
$\langle 3/2\|$	0	0	$2\sqrt{3}$	0
$\langle 1/2\|$	0	0	0	$2\sqrt{3}$
$\langle -1/2\|$	0	0	0	0
$\langle -3/2\|$	0	0	0	0

S_-^2

	$\|3/2\rangle$	$\|1/2\rangle$	$\|-1/2\rangle$	$\|-3/2\rangle$
$\langle 3/2\|$	0	0	0	0
$\langle 1/2\|$	0	0	0	0
$\langle -1/2\|$	$2\sqrt{3}$	0	0	0
$\langle -3/2\|$	0	$2\sqrt{3}$	0	0

$S_+^2 + S_-^2$

	$\|3/2\rangle$	$\|1/2\rangle$	$\|-1/2\rangle$	$\|-3/2\rangle$
$\langle 3/2\|$	0	0	$2\sqrt{3}$	0
$\langle 1/2\|$	0	0	0	$2\sqrt{3}$
$\langle -1/2\|$	$2\sqrt{3}$	0	0	0
$\langle -3/2\|$	0	$2\sqrt{3}$	0	0

$S = 5/2$

S_z

	$\|5/2\rangle$	$\|3/2\rangle$	$\|1/2\rangle$	$\|-1/2\rangle$	$\|-3/2\rangle$	$\|-5/2\rangle$
$\langle 5/2\|$	5/2	0	0	0	0	0
$\langle 3/2\|$	0	3/2	0	0	0	0
$\langle 1/2\|$	0	0	1/2	0	0	0
$\langle -1/2\|$	0	0	0	-1/2	0	0
$\langle -3/2\|$	0	0	0	0	-3/2	0
$\langle -5/2\|$	0	0	0	0	0	-5/2

S_+

	$\|5/2\rangle$	$\|3/2\rangle$	$\|1/2\rangle$	$\|-1/2\rangle$	$\|-3/2\rangle$	$\|-5/2\rangle$
$\langle 5/2\|$	0	$\sqrt{5}$	0	0	0	0
$\langle 3/2\|$	0	0	$2\sqrt{2}$	0	0	0
$\langle 1/2\|$	0	0	0	3	0	0
$\langle -1/2\|$	0	0	0	0	$2\sqrt{2}$	0
$\langle -3/2\|$	0	0	0	0	0	$\sqrt{5}$
$\langle -5/2\|$	0	0	0	0	0	0

S_-

	$\|5/2\rangle$	$\|3/2\rangle$	$\|1/2\rangle$	$\|-1/2\rangle$	$\|-3/2\rangle$	$\|-5/2\rangle$
$\langle 5/2\|$	0	0	0	0	0	0
$\langle 3/2\|$	$\sqrt{5}$	0	0	0	0	0
$\langle 1/2\|$	0	$2\sqrt{2}$	0	0	0	0
$\langle -1/2\|$	0	0	3	0	0	0
$\langle -3/2\|$	0	0	0	$2\sqrt{2}$	0	0
$\langle -5/2\|$	0	0	0	0	$\sqrt{5}$	0

$S = 5/2$

S_x

	$\|5/2\rangle$	$\|3/2\rangle$	$\|1/2\rangle$	$\|-1/2\rangle$	$\|-3/2\rangle$	$\|-5/2\rangle$
$\langle 5/2\|$	0	$\sqrt{5}/2$	0	0	0	0
$\langle 3/2\|$	$\sqrt{5}/2$	0	$\sqrt{2}$	0	0	0
$\langle 1/2\|$	0	$\sqrt{2}$	0	3/2	0	0
$\langle -1/2\|$	0	0	3/2	0	$\sqrt{2}$	0
$\langle -3/2\|$	0	0	0	$\sqrt{2}$	0	$\sqrt{5}/2$
$\langle -5/2\|$	0	0	0	0	$\sqrt{5}/2$	0

S_y

	$\|5/2\rangle$	$\|3/2\rangle$	$\|1/2\rangle$	$\|-1/2\rangle$	$\|-3/2\rangle$	$\|-5/2\rangle$
$\langle 5/2\|$	0	$-i\sqrt{5}/2$	0	0	0	0
$\langle 3/2\|$	$i\sqrt{5}/2$	0	$-i\sqrt{2}$	0	0	0
$\langle 1/2\|$	0	$i\sqrt{2}$	0	$-3i/2$	0	0
$\langle -1/2\|$	0	0	$3i/2$	0	$-i\sqrt{2}$	0
$\langle -3/2\|$	0	0	0	$i\sqrt{2}$	0	$-i\sqrt{5}/2$
$\langle -5/2\|$	0	0	0	0	$i\sqrt{5}/2$	0

S_x^2

	$\|5/2\rangle$	$\|3/2\rangle$	$\|1/2\rangle$	$\|-1/2\rangle$	$\|-3/2\rangle$	$\|-5/2\rangle$
$\langle 5/2\|$	5/4	0	$\sqrt{10}/2$	0	0	0
$\langle 3/2\|$	0	13/4	0	$3/\sqrt{2}$	0	0
$\langle 1/2\|$	$\sqrt{10}/2$	0	17/4	0	$3/\sqrt{2}$	0
$\langle -1/2\|$	0	$3/\sqrt{2}$	0	17/4	0	$\sqrt{10}/2$
$\langle -3/2\|$	0	0	$3/\sqrt{2}$	0	13/4	0
$\langle -5/2\|$	0	0	0	$\sqrt{10}/2$	0	5/4

$S = 5/2$

S_y^2

	$\|5/2\rangle$	$\|3/2\rangle$	$\|1/2\rangle$	$\|-1/2\rangle$	$\|-3/2\rangle$	$\|-5/2\rangle$
$\langle 5/2\|$	5/4	0	$-\sqrt{10}/2$	0	0	0
$\langle 3/2\|$	0	13/4	0	$-3\sqrt{2}/2$	0	0
$\langle 1/2\|$	$-\sqrt{10}/2$	0	17/4	0	$-3\sqrt{2}/2$	0
$\langle -1/2\|$	0	$-3\sqrt{2}/2$	0	17/4	0	$-\sqrt{10}/2$
$\langle -3/2\|$	0	0	$-3\sqrt{2}/2$	0	13/4	0
$\langle -5/2\|$	0	0	0	$-\sqrt{10}/2$	0	5/4

$S_x^2 - S_y^2$

	$\|5/2\rangle$	$\|3/2\rangle$	$\|1/2\rangle$	$\|-1/2\rangle$	$\|-3/2\rangle$	$\|-5/2\rangle$
$\langle 5/2\|$	0	0	$\sqrt{10}$	0	0	0
$\langle 3/2\|$	0	0	0	$3\sqrt{2}$	0	0
$\langle 1/2\|$	$\sqrt{10}$	0	0	0	$3\sqrt{2}$	0
$\langle -1/2\|$	0	$3\sqrt{2}$	0	0	0	$\sqrt{10}$
$\langle -3/2\|$	0	0	$3\sqrt{2}$	0	0	0
$\langle -5/2\|$	0	0	0	$\sqrt{10}$	0	0

S_z^2

	$\|5/2\rangle$	$\|3/2\rangle$	$\|1/2\rangle$	$\|-1/2\rangle$	$\|-3/2\rangle$	$\|-5/2\rangle$
$\langle 5/2\|$	25/4	0	0	0	0	0
$\langle 3/2\|$	0	9/4	0	0	0	0
$\langle 1/2\|$	0	0	1/4	0	0	0
$\langle -1/2\|$	0	0	0	1/4	0	0
$\langle -3/2\|$	0	0	0	0	9/4	0
$\langle -5/2\|$	0	0	0	0	0	25/4

$S = 5/2$

S_+^2

	$\|5/2\rangle$	$\|3/2\rangle$	$\|1/2\rangle$	$\|-1/2\rangle$	$\|-3/2\rangle$	$\|-5/2\rangle$
$\langle 5/2\|$	0	0	$2\sqrt{10}$	0	0	0
$\langle 3/2\|$	0	0	0	$6\sqrt{2}$	0	0
$\langle 1/2\|$	0	0	0	0	$6\sqrt{2}$	0
$\langle -1/2\|$	0	0	0	0	0	$2\sqrt{10}$
$\langle -3/2\|$	0	0	0	0	0	0
$\langle -5/2\|$	0	0	0	0	0	0

S_-^2

	$\|5/2\rangle$	$\|3/2\rangle$	$\|1/2\rangle$	$\|-1/2\rangle$	$\|-3/2\rangle$	$\|-5/2\rangle$
$\langle 5/2\|$	0	0	0	0	0	0
$\langle 3/2\|$	0	0	0	0	0	0
$\langle 1/2\|$	$2\sqrt{10}$	0	0	0	0	0
$\langle -1/2\|$	0	$6\sqrt{2}$	0	0	0	0
$\langle -3/2\|$	0	0	$6\sqrt{2}$	0	0	0
$\langle -5/2\|$	0	0	0	$2\sqrt{10}$	0	0

$S_+^2 + S_-^2$

	$\|5/2\rangle$	$\|3/2\rangle$	$\|1/2\rangle$	$\|-1/2\rangle$	$\|-3/2\rangle$	$\|-5/2\rangle$
$\langle 5/2\|$	0	0	$2\sqrt{10}$	0	0	0
$\langle 3/2\|$	0	0	0	$6\sqrt{2}$	0	0
$\langle 1/2\|$	$2\sqrt{10}$	0	0	0	$6\sqrt{2}$	0
$\langle -1/2\|$	0	$6\sqrt{2}$	0	0	0	$2\sqrt{10}$
$\langle -3/2\|$	0	0	$6\sqrt{2}$	0	0	0
$\langle -5/2\|$	0	0	0	$2\sqrt{10}$	0	0

$S = 5/2$

S_z^4

	$\|5/2\rangle$	$\|3/2\rangle$	$\|1/2\rangle$	$\|-1/2\rangle$	$\|-3/2\rangle$	$\|-5/2\rangle$
$\langle 5/2\|$	$\frac{625}{16}$	0	0	0	0	0
$\langle 3/2\|$	0	$\frac{81}{16}$	0	0	0	0
$\langle 1/2\|$	0	0	$\frac{1}{16}$	0	0	0
$\langle -1/2\|$	0	0	0	$\frac{1}{16}$	0	0
$\langle -3/2\|$	0	0	0	0	$\frac{81}{16}$	0
$\langle -5/2\|$	0	0	0	0	0	$\frac{625}{16}$

S_x^4

	$5/2\rangle$	$3/2\rangle$	$1/2\rangle$	$-1/2\rangle$	$-3/2\rangle$	$-5/2\rangle$
$\langle 5/2\|$	$\frac{65}{16}$	0	$\frac{22\sqrt{10}}{8}$	0	$\frac{3\sqrt{5}}{2}$	0
$\langle 3/2\|$	0	$\frac{241}{16}$	0	$\frac{90\sqrt{2}}{8}$	0	$\frac{3\sqrt{5}}{2}$
$\langle 1/2\|$	$\frac{22\sqrt{10}}{8}$	0	$\frac{401}{16}$	0	$\frac{90\sqrt{2}}{8}$	0
$\langle -1/2\|$	0	$\frac{90\sqrt{2}}{8}$	0	$\frac{401}{16}$	0	$\frac{22\sqrt{10}}{8}$
$\langle -3/2\|$	$\frac{3\sqrt{5}}{2}$	0	$\frac{90\sqrt{2}}{8}$	0	$\frac{241}{16}$	0
$\langle -5/2\|$	0	$\frac{3\sqrt{5}}{2}$	0	$\frac{22\sqrt{10}}{8}$	0	$\frac{65}{16}$

$S = 5/2$

S_y^4

	$\|5/2\rangle$	$\|3/2\rangle$	$\|1/2\rangle$	$\|-1/2\rangle$	$\|-3/2\rangle$	$\|-5/2\rangle$
$\langle 5/2\|$	$\frac{65}{16}$	0	$\frac{-22\sqrt{10}}{8}$	0	$\frac{3\sqrt{5}}{2}$	0
$\langle 3/2\|$	0	$\frac{241}{16}$	0	$\frac{-90\sqrt{2}}{8}$	0	$\frac{3\sqrt{5}}{2}$
$\langle 1/2\|$	$\frac{-22\sqrt{10}}{8}$	0	$\frac{401}{16}$	0	$\frac{-90\sqrt{2}}{8}$	0
$\langle -1/2\|$	0	$\frac{-90\sqrt{2}}{8}$	0	$\frac{401}{16}$	0	$\frac{-22\ 10}{8}$
$\langle -3/2\|$	$\frac{3\sqrt{5}}{2}$	0	$\frac{-90\sqrt{2}}{8}$	0	$\frac{241}{16}$	0
$\langle -5/2\|$	0	$\frac{3\sqrt{5}}{2}$	0	$\frac{-22\sqrt{10}}{8}$	0	$\frac{65}{16}$

$S_x^4 + S_y^4$

	$\|5/2\rangle$	$\|3/2\rangle$	$\|1/2\rangle$	$\|-1/2\rangle$	$\|-3/2\rangle$	$\|-5/2\rangle$
$\langle 5/2\|$	$\frac{65}{8}$	0	0	0	$3\sqrt{5}$	0
$\langle 3/2\|$	0	$\frac{241}{8}$	0	0	0	$3\sqrt{5}$
$\langle 1/2\|$	0	0	$\frac{401}{8}$	0	0	0
$\langle -1/2\|$	0	0	0	$\frac{401}{8}$	0	0
$\langle -3/2\|$	$3\sqrt{5}$	0	0	0	$\frac{241}{8}$	0
$\langle -5/2\|$	0	$3\sqrt{5}$	0	0	0	$\frac{65}{8}$

```
$JOB  10020064  MAGUIRE  IBJOB  3.0  3000
$*
$*
$*    PLEASE LOAD CALCOMP TAPE ON A8
$*
$*
$PAUSE
$EXECUTE  IBJOB
$IBJOB  FIOCS,CALCOM,MAP
C     THE PROGRAM EVALUATES THE EIGENVALUES FOR VARIOUS NUMERICAL
C     VALUES OF THE SPIN HAMILTONIAN PARAMETERS AS A FUNCTION OF
C     INCREASING MAGNETIC FIELD. THESE EIGENVALUES ARE THEN PLOTTED ON
C     CALCOMP USING THE ENPLOT ROUTINE.
$IBFTC MAIN
      DIMENSION DD(2000)
      COMMON /CONST/ G,D,A,B,ZETA,TAU,RHO,DELTA,I,DD,K
      CALL START
      CALL PLOT(1.0,1.0,-3)
    1 READ (5,100) G,D,A,B,III
  100 FORMAT (4E15.6,11X,I1)
      IF (III.EQ.1)GO TO 3
      WRITE (6,200)
  200 FORMAT (1H1,40X,25HCOMPUTED ENERGY VALUES )
      WRITE (6,300) G,D,A,B
  300 FORMAT (////10X,7HG*BETA= ,E15.6,10X,2HD= ,E15.6,10X,2HA=,E15.6
     *  10X,2HB=, E15.6)
      CALL ENERG
      CALL PLOT(11.0,0.0,-3)
      GO TO 1
    3 CALL ENPLOT(0,0)
      STOP
      END
```

```
$IBFTC IENERG
      SUBROUTINE ENERG
      DIMENSION DD(2000), FIELD(200), X(200), Y(200)
      COMMON /CONST/ G,D,A,B,ZETA,TAU,RHO,DELTA,I,DD,K
      ZETA=6.25*D + 39.0625*A + 8.125*B
      TAU=2.25*D + 5.0625*A + 30.125*B
      RHO=0.25*D + 0.0625*A + 50.125*B
      DELTA=2.0*D + 17.0*A - 11.0*B
      WRITE (6,100) ZETA,TAU,RHO,DELTA
  100 FORMAT (///10X,5HZETA=,E16.6,10X,4HTAU=,E16.6,10X,4HRHO=,E16.6,
     *        10X,6HDELTA=,E16.6)
      WRITE (6,200)
  200 FORMAT (1H1,3X,1HH,14X,2HE1,18X,2HE2,18X,2HE3,18X,2HE4,18X,2HE5,
     *           18X,2HE6/)
      K=1
      I=1
      DO 10 IH = 1,161
      H = (IH-1) * 50
      FIELD(IH) = H
      DO 5 L=1,6
      DD(K) = H
      K= K+1
    5 CONTINUE
   10 CALL CALC(H)
      CALL SCALE(FIELD,8.0,161,1)
      CALL SCALE(DD,20.0,966,1)
      YMIN = -DD(967)/DD(968)
      CALL AXIS(0.0,YMIN,5HFIELD,-5, 8.0, 0.0, FIELD(162),FIELD(163))
      CALL AXIS(0.0, 0.0, 6HENERGY, 6, 20.0, 90.0, DD(967), DD(968))
      X(162) = FIELD(162)
      X(163) = FIELD(163)
      Y(162) = DD(967)
      Y(163) = DD(968)
      DO 21 J= 1,6
      DO 22 K = 1, 161
      JJ= J+(K-1)*6
      X(K) = FIELD(K)
   22 Y(K) = DD(JJ)
   21 CALL LINE(X,Y, 161, 1, 0,0)
      RETURN
      END
```

```
$IBFTC CALCX
      SUBROUTINE CALC(H)
      DIMENSION DD(2000)
      COMMON /CONST/ G,D,A,B,ZETA,TAU,RHO,DELTA,I,DD,K
      IH=H+0.1
      C0=G*H
      C1=0.5*(C0+ZETA+TAU)
      C2=C0+C0+DELTA
      C3=SQRT(C2*C2+45.0*B*B)
      E1=C1+C3
      E5=C1-C3
      C1=C1-C0
      C2=-C0-C0+DELTA
      C3=SQRT(C2*C2+45.0*B*B)
      E2=C1+C3
      E6=C1-C3
      E3=RHO+0.5*C0
      E4=E3-C0
      DD(I) = E1
      DD(I+1) = E2
      DD(I+2) = E3
      DD(I+3) = E4
      DD(I+4) = E5
      DD(I+5) = E6
      I=I+6
      WRITE (6,100)IH, E1,E2,E3,E4,E5,E6
  100 FORMAT (I6,6E20.4)
      RETURN
      END
```

```
$JOB  10020064  MAGUIRE  IBJOB  3.0  3000
$EXECUTE  IBJOB
$IBJOB  ICIST
C     THIS PROGRAM INITIALLY CALCULATES THE EIGENVALUES FOR VARIOUS
C     VALUES OF THE SPIN HAMILTONIAN PARAMETERS AND THEN BY MEANS OF THE
C     SUBROUTINE SEARCHES FOR TRANSITIONS BETWEEN THESE EIGENVALUES AS A
C     FUNCTION OF THE MAGNETIC FIELD.
$IBFTC MAIN
      DIMENSION DD(2,2000)
      COMMON/CONS /E1,E2,E3,E4,E5,E6,IH
      COMMON /CONST/ G,D,A,B,ZETA,TAU,RHO,DELTA,I,DD,K
    1 READ (5,100) G,D,A,B,III
  100 FORMAT (4E15.6,11X,I1)
      IF (III.EQ.1)GO TO 3
      WRITE (6,200)
  200 FORMAT (1H1,40X,25HCOMPUTED ENERGY VALUES )
      WRITE (6,300) G,D,A,B
  300 FORMAT (////10X,7HG*BETA= ,E15.6,10X,2HD= ,E15.6,10X,2HA=,E15.6,
     *        10X,2HB=, E15.6)
      CALL ENERG
      CALL PINIST(DD,660)
      GO TO 1
    3 STOP
      END
```

```
$IBFTC IENERG
      SUBROUTINE ENERG
      DIMENSION DD(2,2000)
      COMMON /CONST/ G,D,A,B,ZETA,TAU,RHO,DELTA,I,DD,K
      COMMON/CONS /E1,E2,E3,E4,E5,E6,IH
      ZETA=6.25*D + 39.0625*A + 8.125*B
      TAU=2.25*D + 5.0625*A + 30.125*B
      RHO=0.25*D + 0.0625*A + 50.125*B
      DELTA=2.0*D + 17.0*A - 11.0*B
      WRITE (6,101) ZETA,TAU,RHO,DELTA
  101 FORMAT (///10X,5HZETA=,E16.6,10X,4HTAU=,E16.6,10X,4HRHO=,E16.6,
     *        10X,6HDELTA=,E16.6)
      WRITE (6,200)
  200 FORMAT (1H1,3X,1HH,14X,2HE1,18X,2HE2,18X,2HE3,18X,2HE4,18X,2HE5,
     *        18X,2HE6/)
      K=1
      I=1
      DO 10 IH = 1,161
      H = (IH-1) * 50
      DO 5 L=1,6
      DD(1,K)=H
      K= K+1
    5 CONTINUE
   10 CALL CALC(H)
      RETURN
      END
```

```
      C
      SUBROUTINE CALC(H)
      DIMENSION DD(2,2000),FMT(15)
      COMMON /CONST/ G,D,A,B,ZETA,TAU,RHO,DELTA,I,DD,K
      COMMON/CONS /E1,E2,E3,E4,E5,E6,IH
      DATA FMT/6H(1H0, ,6H27H TR,6HANSITI,6HON EXP,6HECTED ,6HAT H =,
     A6H,I6,6X,6H,9H BE,6HTWEEN ,6H,    ,6H      ,6H,6H AN,6HD  ,  ,
     B6H      ,6H)    /
      DATA E11,E22,E33,E44,E55,E66/4H2HE1,4H2HE2,4H2HE3,4H2HE4,4H2HE5,4H
     A2HE6/
      IH=H+0.1
      C0=G*H
      C1=0.5*(C0+ZETA+TAU)
      C2=C0+C0+DELTA
      C3=SQRT(C2*C2+45.0*B*B)
      E1=C1+C3
      E5=C1-C3
      C1=C1-C0
      C2=-C0-C0+DELTA
      C3=SQRT(C2*C2+45.0*B*B)
      E2=C1+C3
      E6=C1-C3
      E3=RHO+0.5*C0
      E4=E3-C0
      DD(2,I) = E1
      DD(2,I+1) = E2
      DD(2,I+2) = E3
      DD(2,I+3) = E4
      DD(2,I+4) = E5
      DD(2,I+5) = E6
      I=I+6
  102 FORMAT (I6,6E20.4)
      WRITE (6,102) IH, E1,E2,E3,E4,E5,E6
      FMT(11) = E11
      FMT(14) = E22
      X = E1 - E2
      IF((X-.313).LT.0.01.AND.(X-.313).GT.-0.01) WRITE(6,FMT)IH
      FMT(14) = E33
      X = E1 - E3
      FMT(14) = E44
      X = E1 - E4
      IF((X-.313).LT.0.01.AND.(X-.313).GT.-0.01) WRITE(6,FMT)IH
      FMT(14) = E55
      X = E1 - E5
      IF((X-.313).LT.0.01.AND.(X-.313).GT.-0.01) WRITE(6,FMT)IH
      FMT(14) = E66
      X = E1 - E6
      IF((X-.313).LT.0.01.AND.(X-.313).GT.-0.01) WRITE(6,FMT)IH
      FMT(11) = E22
      FMT(14) = E11
      X = E2 - E1
      IF((X-.313).LT.0.01.AND.(X-.313).GT.-0.01) WRITE(6,FMT)IH
      FMT(14) = E33
      X = E2 - E3
      IF((X-.313).LT.0.01.AND.(X-.313).GT.-0.01) WRITE(6,FMT)IH
      FMT(14) = E44
      X = E2 - E4
      IF((X-.313).LT.0.01.AND.(X-.313).GT.-0.01) WRITE(6,FMT)IH
      FMT(14) = E55
```

```
      X = E2 - E5
      IF((X-.313).LT.0.01.AND.(X-.313).GT.-0.01) WRITE(6,FMT)IH
      FMT(14) = E66
      X = E2 - E6
      IF((X-.313).LT.0.01.AND.(X-.313).GT.-0.01) WRITE(6,FMT)IH
      FMT(11) = E33
      FMT(14) = E11
      X = E3 - E1
      IF((X-.313).LT.0.01.AND.(X-.313).GT.-0.01) WRITE(6,FMT)IH
      FMT(14) = E22
      X = E3 - E2
      IF((X-.313).LT.0.01.AND.(X-.313).GT.-0.01) WRITE(6,FMT)IH
      FMT(14) = E44
      X = E3 - E4
      IF((X-.313).LT.0.01.AND.(X-.313).GT.-0.01) WRITE(6,FMT)IH
      FMT(14) = E55
      X = E3 - E5
      IF((X-.313).LT.0.01.AND.(X-.313).GT.-0.01) WRITE(6,FMT)IH
      FMT(14) = E66
      X = E3 - E6
      IF((X-.313).LT.0.01.AND.(X-.313).GT.-0.01) WRITE(6,FMT)IH
      FMT(11) = E44
      FMT(14) = E11
      X = E4 - E1
      IF((X-.313).LT.0.01.AND.(X-.313).GT.-0.01) WRITE(6,FMT)IH
      FMT(14) = E22
      X = E4 - E2
      IF((X-.313).LT.0.01.AND.(X-.313).GT.-0.01) WRITE(6,FMT)IH
      FMT(14) = E33
      X = E4 - E3
      IF((X-.313).LT.0.01.AND.(X-.313).GT.-0.01) WRITE(6,FMT)IH
      FMT(14) = E55
      X = E4 - E5
      IF((X-.313).LT.0.01.AND.(X-.313).GT.-0.01) WRITE(6,FMT)IH
      FMT(14) = E66
      X = E4 - E6
      IF((X-.313).LT.0.01.AND.(X-.313).GT.-0.01) WRITE(6,FMT)IH
      FMT(11) = E55
      FMT(14) = E11
      X = E5 - E1
      IF((X-.313).LT.0.01.AND.(X-.313).GT.-0.01) WRITE(6,FMT)IH
      FMT(14) = E22
      X = E5 - E2
      IF((X-.313).LT.0.01.AND.(X-.313).GT.-0.01) WRITE(6,FMT)IH
      FMT(14) = E33
      X = E5 - E3
      IF((X-.313).LT.0.01.AND.(X-.313).GT.-0.01) WRITE(6,FMT)IH
      FMT(14) = E44
      X = E5 - E4
      IF((X-.313).LT.0.01.AND.(X-.313).GT.-0.01) WRITE(6,FMT)IH
      FMT(14) = E66
      X = E5 - E6
      IF((X-.313).LT.0.01.AND.(X-.313).GT.-0.01) WRITE(6,FMT)IH
      FMT(11) = E66
      FMT(14) = E11
      X = E6 - E1
      IF((X-.313).LT.0.01.AND.(X-.313).GT.-0.01) WRITE(6,FMT)IH
```

```
      IF((X-.313).LT.0.01.AND.(X-.313).GT.-0.01) WRITE(6,FMT)IH
      FMT(14) = E33
      X = E6 - E3
      IF((X-.313).LT.0.01.AND.(X-.313).GT.-0.01) WRITE(6,FMT)IH
      FMT(14) = E44
      X = E6 - E4
      IF((X-.313).LT.0.01.AND.(X-.313).GT.-0.01) WRITE(6,FMT)IH
      FMT(14) = E55
      X = E6 - E5
      IF((X-.313).LT.0.01.AND.(X-.313).GT.-0.01) WRITE(6,FMT)IH
      RETURN
      END
```

```
$DATA
 .934860 E-04  0.900000 E-01  0.186000 E-02  0.186000 E-02
 .934860 E-04  0.950000 E-01  0.163000 E-02  0.163000 E-02
 .934860 E-04  0.794500 E-01  0.163000 E-02  0.163000 E-02
 .934860 E-04  0.467300 E-01  0.163000 E-02  0.163000 E-02
 .934860 E-04  0.000000 E-01  0.163000 E-02  0.163000 E-02
                                                          1
$EOF
```